TERAHERTZ TIME DOMAIN METHODS FOR MATERIAL CHARACTERIZATION OF LAYERED DIELECTRIC MEDIA

By

Jose Ale Hejase

A DISSERTATION

Submitted to
Michigan State University
in partial fulfillment of the requirements
for the degree of

DOCTOR OF PHILOSOPHY

Electrical Engineering

2012

ABSTRACT

TERAHERTZ TIME DOMAIN METHODS FOR MATERIAL CHARACTERIZATION OF LAYERED DIELECITRIC MEDIA

By

Jose Ale Hejase

Material characterization methods for layered dielectric media are highly sought after in many fields including nondestructive evaluation, structural health monitoring, security imaging, biological tissue inspection and agricultural and industrial quality assurance. On the other hand, the still under-explored Terahertz frequency range shows great promise and advantages for imaging and spectroscopy. As such, this dissertation provides a library of material parameter extraction tools of single and multiple layered dielectric mediums for different circumstances and using a variety of measurement and analysis criteria. The conditions required for using each characterization method are laid out. The background theory of the methods is based upon electromagnetic waves transmission and reflection phenomena at interfaces, wave propagation and Fourier optics. Because material characterization is an inverse problem solution, optimization and root finding methods were required to that effect. The optimization method utilized was the Nelder-Mead Simplex method while the root finding method was the Secant method. The inverse problem solution setups and special considerations for each of the characterization tools are presented. The operation validation and material characterization examples for each method are demonstrated. Additionally, the limitations of the methods are discussed along with error analysis pertaining to crucial input parameters. On the other hand, a measurement component for fine spatial resolution interrogation is designed, fabricated and tested. This component can be used in conjunction with the methods presented in this research study for simultaneous imaging and spectroscopy/material characterization of structures. The

possible future investigation routes related to the research presented in this dissertation are discussed in the conclusion. .

To the memory of my dear grandmother,
Charifa Ibrahim Hejase

ACKNOWLEDGEMENTS

It has been about four and half years since joining the PhD program at Michigan State University. As this journey comes to an end, I would like to express my gratitude to several people without whom successful completion of my degree would not have been possible.

First and foremost, I thank my advisor Dr. Premjeet Chahal whose valuable research direction greatly facilitated this journey. Through Dr. Chahal, I was introduced to many disciplines pertaining to applied electromagnetics research, thus increasing my horizons. I am especially grateful for his understanding, motivation, emphasis on team work, encouragement to publish journals and attend conferences and his belief in me.

Second, I would like to thank my committee members Dr. Lalita Udpa, Dr. Shanker Balasubramaniam, Dr. Edward J. Rothwell, Dr. Rigoberto Burgueno and Dr. Pradeep Ramuhalli for their research advice and support. Particularly, I wish to thank Dr. Ramuhalli for being the person to open the door for me to join MSU in the first place. I also wish to express sincere appreciation to Dr. Rothwell for our many technical discussions and more importantly for being a wise mentor and great example to me.

Third, I would like to thank the members of the EM group and the Terahertz Systems Laboratory for all the help, friendships and experiences they provided me. The friendships I have developed with them will last long after I leave MSU.

Fourth, I am thankful to the National Science Foundation for partially funding my research. I am thankful to the graduate school and the college of engineering for awarding me the graduate office fellowship twice and two conference travel grants. I also thank the department of electrical

and computer engineering for awarding the dissertation completion fellowship which was instrumental in the facilitation of completing my degree.

Fifth, I would like to thank Dr. Percy Pierre for inducting me into the Alfred Sloan scholars student group at Michigan State University. Through my participation in the Sloan scholars group, I managed to meet many outstanding peers, attend a national workshop on teaching and mentoring and receive the Sloan scholarship.

Finally, certain people have had a major effect on my life and contributed to the successes that have happened in it. I will never be able to thank them enough. These people are: my father, Ale, the captain of my life and the person I strive to be like; my mother, Layla, my God sent blessing; my loyal brother, Hussein, the person I can always depend on; my sweet sister, Charifa, who is always there to support me; my skilled brother, Ahmad, who always finds a way to cheer me up and my soul mate, Layal, who has been the glowing star of my life from the moment she entered it.

TABLE OF CONTENTS

LIST OF TABLES ... ix

LIST OF FIGURES ... x

CHAPTER 1 ... 1
INTRODUCTION ... 1
1.1 Terahertz Nondestructive Evaluation ... 1
1.1.1 Definition ... 1
1.1.2 Literature Overview ... 5
1.2 Terahertz Material Characterization ... 9
1.2.1 Problem Statement ... 9
1.2.2 Terahertz Time Domain System ... 10
1.2.3 Current Terahertz Time Domain Material Characterization Techniques ... 13
1.3 Research Motivation and Objectives ... 18
1.4 Dissertation layout ... 21

CHAPTER 2 ... 22
SINGLE LAYER MATERIAL CHARACTERIZATION METHODS ... 22
2.1 Reference Requiring Method ... 22
2.1.1 Problem Definition and Motivation ... 22
2.1.2 Characterization Method Theory ... 23
2.1.3 Optimization Procedure and Setup ... 26
2.1.4 Method Validation and Results ... 29
2.1.5 Moisture Content Examination Example ... 35
2.1.6 Error Analysis and Disucssion ... 36
2.2 Self Calibrating Method ... 41
2.2.1 Problem Definition and Motivation ... 41
2.2.2 Characterization Method Theory ... 42
2.2.3 Optimization Procedure and Setup ... 47
2.2.4 Signal Artifacts Removal Technique ... 49
2.2.5 Method Validation and Results ... 55
2.2.6 Method Limitations ... 60
2.2.7 Error Analysis and Discussion ... 61

CHAPTER 3 ... 67
METHODS FOR CHARACTERIZATION OF MULTIPLE LAYER MEDIA ... 67
3.1 The Multiple Angle Method ... 67
3.1.1 Problem Definition and Motivation ... 67
3.1.2 Characterization Method Theory ... 68
3.1.3 Inverse Problem Root-Finding Setup ... 71
3.1.4 Forward Problem Solution and Validation ... 72
3.1.5 Inverse Problem Solution from Synthesized Data ... 76

3.1.6 Inverse Problem Solution from Measured Data ... 82
3.1.7 Error Analysis and Discussion ... 92
3.2 The Input and Output Field Distribution Method ... 97
3.2.1 Problem Definition and Motivation ... 97
3.2.2 Characterization Method Theory ... 99
3.2.3 Inverse Problem Root-Finding Setup ... 103
3.2.4 Forward Problem Solution from Synthesized Data ... 105
3.2.5 Inverse Problem Solution from Synthesized Data ... 110
3.2.6 Experimental Implementation Discussion ... 116
3.2.6.1 Phase Reversing Zone Plate Lens: Design and Experimental Testing ... 116

CHAPTER 4 ... 121
TOOLS FOR SMALL AREA INTERROGATION AND SPECTROSCOPY – CHARACTERIZATION OF COMPOSITE MATERIAL STRUCTURES ... 121
4.1 Problem Definition and Motivation ... 121
4.2 THz Dielectric Subwavelength Focusing Probe ... 124
4.2.1 Probe Design ... 124
4.2.2 Probe Simulation ... 125
4.2.2 Probe Fabrication and Experimental Testing ... 128
4.2.3.1 Bandwidth Testing ... 128
4.2.3.2 Imaging Resolution Testing ... 129
4.2.3.3 Simulataneous Imaging and Spectroscopy Experiment ... 132

CHAPTER 5 ... 135
CONCLUSIONS AND FUTURE WORK ... 135
5.1 Conlusions ... 135
5.2 Future Work ... 140

APPENDICES ... 142

BIBLIOGRAPHY ... 251

LIST OF TABLES

Table 2-1. Dielectric Properties Comparison……………………………………………………34

LIST OF FIGURES

Figure 1-1. Typical NDE system ("For interpretation of the references to color in this and all other figures, the reader is referred to the electronic version of this dissertation.")……………….…………………………………..………...……………….…..2

Figure 1-2. Leaf moisture examination using THz radiation ……….…………………………..…...3

Figure 1-3. Concealed object detection using THz radiation……………………………………..4

Figure 1-4. Delamination thickness detection using THz radiation…………………...………4

Figure 1-5. Magnitude of the THz signal transmitted through moist air (THz frequencies) [14]...7

Figure 1-6. Forward and inverse problems of material characterization…………………...……..9

Figure 1-7. THz time domain system measurement setup – reflection mode…………………...10

Figure 1-8. THz time domain system measurement setup – transmission mode……………..….12

Figure 1-9. T-ray 2000 time-domain THz system……………………………………………….12

Figure 1-10. THz ellipsometry measurement setup [32]……..………………………………….15

Figure 1-11. (a) THz DTDS measurement setup (b) Sample close-up view [34]……………….16

Figure 1-12. The ultimate goal which the dissertation contributes towards…………………….…….19

Figure 2-1. Reference requiring method idealized measurement setup...…………………….…….22

Figure 2-2. Typical reference (air background) and sample (Alumina) THz time-domain signals.. ………………..…………………………………………………………………………..………24

Figure 2-3. (a) Dielectric constant of glasses, (b) Loss-tangent of glasses..……………….………30

Figure 2-4. (a) Dielectric constant of ceramic and semiconductors, (b) Loss-tangent of ceramic and semiconductors………………………..……………………………………………….………31

Figure 2-5. (a) Dielectric constant of organic materials, (b) Loss-tangent of organic materials...31

Figure 2-6. (a) Dielectric constant of organic materials, (b) Loss-tangent of organic materials...31

Figure 2-7. (a) Dielectric constant of polymer-ceramic composites, (b) Loss-tangent of polymer-ceramic composites…………………………………………………………………………....33

Figure 2-8. (a) Relative dielectric constants of the moist and dry Polyimide samples, (b) Loss tangents of the moist and dry Polyimide samples…………………………………………......35

Figure 2-9. (a) Extracted material properties of "B" for measured thickness=0.5mm, (b) Extracted material properties of "B" for measured thickness=1mm…………….………….....37

Figure 2-10. (a) Extracted material properties of "A" for measured thickness=1.3mm, (b) Extracted material properties of "C" for measured thickness=0.6mm………….……………....39

Figure 2-11. Sketch of idealized measurement setup...…………………...…………………42

Figure 2-12. Received time-domain signal for a typical sample showing multiple transmissions under ideal conditions……………………………………......………….………………43

Figure 2-13. Example time-domain signals obtained from the measurement…..………………49

Figure 2-14. Sample signal along with the shifted archived time-domain signal.....…………….51

Figure 2-15. Sample Signal and First Subtraction Result……………...…………..…………….52

Figure 2-16. Second Subtraction Result………………………......………….…………52

Figure 2-17. Measured and Final Sample Signals…………………...………….………….54

Figure 2-18. Extracted dielectric properties of Al2O3………………...………………...……….56

Figure 2-19. Extracted dielectric properties of HDPE…….…………...……………...………….57

Figure 2-20. Extracted dielectric properties of Quartz………………...……………..………….58

Figure 2-21. Extracted dielectric properties of InP…….….………...……………….....……….59

Figure 2-22. Extracted dielectric properties of doped Si….…………...…………………..…….59

Figure 2-23. (a) Extracted material properties of "B" for measured thickness=0.5mm, (b) Extracted material properties of "B" for measured thickness=1mm...………..……………..….62

Figure 2-24. (a) Extracted material properties of "A" for measured thickness=1.3mm, (b) Extracted material properties of "C" for measured thickness=0.6mm………..……………..….64

Figure 3-1. Sketch of the idealized measurement setup……..………...……………….....……….68

Figure 3-2. Experiment measurement setup (top view)…..…………...………………..……….73

Figure 3-3. Typical measured reference signal through air (or delayed incident signal).……….73

Figure 3-4. Measured and calculated signals through the single layer dielectric stack...……….74

Figure 3-5. Measured and calculated signals through the two layer dielectric stack…...……….75

Figure 3-6. Extracted properties of the single layer stack……………………..………………...77

Figure 3-7. Extracted properties of the two layer stack (known thicknesses)………….……….79

Figure 3-8. Extracted properties of the two layer stack (unknown thicknesses)……….……….81

Figure 3-9. HDPE single layer stack extracted material properties and thickness……..……….85

Figure 3-10. Si single layer stack extracted material properties and thickness….……..……….86

Figure 3-11. Pyrex single layer stack extracted material properties and thickness…….……….87

Figure 3-12. PC single layer stack extracted material properties and thickness…..……..……….89

Figure 3-13. HDPE-Si two layer stack extracted material properties………………..…..……….91

Figure 3-14. Pyrex-Si two layer stack extracted material properties…..……………...……….92

Figure 3-15. Extracted material parameters for the assumed incident angle settings of (a) 0-degrees, (b) 20-degrees, (c) 40-degrees and (d) 60-degrees…………...……………...……….94

Figure 3-16. Extracted properties for the assumed incident angle pair (60- and 40- degrees) (a) 2 matching equations for 60-degrees incidence (b) 2 matching equations for 40-degrees incidence………………………………………………………………………………………95

Figure 3-17. Idealized model for the input and output field distribution method……..……….98

Figure 3-18. Theoretical model for the characterization method……...……………...……….99

Figure 1-19. Waveform of the incident plane wave upon the PRZP…..……………...……...105

Figure 3-20. Magnitude of the Fourier transform of $E_i(t)$…..………...……………...……...106

Figure 3-21. Magnitude of the input field distribution at 60mm……...……………...……...107

Figure 3-22. Magnitude of the output field distribution for a 30mm material system of air…...108

Figure 3-23. Magnitude of the output field distribution for a 30mm thick material having $n=3$ and k=0……………………………………...……………...……………...……...109

Figure 3-24. Extracted parameters of the single layer stack…………...………………..…..…112

Figure 3-25. Extracted parameters of the two layer stack……………..……………….……...114

Figure 3-26. Extracted parameters of the three layer stack…………...………………..……...115

Figure 3-27. PRZP design structure……………………….…...……………….……...117

Figure 3-28. PRZP field distribution measurement setup………..…...………………..……….119

Figure 3-29. Magnitude of field distribution as a result of the PRZP measured at: (a) 15.5mm and (b) 20mm…………………………………………………...……………….……….119

Figure 4-1. Composite structure, homogeneous along the direction normal to its surface…….121

Figure 4-2. Composite structure, heterogeneous along all directions…...……………..……….122

Figure 4-3. Conical probe geometry……………………..……...………………..……….124

Figure 4-4. True design versus simulated design (red)……………….………………..……….126

Figure 4-5. Complex field distribution magnitude (red=highest intensity, blue=lowest intensity)...127

Figure 4-6. Electric field complex magnitude 0.15mm away from the tip……….…..……….127

Figure 4-7. Probe measurement setup……………………………...………………..……….128

Figure 4-8. Transmitted signal magnitude spectrum.………………...………………..……….129

Figure 4-9. Resolution measurement for the conical focusing probes………………………….130

Figure 4-10. Fourier transform magnitude at 212.5 GHz……………….……………...…….131

Figure 4-11. Gradient of the magnitude of the Fourier transform with it half power resolution.132

Figure 4-12. Resolution as a Function of Frequency for the Conical Probe………………..….132

Figure 4-13. Leaf imaged window………………….………………...………………..……….133

Figure 4-14. Leaf images at different frequencies.....………………...………………..……….134

Figure A-1. Nelder and Mead Simplex method possible movements..………………..……….143

CHAPTER 1

INTRODUCTION

1.1 Terahertz Nondestructive Evaluation

1.1.1 Definition

Until recently, the wide Terahertz (THz) frequency spectrum (0.1 to 10 THz) has been one of the least explored sections of the Electromagnetic spectrum due to the lack of availability of THz sources and detectors. However, because of recent technological advances combining optical and electronic systems, THz systems have been significantly advanced. The mechanism utilized in most of these developments involves the use of mode-locking femtosecond lasers in order to excite photoconductive switches which generate THz radiation [1].

The use of THz radiation can have major benefits in many areas such as high frequency circuits, spectroscopy, imaging, high bandwidth communications and different types of sensing. However, such uses are still in their infancy. Several reasons are behind this lag. Partly, the inability to generate THz signals efficiently until the past two decades. Also, THz systems were not commercia1lly available except until this past decade. Moreover, THz systems are expensive, bulky and require significant upkeep. Research groups carrying out research in the THz spectrum are few in number and thus the know-how and the availablility of necessary tools is still limited [2]. As a result, further investigations in this spectral region will prove to be very useful towards utilizing THz radiation to its full capacity in many applications.

One of the emerging fields of THz is the use of THz radiation for nondestructive evaluation (NDE). THz NDE revolves around the development of techniques to examine structures and specimens without putting the integrity of the specimen in jeopardy. The area of NDE includes

measurement techniques, signal processing and data analysis. An example of an NDE system is shown in Figure 1-1. Here a sample containing a defect is interrogated with a wave, in this case a THz wave, using a quasi-optical setup. The interaction of the sample with the wave is then recorded using a measurement transducer. The measured interactions in addition to the excitation signal are then processed and analyzed. The result of the processing may be in the form of flaw detection or flaw characterization.

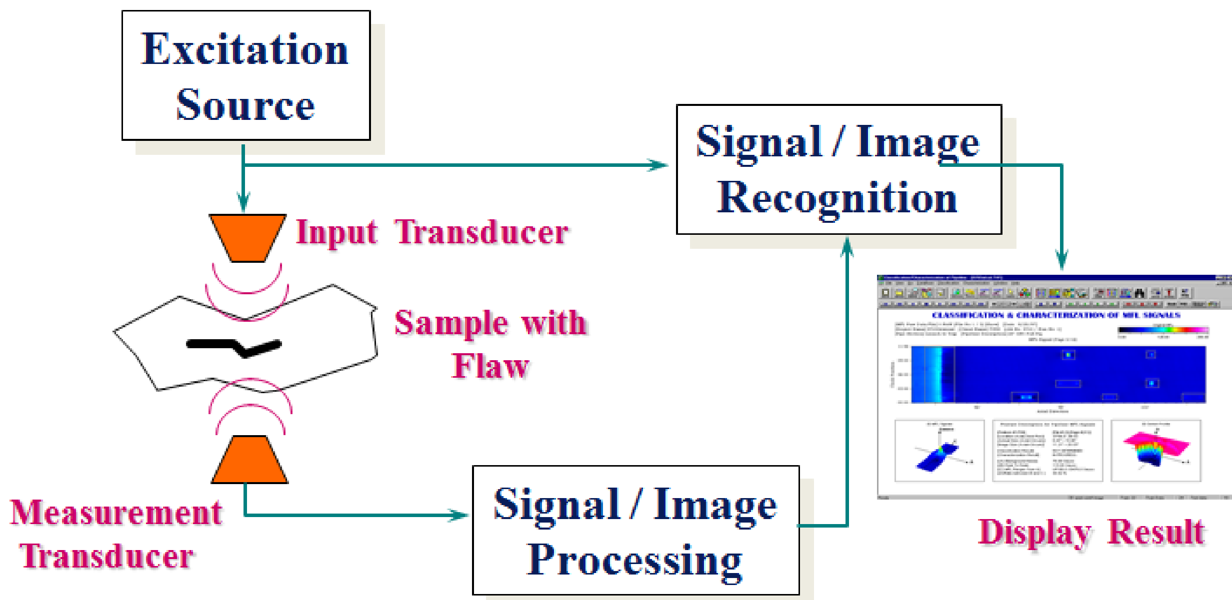

Figure 1-1. Typical NDE system ("For interpretation of the references to color in this and all other figures, the reader is referred to the electronic version of this dissertation.")

Interest in the use of THz for NDE is due to several reasons. First, material spectral fingerprints are very abundant in the THz frequency range making THz radiation very attractive for use in material spectroscopy. Second, THz radiation is known to be non-ionizing and thus is safer for biomedical (and biological studies) applications than X-rays. Third, the wavelengths at THz frequencies are smaller than at microwave frequencies thus resulting in higher resolution imaging when compared to more common microwave imaging techniques. Fourth, a wide variety of materials (e.g., paper, plastics, dielectric composites, etc.) are transparent at THz frequencies making THz attractive for use in NDE of such materials and structures. Fifth, while

highly conducting materials are not transparent at THz frequencies, THz radiation can be used to examine their surface (e.g., roughness, corrosion, oxidation, etc) or coatings on these surfaces. All these different reasons infer the applicability of THz radiation for NDE applications spanning and not limited to: security applications, bio-imaging, spectroscopy, moisture content examination, material characterization and composite materials inspection [3]. Figure 1-2 shows an example of using THz radiation for monitoring the moisture content of a leaf as a function of drying-time. The amplitude of the signal transmitted through the leaf increases as a function of time. This can be attributed to the fact that the leaf loses moisture overtime thus decreasing the attenuation of the transmitted THz signal. Figure 1-3 shows an example where THz radiation was used in order to detect an embedded chip and loop antenna within a smart plastic card. Figure 1-4 shows different measured time domain THz signals as a function of increase in delamination gap between two Polyethylene terephthalate (PET) films. The uniqueness of each of the waveforms shown in the figure infers that THz radiation can be used to inspect structures having very thin delamination (for example: peeling of paint from surface).

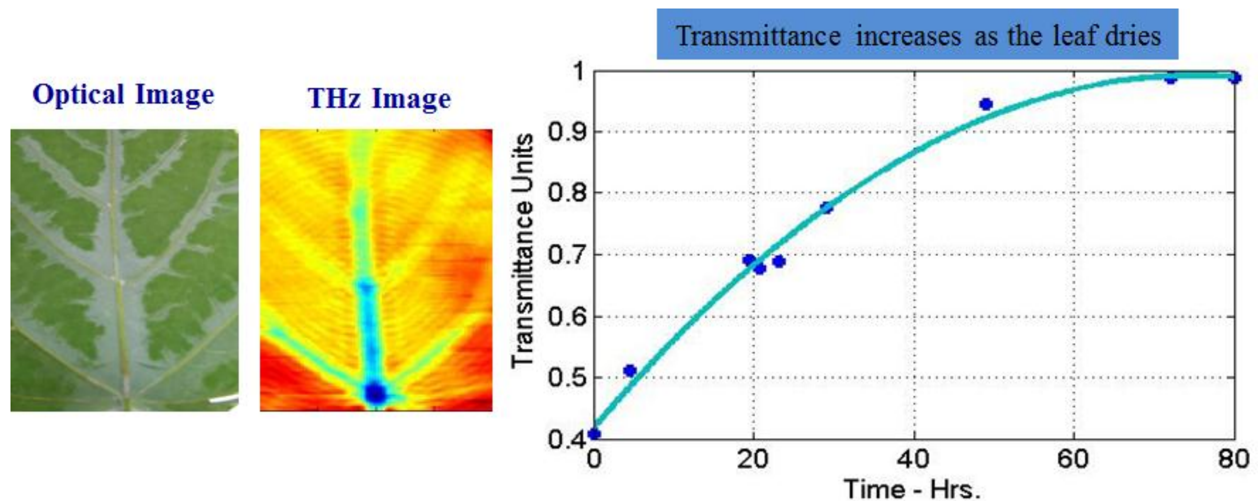

Figure 1-2. Leaf moisture examination using THz radiation

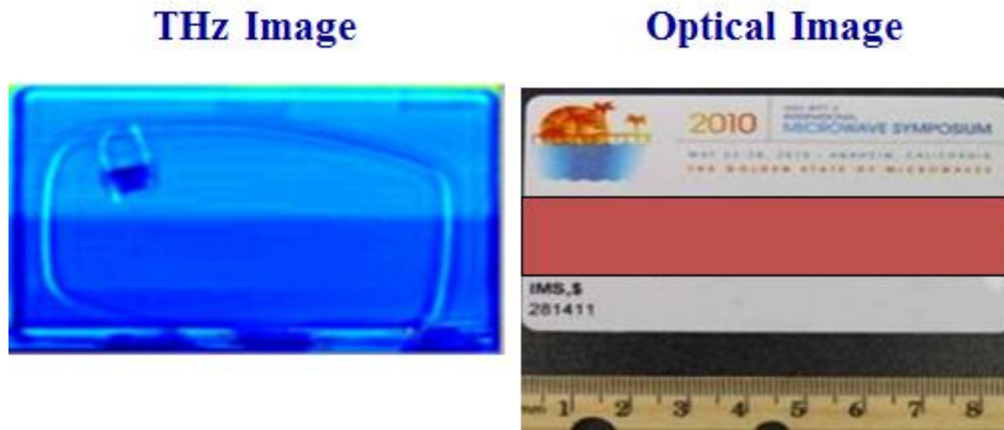

Figure 1-3. Concealed object detection using THz radiation

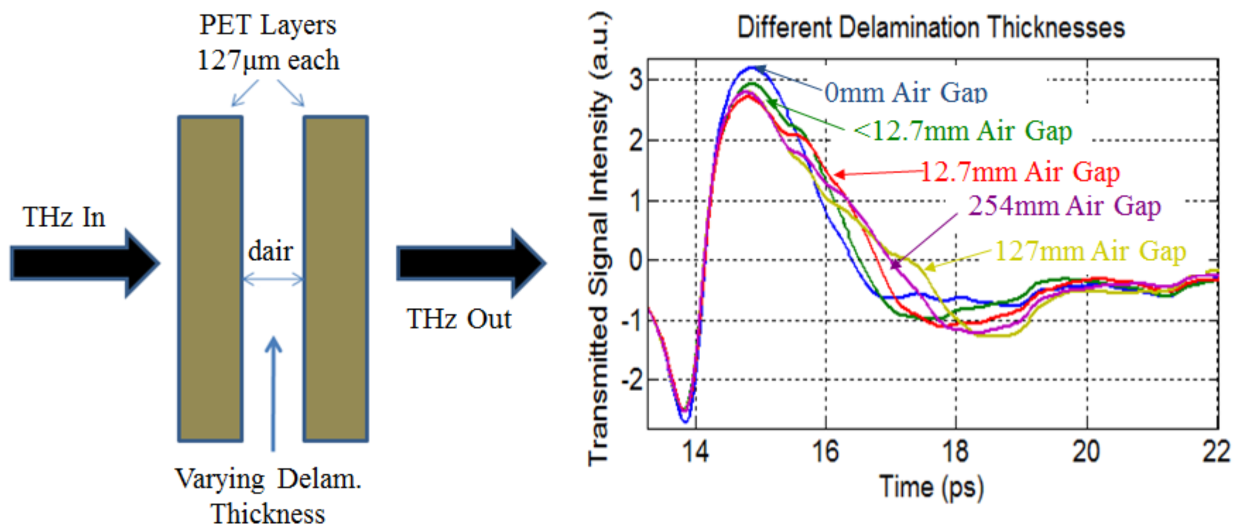

Figure 1-4. Delamination thickness detection using THz radiation

THz NDE can be sub-grouped into four categories of study based on the use and end results. These are as follows:

1. The use of THz radiation for obtaining physical dimensions of different structures
2. The use of THz radiation for obtaining material properties of structures as a function of frequency
3. The use of THz radiation for obtaining spectral information about structures coming short of material properties (detecting a change in the material properties)

4. The use of THz radiation for obtaining structural information coming short of dimensions (detecting a change in the structure).

1.1.2 Literature Overview

Many examples related to the use of THz radiation to examine structures have been documented. These are reviewed here briefly.

In [4], THz imaging was utilized to examine voids and disbands in foam insulation of a space shuttle external tank. Additionally, the ability to use THz radiation for metallic and nonmetallic weapon detection was shown. A main contribution of [4] was the demonstration of the feasibility to use THz radiation to do fast large area imaging scans. In [5], NDE of IC packages was done for delamination detection at 109 GHz using open ended coaxial cable focusing probes while monitoring the reflection. Features from THz time domain measurements have been used in order to detect flaws (or contiminants) in a chocolate bar towards a quick detection technique for chocolate bar quality assurance [6]. THz time domain measurements have been used to detect surface roughness of metallic structures with roughness varying between 0.8 μm up to 100 μm [7]. The reflection spectrum was shown to be almost identical for average roughness varying from 0.8 μm up to 3.2 μm. Above 3.2 μm, the surface roughness effect on the reflection magnitude spectrum was shown to be pronounced [7].

In [8], THz radiation was used to estimate crop yield. Veins, leafs, and fruit berries have different spectral signatures. These signatures are determined by physical dimensions and dielectric properties. The inspection process was carried out at a 1m standoff thus showing feasibility for use in agricultural quality assurance. THz radiation has also shown promise to monitor minute changes in live cells including cell growth, cell volume and morphology changes over time [9]. Using THz radiation, imaging and discrimination of localized heat damage spots

on aircraft composites has been shown in [10]. Additionally, discrimination between hidden explosive versus non-explosive materials has been demonstrated in [11].

Some research work has been done on target reconstruction using different tomography techniques in the THz range [12-13]. These studies have developed reconstruction algorithms for THz tomography based on diffraction theory and electromagnetic scattering. While THz tomography has limited applications compared to X-ray tomography due to the limited penetration depth of THz radiation in highly moist environments, it still can be used as a safer alternative for certain types of image reconstruction involving humans such as under-skin tumor imaging.

One example of capitalizing on the abundance of material spectral features in the THz frequency range is material moisture content examination. Moisture content in objects has been known to affect their integrity. The advantage of using THz radiation to monitor moisture content is that moisture absorption peaks are highly concentrated in the THz frequency range and have strong absorption features. Several studies have shown this characteristic including [14]. In another work, the ability of THz radiation to detect the water content in paper has been demonstrated. This was done by examining the effects on the phase and magnitude of a transmitted THz signal through pieces of paper having different moisture levels [15]. Figure 1-5 shows the magnitude spectrum of a THz signal transmitted through moist air. Absorption peaks are labeled in the figure.

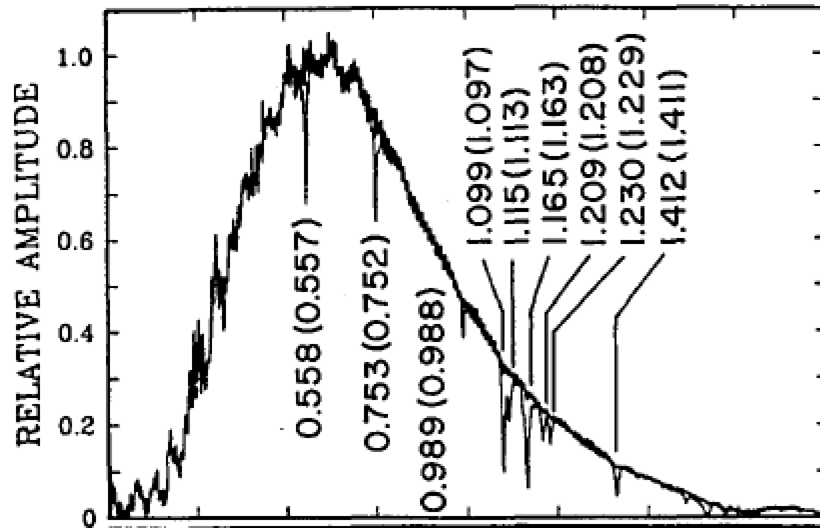

Figure 1-5. Magnitude of the THz signal transmitted through moist air (THz frequencies) [14]

One of the main advantages of X-ray imaging and interrogation is the high resolution images that can be resolved. Recent progress in the area of THz near field imaging has shown that ultra fine resolution can be achieved by using X-ray inspired imaging techniques or focusing tools. This includes the use of scanning near field optical microscopy for THz imaging where sub-micron resolution has been demonstrated [16]. The applications of such focusing include inspection of very fine features in biological tissue reaching cell level or even nondestructive evaluation of semiconductors such as solar cell for micro-crack detection. Other instances where sub-wavelength focusing has been achieved include the use of waveguide apertures [17-18] and dielectric probes [19-20]. While the resolution achieved by such methods is not as high as scanning near field optical microscopy, they do provide faster measurements and more flexibility in the measurement setup while still proving useful in a variety of possible applications such as concealed object inspection [17], mineralogy studies [19] and pore/void detection [18].

A major motivation behind the emergence of THz NDE is the ability of THz radiation to penetrate through most optically opaque materials (largely dielectric materials). A variety of materials that have been characterized in the literature are proof that THz radiation can be used

in NDE of structures composed of these materials. In [21], several high dielectric constant and low loss materials were characterized at THz frequencies. The availability of such substrates with such characteristics might be advantageous as photonic crystal substrates for terahertz frequency antennas. The measured substrates included Alumina, Silicon, Zirconium and others. In [22] and [23], THz material characterization is carried out for several oxide materials. In [24], low loss polymers that are not attacked by chemicals and thus compatible with microfluidics sensing and bio-imaging have been characterized at THz frequencies. In [25], different polymers, oils and glasses were characterized. The ability of THz radiation to distinguish between used, overused and unused oils was shown. Also shown was the ability of THz radiation to distinguish between cured and uncured SU8 (photo-epoxy material). This discrimination capability was possible as the dielectric properties were shown to be different related to the degree of cross-linking of the polymer chains.

The properties of the materials mentioned in the above paragraph were extracted using different material characterization methods. One crucial area of THz NDE involving computation and measurements is material characterization. The material characterization problem definition and its importance are discussed in the next subsections along with a survey of available methods and techniques.

1.2 Terahertz Material Characterization

1.2.1 Problem Statement

Characterizing materials at THz frequencies is a challenging inverse problem. Here, the resultant of the interaction of THz radiation with a material system is used in order to determine the properties of that system. In most instances, these are the dielectric properties such as permittivity and loss tangent or refractive index and absorption coefficient. The process of extracting the material properties is the inverse problem solution and the essence of the material characterization. This is the opposite of the forward problem solution where the resultant of the interaction of the THz radiation with the material system is to be predicted while knowing the properties of the system. Figure 1-6 shows a systems-based block diagram summarizing the forward and inverse problems pertaining to material characterization.

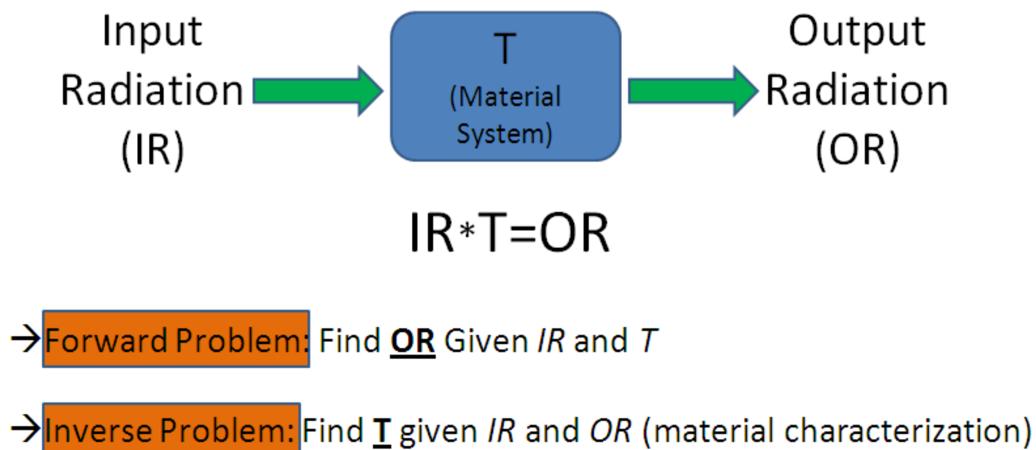

Figure 1-6. Forward and inverse problems of material characterization

The apparent need for material characterization methods is to extract properties of unknown samples. However, given an object to test noninvasively the more information extracted about that object the better. The characteristics of the materials that form the object and their location within the object are the utmost information that can be achieved. As a result, a variety of versatile material characterization methods and techniques are required in order to achieve more

efficient, reliable and informative nondestructive testing. The next subsections present the THz time domain system configuration and material characterization techniques currently available for THz time domain signals.

1.2.2 Terahertz Time Domain System

This dissertation presents new THz material characterization methods which employ time domain signals in the process. However, prior to discussing the methods available in the literature it is probably worth introducing what a typical THz time domain system entails, how it operates and briefly discuss its limitations.

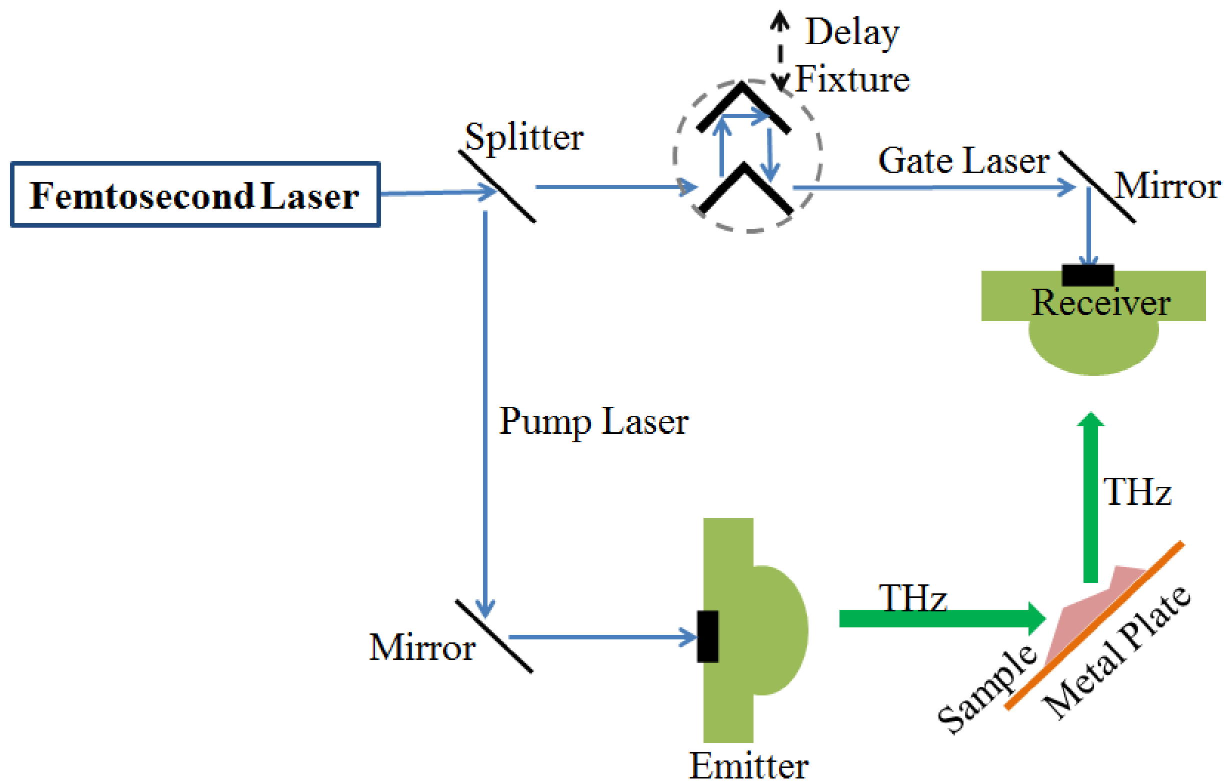

Figure 1-7. THz time domain system measurement setup – reflection mode

As mentioned before, common THz time domain systems use femtosecond mode-locking lasers in order to generate THz radiation. Such systems have two photoconductive switches, one placed at an emitter level and one at a receiver level. The emitter level switch generates radiation

when excited with a pump laser pulse while the receiver level switch detects them triggered by a separate gate laser pulse delivered through a time delay fixture [26]. Plano-convex lenses can be placed on the photoconductive switches. This results in collimated THz radiation travelling from the emitter to the plano-convex lens at the receiver where it is focused on to the detecting photoconductive switch. THz radiation is detected at the receiver by scanning through the time delay. Measurements can be taken in transmission mode and in reflection mode by changing the emitter's and receiver's locations. The range of frequencies that can be achieved on common systems ranges from 100 GHz up to 2.5 THz. Figures 1-7 and 1-8 show sketches of a THz time domain system set up for reflection and transmission measurements respectively. Due to the emitter and receiver being separate parts of the system, they would have to be placed at an angle in order to carry out reflection measurements. A metal plate can be placed behind the sample if needed. Figure 1-7 shows one type of reflection measurement configurations used for THz time domain systems. In transmission mode measurements, the sample is place in between the transmitter and receiver as shown in Figure 1-8.

Figure 1-9 shows a commercially available THz time domain system. This system is the T-ray 2000 from picometrix. Labels of its different parts are shown in the figure. The T-ray 2000 is the system that is utilized to carry out the measurement portion of this dissertation. THz time-domain NDE computational and experimental techniques are constrained by current THz systems limitations. Particularly of interest are the limitations pertaining to material characterization techniques. The emitted power of current THz systems is not very high, thus limiting the operation of current THz systems in the lower end of the THz range (up to around 2.5 THz) [2]. This limits the frequency range where materials can be characterized. On the other hand, THz time-domain systems may experience power drifts and time shifts over short periods

of times. While these effects are not very pronounced, under certain circumstances they may result in erroneous extracted material parameters.

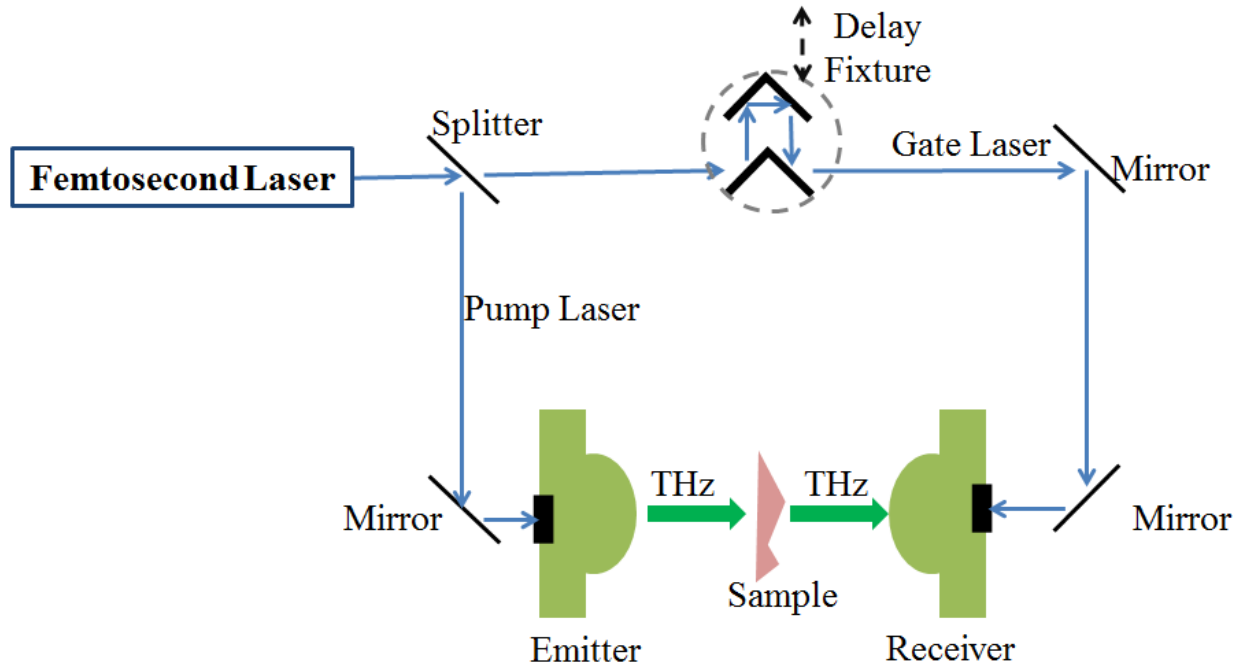

Figure 1-8. THz time domain measurement setup – transmission mode

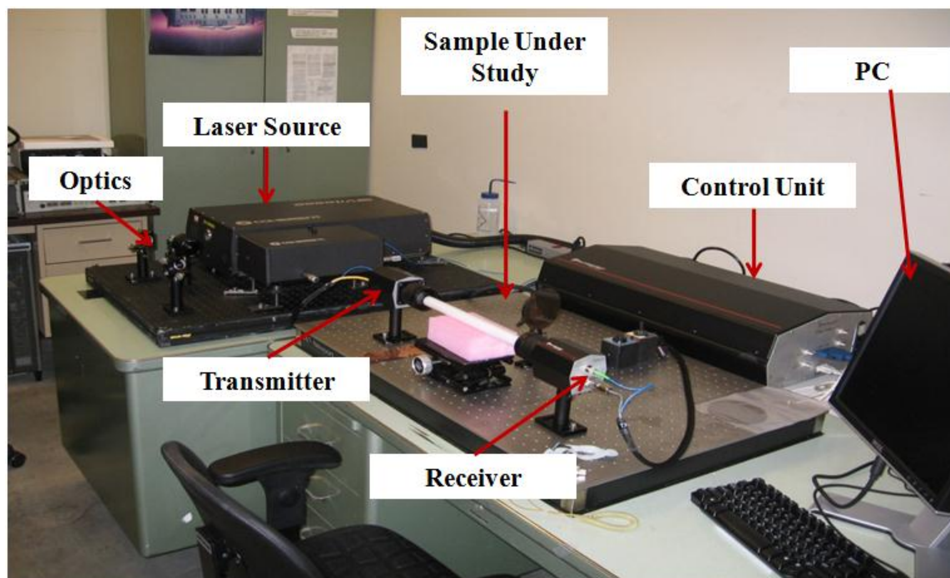

Figure 1-9. T-ray 2000 time-domain THz system

1.2.3 Current Terahertz Time Domain Material Characterization Techniques

The different THz time domain material characterization techniques documented in the literature were essential to this research. These methods provided crucial knowledge that was built upon in this dissertation. On the other hand, some of their limitations provided motivation to certain parts of the dissertation research.

The most common technique for carrying out THz time-domain material characterization is a transmission mode single layer material characterization method. This has been discussed in great detail in literature, including refs. [27-31]. The differences between the previous works were minimal in which incremental improvements were introduced chronologically. The background for all these works is more or less the same. In this technique, a transmission mode setup is used (see Figure 1-8). Normally incident time-domain reference (typically through air), $E_r(t)$, and sample, $E_s(t)$, transmission measurements are collected. The Fourier transforms, $E_r(\omega)$ and $E_s(\omega)$ respectively, of these acquired signals are then calculated. By dividing $E_s(\omega)$ by $E_r(\omega)$, a measured frequency domain transmission coefficient, $T_m(\omega)$, can be found. It is well known from electromagnetic theory of wave propagation in mediums that the transmission coefficient is a function of the material properties and thickness of the medium that the wave propagates. Consequently, the material characterization method proceeds by defining a calculated frequency domain transmission coefficient, $T_c(\omega)$. $T_c(\omega)$, for normal incidence is described as

$$T_c(\omega) = \frac{T_{as}(\omega) T_{sa}(\omega) \exp\left(-j\omega \tilde{n}_s\, l/c\right)}{1 + \Gamma_{as}(\omega)\Gamma_{sa}(\omega)\exp\left(-2j\omega \tilde{n}_s\, l/c\right)}, \qquad (1\text{-}1)$$

where, $\tilde{n}_s$ ($\tilde{n}_s = n_s - jk_s$) is the complex index of refraction of the sample, l is the thickness of the sample, c is the speed of light in air, $T_{as}(\omega)$ and $\Gamma_{as}(\omega)$ are interfacial transmission and

reflection coefficients when the wave is travelling from air into the sample, and $T_{sa}(\omega)$ and $\Gamma_{sa}(\omega)$ are the interfacial transmission and reflection coefficients when the wave is travelling from the sample to air. The expression which describes $\Gamma_{as}(\omega)$ is

$$\Gamma_{as}(\omega) = \frac{(n_s - jk_s) - 1}{1 + (n_s - jk_s)}. \tag{1-2}$$

The rest of the interfacial coefficients are described as,

$$\Gamma_{sa}(\omega) = -\Gamma_{as}(\omega), \tag{1-3}$$

$$T_{as}(\omega) = 1 - \Gamma_{as}(\omega), \tag{1-4}$$

$$T_{sa}(\omega) = 1 + \Gamma_{as}(\omega). \tag{1-5}$$

Given $T_m(\omega)$, the unknown material properties (n_s and k_s) are found through an extraction process using an optimization algorithm. The condition that must be satisfied to arrive at the true material properties is $T_m(\omega) = T_c(\omega)$. More details on this material parameter extraction procedure are provided in chapter two.

The above theory has been applied as the basis for many material characterization methods. The differences between the different implementations include the addition of thickness optimization modules, oblique incidence usage capability, different optimization methods and noise treatment techniques.

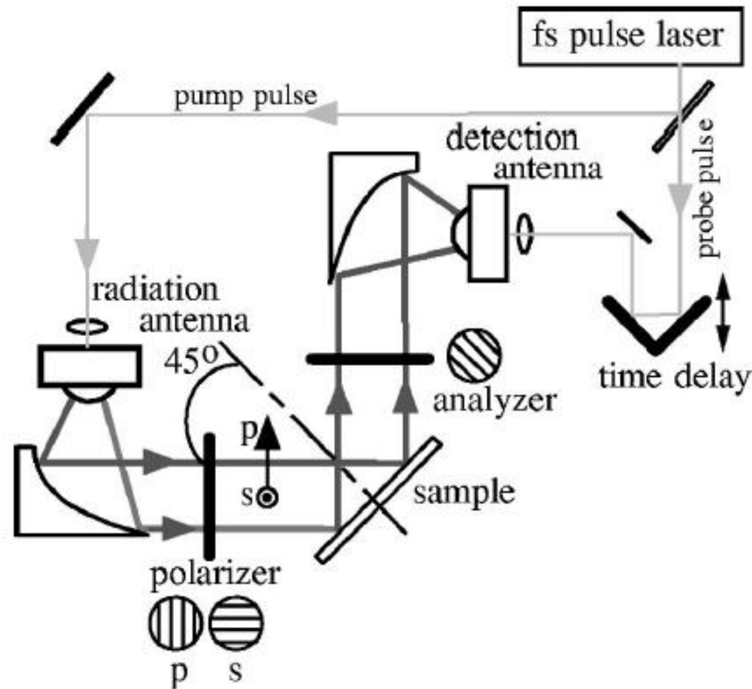

Figure 1-10. THz ellipsometry measurement setup [32]

Another technique for material characterization used at THz frequencies is THz ellipsometry [32-33]. Ellipsometry is a material characterization technique commonly used at other frequency ranges (for example: optical). The change in the polarization of a reflected wave due to oblique incidence on a dielectric sample is associated with the material properties of the sample. As a result the inverse problem entails finding the material properties of the dielectric slab causing a specific change in polarization. Fig. 1-10 shows a typical THz ellipsometry measurement system. The transmitter and receiver of a typical time-domain THz system radiate and detect linearly polarized waves. In the THz ellipsometry system, the transmitter and receiver are rotated such that perpendicular (s-) and parallel (p-) polarizations can be obtained when using a polarizer. The polarizer angle that results in perpendicular polarization is 90 degrees different from the one resulting in parallel polarization. The parallel or perpendicular polarized wave resulting from the polarizer after the wave impinges upon the sample under examination. The polarization of the reflected signal will change as a result of the reflection due to the sample properties. The changes

in the amplitude and phase of the recorded waves due to parallel and perpendicular incidence are utilized in order to find the dielectric properties of the sample under test. This method is further discussed in [32-33]. One advantage of THz ellipsometry is that the sample does not have to be moved in order to measure a reference sample (unlike transmission time-domain material characterization method discussed earlier) thus decreasing experimental error. On the other hand, the extracted material properties of the sample are highly sensitive to any uncertainty in the angle of oblique incidence of the wave impinging upon the sample and the extinction ratio of the polarizers.

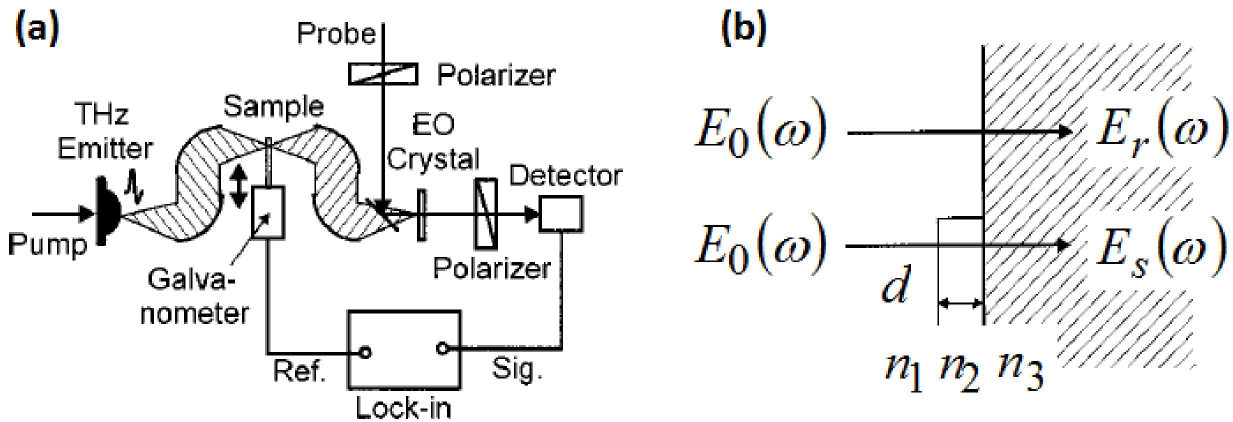

Figure 1-11. (a) THz DTDS measurement setup (b) Sample close-up view [34]

Another method used for THz material characterization is THz differential time-domain spectroscopy (DTDS) [9, 34-36]. Using this method, material properties of ultrathin films can be extracted unlike the traditional THz material time-domain material characterization methods. The THz-DTDS measurement setup is shown in Figure 1-11 (a). THz-DTDS requires two signals in order to carry out the characterization. These are a signal transmitted through a reference material, $E_r(t)$, and a signal equaling the difference between the signal transmitted through the sample film and the reference material, $E_{diff}(t) = E_s(t) - E_r(t)$. At first it might seem trivial to obtain these signals from the transmission setup shown in Figure 1-8, however,

THz system noise and instabilities are of the same order of magnitude (and maybe higher) as changes in amplitude and phase seen due to wave transmission through ultrathin films. In THz DTDS, the sample under study (see Figure 1-11 (b)) is moved in and out of the THz beam using a galvanometer. The movement alternates between placing the film and reference in the THz beam path. A lock-in amplifier synchronized to the galvanometer oscillation signal is used in order to measure the differential signal thus highly increasing the SNR. The same experimental setup is used in order to acquire $E_{diff}(t)$ and $E_r(t)$. $E_r(t)$ can be thought of as a differential measurement as well if the film part of the sample fixture (see Figure 1-11 (b)) is blocked with a metal plate to prevent transmission through the film, thus causing the galvanometer to alternate between the reference sample and the metal plate.

While the techniques described above provide solutions for many material characterization inverse problem scenarios, they still have certain shortcomings. The available methods served as a valuable source towards building the research disseminated by this dissertation and their shortcomings provided many motivations for it. The motivation, objectives and dissertation layout are discussed in the next sections.

1.3 Research Motivation and Objectives

Most documented methods require a reference measurement in addition to the sample measurement in order to carry out the material characterization. This fact is a shortcoming due to time and amplitude drifts inherent in THz systems. Reference and sample measurements are collected at different times and thus if not taken in short time proximity after each other may result in erroneous material characteristics due to the signal drift. Additionally, in case of a simultaneous imaging and material characterization pixel scans of a single layer heterogeneous material sample, a reference measurement is required for every pixel thus placing a high time cost on the scan. Second, most documented methods require the knowledge of the thickness of the sample understudy in order to extract its dielectric properties. This is hindering as the uncertainty in thickness measurements leads to error in material parameter extraction. Few schemes that can be used in conjunction with material parameter extraction techniques have been developed. One method commonly used is the total variation technique first presented in [27] and used in conjunction with the common transmission mode THz material characterization technique. Given a discrete set of thicknesses in a specific range (usually dictated by the uncertainty of the measured thickness), the material properties of a dielectric sample can be obtained for each thickness. The material properties are frequency dependent. The total variation measure is a smoothness measure which makes use of the fact that within a certain limited frequency range (like the lower THz range), solids' material properties do not change drastically between consecutive frequency samples. Hence, the properties extracted with the lowest total variation measure along with the corresponding thickness are the properties of the sample under test. A limitation of the total variation method is that it is highly sensitive to system noise. Robust methods capable of extracting the thickness along with the material properties of the

sample would be highly advantageous in applications where measuring the thickness is not appealing due to logistic or time constraints. Third, the present literature lacks THz material characterization methods for stacked layers of dielectrics. The availability of such methods can be very useful for many applications.

This research builds upon the work that has been documented in the literature as presented above. Realizing the importance of evaluation of objects in a wide variety of applications and under various scenarios, the goal of the dissertation research is to provide measurement and data analysis techniques in order to carry out material characterization of structures. The ultimate goal which the dissertation research contributes towards is the characterization of a structure as shown in Figure 1-12 using THz radiation. Given a highly complex 3D composite system (see Figure 1-12), the task would be to extract the material parameters of the homogeneous sections of the system.

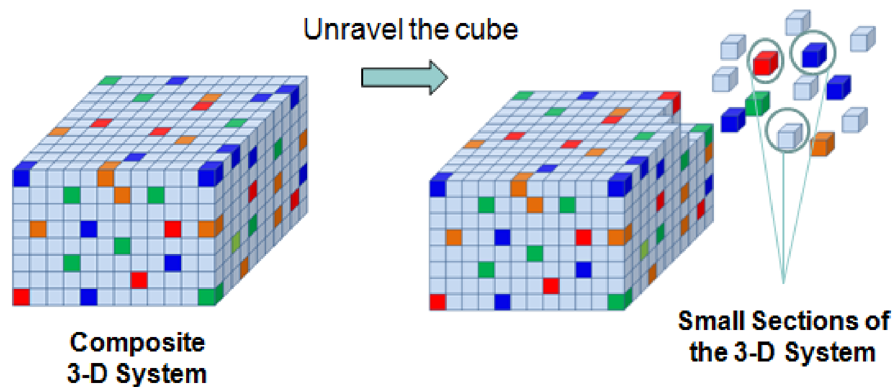

Figure 1-12. The ultimate goal which the dissertation contributes towards

Several tasks are carried out as steps towards that ultimate goal while at the same time overcoming challenges of previously documented material characterization methods. The steps are special cases of the ultimate goal to be achieved.

First, two single homogeneous dielectric layer material characterization methods are presented. The first is a reference requiring method based upon the single layer transmission THz

material characterization method presented in [27]. In essence, it is similar to the method demonstrated in [27] with minor incremental improvements in the optimization process. The main motivation behind working with this method was in order to characterize various materials to be used as a benchmark for the accuracy of the other methods developed as a result of this dissertation. The second is the self-calibrating single layer material characterization method which doesn't require a reference signal to carry out the material characterization thus decreasing the measurement time requirements and overcoming the THz system drifts.

Second, a material characterization method employing different incident angle signals transmitted through the structure under test is developed. This method allows for single and multiple dielectric layer material characterization along with thickness extraction of different layers.

Third, a method that employs input and output field distributions of a multi-feature wave transmitted through a material system under test is developed. This new measurement method can be utilized to characterize single and multiple layer dielectric material systems in parallel with layer thickness extraction.

Fourth, while the methods mentioned above provide solutions for characterizing layers in the direction normal to the layer surfaces, solutions are needed to realize the characterization of a 3D composite system having heterogeneity also along the direction parallel to the surface. Towards this endeavor, focusing probes have been developed. These focus THz radiation into small regions of the structure understudy and can be used in conjunction with the developed material characterization methods to characterize structures that are not homogenous along the direction parallel to their surface.

1.4 Dissertation Layout

The next chapters of this dissertation proceed in the following fashion. Chapter 2 presents the single layer material characterization methods. For each method the background theory, inverse problem optimization setup, method experimental validation results and an error analysis study are presented. Chapter 3 presents the methods capable of carrying out both multiple and single layer material characterization along with thickness extraction. For the multiple angle method the background theory, inverse problem root finding setup, forward problem experimental validation, inverse problem solution from synthesized and experimentally measured signals and an error analysis study are presented. On the other hand, for the input and output field distribution method the background theory, inverse problem root finding setup, forward and inverse problem solutions from synthesized signal, experimental feasibility and implementation discussion are presented. Chapter 4 pertains to the focusing probes. The probe design, simulation studies and experimental testing are presented. The dissertation is concluded in chapter 5 along with the presentation of possible future work routes.

CHAPTER 2

SINGLE LAYER MATERIAL CHARACTERIZATION METHODS

2.1 The Reference Requiring Method

Note: This work is part of [37]. The Matlab material characterization code associated with this method is presented in Appendix C.

2.1.1 Problem Definition and Motivation

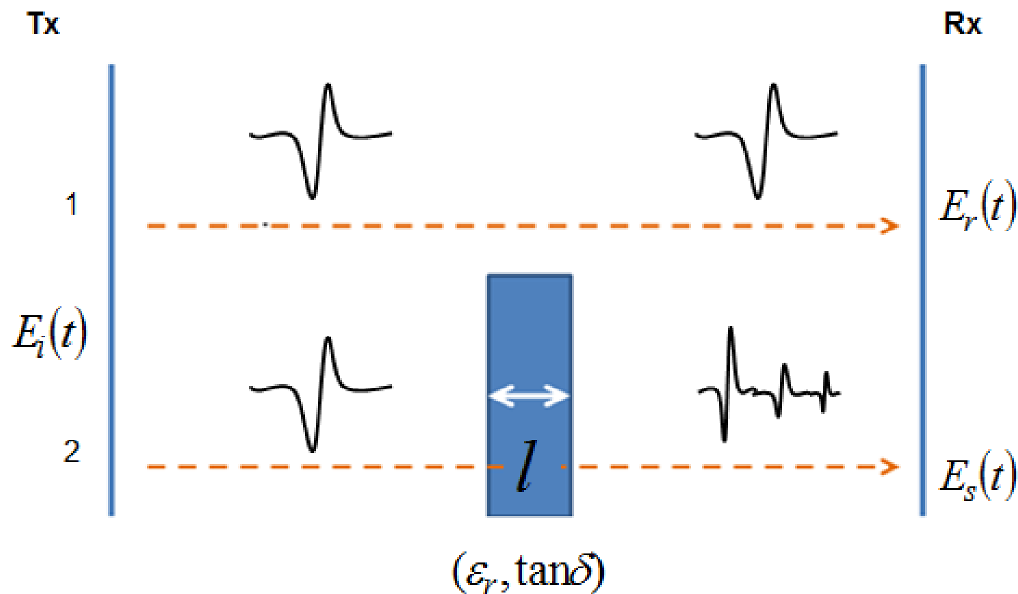

Figure 2-1. Reference requiring method idealized measurement setup

Given a dielectric slab with a known thickness, the reference requiring method is used to find the dielectric properties of the slab using a THz signal transmitted through the slab and its relation to a THz signal transmitted through a reference material (typically air). Figure 2-1 shows the corresponding idealized measurement setup for the method where Tx and Rx are the transmitter and receiver modules respectively and $E_i(t)$, $E_r(t)$, and $E_s(t)$ are the incident, reference and sample THz time-domain signals respectively. The reference requiring method

presented here builds upon the background theory in [27]. Particularly, the characterization method uses a different optimization algorithm, the Nelder-Mead method which is more robust to signal noise. Additionally, the extraction of the material properties is done independently at every frequency sample unlike [27] where the extraction is done in the whole frequency range at once thus being more prone to contain errors. Note that similar changes to [27] were done in [30] but discovered by the author after the completion of this section of chapter 2.

2.1.2 Characterization Method Theory

As mentioned earlier, this method utilizes two different signals collected from a transmission mode measurement setup. These are a reference signal and a sample signal. The reference measurement is taken when the sample is removed from the path of the THz radiation beam. To minimize measurement errors due to drift in THz signal generation and detection, sample measurements and reference signal measurements were carried out in close time proximity from each other. The different considerations taken during the measurement procedure and the data analysis method are as follows:

1) The electromagnetic time domain pulse was normally incident on the sample

2) The samples tested were flat and had smooth surfaces

3) The THz system signal (through air) had acceptable noise levels (high signal-to noise ratio (SNR)) up to 2.5 THz

4) The size of the time window when the data is collected was 80 ps

5) The sampling period of the time pulse (of the reference and sample signals) was 0.03941 ps, which when considering the time-domain signal's 2048 samples, gives a frequency domain resolution of approximately 12.5 GHz.

The process begins by acquiring the two time-domain signals sequentially. These are the

reference signal through air (sample removed from the path of the beam) and the sample signal (signal transmitted through the sample under test). Figure 2-1 depicts the measurements along with notations used in the discussion of the material parameter extraction theory.

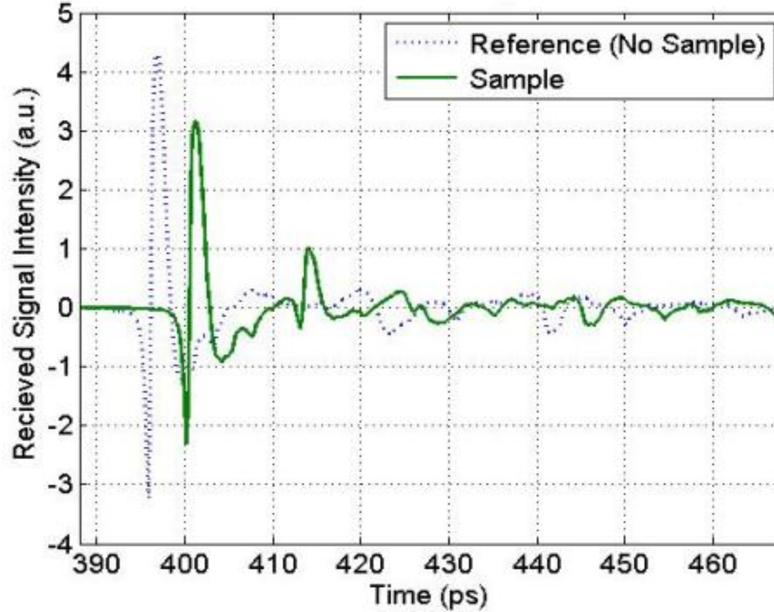

Figure 2-2. Typical reference (air background) and sample (Alumina) THz time-domain signals

The reference signal, $E_r(t)$, is simply the incident signal, $E_i(t)$, delayed in time (by p) due to traveling a certain distance in air. The sample signal, $E_s(t)$, on the other hand is $E_i(t)$ delayed in time (by $p1$) due to traveling a different distance in air and convoluted with the time-domain transmission coefficient $T(t)$ which is a function of the dielectric substrate having thickness l. The expressions for $E_r(t)$ and $E_s(t)$ are

$$E_r(t) = E_i(t - p), \tag{2-1}$$

and

$$E_s(t) = E_i(t - p1) * T(t). \tag{2-2}$$

Figure 2-2 shows example measured time-domain (80ps time window with 2048 measured data points) reference and sample (0.635mm thick Alumina, Al_2O_3) signals. A delay in time, a change

in amplitude and multiple transmissions from the substrate are visible in the time-domain sample signal.

The frequency spectrum was calculated by Fourier transforming the time-domain signals. The expressions for the Fourier transforms are

$$E_r(\omega) = E_i(\omega)\exp\left(-j\omega\tilde{n}_{air}\, x/c\right), \tag{2-3}$$

and

$$E_s(\omega) = E_i(\omega)\exp\left(-j\omega\tilde{n}_{air}\,(x-l)/c\right)T(\omega), \tag{2-4}$$

where $\tilde{n}_{air}$ ($\tilde{n}_{air} = 1.00027 - j0$) is the complex index of refraction of air [27], c is the speed of light in free space, x is the distance between the transmitter and receiver and l is the thickness of dielectric sample under test. The frequency domain transmission coefficient, $T(\omega)$, is a function of the complex index of refraction of the sample, $\tilde{n}_s$ ($\tilde{n}_s = n - jk$), and its thickness, l, and is described by [38]

$$T(\omega) = \frac{T_{as}(\omega)T_{sa}(\omega)\exp\left(-j\omega\tilde{n}_s\, l/c\right)}{1+\Gamma_{as}(\omega)\Gamma_{sa}(\omega)\exp\left(-2j\omega\tilde{n}_s\, l/c\right)}, \tag{2-5}$$

where $T_{as}(\omega)$ and $\Gamma_{as}(\omega)$ are the interfacial transmission and reflection coefficients between air and the sample under test and $T_{sa}(\omega)$ and $\Gamma_{sa}(\omega)$ are the interfacial transmission and reflection coefficients at the interface between the sample under test and air. The expressions describing the interfacial transmission and reflection coefficients for normal incidence are

$$T_{op}(\omega) = \frac{2(n_o - jk_o)}{(n_o - jk_o) + (n_p - jk_p)}, \tag{2-6}$$

and

$$\Gamma_{op}(\omega) = \frac{(n_p - jk_p) - (n_o - jk_o)}{(n_o - jk_o) + (n_p - jk_p)}, \tag{2-7}$$

respectively, where o and p can be the sample understudy or air.

A ratio of the Fourier transforms of the measured signals can be obtained and is expressed as

$$O(\omega) = \frac{E_s(\omega)}{E_r(\omega)}. \tag{2-8}$$

The modeled ratio which is a function of the properties of the material under test is described by

$$\hat{O}(\omega) = \exp\left(j\omega\tilde{n}_a\, l/c\right)\frac{T_{as}(\omega)T_{sa}(\omega)\exp\left(-\,j\omega\tilde{n}_s\, l/c\right)}{1+\Gamma_{as}(\omega)\Gamma_{sa}(\omega)\exp\left(-2\,j\omega\tilde{n}_s\, l/c\right)}. \tag{2-9}$$

Hence, the material properties can be found by minimizing the difference between the measured and modeled ratios in (2-8) and (2-9) respectively. The next subsection lays out the optimization procedure and setup.

2.1.3 Optimization Procedure and Setup

Although the collected data contains the material properties information inherently, the material properties can't be extracted analytically. An optimization process has to take place where the ratio $\hat{O}(\omega)$ can be optimized towards matching the measured ratio $O(\omega)$. The optimization goal would be achieved by finding appropriate values for the complex index of refraction of the sample at each frequency.

The material properties to be extracted are the real part of the refractive index of the sample, n, and the imaginary part of the refractive index, k. The properties are frequency dependent; hence, it was chosen to optimize independently at all frequency points. The properties of materials were extracted between 300 GHz and an upper frequency limit chosen based on the signal level of the magnitude of the Fourier transform of the time-domain sample signal. Above 2.5 THz the signal is at the noise level. The average of the magnitude of the magnitude spectrum

above 2.5 THz was used as the noise floor measure. The frequency corresponding to twenty times the noise floor was chosen as the upper limit of the frequency range for characterizing all the materials. Given that the calculated and measured material property ratios are complex quantities and frequency dependent, the fitness function was chosen to minimize the difference between the magnitudes and the phases of the ratios at all frequency points. The fitness function $F(\omega)$ that is used to carry out the optimization is

$$F(\omega) = \left| \left| \, |O(\omega)| - \left|\hat{O}(\omega)\right| \, \right| + \left| \, \angle O(\omega) - \angle \hat{O}(\omega) \, \right| \right|. \tag{2-10}$$

The calculation of the phase difference requires extra precaution. Phase is determined in radians and the same angle can be described in two ways, positively or negatively. This may lead to extracting incorrect material properties. In order to remedy this effect, if faced with a phase difference that is greater than π or less than $-\pi$ during the optimization process, the phase difference is substituted with the result obtained by subtracting the 2π from its absolute value.

The optimization technique utilized in this study is the Nelder and Mead modified simplex method [39-41]. The simplex method is an unconstrained direct search multivariable optimization algorithm. A regular simplex is a polyhedron with N+1 equidistant points, where N is the dimension (number of variables) of the multivariable optimization. In the problem at hand, the regular simplex was chosen to be a triangle as the optimization is done for two variables. The fitness function is calculated at every vertex. The vertex point that has the highest (or worst) fitness function value is updated based on the rules defined in [40]. The optimization stops once the fitness function reaches the threshold set at the beginning of the optimization $\left(< 10^{-10}\right)$ or once the standard deviation of the fitness function values at all the vertices is very small $\left(< 10^{-10}\right)$. More details on the optimization method implementation can be found in [39-41] and

Appendix A of this dissertation.

Given a measured value of the thickness of the substrate understudy, a discrete array of thicknesses is created. The array will include a range of thicknesses limited by the uncertainty of the thickness measurement. For example, if the uncertainty of the measurement is 5%, the upper limit of the range of thicknesses would be the measured value added to 5% of the measured value. The characterization process first begins by picking a thickness from the array created earlier. Guesses of the real and imaginary parts of the refractive index are made. The initial guesses are chosen to be the same at all frequencies. The procedure applied to find these initial guesses is detailed in [27]. By examining the time delay of the sample signal with respect to the reference signal, the initial guess for the real part of the refractive index can be found. The expression to finding an initial guess for the real part of the refractive index of the sample is

$$n_{initial} - 1.00027 = \frac{c\Delta t}{l}, \tag{2-11}$$

where Δt is the time delay of the sample signal with respect to the reference signal and $n_{initial}$ is the initial guess for the real part of the refractive index. Using the initial guess of the real part of the refractive index, the initial guess for the imaginary part of the refractive index is taken to be the highest value chosen such that the absolute maximum of the inverse Fourier transform of the calculated ratio in (2-9) is less than or equal to the absolute maximum of the inverse Fourier transform of the measured ratio in (2-8). After the initial guesses have been made, a frequency is selected. The Nelder and Mead modified simplex method is applied at that frequency in order to find the optimal values of the real and imaginary parts of the index of refraction which minimize (2-10) at that frequency. The optimization procedure is then repeated for all the other frequencies. This process is carried out at all the thicknesses present in the discrete thicknesses array. As mentioned in [27], the optimal thickness can be chosen by calculating a total variation

measure of degree two for each set of material properties found. The total variation method of degree two is a smoothness measure which is based upon the fact that for solids', material properties do not change drastically between two consecutive frequency samples. Instead, the material properties vary smoothly across the whole frequency range. More details on the total variation of degree two can be found in [27]. After the measure is calculated for each thickness, the thickness that corresponds to the deepest local minimum (in a thickness versus total variation degree two plot) is selected as the optimal thickness. Consequently, the material properties corresponding to that optimal thickness are the optimal properties.

2.1.4 Method Validation and Results

In this section, the material characterization method described above is utilized in order to obtain the dielectric properties of different materials. The materials characterized include organics, inorganics and polymer-ceramic composites. The information is presented in the form of the relative dielectric constant, ε_r, and the loss tangent, $\tan\delta$. These parameters are calculated from the real part of the index of refraction, n, and the extinction coefficient, k, found using the characterization method. The relative dielectric constant is related to the index of refraction and extinction coefficient by $\varepsilon_r = n^2 - k^2$. The loss tangent is related to the index of refraction and extinction coefficient by $\tan\delta = 2nk/\left(n^2 - k^2\right)$. The substrates and films examined had physical thicknesses ranging from 50 µm to 3.5 mm. Note that a ringing effect might be observed in the extracted parameters. This ringing effect is due to the nonzero truncated ends of the measured time-domain signals (see Figure 2-2).

The inorganic substrates characterized in this research are doped indium phosphide (InP), doped silicon (Si), alumina (Al_2O_3), Pyrex Borosilicate glass and Quartz glass. The glass materials relative dielectric constants and loss tangents are shown in Figure 2-3. The ceramic and

semiconducting materials' relative dielectric constants and loss tangents are shown in Figure 2-4. The availability of high dielectric constant materials with low loss tangents is crucial and very useful for the field of THz packaging and integration. The ability of THz radiation to inspect such materials shows great promise in the field of NDE of THz electronic packages. Aside from Pyrex, the characterized materials here are clearly low loss ($\tan\delta < 0.02$) over the measured frequency range. Also Al_2O_3, Si and InP have high relative dielectric constants ($9.3 \le \varepsilon_r \le 12.4$). Semiconductors, such as Si and InP are needed in the fabrication of THz active components. Undoped Si and InP have been characterized in the past showing almost no dielectric loss [27]. In this study, doped Si and InP substrates are characterized instead of the undoped materials. In general such doped semiconductors are used in fabrication of actual devices and were thus chosen to be characterized here.

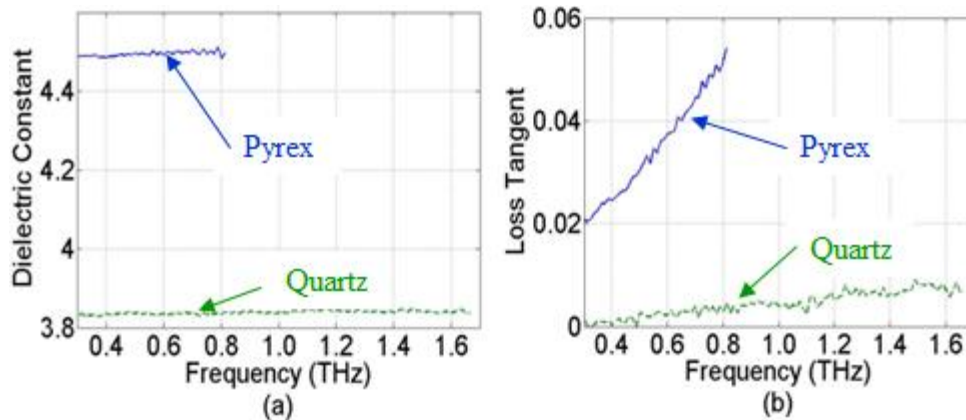

Figure 2-3. (a) Dielectric constant of glasses, (b) Loss-tangent of glasses

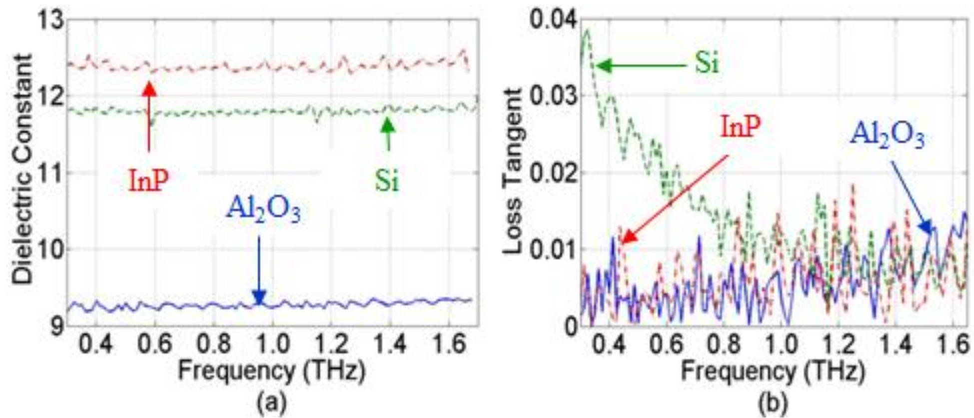

Figure 2-4. (a) Dielectric constant of ceramic and semiconductors, (b) Loss-tangent of ceramic and semiconductors

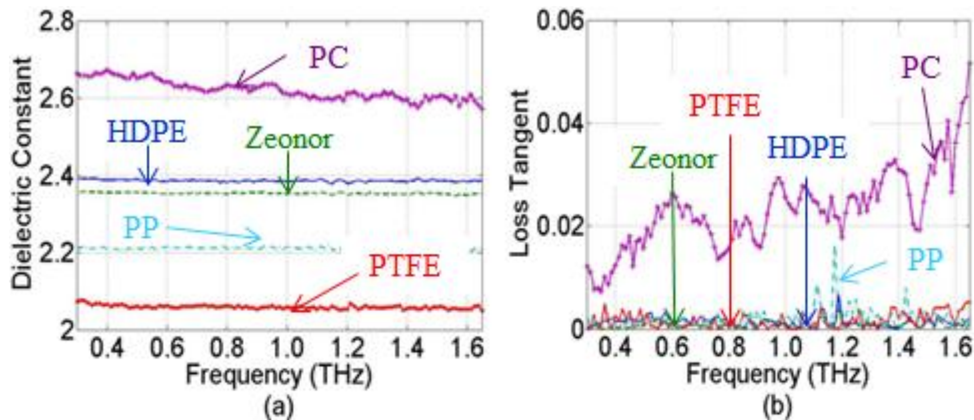

Figure 2-5. (a) Dielectric constant of organic materials, (b) Loss-tangent of organic materials

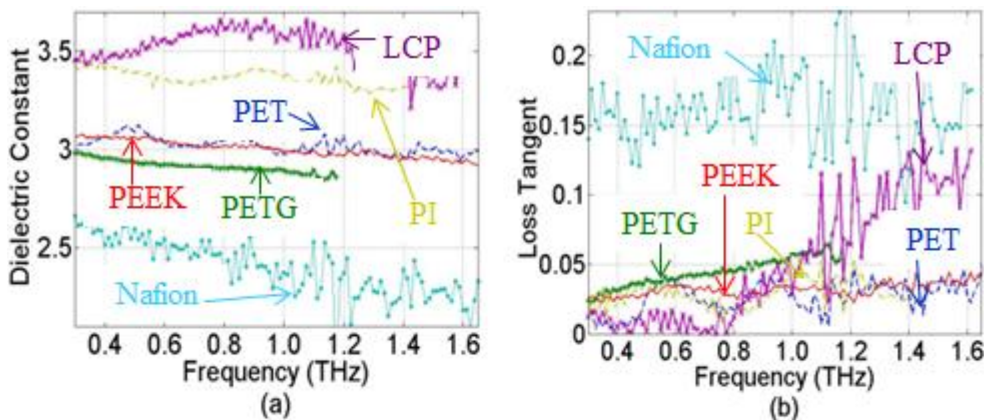

Figure 2-6. (a) Dielectric constant of organic materials, (b) Loss-tangent of organic materials

THz packaging utilizes materials with low dielectric constants and loss tangents. Again, the ability to characterize such materials shows great promise in the area of THz NDE of electronic packages. For this reason, a host of organic materials were characterized under this study. These

are: high density polyethylene (HDPE), polyethylene terephthalate (PET), polyethylene terephthalate glycol (PETG), polycarbonate (PC), polypropylene (PP), polytetrafluoroethylene (PTFE), polynorbornene (Zeonor 1020R) from Zeon Chemicals, polyether ether ketone (PEEK), polyimide (PI), liquid crystal polymer (ULTRALAM LCP) and Nafion. The relative dielectric constants and loss tangents of HDPE, Zeonor, PC, PTFE and PP are presented in Figure 2-5; while the relative dielectric constants and loss tangents of PET, PETG, PEEK, Nafion, PI and LCP are shown in Figure 2-6. With $\tan\delta < 0.02$ assumed to be the criterion to classify between low loss and high loss organic materials; it can be immediately concluded from the results that materials like HDPE, Zeonor, PTFE and PP are low-loss materials while others like Nafion and PETG are higher-loss substrate materials. A third category of materials includes materials such as PET (low loss below 500 GHz), show lower dielectric loss in certain frequency bands.

The polymer-ceramic composite substrates characterized here were obtained from Rogers Corporation. The substrates obtained are PTFE-ceramic composites, intended for use in microwave and RF applications. The dielectric constant is modified by changing the volume loading of the base polymer material with high dielectric constant ceramic particles [42]. Although they had been characterized (and documented by Roger's) at lower frequencies (< 10 GHz), no information exists on their properties in the higher frequency range, and to our knowledge these are characterized in the THz spectral region for the first time. The boards characterized are RO-3003, RO-3006, and RO-3010. Figure 2-7 shows the relative dielectric constant and loss tangent values of the polymer-ceramic composite materials. The dielectric constant of these materials remains high in the THz spectral region. However, the loss-tangent is also high for substrates containing a higher concentration of ceramic. This may be largely due to scattering of THz waves by the ceramic particles and potentially voids in the substrate. In the

future, the use of nanocomposites would be a useful approach to tailoring high dielectric constant materials for THz applications [42]. With respect to THz NDE, the results obtained for the composite materials infer that THz radiation can be used to inspect different loading within a composite material, grain size within a material by increased or decreased scattering in addition to material characterization.

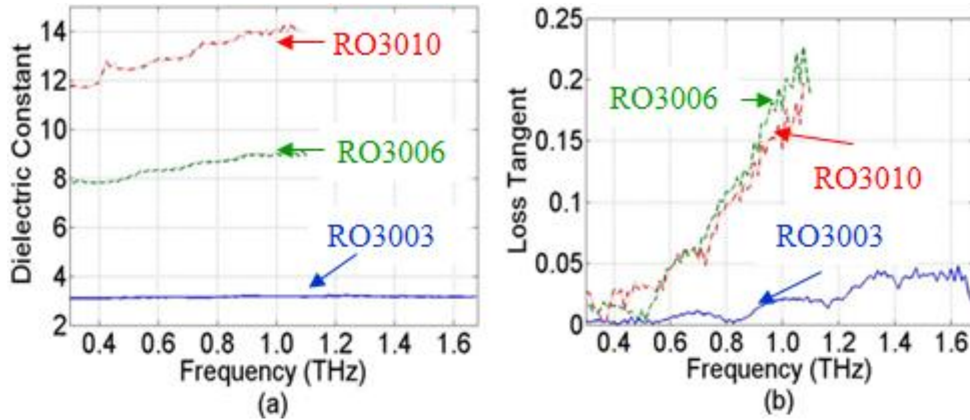

Figure 2-7. (a) Dielectric constant of polymer-ceramic composites, (b) Loss-tangent of polymer-ceramic composites

The repeatability of the measurements and the characterization results has been validated in three different ways. In the first approach, the characterization of some of the samples of Figures 2-5 and 2-6 was carried out at different times and the results were similar within less than 1% difference. In the second approach, the characterization of two samples with different thickness but made from the same material showed material characteristics with less than 3% difference.

Finally, as a third approach, some of the extracted parameters here were compared with material parameters present in the literature. Table 2-1 shows extracted dielectric properties at a single frequency of selected substrates placed in comparison with properties of the same materials available from the literature. It is apparent that the properties extracted using the reference requiring method are very similar to material properties readily available in the literature. Minor differences may be attributed to things like THz radiation source instabilities,

thickness measurement uncertainty, different extraction processes (for example [43] uses a less accurate analytic approach), different environment conditions (temperature and humidity) at the time of measurements (for example, PI dielectric properties are affected by the moisture and temperature levels in the room at the time of measurement), different surface roughness of samples measured and differences in manufacturability.

Table 2-1. Dielectric Properties Comparison

	Reference Requiring Method		Literature		
Material	ε_r	$\tan\delta$	ε_r	$\tan\delta$	Reference
InP (1THz)	12.33	0.009	12.39	0.006	[27]
Quartz (1THz)	3.84	0.004	3.84	0.0037	[25]
Al_2O_3 (1THz)	9.3	0.003	9.28	0.004	[21]
PC (1THz)	2.61	0.027	2.67	0.028	[25]
Zeonor (1THz)	2.35	0.001	2.28	0.001	[24]
HDPE (1THz)	2.38	0.002	2.37	0.002	[25]
PTFE (1THz)	2.06	0.0004	2.08	0.008	[43]
PP (1THz)	2.21	0.002	2.28	0.008	[43]
PI_d^* - PI_m^* (1THz)	3.25-3.37	0.021-0.037	3.22	0.05	[44]
PET (1THz)	2.98	0.031	2.93	0.063	[43]
Pyrex (0.8THz)	4.48	0.052	4.45	0.05	[25]

*PI_d is a dried polyimide sample, lacking moisture content.

*PI_m is a polyimide sample taken from an uncontrolled environment characterized by having some moisture in it. The properties pertaining to this sample are presented in the material characterization results.

The close comparison presented through this table infers the accuracy of the characterization carried out and the capability of reproducing results published in the past by other researchers.

2.1.5 Moisture Content Examination Example

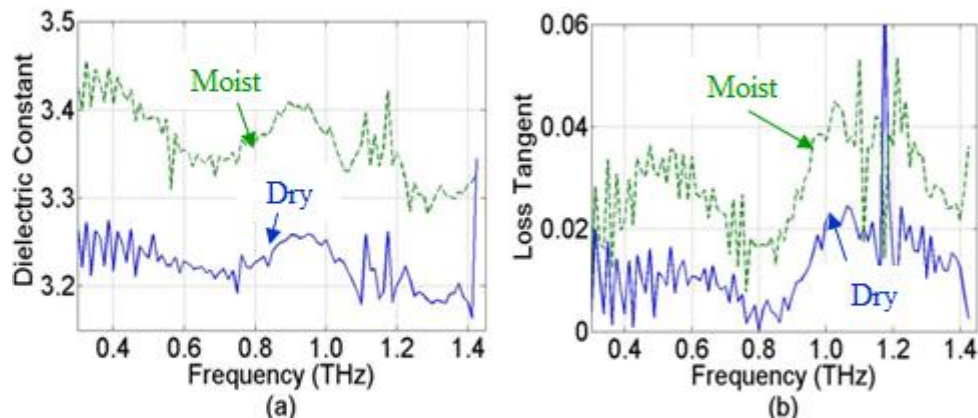

Figure 2-8. (a) Relative dielectric constants of the moist and dry Polyimide samples, (b) Loss tangents of the moist and dry Polyimide samples

Presence of moisture can jeopardize the integrity of structures (for example it may lead to early failure of electronic parts). THz radiation can be used to detect small amounts of moisture ingression in dielectric films. An experiment has been carried out in order to show how moisture content can be detected in a polyimide film, a widely used electronic packaging substrate. The experimental setup involved using two pieces of a polyimide substrate having similar physical and material properties. One of the substrates was put in an oven heated at constant temperature of 80° C for 16 hours in a dry environment to remove any moisture from the film prior to the measurements. The second substrate was used as received (expected to have moisture content within). Four signals were then collected, one through each sample and a corresponding reference measurement for each. Each pair of signals was then used in order to extract the dielectric permittivity and loss tangent for each sample as discussed earlier. It has been shown in the literature at lower frequencies (up to 100 GHz), that humidity leads to an increase in loss

tangent and the dielectric permittivity of Polyimide [45]. A similar effect is attained at THz frequencies and this is shown in Figure 2-8. This simple experiment shows that THz radiation can be used in characterizing moisture ingression in dielectric films and in detection of early packaging failure due to moisture.

2.1.6 Error Analysis and Discussion

Uncertainty in the measurements might result in errors in the extracted material parameters. The uncertainties might have slight or significant effect on the extracted parameters. Of specific interest are the measured inputs required to run the material characterization method. Particularly of concern is the thickness input of the sample to be characterized. The samples thicknesses used for the characterization method described above where acquired using a digital caliper having a thickness measurement accuracy of ±0.02mm. In this section, an error analysis is carried out in order to examine the effect of the thickness measurement uncertainty on the extracted parameters.

For a given a dielectric sample it is assumed that its true thickness lies within ±0.02mm of the measured thickness. A population of 1000 possible true sample thicknesses is generated at random from a normal distribution having the measured thickness as a mean and 0.01mm as the standard deviation. For every sample thickness the forward problem was solved resulting in a synthesized sample signal calculated from a measured reference signal. The same measured reference signal was used for every forward problem solution. For every synthesized sample signal the inverse problem was solved using the measured thickness. Afterwards, the mean and standard deviation of the extracted properties was found at every single frequency. The resulting mean along with two times the standard deviation error bars were then plotted on the same graph.

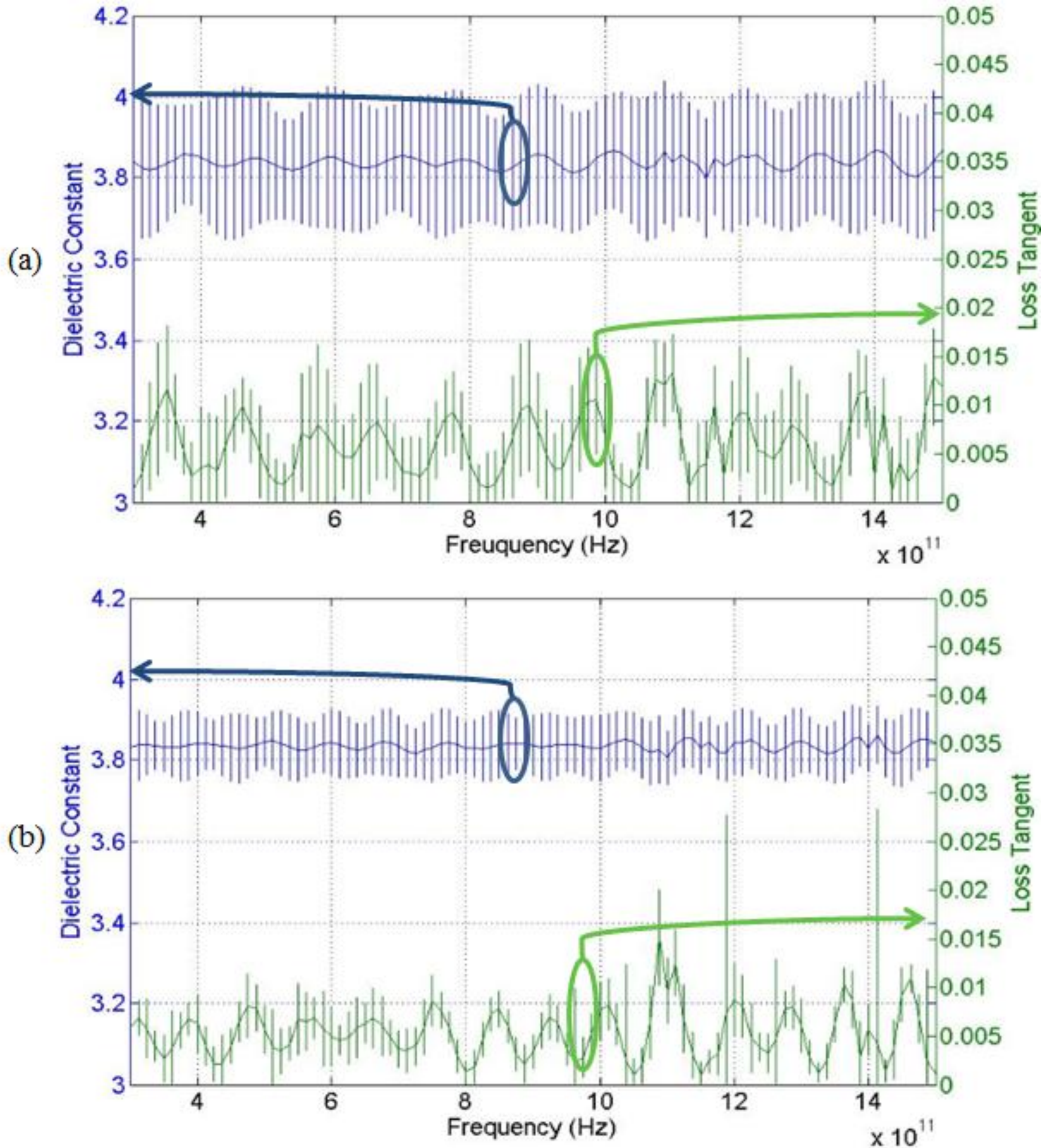

Figure 2-9. (a) Extracted material properties of "B" for measured thickness=0.5mm, (b) Extracted material properties of "B" for measured thickness=1mm

Three modeled materials were used in order to carry out the thickness error analysis study for the reference requiring material characterization method. The materials' properties across the whole frequency range were "A": $\varepsilon_r 1$=2.372 and $\tan\delta 1$=0.005 (approximating the material properties of a low loss polymer), "B": $\varepsilon_r 2$=3.822 and $\tan\delta 2$=0.005 (approximating the

material properties of a low loss glass) and “C”: $\varepsilon_r 3=11.7$ and $\tan\delta 3=0.005$ (approximating the properties of a low loss semiconductor). Two different tests were carried out. First, the sensitivity of the material characterization method was examined for the same material (“B”) at two different measured thicknesses. The two different measured thicknesses of “B” were chosen to be 0.5mm and 1mm. Second, the sensitivity of the method was tested for the three different materials (“A”, “B” and “C”) having the same optical thicknesses. Note that the optical thickness of a material is its physical thickness multiplied by its refractive index. The measured thicknesses of “A”, “B” and “C” were chosen to be 1.3mm, 1mm and 0.6mm, respectively. Note that the results of the 1mm material “B” were not recalculated as this was done in the first test.

Figure 2-9 shows the mean and standard deviation of the extracted properties at each frequency for the two measured thicknesses of “B”. Upon comparing Figure 2-9 (a) and (b), it can be seen that the means of the extracted material properties of “B” for both thicknesses are almost the same. However, it can also be seen that the error bars for the 0.5mm thick sample are larger. This means that for the same material properties, the reference requiring method extraction procedure is more sensitive to the thickness measurement uncertainty as the thickness decreases.

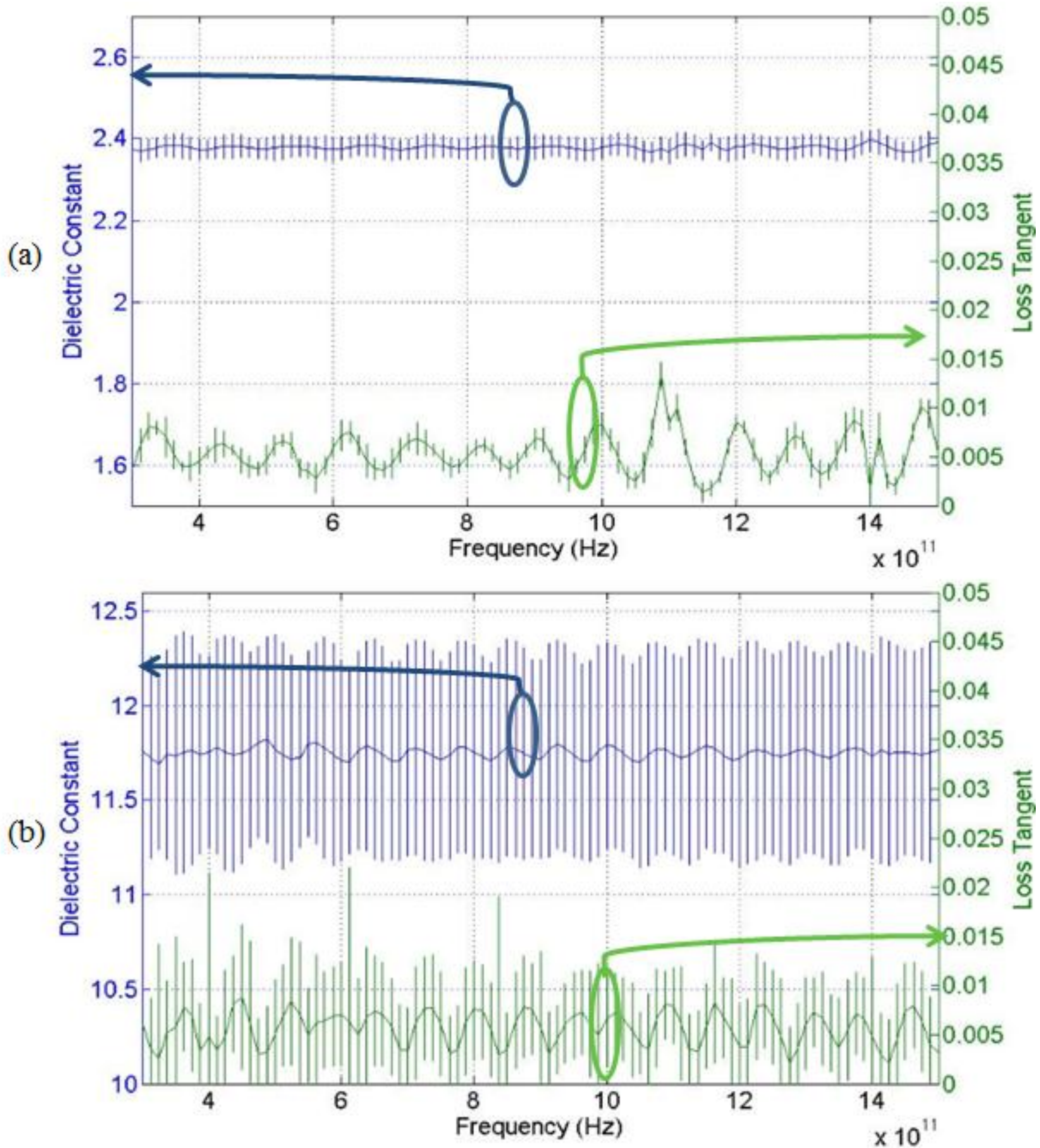

Figure 2-10. (a) Extracted material properties of “A” for measured thickness=1.3mm, (b) Extracted material properties of “C” for measured thickness=0.6mm

Figure 2-10 shows the mean and standard deviation of the material properties extracted for “A” and “C” each at its measured thickness. Although the material samples “A” and “C” from Figure 2-10 (a) and (b) and “B” from Figure 2-9 (b) all had the same optical thickness, the error bars grew significantly larger for the material having a higher dielectric constant. From this

observation, it can be concluded that the reference requiring method is not equally sensitive to the thickness measurement uncertainty for materials having the same optical thickness. Using the results obtained from both of the error analysis tests, a third conclusion can be made. Given two materials having the same thickness, the reference requiring method is more sensitive to the thickness accuracy measurement for the material that has a higher dielectric constant. This can be deduced when comparing the results shown in Figures 2-9 (a) and 2-10 (b). Although the lower dielectric constant material "B" in Figure 2-9 (a) had a lesser physical thickness than the higher dielectric constant material "C" in Figure 2-10 (b) the error bars on the extracted properties for "C" were significantly larger.

2.2 Self Calibrating Method

Note: This work is part of [46]. The Matlab material characterization code associated with this method is presented in Appendix D.

2.2.1 Problem Definition and Motivation

In a typical material characterization scheme, information pertaining to some unknown material is acquired and then analyzed in order to extract the dielectric properties of the material. Several techniques have been developed for THz time-domain material characterization. These techniques involve different assumptions and hence work on different groups of materials. In classical THz time-domain techniques, the information acquired before analysis is usually a signal representing a transient plane wave transmitted through the sample under test, and a signal for the transient plane wave transmitted through a reference sample of known material properties [25, 27-30]. While under ideal experimental conditions these methods produce dependable extracted parameters, they still have shortcomings. With the classical techniques, differences between the sample and reference measurements are mainly due to the wave propagation through the sample. However, minor differences between the two measured signals arise due to THz system instabilities causing different drifts in power and delays in time. These differences give rise to small errors in the extracted material parameters if the measured signals are collected in very close time proximity from each other. An increasing error in the extracted parameters is realized with more time proximity between the collection of the measurements. Additonally, in a real-time simultaneous imaging and spectroscopy scan of an inhomogeneous sample, obtaining a reference measurement for each pixel might prove time consuming and logistically difficult when the sample is large. More desirable would be one reference measurement for the whole

scan. Unfortunately, this is precluded due the instabilities inherent in existing THz time-domain systems.

This study provides an alternative method for characterizing materials using THz time-domain signals. The method requires only a sample signal while there is no need for a reference signal. Instead of using the relations between a reference and sample signal, this method employs the relations between the multiple transmissions of the pulsed signal through the sample under test in order to extract its material properties. The technique demonstrated in this section improves on previous traditional single layer characterization methods in decreasing the time required for measurements and in overcoming THz system drifts and instabilities issues in the extracted parameters.

2.2.2 Characterization Method Theory

Consider a transient plane wave with an inverted Gaussian monocycle time-domain waveform, incident through air from a stationary collimating source. Assume that the wave impinges normally upon a planar dielectric slab of finite thickness and unknown dielectric properties. The waveform representing the wave transmitted through the slab is collected at a stationary receiver located on the same straight line as the transmitter and dielectric slab, a distance d from the transmitter. Figure 2-11 shows a descriptive sketch of the setup.

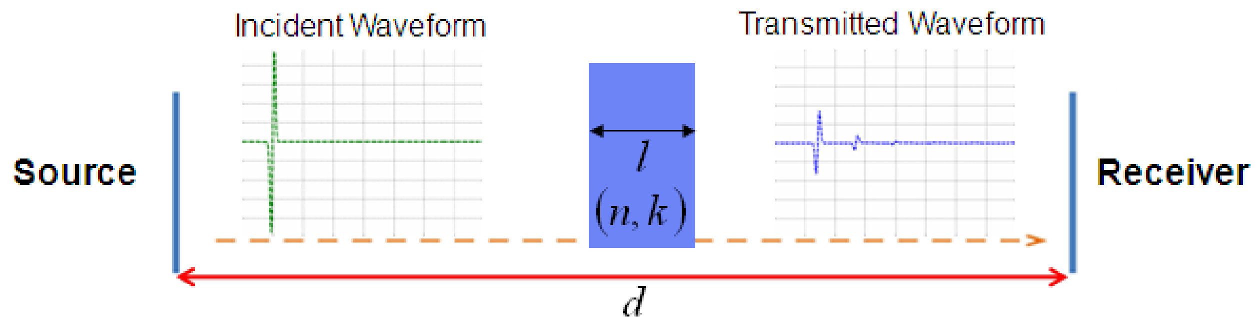

Figure 2-11. Sketch of idealized measurement setup

The acquired waveform is the convolution of the waveform of the incident plane wave, delayed in time due to traveling a certain distance in air, with the global time-domain transmission coefficient of the sample, $T(t)$. The global time-domain transmission coefficient is a function of the thickness of the slab, l, its refractive index, n, and its extinction coefficient, k. The expression for the time-domain waveform acquired at the receiver is

$$E_s(t) = E_i(t-p) * T(t), \tag{2-12}$$

where t is time, $p = (d-l)/c$ is the travel time through air (where c is the speed of light in air), and $E_i(t)$ is the waveform of the incident field.

The received signal consists of multiple events representing multiple transmissions of the wave through the sample. This is due to the mismatches in the media properties at the interface between the dielectric slab and air. Figure 2-12 shows a signal transmitted through a typical dielectric slab. The first, second and third transmissions are clearly seen. Although there are an infinite number of multiple transmissions, only the first few have non-negligible amplitudes.

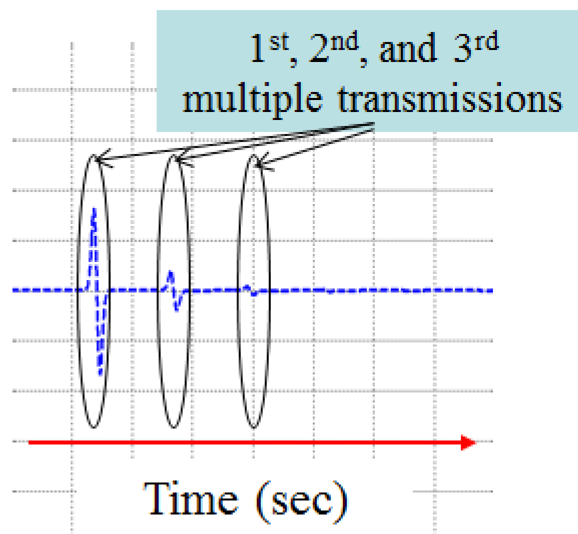

Figure 2-12. Received time-domain signal for a typical sample showing multiple transmissions under ideal conditions

In order to proceed with the theoretical description, the Fourier transform of the received signal is computed as

$$E_s(\omega) = E_i(\omega)\exp\left[-j\omega\tilde{n}_a(d-l)/c\right]T(\omega), \tag{2-13}$$

where the complex index of refraction of air is $\tilde{n}_a = 1.00027 - j0$ [27] and $T(\omega)$ is the global frequency domain transmission coefficient. The expression for $T(\omega)$ can be easily found [38] and is described by

$$T(\omega) = \frac{T_{as}(\omega)T_{sa}(\omega)\exp\left(-j\omega\tilde{n}_s l/c\right)}{1+\Gamma_{as}(\omega)\Gamma_{sa}(\omega)\exp\left(-2j\omega\tilde{n}_s l/c\right)}, \tag{2-14}$$

where $\tilde{n}_s = n - jk$ is the complex refractive index of the dielectric slab, $T_{as}(\omega)$ and $\Gamma_{as}(\omega)$ are the interfacial transmission and reflection coefficients, respectively, when the transient plane wave is traveling from air to the dielectric sample, and $T_{sa}(\omega)$ and $\Gamma_{sa}(\omega)$ are the interfacial transmission and reflection coefficients, respectively, when the transient plane wave is traveling from the dielectric sample to air.

The expression describing $\Gamma_{as}(\omega)$ is

$$\Gamma_{as}(\omega) = \frac{\tilde{n}_s - \tilde{n}_a}{\tilde{n}_a + \tilde{n}_s}. \tag{2-15}$$

The rest of the interfacial coefficients, $\Gamma_{sa}(\omega)$, $T_{as}(\omega)$, and $T_{sa}(\omega)$, can be described in terms of $\Gamma_{as}(\omega)$ by

$$\Gamma_{sa}(\omega) = -\Gamma_{as}(\omega), \tag{2-16}$$

$$T_{as}(\omega) = 1 - \Gamma_{as}(\omega), \tag{2-17}$$

and

$$T_{sa}(\omega) = 1 + \Gamma_{as}(\omega). \tag{2-18}$$

The various multiple transmissions are easily identified when the global transmission coefficient is expanded in a binomial series. The binomial series for $T(\omega)$ is

$$\begin{aligned}
T(\omega) &= T_{as}(\omega)T_{sa}(\omega)\exp\left(-j\omega\tilde{n}_s\, l/c\right) \\
&- T_{as}(\omega)T_{sa}(\omega)\exp\left(-j\omega\tilde{n}_s\, l/c\right)\left[\Gamma_{as}(\omega)\Gamma_{sa}(\omega)\exp\left(-2j\omega\tilde{n}_s\, l/c\right)\right] \\
&- T_{as}(\omega)T_{sa}(\omega)\exp\left(-j\omega\tilde{n}_s\, l/c\right)\left[\Gamma_{as}(\omega)\Gamma_{sa}(\omega)\exp\left(-2j\omega\tilde{n}_s\, l/c\right)\right]^2 \\
&- \ldots
\end{aligned} \qquad (2\text{-}19)$$

By taking the inverse Fourier transform of (2-19), an infinite series describing $T(t)$ can be obtained. The summation of the first three terms is

$$\begin{aligned}
T(t) &= \left[T_{as}(t) * T_{sa}(t) * f_s(t)\right]U(t-\tau_s) \\
&- \left[T_{as}(t) * T_{sa}(t) * \Gamma_{as}(t) * \Gamma_{sa}(t) * f_s(t)^{*3}\right]U(t-3\tau_s) \\
&- \left[T_{as}(t) * T_{sa}(t) * \Gamma_{as}(t) * \Gamma_{sa}(t) * \Gamma_{as}(t) * \Gamma_{sa}(t) * f_s(t)^{*5}\right]U(t-5\tau_s) \\
&- \ldots
\end{aligned}, \qquad (2\text{-}20)$$

where $f_s(t) = F^{-1}\left\{\exp\left(-j\omega\tilde{n}_s\, l/c\right)\right\}$ is the time-domain dispersion function due to one-way propagation in the dielectric slab, $f_s(t)^{*n}$ is short-hand notation for n convolutions of $f_s(t)$, τ_s is the one-way transit time across the slab, and the unit step functions account for the causality of the various multiple transmissions. In the case of a dispersionless material, $f_s(t)$ is merely the impulse function, $\delta(t-\tau_s)$, which accounts for the propagation delay through the slab. Inserting (2-20) in (2-12) gives

$$
\begin{aligned}
&E_s(t)=\left[E_i(t-p)*T_{as}(t)*T_{sa}(t)*f_s(t)\right]U(t-\tau_s)\\
&-\left[E_i(t-p)*T_{as}(t)*T_{sa}(t)*\Gamma_{as}(t)*\Gamma_{sa}(t)*f_s(t)^{*3}\right]U(t-3\tau_s)\\
&-\left[E_i(t-p)*T_{as}(t)*T_{sa}(t)*\Gamma_{as}(t)*\Gamma_{sa}(t)*\Gamma_{as}(t)*\Gamma_{sa}(t)*f_s(t)^{*5}\right]U(t-5\tau_s)\\
&-\ldots
\end{aligned}
\quad . \quad (2\text{-}21)
$$

The three multiple transmissions shown in Figure 2-12 are described by the three terms of the summation shown in (2-21). It is seen that each successive transmission undergoes an additional time delay of $2\tau_s$ associated with a two way dispersion of $f_s(t)^{*2}=f_s(t)*f_s(t)$. Now, assume $W(t)$ to be a time-domain window of unity amplitude between $t=p$ and $t=2\tau_s+p$, and zero elsewhere. Multiplying $E_s(t)$ by $W(t)$ results in the isolation of the beginning section of $E_s(t)$. This section is that portion of the first multiple transmission

$$E_a(t)=\left[E_i(t-p)*T_{as}(t)*T_{sa}(t)*f_s(t)\right]U(t-\tau_s)W(t) \quad (2\text{-}22)$$

that lies in $p\le t\le p+2\tau_s$. If dispersion is low and the dielectric slab is sufficiently optically thick such that the second multiple transmission is sufficiently delayed in time, then $E_a(t)$ is a good approximation of the first multiple transmission $E_1(t)$:

$$E_a(t)\approx E_1(t)=\left[E_i(t-p)*T_{as}(t)*T_{sa}(t)*f_s(t)\right]U(t-\tau_s). \quad (2\text{-}23)$$

The Fourier transform of the first multiple transmission can be expressed as

$$E_1(\omega)=E_i(\omega)\exp\left[-j\omega\tilde{n}_a(d-l)/c\right]T_{as}(\omega)T_{sa}(\omega)\exp\left(-j\omega\tilde{n}_s\, l/c\right). \quad (2\text{-}24)$$

Dividing (2-24) by the spectrum of the measured signal (2-13), results in a ratio. After simplification the ratio can be expressed as

$$\frac{E_1(\omega)}{E_s(\omega)}=1-\Gamma_{as}^2\exp\left(-2j\omega\tilde{n}_s\, l/c\right). \quad (2\text{-}25)$$

Note that this normalization completely eliminates the spectrum of the incident waveform, $E_i(\omega)$, leaving a simple expression that is a function of the unknown material constants n and k. Thus, the material constants can be found by minimizing the difference between the measured signal ratio and the model (2-25) without knowledge of the incident waveform. The optimization procedure is explained in the next subsection.

2.2.3 Optimization Procedure and Setup

Let $M(\omega)$ be the ratio of $E_1(\omega)$ to $E_s(\omega)$ obtained from the measured waveform and $\hat{M}(\omega)$ be the theoretical ratio given by (2-25). After approximating $\tilde{n}_a$ to 1, the expression for $\hat{M}(\omega)$ in terms of the material properties of the dielectric slab may be written as

$$\hat{M}(\omega)=1-\Gamma_{as}^2\exp(-2j\omega\tilde{n}_s\, l/c)=1-\left(\frac{n-jk-1}{1+n-jk}\right)^2\exp[-2j\omega(n-jk)l/c]. \quad (2\text{-}26)$$

Minimizing the difference between $\hat{M}(\omega)$ and $M(\omega)$ will yield the dielectric properties of the slab, n and k. Since the ratios are frequency dependent complex quantities, the objective function was chosen to minimize the sum of the differences between the magnitudes (in absolute scales) and the phases (in radians) of the measured and calculated ratios at each frequency. The expression for the objective function is

$$f(\omega)=C_1\left|\,|M(\omega)|-|\hat{M}(\omega)|\,\right|+C_2\left|\angle M(\omega)-\angle\hat{M}(\omega)\right|. \quad (2\text{-}27)$$

Where C_1 and C_2 are weighting constants. Upon implementation, this objective function gave acceptable results for the simple case $C_1=C_2=1$.

The optimization method chosen to minimize (2-27) is the Nelder and Mead Simplex method [39-41]. The dimension of the simplex polyhedron was chosen as $N=2$ since two variables are

included in the optimization. The iterative procedure used is detailed in [40] and Appendix A. The optimization is carried out to minimize (2-27) at each individual frequency sample. The optimization for the material properties at a certain frequency is terminated if the value of the objective function at one of the vertices of the simplex becomes appropriately small [39] (less than 10^{-10}) or the function values at the vertices become appropriately close to each other [39] (standard deviation less than 10^{-10}). The obtained variables at the vertex with the lowest function value are then considered to be the solution at that frequency. In this work, the reflection, expansion, contraction and shrinking factors are 1, 2, 0.5, and 0.5 respectively. These values were chosen based on previous applications of the Nelder Mead simplex method [39-41].

The base point for the initial simplex at every frequency is determined by certain initial guesses of n and k. Given $E_s(t)$, the initial guess for n at all frequencies is determined using

$$n_{initial} = \frac{c\Delta t}{2l}, \tag{2-28}$$

where Δt is the time difference between the two peaks of the first two consecutive multiple transmissions. Using $n_{initial}$ and assuming an initial extinction coefficient value of $k_{initial} = 0$ at all frequencies, an initial guess for $\hat{M}(\omega)$ can be found using (2-26). Afterwards, very small increments of 10^{-5} are added to $k_{initial}$ while comparing $A = \sum_{i=1}^{q} \left|\hat{M}(\omega_i)\right|$ and $B = \sum_{i=1}^{q} \left|M(\omega_i)\right|$, where $\{\omega_i\}$ are the frequency samples and q is the total number of frequency samples in the frequency range over which the dielectric properties are extracted. The choice of frequency range is discussed in the validation results section. The value of $k_{initial}$ that results in the minimum difference between A and B is the initial guess for k used to specify the base point. It is worth noting that all base points for the initial guesses at all frequencies are identical. Hence, the initial

simplex polyhedron is the same at all frequencies. The two other vertices of the simplex are found as described in [39] with the scale factor, α, chosen to be 0.01.

2.2.4 Signal Artifacts Removal Technique

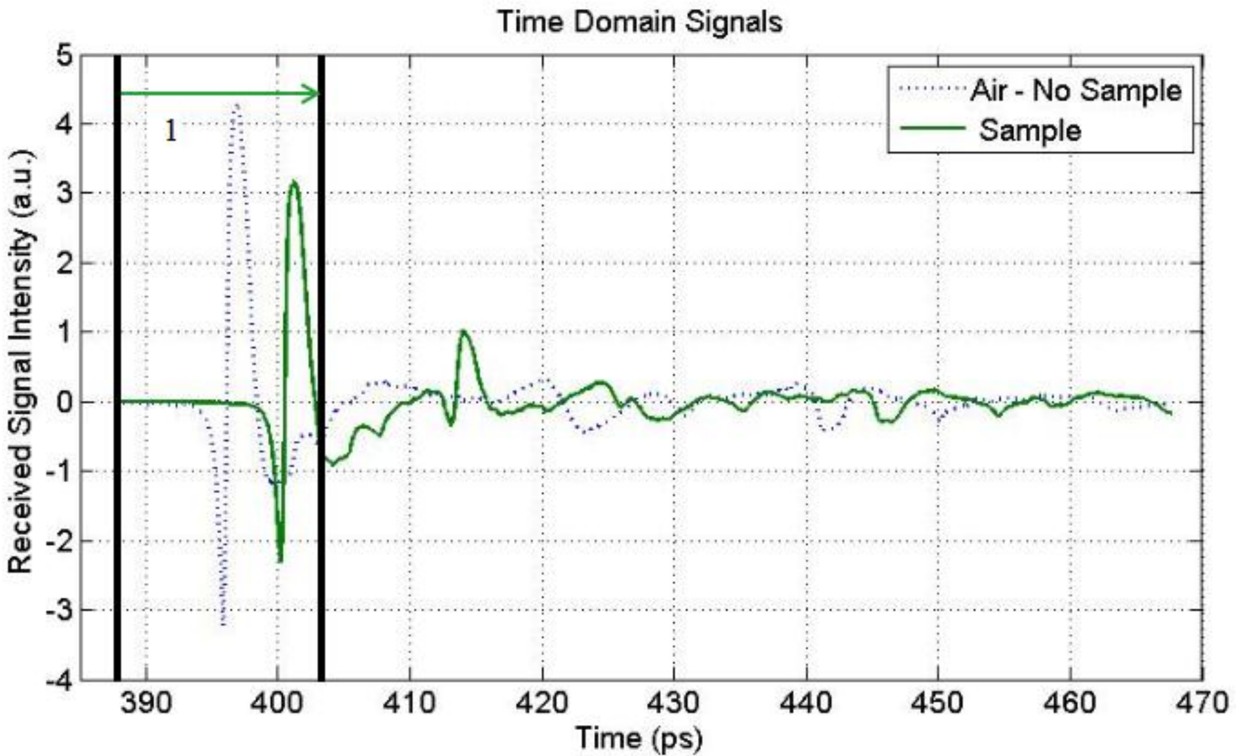

Figure 2-13. Example time-domain signals obtained from the measurement

In any realistic scenario, the waveform of the transient plane wave transmitted through the test substrate is not only a function of the substrate properties, but is also dependent on the properties of the apparatus. Temporal artifacts in the radiated waveform result from things like wire bonds of the antenna packages and fabrication imperfections. Additionally, extraneous effects are introduced by the measurement system and affect the shape of the acquired waveform. Unless these extraneous effects are removed, significant errors in n and k can be expected upon extraction. It is worth noting that while these artifacts are systematic and unchanging, the measured waveforms differ from one signal to the next due to fluctuations in power level or drifts in the time base. It is thus necessary to use an archived reference waveform

measured with the sample absent to remove the extraneous effects from the signal obtained with any sample present.

Begin with the waveform for the plane wave transmitted through the sample under test. Figure 2-13 shows typical measured waveforms. The dotted waveform is $E_{im}(t)$, a measured sample signal of the wave transmitted through air, and the solid line waveform is $E_{sm}(t)$, a sample signal transmitted through an Alumina sample. $E_{im}(t)$ is an archived signal that is not required to be collected every time a sample is to be characterized. As can be clearly observed, the signals are different from the idealized time-domain signals shown in Figures 2-11 and 2-12. The extra fluctuations are due to the measurement apparatus and the signal generating system. The signals were each measured at 2048 time points covering an 80ps time window. Extraneous system effects are present at every multiple transmission in the measured sample signal. Hence, the second multiple transmission overlays with the extraneous system effects of the first multiple transmission, and the third multiple transmission overlays with the extraneous system effects of the first and second multiple transmissions, etc. It is clear then that since the first multiple transmission is the first time event of the transmitted signal, it doesn't overlay with any previously generated extraneous system effects. This is clearly observable in Figure 2-13 where $E_{sm}(t)$ lacks any signal fluctuations prior to the first multiple transmission.

Based on these observations, a technique that aims to remove the extraneous system effects generated at each multiple transmission is conceived. It is assumed that the pattern of extraneous system effects at a multiple transmission is a signal that follows its monocycle-like pulse. Then the archived time-domain signal may be shifted a time τ_s such that it aligns with the sample signal to form the waveform, $E_{im}(t-\tau_s)$. Figure 2-14 shows $E_{im}(t-\tau_s)$ and $E_{sm}(t)$.

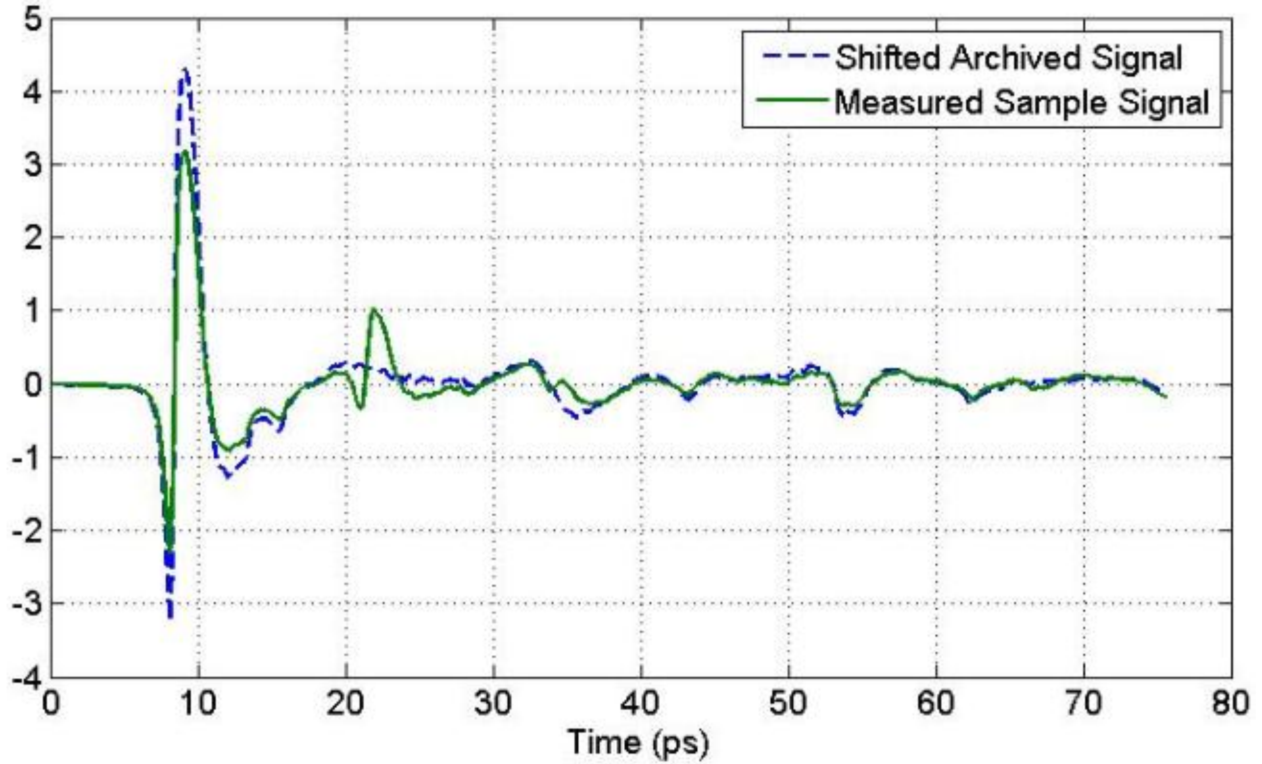

Figure 2-14. Sample signal along with the shifted archived time-domain signal

Next, $E_{im}(t-\tau_s)$ is scaled such that its peak intensity matches that of $E_{sm}(t)$. After that, the scaled signal is subtracted from $E_{sm}(t)$, resulting in the removal of the artifacts in the signal produced during the first multiple transmission. Figure 2-15 shows $E_{sm}(t)$ and the subtracted signal.

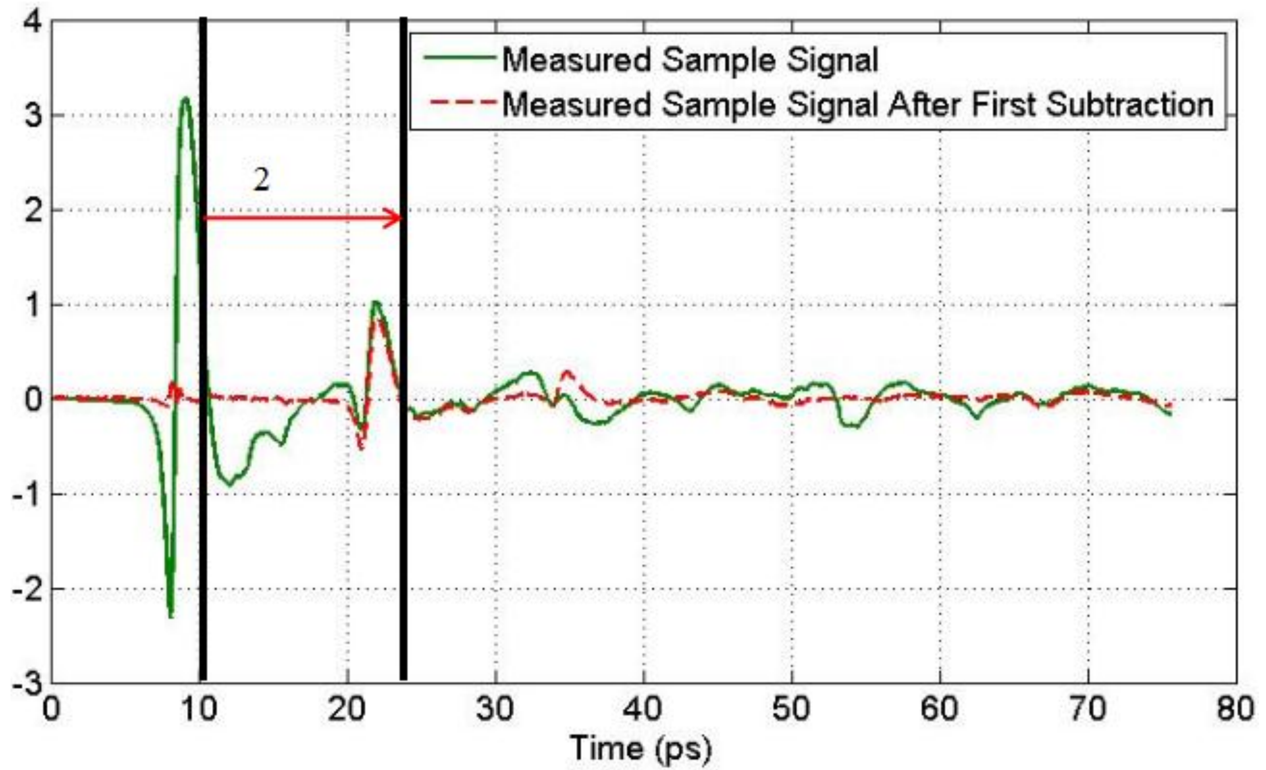

Figure 2-15. Sample Signal and First Subtraction Result

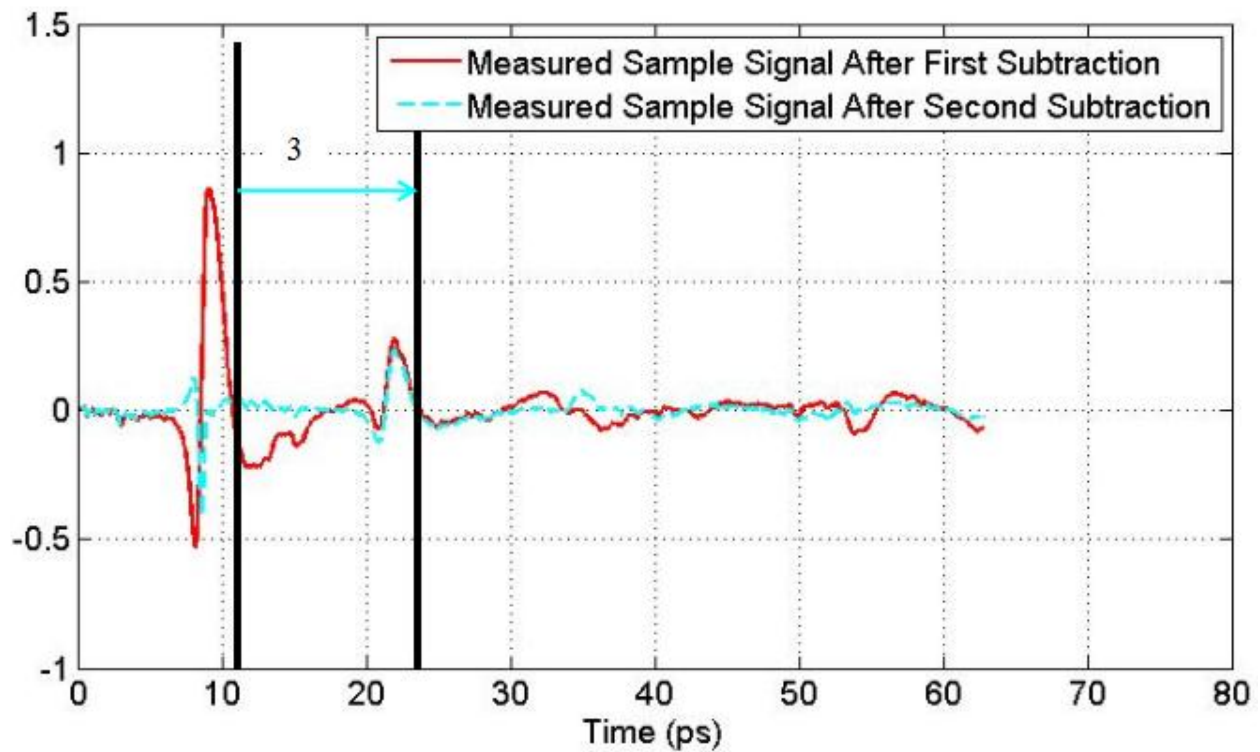

Figure 2-16. Second Subtraction Result

From Figure 2-15, it can be seen that the subtraction produces a cleaner version of the second multiple transmission, and that the third and fourth multiple transmissions become more visible. It can also be observed that the subtraction is nearly complete up to the time of the mono-cycle like pulse of the second multiple transmission, with only minor fluctuations due to time sampling and dispersion.

The final sample signal with the extraneous system effects removed is composed of a set of patched signal sections. The first signal section occupies the region between the two vertical line markers of the solid line waveform in Figure 2-13. This section contains the mono-cycle like pulse of the first multiple transmission. The signal section lying in between the two vertical line markers of the dashed waveform in Figure 2-15 is the next patch belonging to the sample signal with no system effects. This section contains the mono-cycle like pulse of the second multiple transmission.

The signal artifacts removal process proceeds by shifting and scaling $E_{im}(t)$ to align its peak in time and match in intensity with the peak of the first mono-cycle like pulse of the dashed waveform in Figure 2-14. The scaled and shifted signal is then subtracted from the dashed waveform of Figure 2-14. The resulting signal from the subtraction is shown as the dashed waveform in Figure 2-16, while the solid line waveform in Figure 2-16 represents the original waveform before subtraction. From the waveform resulting from the subtraction in Figure 2-16, it can be seen that the subtraction results in a clean version of the third multiple transmission and a cleaner representation of the fourth multiple transmission. It can also be observed that the subtraction is nearly complete up to the third multiple transmission, with fluctuations occurring due to time sampling and dispersion. The signal section lying in between the two vertical line markers of dashed waveform in Figure 2-16 is the next patch belonging to the sample signal with

no system effects. This section contains the mono-cycle like pulse of the third multiple transmission. The shifting, scaling and subtraction operation is repeated for all the multiple transmissions in the sample signal time window that are above noise level. The final sample signal used for the self-calibrating method, with the extraneous effects removed, is a series of patched signal segments from the successive subtractions. This signal is shown in Figure 2-17 along with the measured sample signal.

The transmitted signal multiples through a slab are not only scaled and time delayed versions of the signal transmitted through air, they are also stretched due to dispersive effects. Hence, the signal clean-up procedure presented works better when dispersion effects are minimal. This can be clearly concluded from the fact that the procedure presented does not take any signal stretching into consideration.

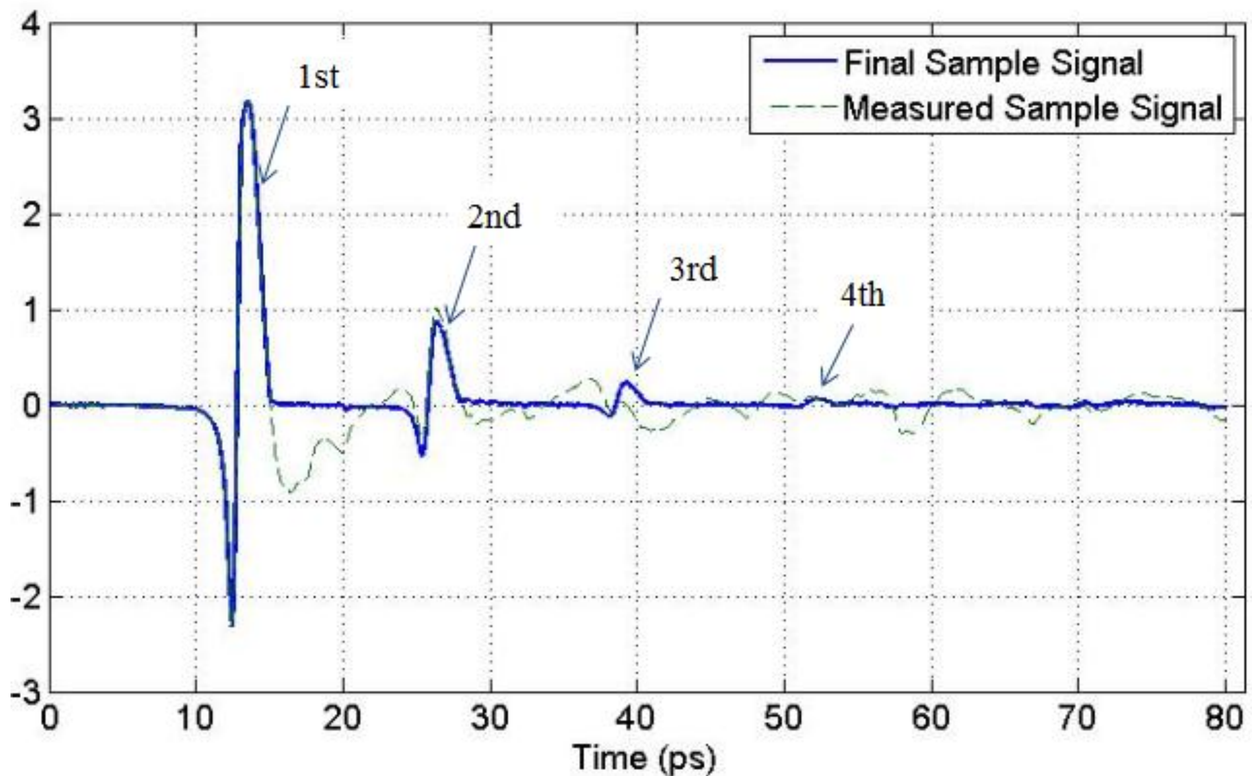

Figure 2-17. Measured and Final Sample Signals

2.2.5 Method Validation and Results

Using the T-ray 2000 THz time-domain system from Picometrix [www.picometrix.com], $E_{sm}(t)$ for the sample under test was acquired. The extraneous measurement system effects present in the acquired signal were removed using the system artifacts removal technique and the archived measured time-domain signal, $E_{im}(t)$, to obtain an approximation to $E_s(t)$. The initial guesses for $n_{initial}$ and $k_{initial}$ were determined as described earlier. The first multiple transmission time domain signal, $E_1(t)$, was then obtained by multiplying by $W(t)$. $W(t)$ is centered at the first multiple transmission of $E_{sm}(t)$ with a $2\tau_s$ width. τ_s is equal to half the time delay between the first and second multiple transmissions of $E_{sm}(t)$.After $E_1(t)$ and $E_s(t)$ were determined, their Fourier transforms were found and the measured ratio, $M(\omega)$, was computed. The Nelder Mead simplex optimization method was then set up and used to minimize the objective function in (2-27) in order to extract the material properties at every frequency sample of the Fourier transform.

Several different material samples were characterized. The dielectric properties of the substrates were extracted in a frequency range for 250 GHz to 1.6 THz. Above 1.6 THz noise effects become more dominant in the extraction, and results may become unreliable.

The samples that were used to validate the method are: Alumina (Al_2O_3), Quartz, High Density Polyethylene (HDPE), Indium Phosphide (InP), and Silicon (Si). These samples were picked because they span a variety of material types: ceramics, polymers, semiconductors and glasses. The thicknesses of the material samples tested are: Al_2O_3 – 0.637mm, Quartz – 1.631mm, HDPE – 1.58mm, InP – 0.63mm, and Si – 0.513mm. Note that an accurate measure of the sample thickness is required for the method to extract the sample's true dielectric properties.

An uncertainty in the thickness of the sample results in an uncertainty in the extracted properties. The accuracy of the sample thickness measure becomes more influential when the sample to be characterized becomes more and more optically thin. The dielectric properties are presented in the form of the dielectric constant, ε_r, and the loss tangent, $\tan\delta$, which were obtained from the extracted n and k using $\varepsilon_r = n^2 - k^2$ and $\tan\delta = \frac{2nk}{n^2 - k^2}$. The extracted material properties were smoothed with a moving average including 21 data points within its averaging window and centered at the data point to be smoothed. The standard deviation of the data within the averaging window was found each time the window was shifted. In order to show the spread of the extracted data before smoothing, standard deviation bars were included in the smoothed results. Each data point has a bar associated with it extending one standard deviation above and another below the data point. For validation completeness, the results presented here are compared to previously published results in the literature at selected frequencies.

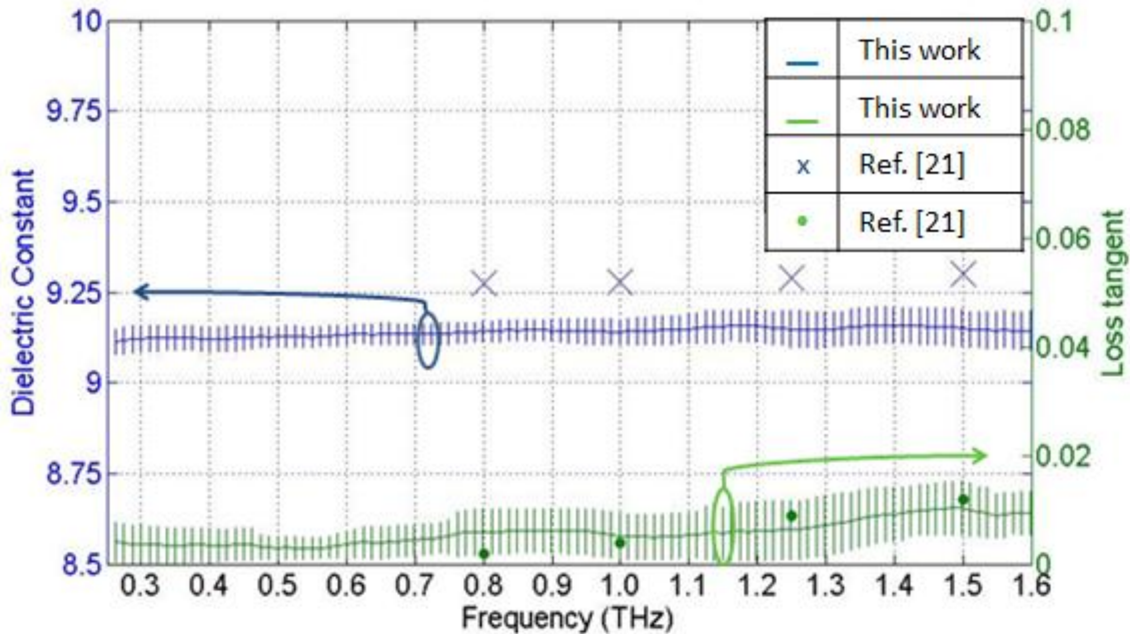

Figure 2-18. Extracted dielectric properties of Al_2O_3

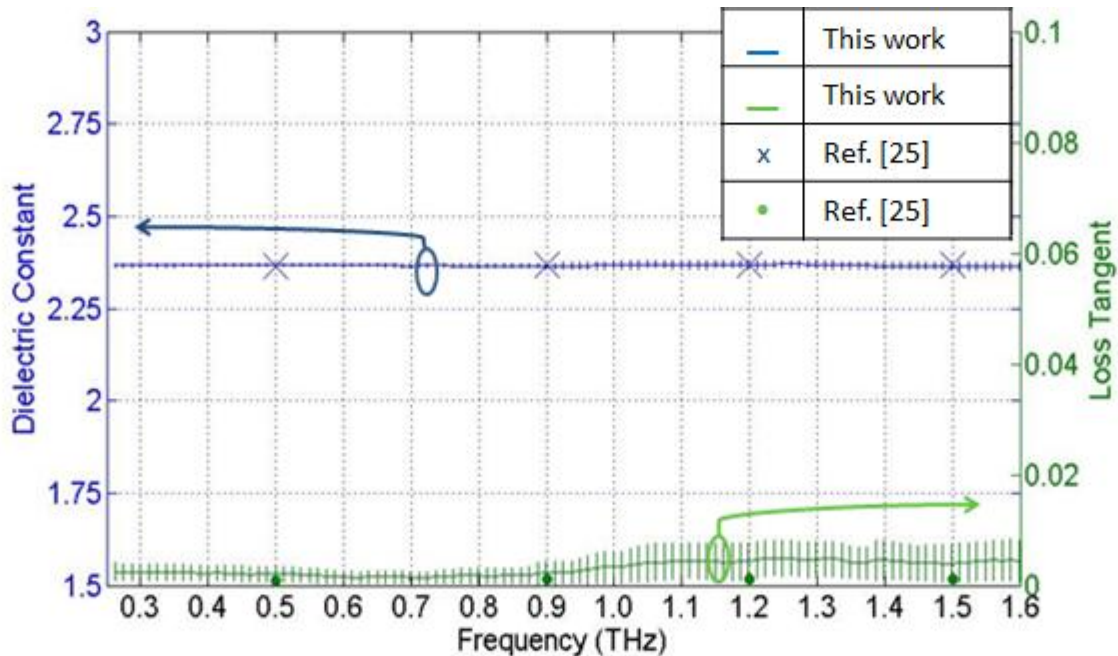

Figure 2-19. Extracted dielectric properties of HDPE

Figure 2-18 shows the dielectric properties obtained for Al_2O_3. These values follow the material parameters shown in [21]. The loss tangent from [21] lies within one standard deviation from the loss tangent obtained using the self-calibrating method. The dielectric constant in [21] differs from the dielectric constant obtained here by less than 1.7%. Possible reasons for this difference are manufacturability, sample thickness uncertainty and inherent system instability differences between the reference signal and sample signal in the reference requiring method of [21]. Figure 2-19 shows the dielectric properties obtained for HDPE. The extracted values follow those results shown in [25] quite well. Upon close comparison, it can be observed that both the dielectric constant and the loss tangent obtained from [25] lie within one standard deviation from the parameters extracted using the self-calibrating method.

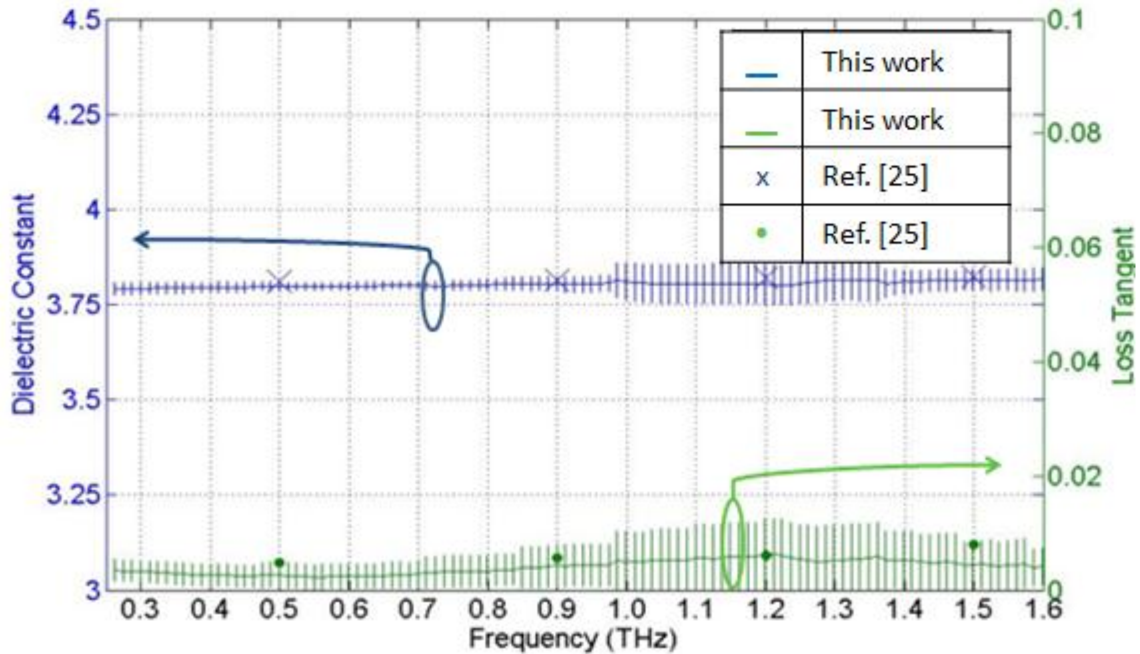

Figure 2-20. Extracted dielectric properties of Quartz

Figure 2-20 presents the characterization results obtained for Quartz. These results closely follow those shown in [25]. Both the dielectric constant and the loss tangent from [25] lie within one standard deviation from the parameters extracted using the self-calibrating method. Figure 2-21 shows the results obtained for the first semiconducting material, InP. The results show that the loss tangent of InP extracted using the self-calibrating method lies within one standard deviation from the loss tangent in [27] while the dielectric constants differ by around 1.2%. Reasons for this difference might again be attributed to thickness uncertainty and the inherent system instability difference between reference and sample signals in the reference requiring method of [27]. Additionally, while both InP samples (in [27] and in this study) are high doped semiconductor samples, the effective doping concentrations might be different resulting in small differences in the extracted parameters.

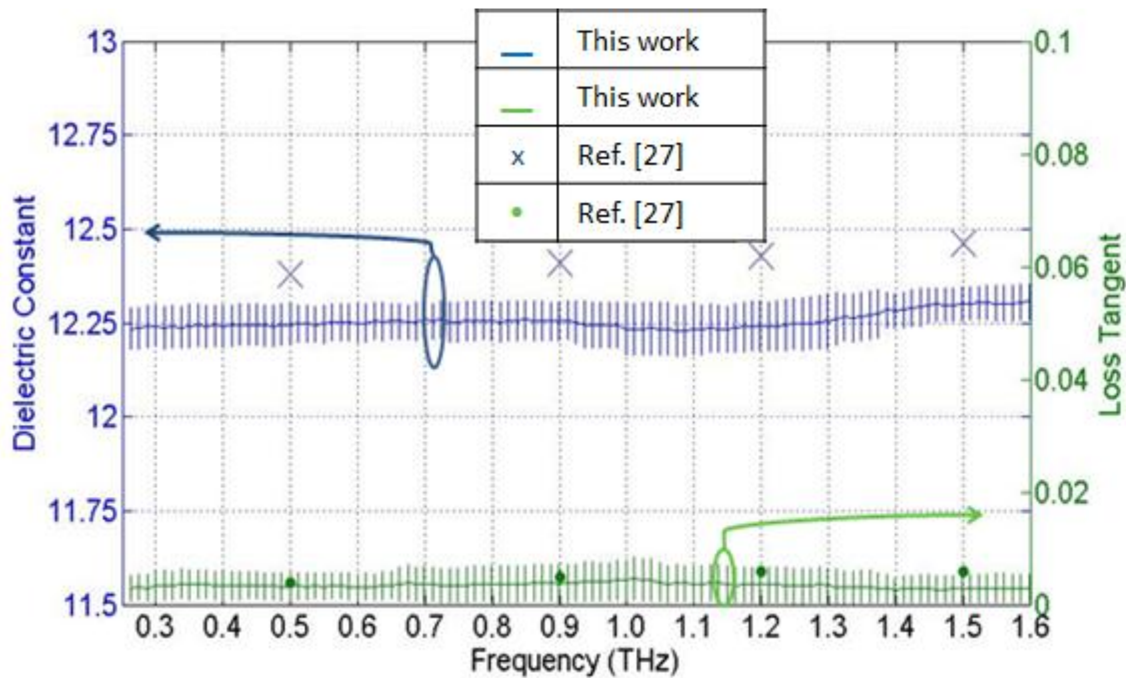

Figure 2-21. Extracted dielectric properties of InP

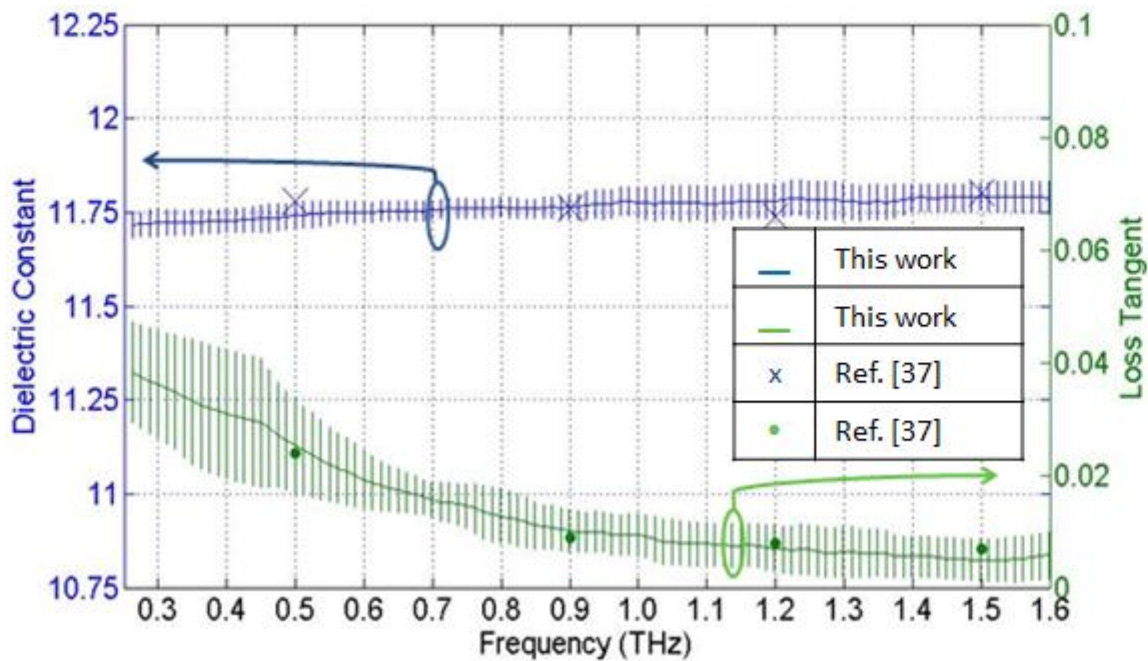

Figure 2-22. Extracted dielectric properties of doped Si

Figure 2-22 presents the extracted dielectric properties for doped Si. Doped Si has lower resistivity than undoped Si. Previous studies show that Si with different resistivities have different material properties [47-48]. It has been shown that the higher the resistivity (lower

doping concentration) the lower the dielectric constant and the lower the loss tangent [48]. The dielectric properties of Si obtained here lie within the range of possible values of Si shown in [48]. Additionally, the extracted properties of Si here match to values presented in [37] for the same wafer using a reference-requiring material parameter extraction method and lie well within one standard deviation from them. Note that in [21], [25], [27], and [37] a measured reference signal was required for characterization whereas the results shown in Figure 2-18 to 2-22 do not require this signal.

2.2.6 Method Limitations

The self-calibrating technique has several implementation constraints which still needs to be resolved. First, in order to to separate the first multiple transmission from the sample signal, the time delay between the first multiple and the second multiple must be sufficiently large than the pulse width (avoid overlap of pulses). This time delay is determined by the optical thickness of the material sample under test. Specifically, the optical thickness is determined by the physical thickness and the refractive index of the sample. Second, for the characterization to be feasible, the total signal power present in at least the second multiple transmission must be above the noise level of the measured signal. Third, the measured signal artifacts removal procedure does not account for all the dispersion effects in the material, and hence the method works best when dispersion is low. Fourth, the sample thickness measurement accuracy affects the extracted results of the dielectric constant. Hence, a highly accurate thickness measurement is required for best characterization. To characterize a sample, the effect of the thickness measurement error can be decreased by using a thicker sample as the uncertainty of the thickness measurement would be less relative to the total thickness of the sample. However, even with these constraints, the method is still applicable to a wide range of materials and useful under many scenarios.

2.2.7 Error Analysis and Discussion

As is mentioned in 2.2.6, one of the parameters which the self-calibrating method is highly prone to is the thickness measurement accuracy of the sample to be characterized. In this section, an error analysis is carried out in order to examine the effect of the thickness measurement uncertainty on the extracted parameters.

For a given a dielectric sample it is assumed that its true thickness lies within ±0.02mm of the measured thickness. A population of 1000 possible true sample thicknesses is generated at random from a normal distribution having the measured thickness as a mean and 0.01mm as the standard deviation. For every sample thickness the forward problem was solved resulting in a synthesized sample signal calculated from a measured reference signal. The same measured reference signal was used for every forward problem solution. For every synthesized sample signal the inverse problem was solved using the measured thickness. Afterwards, the mean and standard deviation of the extracted properties was found at every single frequency. The resulting mean along with two times the standard deviation error bars were then plotted on the same graph.

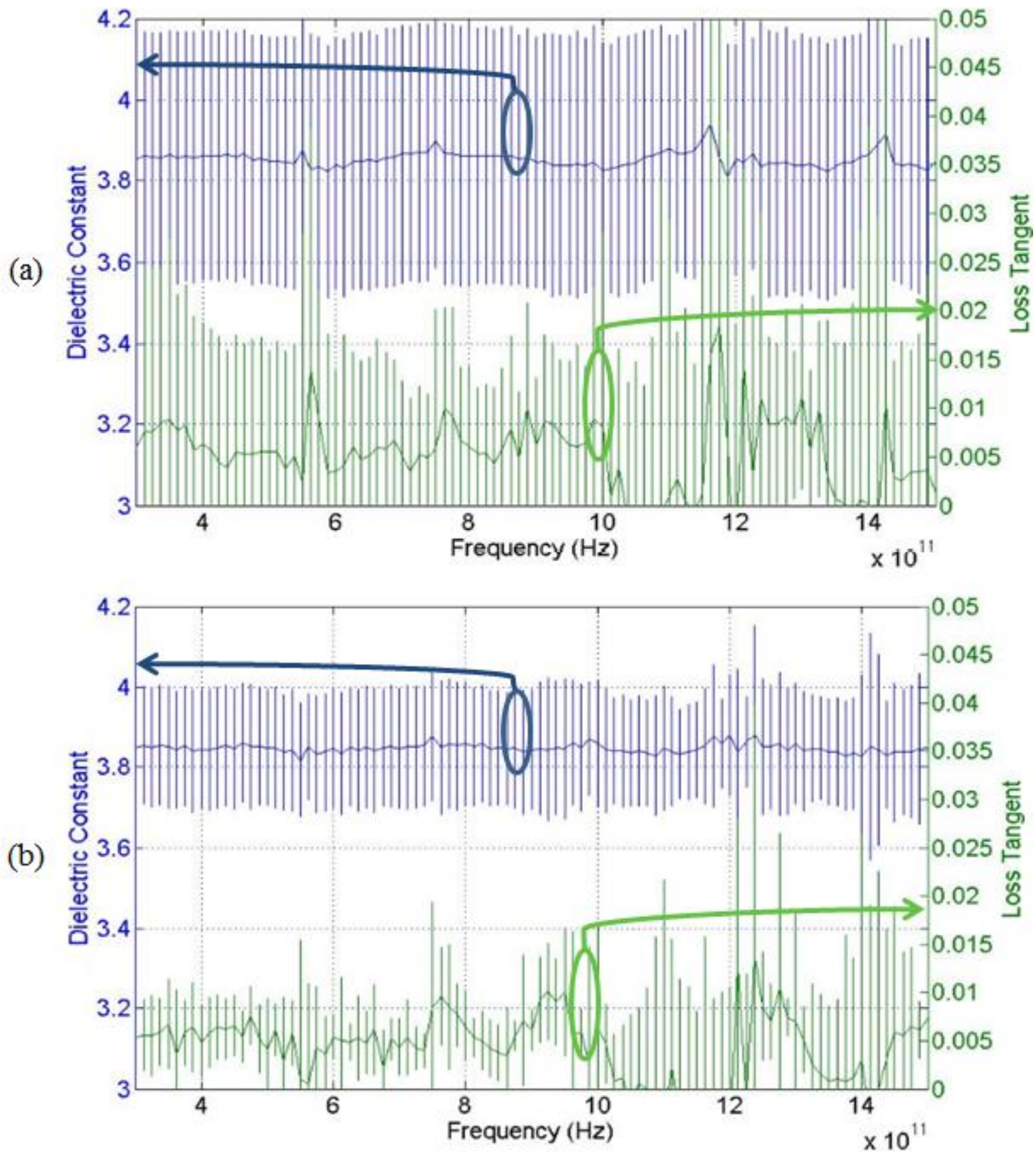

Figure 2-23. (a) Extracted material properties of "B" for measured thickness=0.5mm, (b) Extracted material properties of "B" for measured thickness=1mm

Three modeled materials were used in order to carry out the thickness error analysis study for the self-calibrating material characterization method. The materials' properties across the whole frequency range were "A": $\varepsilon_r 1$=2.372 and $\tan\delta 1$=0.005 (approximating the material properties

of a low loss polymer), "B": $\varepsilon_r 2$=3.822 and $\tan\delta 2$=0.005 (approximating the material properties of a low loss glass) and "C": $\varepsilon_r 3$=11.7 and $\tan\delta 3$=0.005 (approximating the properties of a low loss semiconductor). Two different tests were carried out. First, the sensitivity of the material characterization method was examined for the same material ("B") at two different measured thicknesses. The two different measured thicknesses of "B" were chosen to be 0.5mm and 1mm. Second, the sensitivity of the method was tested for the three different materials ("A", "B" and "C") having the same optical thicknesses. Note that the optical thickness of a material is its physical thickness multiplied by its refractive index. The measured thicknesses of "A", "B" and "C" were picked to be 1.3mm, 1mm and 0.6mm respectively. Note that the results of the 1mm material "B" were not recalculated as this was done in the first test.

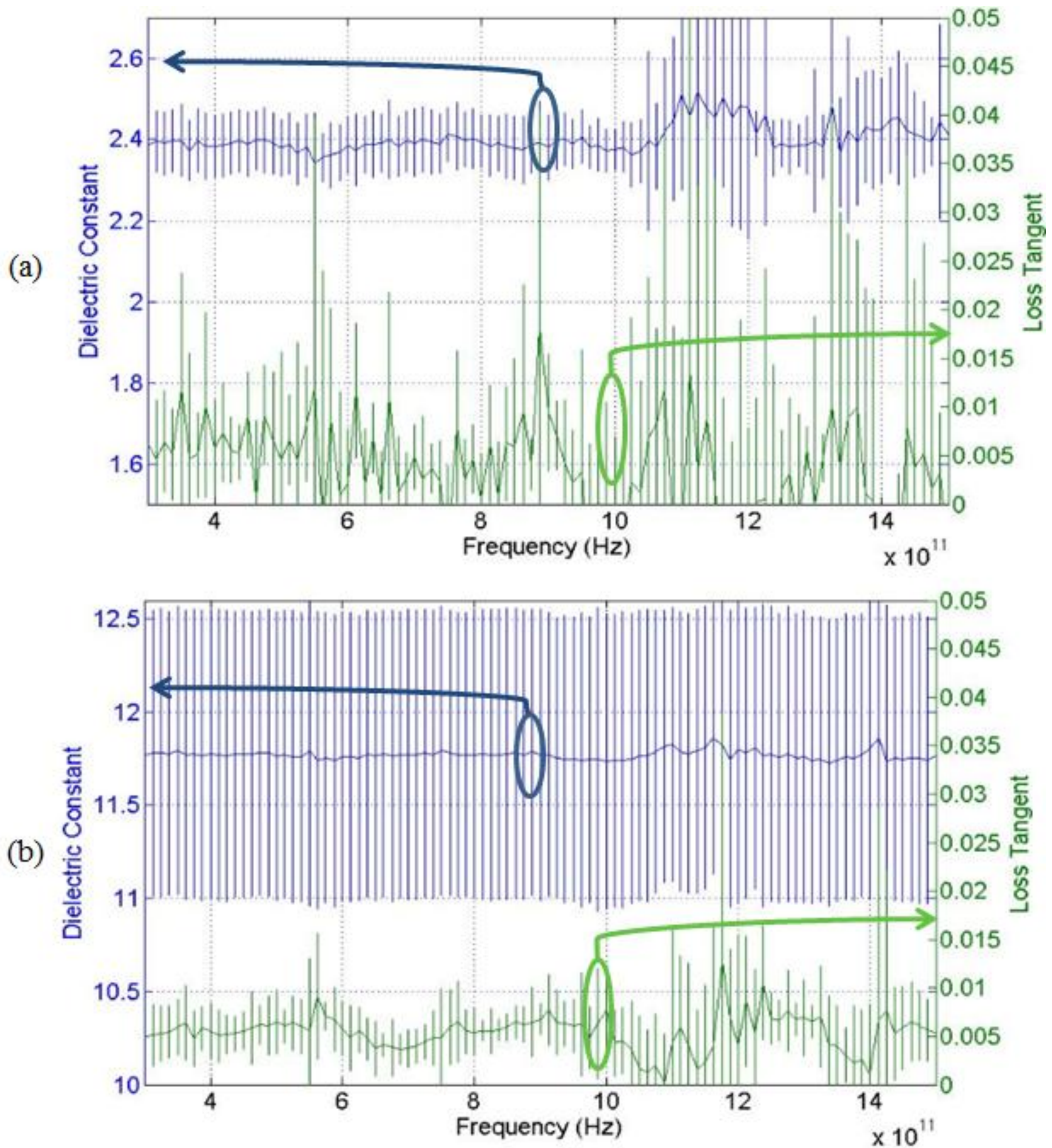

Figure 2-24. (a) Extracted material properties of "A" for measured thickness=1.3mm, (b) Extracted material properties of "C" for measured thickness=0.6mm

Figure 2-23 shows the mean and standard deviation of the extracted properties at each frequency for the two measured thicknesses of "B". Upon comparing Figure 2-23 (a) and (b), it can be seen that the means of the extracted material properties of "B" for both thicknesses are almost the same. However, it can also be seen that the error bars for the 0.5mm thick sample are

larger. This means that for the same material properties, the self-calibrating method is more sensitive to the thickness measurement uncertainty as the thickness decreases.

Figure 2-24 shows the mean and standard deviation of the material properties extracted for "A" and "C" at their measured thicknesses. Although the material samples "A" and "C" from Figure 2-24 (a) and (b) and "B" from Figure 2-23 (b) all have the same optical thickness, the error bars grew significantly larger for the material having a higher dielectric constant. From this observation, it can be concluded that the self-calibrating method is not equally sensitive to the thickness measurement uncertainty for materials having the same optical thickness. Using the results obtained from both of the error analysis tests, a third conclusion can also be made. Given two materials having the same thickness, the self-calibrating method is more sensitive to the thickness accuracy measure for the material that has a higher dielectric constant. This can be deduced when comparing the results shown in Figures 2-23 (a) and 2-24 (b). Although the lower dielectric constant material "B" in Figure 2-23 (a) had a lesser thickness than the higher dielectric constant material "C" in Figure 2-24 (b) the error bars on the extracted properties for "C" were significantly larger.

A few observations can be made upon comparing the error analysis results obtained for the reference requiring (see section 2.1.6) and the self-calibrating methods given that the same modeled materials were used for both studies. First, it is clear from the obtained results that the self-calibrating method is more sensitive to the thickness measurement uncertainty than the reference requiring method. Second, the ringing effect seen in the reference requiring method extracted properties mean and standard deviation is not seen in those of the self-calibrating method(see Figures 2-10 (b) and 2-24 (b)). This is due to the absence of nonzero truncations in the time domain sample signal used for extracting the material properties with the self-

calibrating technique. The nonzero truncations disappear from the measured sample signal after the signal artifacts removal procedure. Third, for the 0.5mm thick material "B" and the 1.3m thick material "A" the self-calibrating method shows significantly higher error bars on the loss tangent than the reference requiring method. This can be explained by two of the method limitations discussed above in section 2.2.6. The higher loss tangent for material "B" is most likely due to the need to have sufficient time delay between the multiple transmissions of the sample signal. On the other hand for "A", the self-calibrating method is more prone to signal power than the reference requiring method as it requires at least the second multiple transmission to be higher than noise level. The higher the number of multiple transmissions captured above noise level, the better the method results. For a low loss polymer material like "A", most of the signal passes through the sample in the first transmission and the second transmission is relatively low in amplitude. This might result in a higher loss tangent uncertainty for the self-calibrating method.

CHAPTER 3

METHODS FOR CHARACTERIZATION OF MULTIPLE LAYER MEDIA

3.1 The Multiple Angle Method

Note: This work is partially documented in [49]. The Matlab material characterization code associated with this method is presented in Appendix E.

3.1.1 Problem Definition and Motivation

The methods provided in chapter 2 cannot be used to carry out multiple layer material characterization or even efficient single layer material characterization with thickness extraction. Methods capable of achieving such feats will prove useful for many applications including manufacturing quality assurance, defect characterization, structural health monitoring, composite material delamination characterization and biotissue inspection.

This section demonstrates the multiple angle method capable of material characterization of multiple dielectric layers along with single layer characterization with thickness extraction. Given a dielectric stack with flat surfaces, an incident electromagnetic plane wave with a monocycle shaped Gaussian waveform is illuminated onto the structure at a certain angle. First, a reference signal (representing a delayed version of the incident plane wave) transmitted through air is measured. Second, signals transmitted through the stack at different angles of incidence are collected. Using these signals and the knowledge of the number of layers in the stack, the proposed method extracts the dielectric properties and thickness of each layer. The number of measurements required is dependent on the number of dielectric layers in the stack.

3.1.2 Characterization Method Theory

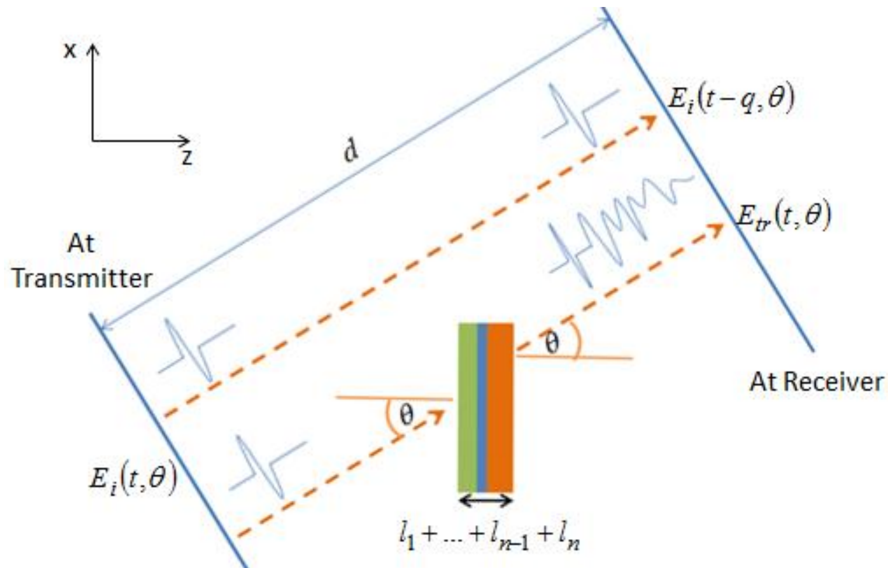

Figure 3-1. Sketch of the idealized measurement setup

As mentioned before, two sets of measurements are required for the multiple angle method: i) a reference measurement, and ii) a number of incident angle dependent sample measurements. The sketch diagram, Figure 3-1, shows an idealized measurement setup of the signals required for the multiple angle method. The incident plane wave is $E_i(t,\theta)$ where t is time and θ is the angle of incidence. The reference measurement, $E_i(t-q,\theta)$, is the incident wave delayed in time by q due to travelling the distance d (see Figure 3-1) between the transmitter and receiver. On the other hand, the wave transmitted through the stack (or sample measurement) can be described as

$$E_{tr}(t,\theta) = E_i(t-p,\theta) * T(t,\theta), \tag{3-1}$$

where $T(t,\theta)$ is the global time domain transmission coefficient due to travelling through the material system and p is a time delay due to travelling a certain distance in air before entering and after exiting the material system. The stack is composed of multiple dielectric layers each

having a thickness, l_i, and dielectric properties, $\tilde{n}_i = n_i - jk_i$ where i is a positive integer number representing a specific layer.

Proceeding with the theoretical description, the Fourier transforms of the measured signals are found. The Fourier transform of the reference measurement, $E_i(t-q,\theta)$, is described as $E_i(\omega,\theta)\exp[-j\omega\tilde{n}_a(d)/c]$ where $\tilde{n}_a = 1.00027 - j0$ [27] is the refractive index of air, ω is the angular frequency in radians and c is the speed of light in air. The Fourier transform of the incidence angle dependent sample measurement is described by

$$E_{tr}(\omega,\theta) = E_i(\omega,\theta)T(\omega,\theta)U(\omega,\theta), \tag{3-2}$$

where $T(\omega,\theta)$ is the Fourier transform of the global time-domain transmission coefficient and $U(\omega,\theta)$ is a phase shift factor resulting from the wave travelling a certain distance in air before entering and after exiting the material system. Respectively, the expressions for $U(\omega,\theta)$ and $T(\omega,\theta)$ are

$$U(\omega,\theta) = \exp\left[-j\omega\tilde{n}_a\, d/c + j\left(\sum_{i=1}^{n} l_i\right)k_{z,0}\right], \tag{3-3}$$

and

$$T(\omega,\theta) = \prod_{i=0}^{n} \exp\left[-jk_{z,i}l_i\right]S_{i,i+1} \text{ , [50]} \tag{3-4}$$

where $i = 0$ and $i = n+1$ are the air before and after the dielectric material system, $k_{z,i}$ is the wave vector component along the z direction and is described by

$$k_{z,i} = \frac{\omega}{c}\sqrt{(\tilde{n}_i)^2 - (\sin(\theta))^2}\ . \tag{3-5}$$

Additionally,

$$S_{i,i+1} = \frac{T_{i,i+1}}{1 - R_{i+1,i}\tilde{R}_{i+1,i+2}\exp\left[-2jk_{z,i+1}l_{i+1}\right]}, \quad (3\text{-}6)$$

where $T_{i,i+1}$ and $R_{i,i+1}$ are interfacial transmission and reflection coefficients respectively and are described in terms of the wave impedances in each layer, Z_i, as

$$T_{i,i+1} = \frac{2Z_{i+1}}{Z_i + Z_{i+1}}, \quad (3\text{-}7)$$

$$R_{i,i+1} = \frac{Z_{i+1} - Z_i}{Z_i + Z_{i+1}}, \quad (3\text{-}8)$$

and

$$\tilde{R}_{i,i+1} = \frac{R_{i,i+1} + \tilde{R}_{i+1,i+2}\exp\left[-2jk_{z,i+1}l_{i+1}\right]}{1 + R_{i,i+1}\tilde{R}_{i+1,i+2}\exp\left[-2jk_{z,i+1}l_{i+1}\right]}. \quad (3\text{-}9)$$

Given the experimental measurement setup, the parallel polarization case is considered and as a result the wave impedance in layer i is given by

$$Z_i = \frac{k_{z,i}\,\eta_i}{k_i}, \quad (3\text{-}10)$$

where $\eta_i = \dfrac{120\pi}{\tilde{n}_i}$ and $k_i = \dfrac{\omega}{c}\tilde{n}_i$ are the intrinsic impedance and wave number in layer i respectively. For a given angle of incidence a ratio, $Q(\omega,\theta)$, of $E_{tr}(\omega,\theta)$ to $E_i(\omega,\theta)\exp[-j\omega\tilde{n}_a(d)/c]$ can be obtained and simplified to

$$\begin{aligned} Q(\omega,\theta) &= \frac{E_{tr}(\omega,\theta)}{E_i(\omega,\theta)\exp[-j\omega\tilde{n}_a(d)/c]} \\ &= T(\omega,\theta)\exp\left[j\left(\sum_{i=1}^{n} l_i\right)k_{z,0}\right]. \end{aligned} \quad (3\text{-}11)$$

3.1.3 Inverse Problem Root Finding Setup

Each layer i in the dielectric stack is associated with three characteristics n_i, k_i and l_i. For a given angle of incidence, $Q(\omega,\theta)$ is a function of the three properties of each layer in the dielectric stack. A calculated set of ratios (obtained at different angles of incidence) can be matched to a measured set of ratios (at the same angles of incidence) by finding the three properties of each layer in the stack. This matching operation is the basis for the multiple angle material parameter extraction method. The objective function for such an operation is described as

$$F = \begin{pmatrix} Q(\omega,\theta_1) \\ Q(\omega,\theta_2) \\ Q(\omega,\theta_3) \\ \downarrow \end{pmatrix}_{meas.} - \begin{pmatrix} Q(\omega,\theta_1) \\ Q(\omega,\theta_2) \\ Q(\omega,\theta_3) \\ \downarrow \end{pmatrix}_{calc.} = 0\,. \tag{3-12}$$

The expression shown in (3-12) is a system of equations. Thus, the matching operation required to extract the properties of each layer is essentially solving a system of equations of a certain number of unknowns. Since, the ratios are complex quantities, two separate equations can be obtained for every measured ratio (magnitude and phase or real and imaginary). This results in decreasing the total number of measurements and as a result the complexity of the problem. Extracting the properties of each layer from the measured signals, requires a total number of ratios (or different angle of incidence measurements) specified by the total number of unknowns. For example, a stack of two layers of which the thicknesses are known has a total of 4 unknowns. Since two equations can be obtained from each ratio (from each angle of incidence), two different ratios are required (or two different angle of incidence sample measurements in addition to the reference measurement). On the other hand, if the thicknesses of the layers are unknown then the total number of unknowns is 6 and thus requiring three different ratios.

In order to solve the system of equations and obtain approximations to the roots (or dielectric layer characteristics to be found), the secant method [51] was used. A description of the secant method is available in Appendix B. Note that the secant method is highly sensitive to initial guesses. The root finding process takes place in two different phases. The first phase consists of running the extraction procedure at each discrete frequency point starting from a set of initial guesses picked at random from uniform distributions. The uniform distributions are possible wide ranges of values which the unknowns to be found lie within. Afterwards, the extracted parameters for the frequency points where the extraction algorithm converged or completed the maximum number of iterations are checked whether they lie within certain intervals set prior to running the extraction. If a certain extracted set of parameters satisfies the intervals, then the second phase begins. If not, then the first phase is run again. The second phase is a rerun of the extraction procedure taking the extracted set of parameters satisfying the intervals from the first phase as initial guesses. An additional provision added to the second phase is that if convergence is achieved at a certain frequency point, the parameters obtained at that frequency are used as the initial guesses for the next frequency. Upon completion of the second phase, the approximations to the extracted layer characteristics are obtained.

3.1.4 Forward Problem Solution and Validation

The forward problem solution was carried out in order to validate the theory and check if it models the experimental measurement procedure and setup well. Before proceeding any further it is worthy to present the measurement setup used for collecting the data utilized in the forward and inverse problem solutions. The top view of the experimental setup used for collecting the measured signals along with the labels and descriptors is shown in Figure 3-2.

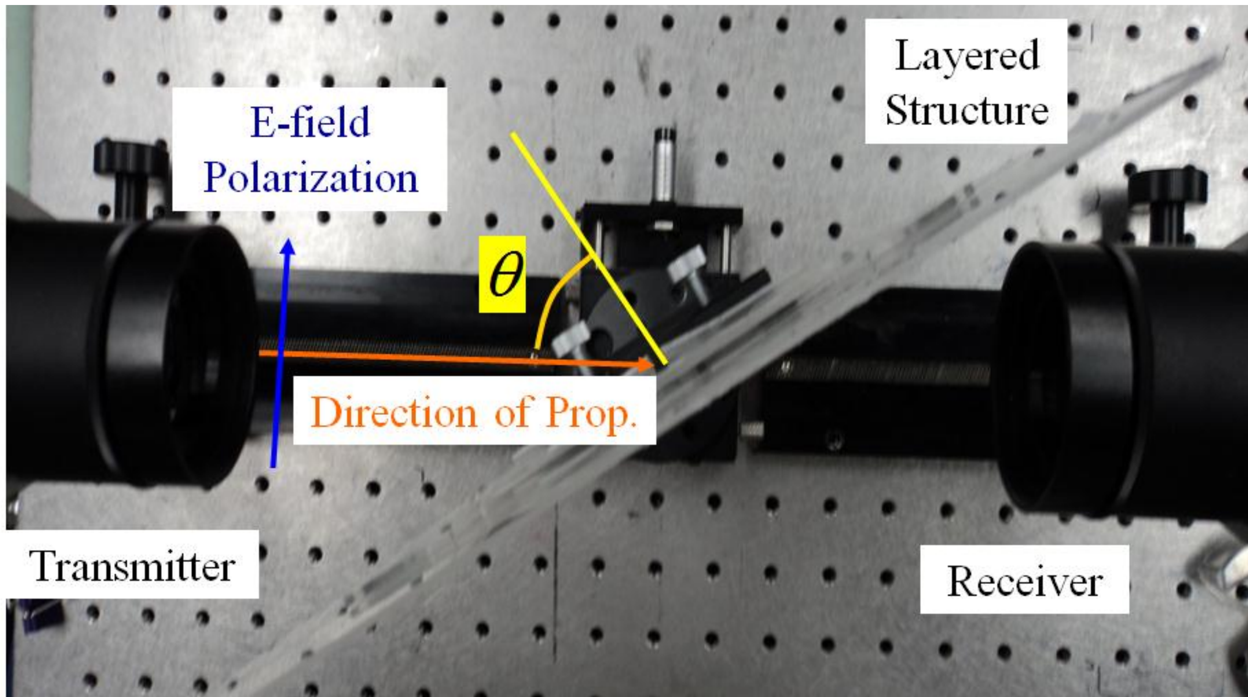

Figure 3-2. Experiment measurement setup (top view)

Figure 3-3 shows a typical reference signal measured through air. This signal simply represents the incident signal delayed in time due to its path length in air between the transmitter and the receiver. Embedded into the THz measured signal is the inherent system response.

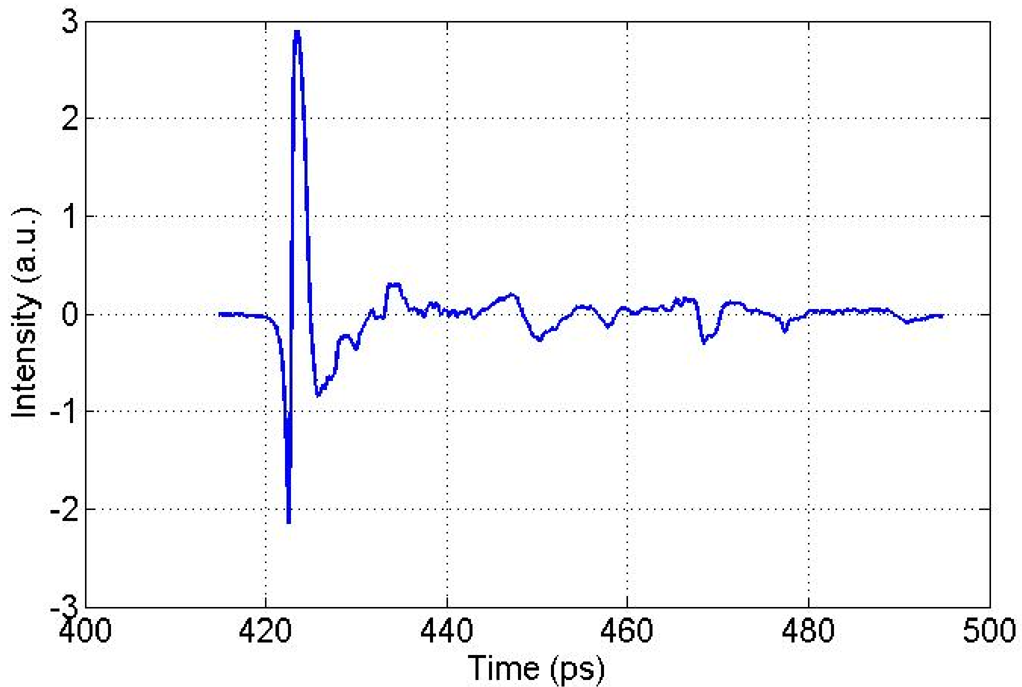

Figure 3-3. Typical measured reference signal through air (or delayed incident signal)

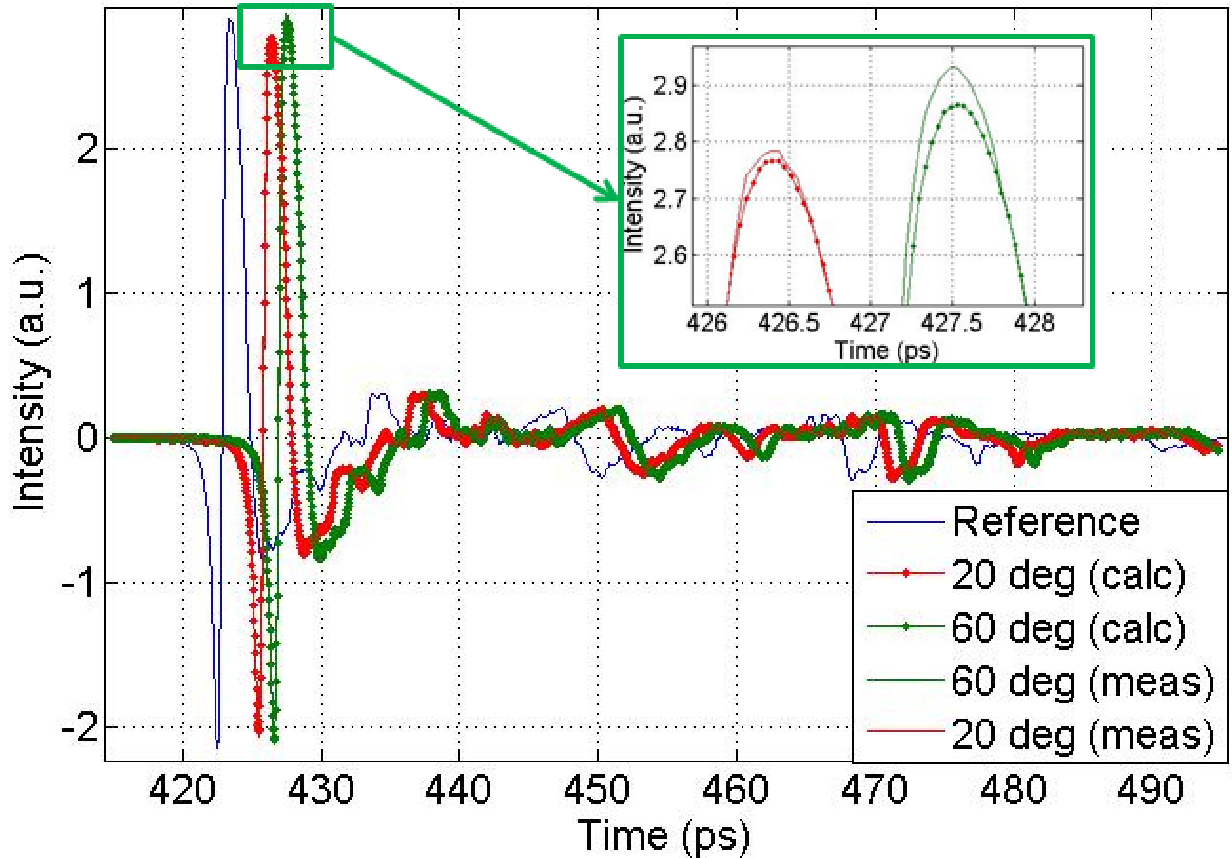

Figure 3-4. Measured and calculated signals through the single layer dielectric stack

Measured signals were obtained for a single layer of HDPE (l =1.595mm) with average dielectric properties across the THz system frequency range of operation being (n =1.535 and k =0.002) [25]. The signals were obtained at two angles of incidence, 20- and 60-degrees. Additionally, calculated signals were obtained using the theory presented earlier and a measured reference signal through air similar to the one shown in Figure 3-3. Figure 3-4 shows the measured signals along with their calculated counter parts for the single layer HDPE stack.

Two layer measurements were obtained for Zeonor 1420-R (l =1.98mm) and Quartz (l =1.631mm) with average dielectric properties across the THz system frequency range of operation being (n =1.5425 and k =0.001) [25] and (n =1.958 and k =0.003) [37], respectively. Measured signals were obtained at two angles of incidence, 20- and 60-degrees. Additionally, calculated signals were obtained using the theory presented earlier and a measured reference

signal through air similar to the one shown in Figure 3-3. Figure 3-5 shows the measured signals along with their calculated counter parts for the two layer stack.

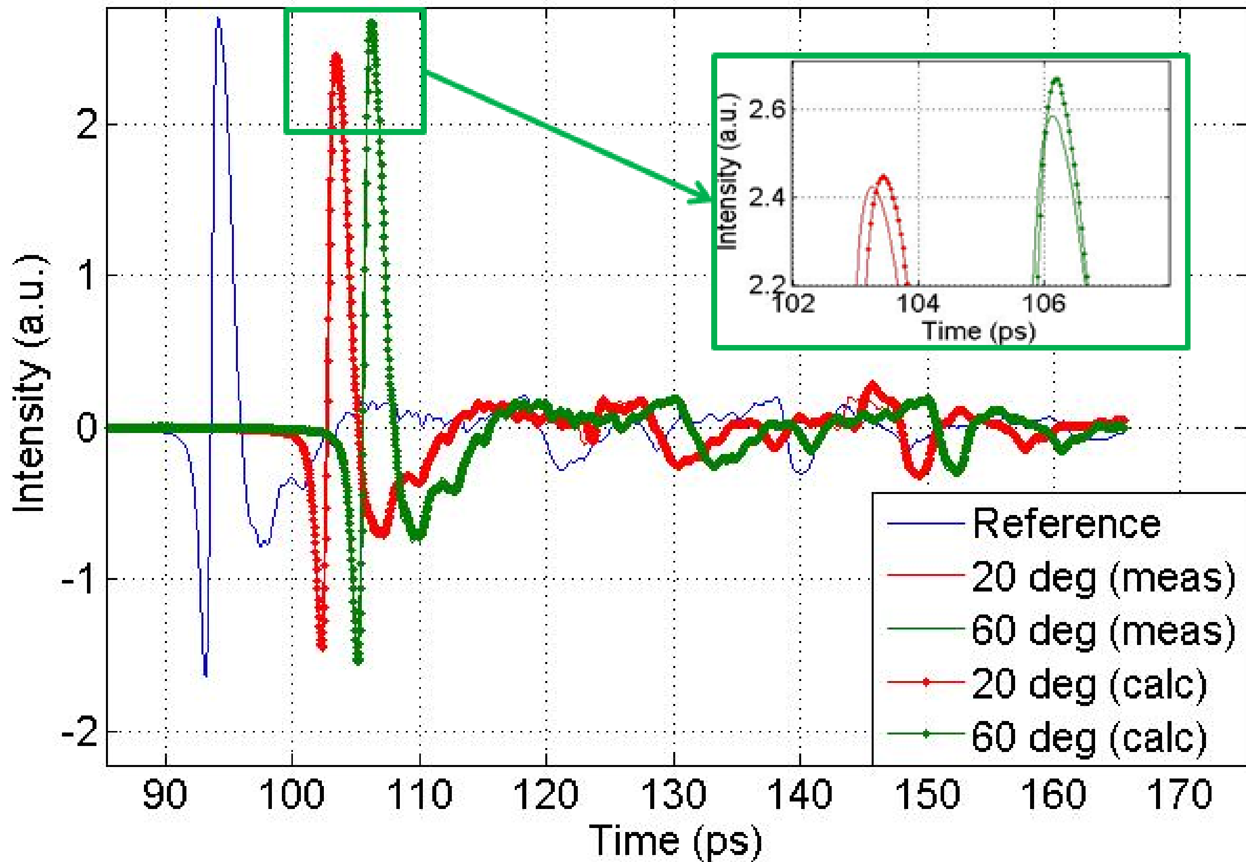

Figure 3-5. Measured and calculated signals through the two layer dielectric stack

The close similarities between the waveforms verify the characterization method modeling and assumptions. The slight differences between the synthesized and measured signals (see indent of Figures 3-4 and 3-5) may have been due to a variety of factors including: i) the measurement incident angle setting accuracy; ii) the thickness measurement uncertainty, iii)the effective average dielectric properties used to generate synthetic signals instead of using the actual frequency dependent properties and iv) for the two layer stack, presence of air gap between the stacked layers.

3.1.5 Inverse Problem Solution From Synthesized Data

Here, three different scenarios were considered and used to test the proposed characterization method. The tests for the characterization method were carried out using synthesized transmitted signals from a measured reference signal. The results for the inverse problem solution were obtained between 0.3 and 1.6 THz with 0.0125 THz steps (found from the sampling period of the measured reference signal =0.0394 ps and the total number of points=2048).

In the first case, it was assumed that the dielectric stack was composed of a single dielectric layer with an unknown thickness. The dielectric layer had a thickness of l=1.1mm. Its refractive index real and imaginary parts across the whole frequency range were n=1.8 and k=0.001, respectively. To sum it up, this problem included three unknowns and as a result three equations were required corresponding to two ratios or two sample measurements at two different angles of incidence. The two angles of incidence were picked to be 30- and 60-deg. The layer properties were solved for at each frequency point. The preliminary initial guesses for the first phase of the root finding process were picked at random in the ranges 1.4 to 1.9, 0 to 0.05 and 0.2mm to 2mm for n, k and l respectively. The extracted parameters obtained from the first phase which were used as the initial guesses for the second phase were: 1.7736, 0.0037 and 1.1165mm for n, k and l respectively. Figure 3-6 shows the extracted material properties for the single layer stack along with the thickness.

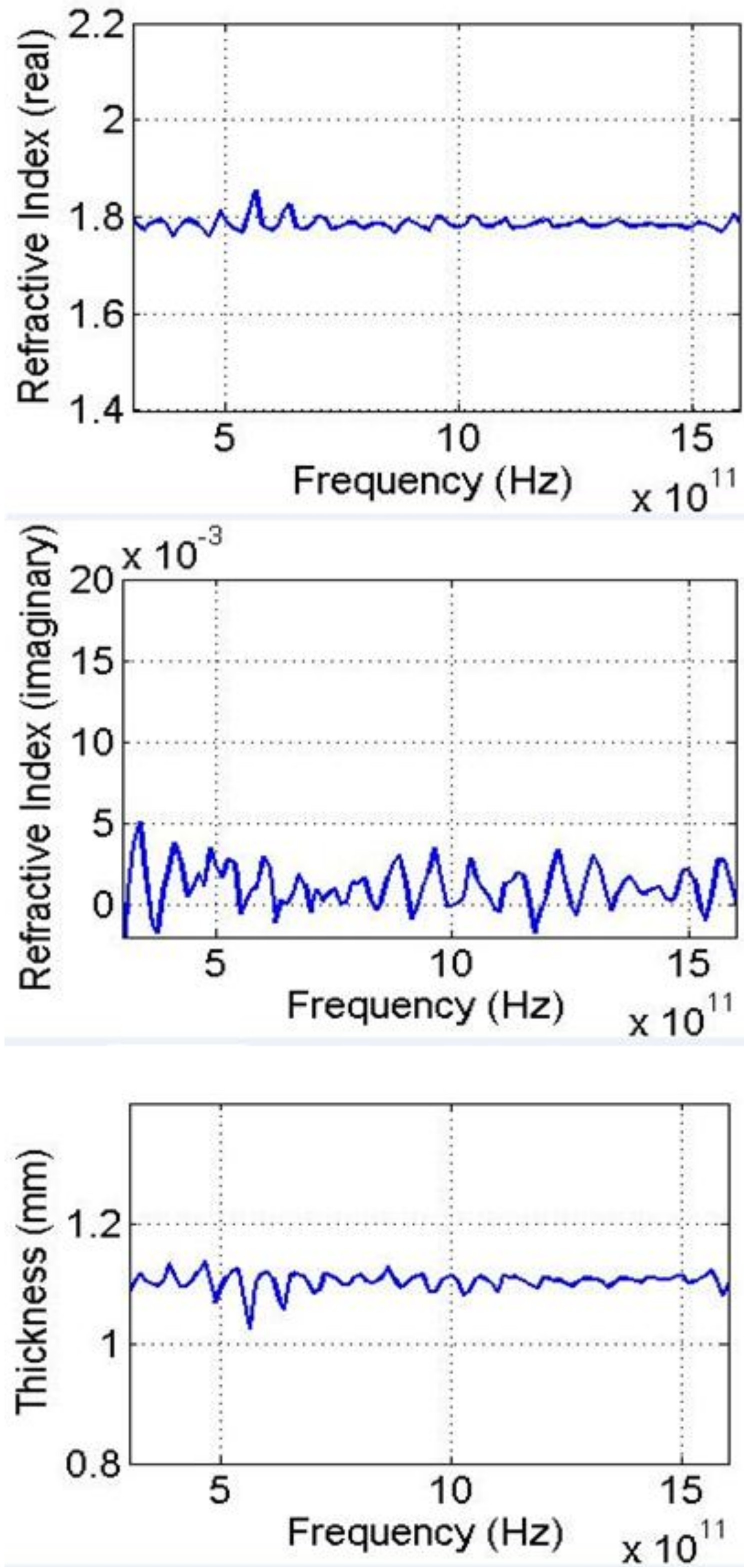

Figure 3-6. Extracted properties of the single layer stack

In the second case, it was assumed that the dielectric stack was composed of two dielectric layers with known thicknesses. The dielectric layers had thicknesses of l_1=1.2mm and l_2=1.98mm, respectively. Their refractive indices real and imaginary parts across the whole frequency range were (n_1=2 and k_1=0.01) and (n_2=1.5425 and k_2=0.01), respectively. To sum it up, this problem included four unknowns and as a result four equations were required corresponding to two ratios or two sample measurements at two angles of incidence. These were picked to be 30- and 60-degrees. The layer properties were solved for at each frequency point. The preliminary initial guesses for the first phase were picked at random in the ranges 1.6 to 2.2, 0 to 0.1, 1.4 to 1.8 and 0 to 0.1 for n_1, k_1, n_2 and k_2 respectively. The extracted parameters obtained from the first phase which were used as the initial guesses for the second phase were: 2.0029, 0.01399, 1.5354 and 0.008639 for n_1, k_1, n_2 and k_2 respectively. Figure 3-7 shows the extracted material properties for the two layer stack. It is clear that the method succeeded in converging to values close to the true properties.

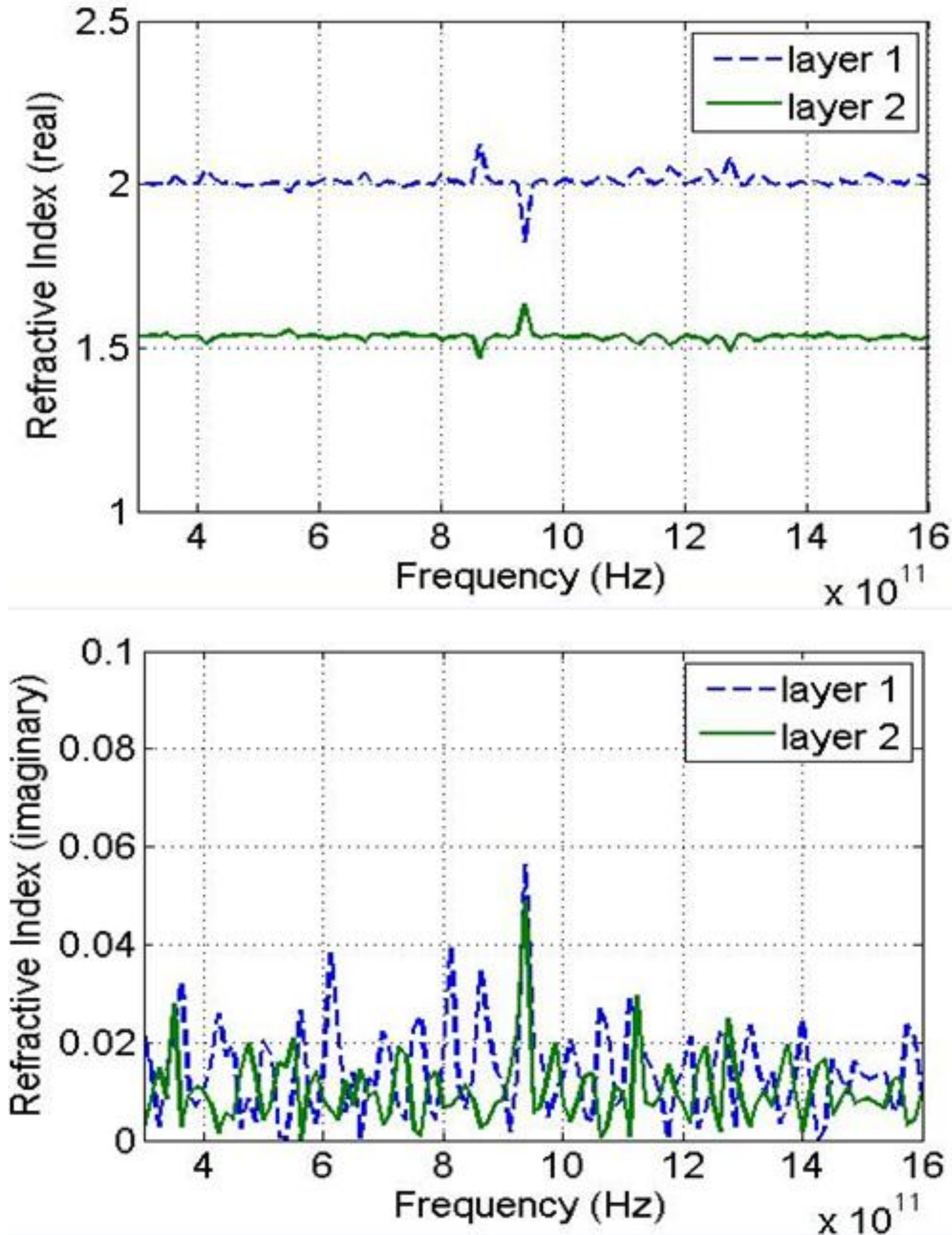

Figure 3-7. Extracted properties of the two layer stack (known thicknesses)

In the third case, it was assumed that the dielectric stack was composed of two dielectric layers with unknown thicknesses. The dielectric layers had thicknesses of l_1=1.98mm and l_2=1.2mm, respectively. Their refractive indices real and imaginary parts across the whole frequency range were (n_1=1.5425 and k_1=0.01) and (n_2=2 and k_2=0.01) respectively. To sum it up, this problem included six unknowns and as a result six equations were required

corresponding to three ratios or three sample measurements at three angles of incidence. These were picked to be 20-, 40- and 60-deg. The layer properties were solved for at each frequency point. The preliminary initial guesses for the first phase were picked at random in the ranges 1.4 to 1.6, 0 to 0.1, 1.8mm to 2.3mm, 1.7 to 2.3, 0 to 0.1 and 0.9mm to 1.4mm for n_1, k_1, l_1 n_2, k_2 and l_2 respectively. The extracted parameters obtained from the first phase which were used as the initial guesses for the second phase were: 1.5627, 0.00998, 1.908mm, 1.9579, 0.00965 and 1.243mm for n_1, k_1, l_1, n_2, k_2 and l_2 respectively. Figure 3-8 shows the extracted material properties for the two layer stack.

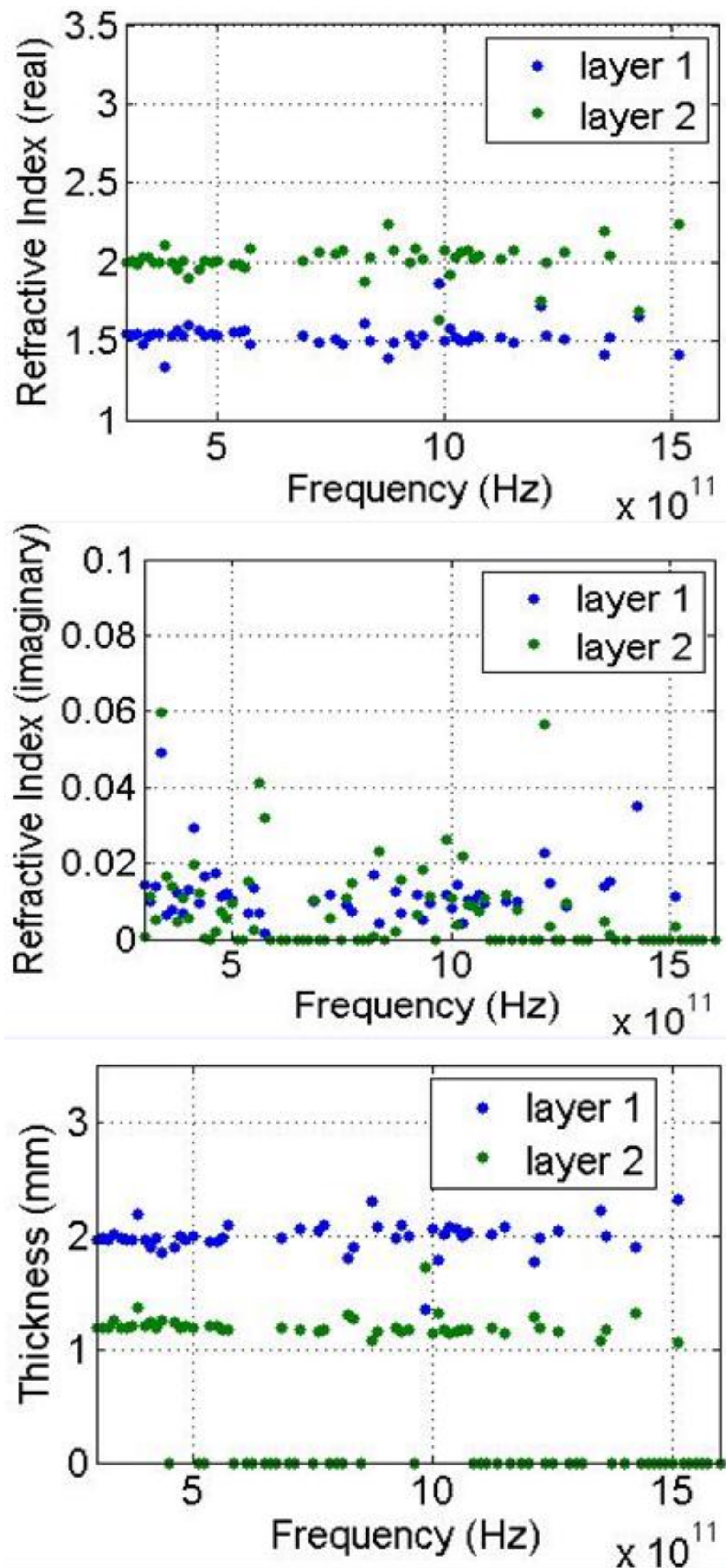

Figure 3-8. Extracted properties of the two layer stack (unknown thicknesses)

Upon examining the results obtained for all the three test cases carried out, it is clear that the method succeeded in converging to values very close to the true properties at most of the frequency samples. Since, this inverse problem solution is for synthesized data, the difference cannot be attributed to the measurement procedure or source instability. However, the minor differences can be attributed to the discretization of the measured time-domain reference signal used to generate the synthesized data. A single time step (0.0394ps) in a material having $n = 1.8$ corresponds to a physical thickness of 0.0145mm, thus the accuracy of the extraction is affected by the discretization as the samples to be characterized become more optically thin. The fluctuations in the extracted parameters are caused by the nonzero truncated ends of the time-domain signals (see Figures 3-3 to 3-5). Comparatively, it is clear that an increasing complexity (more unknowns) results in worse extracted parameters (see Figure 3-6, 3-7 and 3-8). This might be partially attributed to a solution non-uniqueness issue. An example of the solution non-uniqueness issue can be seen in the complimentary outliers in the extracted results at 937 GHz in the refractive index (real) graph of Figure 3-7. One possible solution for the non-uniqueness issue in any future method improvements might be in a multi-objective function constrained optimization. For the third case, the root finding method didn't converge to an answer or complete the root finding process number of iterations at all frequencies. The frequencies at which the root finding process failed are represented by the zeros in Figure 3-8. The increased complexity of the root finding problem is the probable reason for the failure to converge.

3.1.6 Inverse Problem Solution From Measured Data

In this section material sample properties were extracted from measured data. The results for the inverse problem solution were obtained between 0.2 THz and an upper limit determined by the noise floor of the measured signals with 0.0125 THz steps (found from the sampling period

of the measured reference signal =0.0394 ps and the total number of points=2048). Two types of inverse problem solutions were carried out. These were the extraction of parameters of a single layer dielectric stack with unknown thickness and of a two layer dielectric stack with known layer thicknesses. The single layer dielectric stacks characterized along with their thicknesses were: HDPE – 1.595mm, Si – 0.52mm, Pyrex – 0.52mm and Polycarbonate (PC) - 1.11mm. These thicknesses were acquired using a digital caliper accurate to within 0.02mm. The two layer dielectric stacks which were characterized were composed of: HDPE-Si and Pyrex-Si. The dielectric properties are presented in the form of the dielectric constant, ε_r, and the loss tangent, $\tan\delta$, which were obtained from the extracted n and k using $\varepsilon_r = n^2 - k^2$ and $\tan\delta = \frac{2nk}{n^2 - k^2}$. This was done for ease of comparison with the extracted properties from the methods presented in chapter two. The extracted material properties were smoothed with a moving average including 21 data points within its averaging window and centered at the data point to be smoothed. The averaging excluded any frequency points where the method didn't converge to a value or converged to another solution out of the range of possible solutions (used to find the initial guesses for the first phase). The standard deviation of the data within the averaging window was found each time the window was shifted. In order to show the spread of the extracted data before smoothing, standard deviation bars were included in the smoothed results. Each data point has a bar associated with it extending one standard deviation above and another below the data point. For validation completeness, the results presented for this method are compared to the results obtained from the reference requiring method (chapter 2 or [37]) at selected frequencies.

All the sample measurements for the inverse problem solution for the single layer stacks were taken at 60- and 40-deg except for Si (60- and 50-deg). Figure 3-9 shows the results obtained for the HDPE single layer stack. The preliminary initial guesses for the first phase of the root finding process were picked at random in the ranges 1.5 to 2.1, 0 to 0.15 and 0.2mm to 2mm for n, k and l respectively. The extracted parameters obtained from the first phase which were used as the initial guesses for the second phase were: 1.58466, 0.005317 and 1.479mm for n, k and l respectively. The dielectric properties extracted in [37] lie within one standard deviation from those extracted here. Additionally, the mean of the thickness extracted here is 2.8% different from that measured with the digital caliper. Figure 3-10 shows the results obtained for the Si single layer stack. The preliminary initial guesses for the first phase of the root finding process were picked at random in the ranges 3 to 3.8, 0 to 0.15 and 0.2mm to 2mm for n, k and l respectively. The extracted parameters obtained from the first phase which were used as the initial guesses for the second phase were: 3.421, 0.0242 and 0.52mm for n, k and l respectively. The dielectric properties extracted in [37] lie well within one standard deviation from those extracted here. Additionally, the mean of the thickness extracted here is 2.1% different from that measured with the digital caliper.

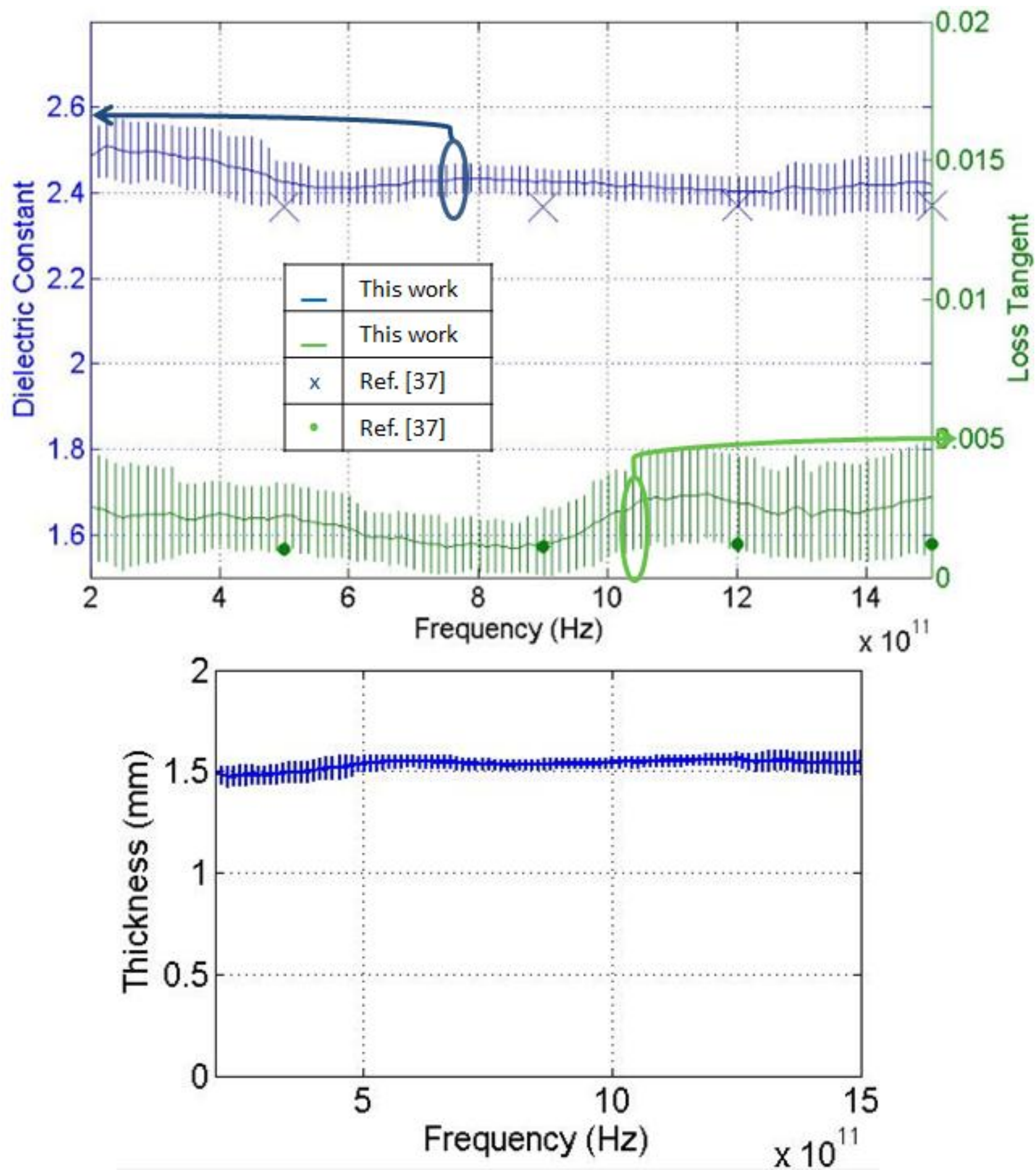

Figure 3-9. HDPE single layer stack extracted material properties and thickness

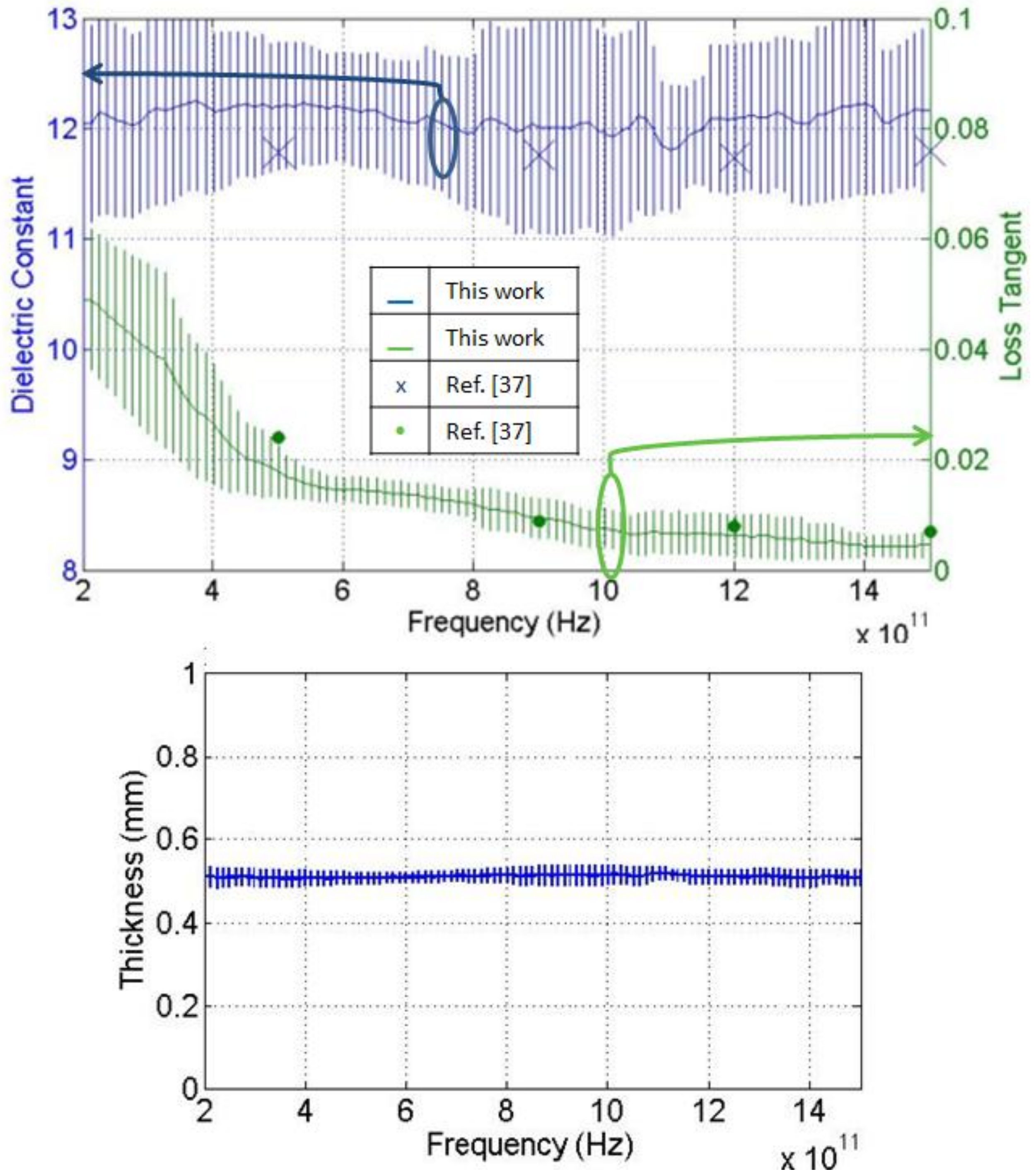

Figure 3-10. Si single layer stack extracted material properties and thickness

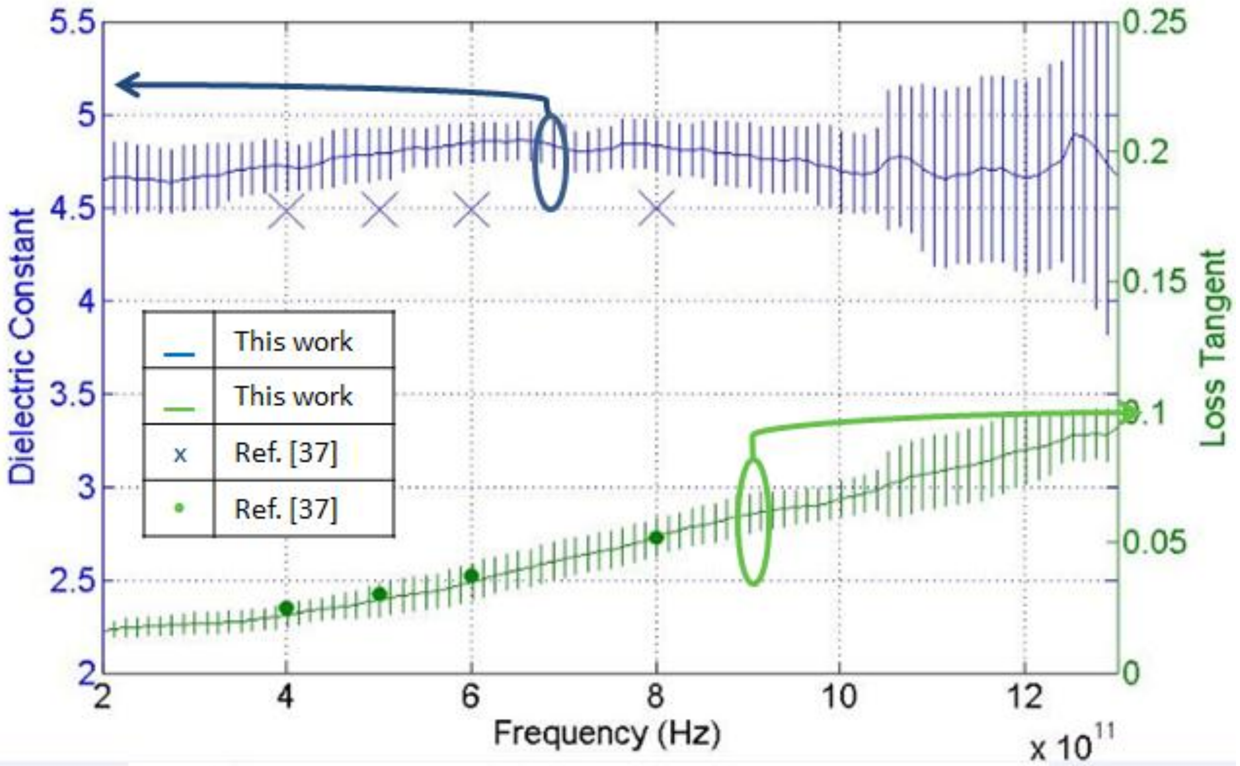

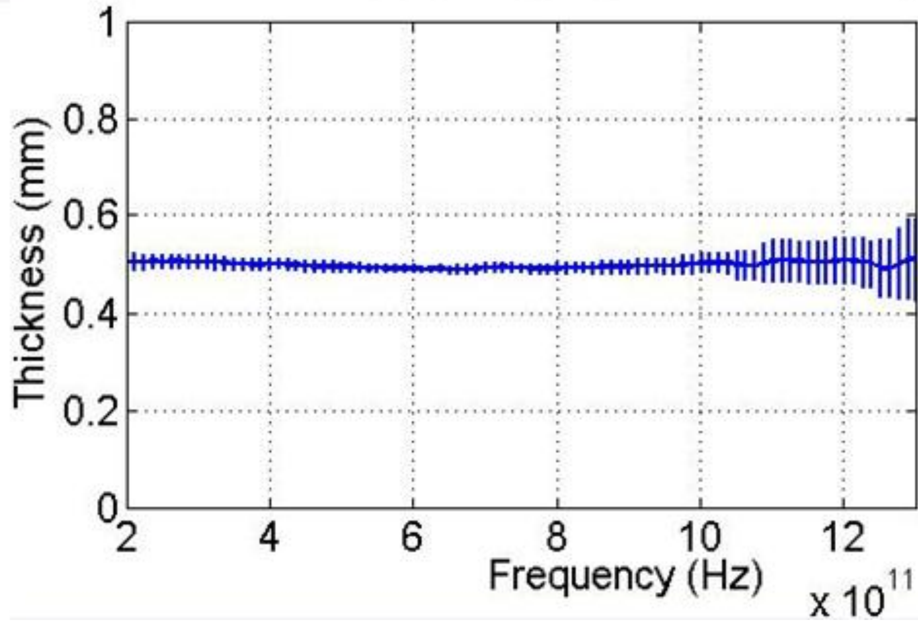

Figure 3-11. Pyrex single layer stack extracted material properties and thickness

Figure 3-11 shows the results obtained for the Pyrex single layer stack. The preliminary initial guesses for the first phase of the root finding process were picked at random in the ranges 1.9 to 2.5, 0 to 0.15 and 0.2mm to 2mm for n, k and l respectively. The extracted parameters

obtained from the first phase which were used as the initial guesses for the second phase were: 2.1559, 0.0158 and 0.5057mm for n, k and l respectively. The extracted dielectric constant differs by about 5% from that obtained in [37], while the loss tangent lies well within one standard deviation. Additionally, the thickness extracted here is 2.88% different from that measured with the digital caliper. Figure 3-12 shows the results obtained for the PC single layer stack. The preliminary initial guesses for the first phase of the root finding process were picked at random in the ranges 1.5 to 2.1, 0 to 0.15 and 0.2mm to 2mm for n, k and l respectively. The extracted parameters obtained from the first phase which were used as the initial guesses for the second phase were: 1.6517, 0.01454 and 1.155mm for n, k and l respectively. The dielectric properties extracted here lie within one standard deviation from those extracted in [37]. Additionally, the thickness extracted here is 0.54% different from that measured with the digital caliper.

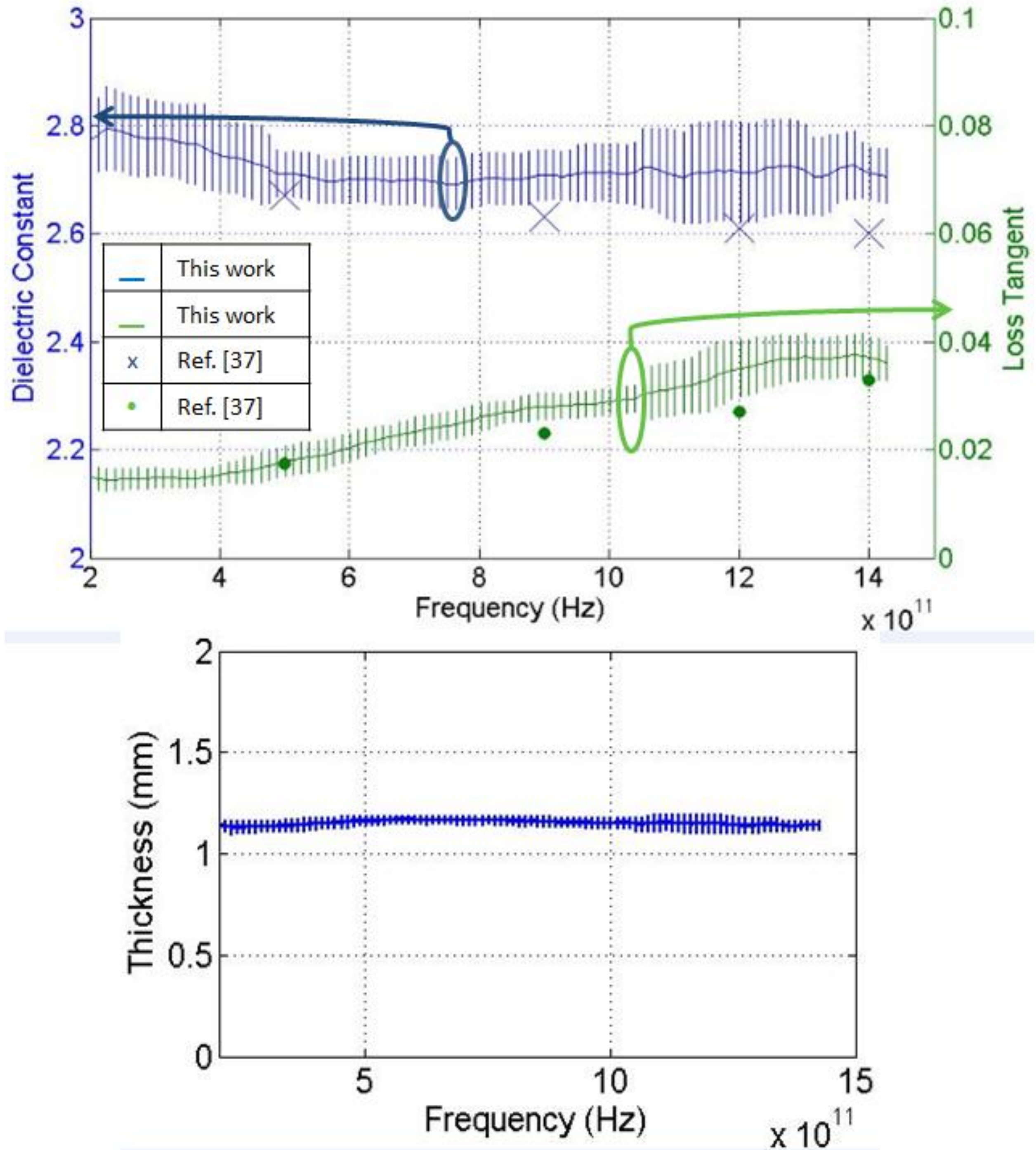

Figure 3-12. PC single layer stack extracted material properties and thickness

The single layer characterization results achieved along with thickness extraction show the contribution of the multiple angle method relative to other single layer material characterization method which don't extract the thickness of the dielectric sample. On the other hand, pertaining

to the obtained results one observation made was that the size of the error bars on the extracted material properties (especially the dielectric constant) increased as the dielectric constant increased. The reason for this is yet to be investigated.

Figure 3-13 shows the results obtained for the Si-HDPE two layer stack. The preliminary initial guesses for the first phase were picked at random in the ranges 3 to 3.8, 0 to 0.2, 1.4 to 1.8 and 0 to 0.2 for n_1, k_1, n_2 and k_2 respectively. The extracted parameters obtained from the first phase which were used as the initial guesses for the second phase were: 3.4077, 0.0348, 1.5263 and 0.00146 for n_1, k_1, n_2 and k_2 respectively. It is clear that the dielectrics constant in [37] lie well within one standard deviation of the dielectric constants extracted here. The extracted loss tangents however appear to be higher than in [37]. A very likely explanation to that might be in any small air gaps between the two layers of the stack not accounted for in the theoretical model. The air gaps possibly came to be when the layers were mechanically pressed against each other to create the two layer stack. These air gaps result in cavities for the THz wave and thus might be causing some attenuation to the signal. Another possible reason for mismatches lies in the instabilities of the source and detector causing different signal drifts in the collected data. Figure 3-14 shows the results obtained for the Pyrex-Si two layer stack. The preliminary initial guesses for the first phase of the extraction process were picked at random in the ranges 1.9 to 2.3, 0 to 0.08, 3 to 3.5 and 0 to 0.08 for n_1, k_1, n_2 and k_2 respectively. The extracted parameters obtained from the first phase which were used as the initial guesses for the second phase were: 2.0938, 0.07, 3.432 and 0.0075 for n_1, k_1, n_2 and k_2 respectively. The dielectric constant results obtained here compared to these in [37] and lie well within one standard deviation of each other. The loss tangent of Si from [37] lies within one standard deviation from the loss tangent extracted here. On the other hand, while the loss tangent in [37] from Pyrex maintains the same

increasing trend as the Pyrex loss tangent extracted using the multiple angle method it is significantly less. Again, this error in the loss tangent can possibly be attributed to air gaps between the layers or measurement system drifts and instabilities.

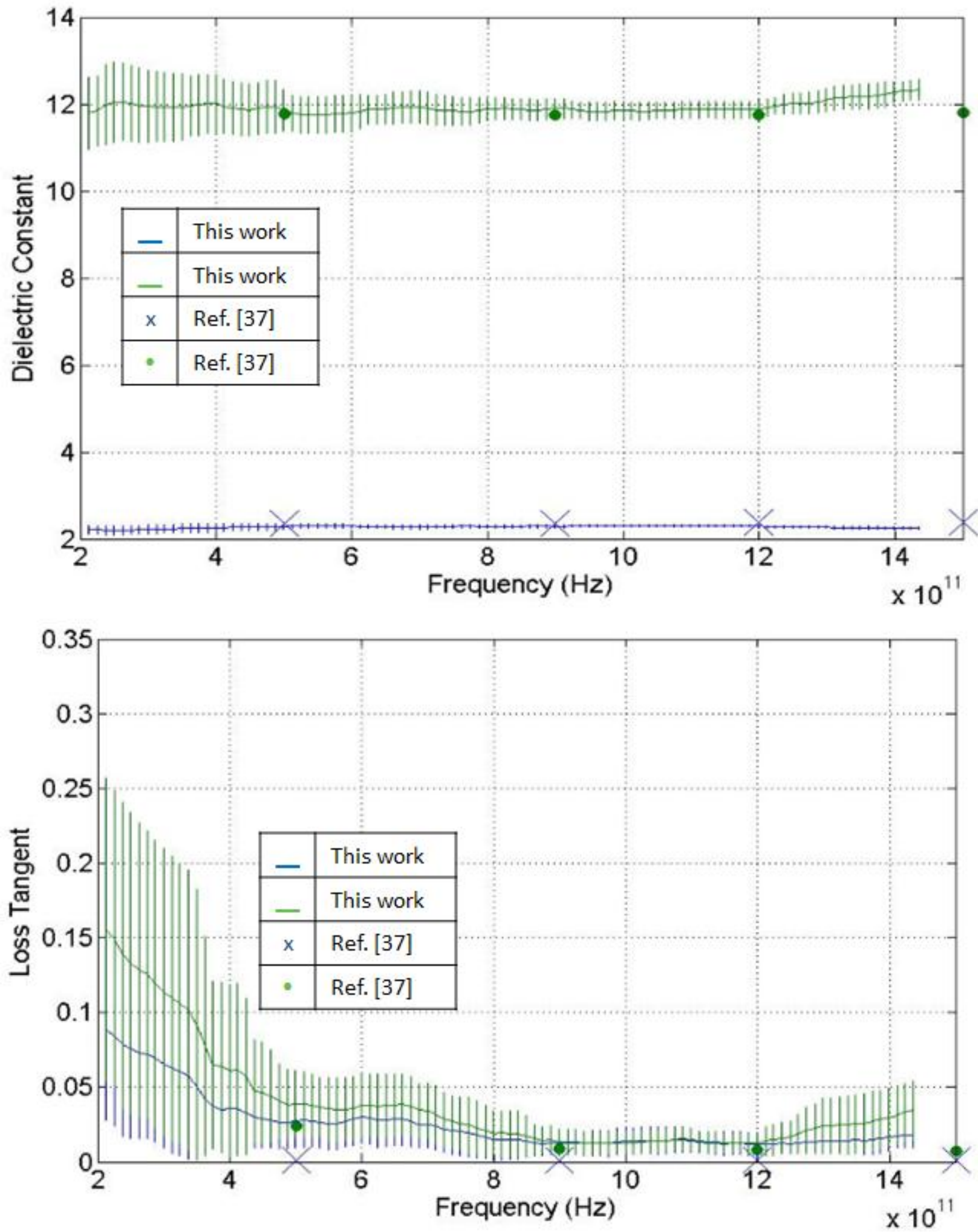

Figure 3-13. HDPE-Si two layer stack extracted material properties

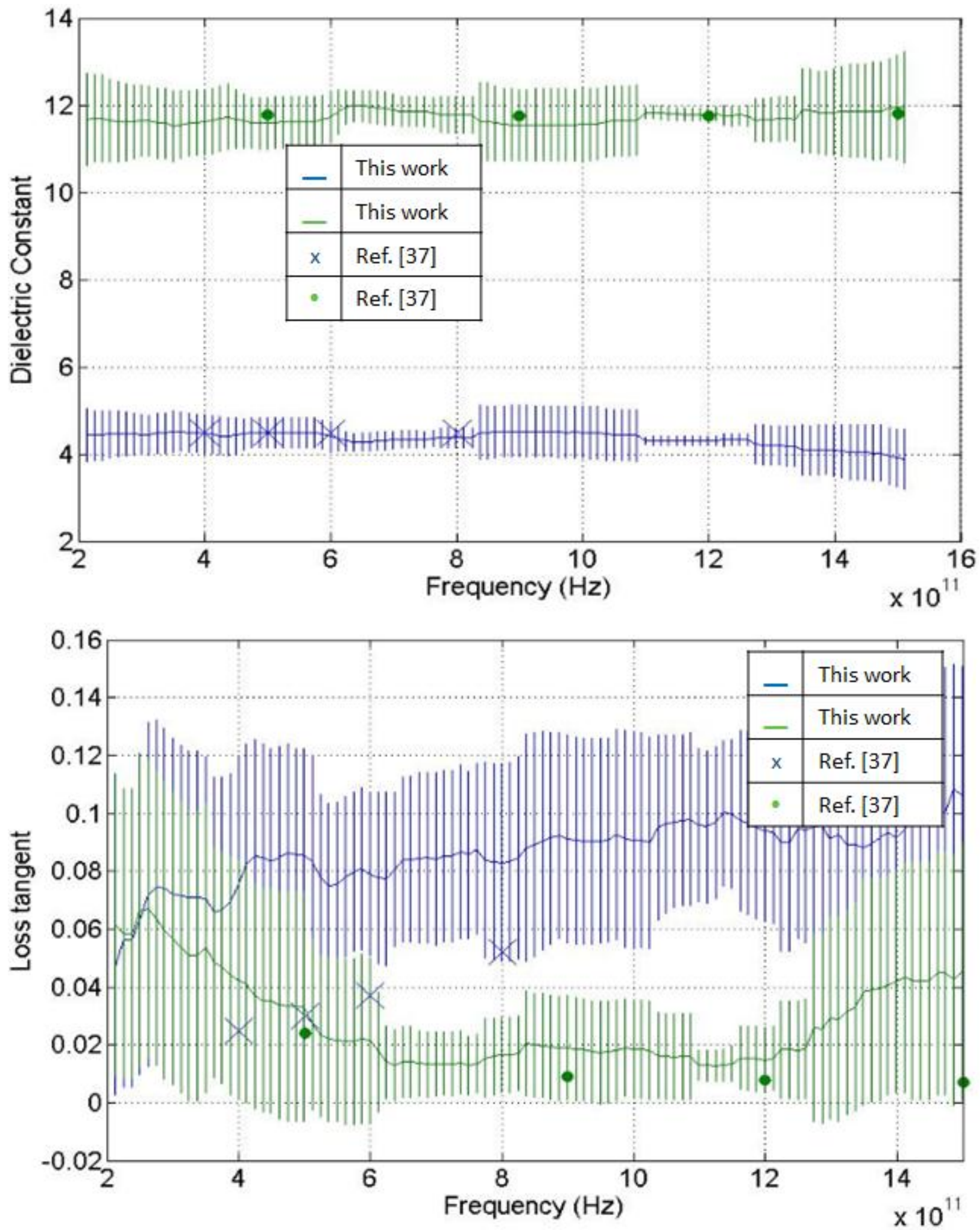

Figure 3-14. Pyrex-Si two layer stack extracted material properties

3.1.7 Error Analysis and Discussion

The multiple angle method requires the measurement of signals transmitted through the sample at an angle. As such, the angle setting in the measurement setup might prove to be a

source of uncertainty in the extracted material parameters. In this section, an error analysis is done in order to examine the effect of the incidence angle setting accuracy on the extracted parameters.

The first study was carried out on the material characterization of a single layer dielectric sample with known thickness for the parallel polarization setup discussed in earlier sections. This characterization requires a single sample signal taken at a chosen angle of incidence in addition to the reference signal through air. For this study, the assumed sample signal angles were chosen to be 0-, 20-, 40- and 60-degrees. The effect of the angle of incidence uncertainty on the extracted parameters is examined. From the measurement setup it was determined that the incident angle setting is accurate to within ±0.5-degrees.

The modeled material used to carry out the error analysis study had the properties: $\varepsilon_r 1 = 3.822$, $\tan\delta 1 = 0.005$ and thickness=1mm. The initial guesses used for the error analysis study were the true modeled material's properties themselves as the goal was to examine the sensitivity of the technique due to the angle setting accuracy only. For the purpose of the discussion that will follow the presentation of the results, it was determined that the Brewster's angle of the modeled material is around 63-degrees.

For each of the assumed sample signal angle settings (0-, 20-, 40- and 60-degrees), a population of 1000 possible true angle settings is generated at random from a normal distribution having the assumed angle setting as a mean and 0.25-degrees as the standard deviation. For every possible true sample signal angle setting generated in the population, the forward problem was solved resulting in a synthesized sample signal calculated from a measured reference signal. The same measured reference signal was used in every forward problem solution. Afterwards, for each synthesized sample signal the inverse problem was solved using the assumed sample

signal angle setting. The mean and standard deviation of the extracted properties were then found at every single frequency. The resulting mean along with two times the standard deviation error bars were then plotted on the same graph. Figure 3-15 shows the means and the errors bars obtained for the extracted parameters of the modeled material using the each of the four sets of synthesized sample signals at assumed angle settings of 0-, 20-, 40- and 60- degrees.

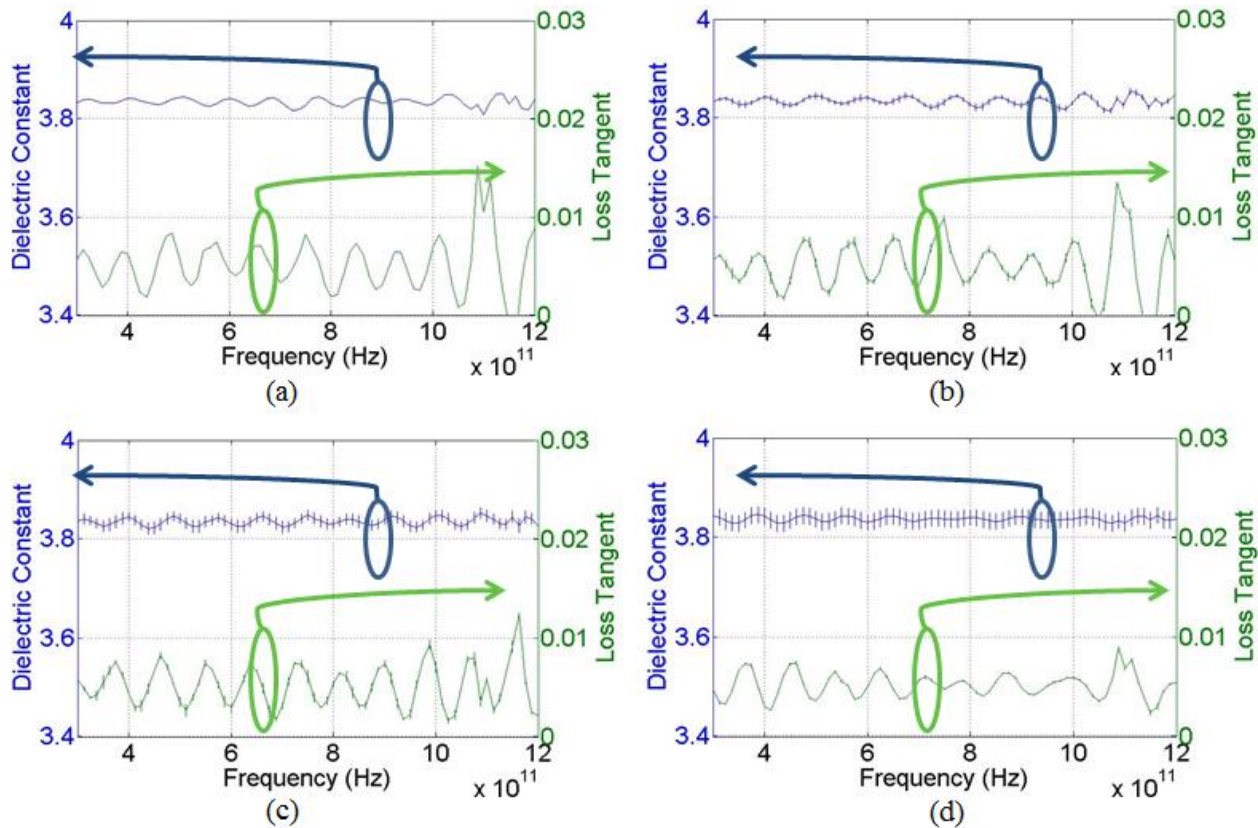

Figure 3-15. Extracted material parameters for the assumed incident angle settings of (a) 0-degrees, (b) 20-degrees, (c) 40-degrees and (d) 60-degrees

From Figure 3-15, it is seen that the method becomes more sensitive to an incident angle approaching the Brewster's angle when extracting the dielectric constant. This is apparent in the increasing size of the error bars. The comparison of the error bars of the extracted loss tangents however shows that the method is slightly more sensitive to the 20- and 40-degrees angles of incidence when extracting the loss tangent. The recurrent peak at around 1.1 THz in the extracted loss tangents of Figure 3-15 may largely be due to moisture absorption (see Figure 1-5) which

would have been present in the measured reference signal used in the forward and inverse problem solutions.

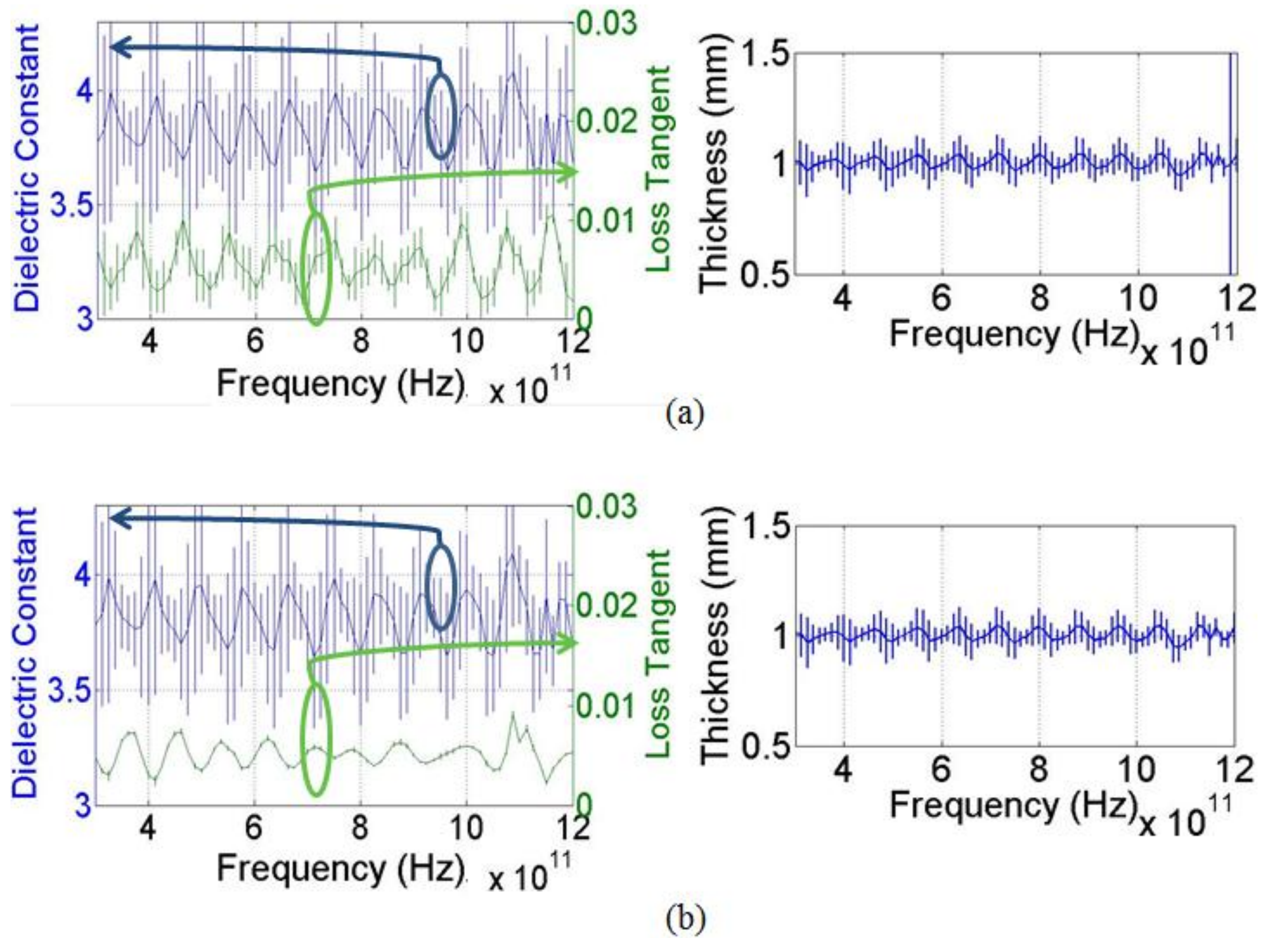

Figure 3-16. Extracted properties for the assumed incident angle pair (60- and 40- degrees) (a) 2 matching equations for 60-degrees incidence (b) 2 matching equations for 40-degrees incidence

The second error analysis study involved the characterization of a single dielectric layer along with thickness extraction. In order to carry out this characterization, two sample signals at two angles are required as the number of unknowns amounts to three and each sample signal can be used to find two unknowns. The assumed sample signal angles used for the study were chosen to be at 40- and 60-degrees. Out of the four possible matching equations (two pairs matching magnitudes and phases of calculated and measured ratios) for the root finding process, three must be picked to complete the characterization. The error analysis study here is run twice. In the

first case, two equations matching the magnitude and phase of a calculated and measured ratio for 60-degrees incidence are used while one equation matching the phase of a calculated and measured ratio for 40-degrees incidence is used. In the second case, two equations matching the magnitude and phase of a calculated and measured ratio for 40-degrees incidence are used while one equation matching the phase of a calculated and measured ratio for 60-degrees incidence is used. Figure 3-16 shows the means and error bars of the extracted dielectric properties and thicknesses for each of the cases.

Upon comparing the results from the two cases obtained, it is clear that the angle setting accuracy affected the possible ranges of the extracted dielectric constant and thickness almost the same in both cases. However, the loss tangent in case (a) was almost unaffected by the angle setting accuracy as opposed to the loss tangent in case (b) which had relatively large error bars. Hence, this leads to the conclusion that under a similar situation and given the angle setting accuracy as the major part of uncertainty in the measurement; the choice of which angle dependent sample signal is used to generate two equations versus one for the root finding algorithm can affect the possible outcome of the material parameter extraction method. Finally, upon comparing the results obtained in Figure 3-16 against the ones obtained in Figure 3-15, it is shown that as the number of angle dependent sample signals increases for the material characterization method the uncertainty in the extracted results increases as well.

3.2 The Input and Output Field Distribution Method

3.2.1 Problem Definition and Motivation

All the material characterization methods presented in this dissertation up until this section were modeled to carry out material characterization of dielectric material systems using a single source and a single detector measurement setup. In the future, THz systems will include a single source and an array of detectors. Such THz systems will have the capability to carry out single shot imaging. Research is currently being carried out to realize such systems. A method facilitating the use of the future multiple detector THz systems for material characterization is needed. Such a method would make use of the field distributions achieved in measurement using an array of detectors. In this section, the input and out field distribution method is presented towards that need.

This method is based upon the angular spectrum propagation concept of Fourier optics [52]. The concept shares similarities with systems theory. Using this concept, the field distribution of an electromagnetic wave at a certain plane can be found if the field distribution of the same wave is known at another plane. The field distribution to be found depends on the known distribution and the medium that the wave has to propagate through in between the two planes. Hence, if the field distribution at two parallel planes is known while the medium material properties between them are unknown an inverse problem can be setup in order to solve for the material properties of the medium.

This method can be further explained if the medium is considered to be a system (see block diagram in Figure 1-6). Under such a consideration, the field distribution at one of the planes bordering the medium is the input field distribution while the other is the output field distribution. Hence given an unchanging medium (or material system), for any input field distribution a unique output field distribution exists.

Consider the medium to be a layered dielectric stack. Using the input and output field distribution at both borders of the stack and the knowledge of the number of layers in the stack, the proposed method provides means to obtain the dielectric properties and thickness of each layer. The number of different input field distributions required (and as a result output field distributions) is dependent on the number of dielectric layers in the stack. Due to that, an efficient way to obtain various input field distributions is required. The THz system alone generates a collimated THz parallel beam. In this research, a 1-D Fresnel phase reversing zone plate (PRZP) lens [53-59] is used to obtain a desired field distribution. Unlike traditional refractive lenses, the PRZP focuses electromagnetic waves through diffraction. It was chosen due to its predictable performance in that it has well spread out focal lengths for different wavelengths of electromagnetic waves and because of the multiple feature field distribution that can be generated as a result of wave propagation through it. Other reasons for choosing the PRZP lens are its ease of fabrication and its overall flat surface making its alignment easier. Figure 3-17 shows the idealized model for the input and output field distribution method used for the analysis in the following sections.

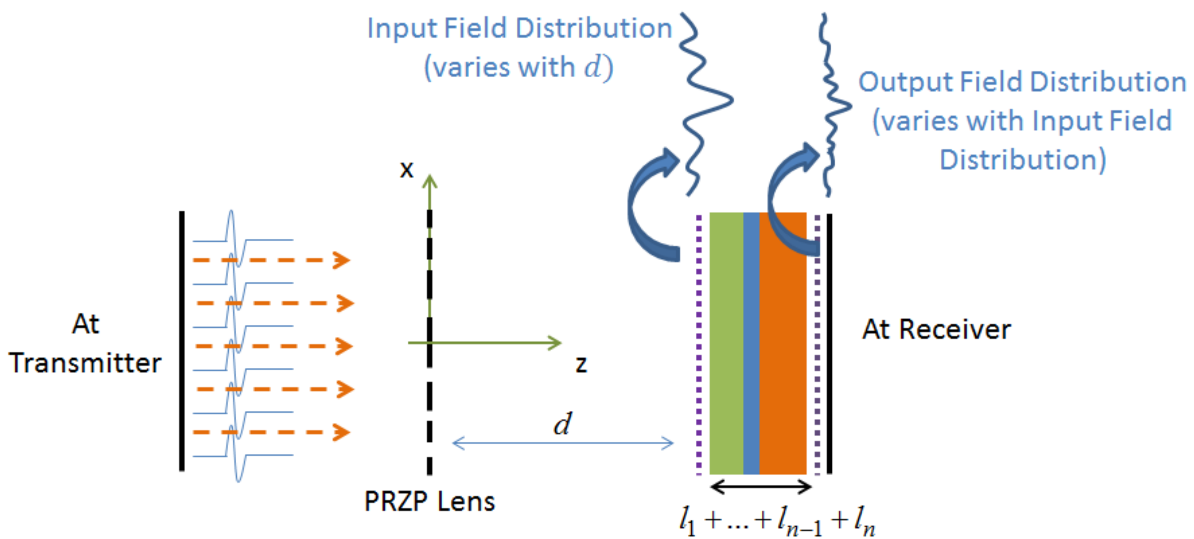

Figure 3-17. Idealized model for the input and output field distribution method

The advantages of the input and output field distribution method over the multiple angle method are its independence from the use of input paramters (such as angle setting for the multiple angle method) and its observed extracted parameter solution uniqueness.

In the next subsections the material characterization method background theory, forward problem solution from synthesized data, the inverse problem solution from synthesized data and a discussion on the method's experimental implementation including the design and experimental testing of a PRZP are presented.

3.2.2 Characterization Method Theory

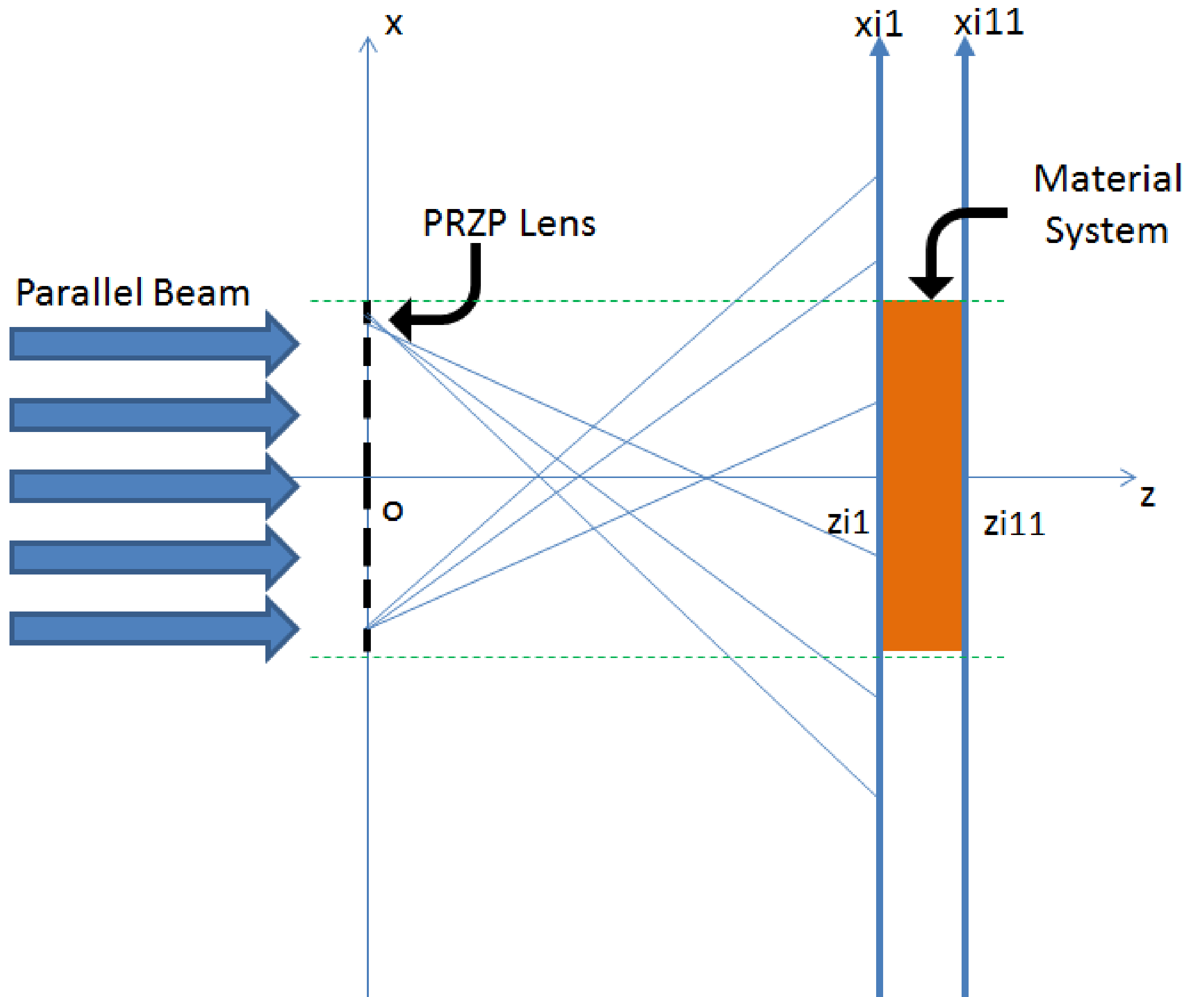

Figure 3-18. Theoretical model for the characterization method

Consider a monochromatic collimated electromagnetic plane wave propagating in the z-direction incident upon a 1-D PRZP lens (see Figure 3-18). The zone plate lens can be described in terms of a transmittance function [60]. The transmittance function is a Fourier series expressed as

$$t_b(x) = \sum_{w=-\infty}^{\infty} b_w \exp\left[-j\left(\pi w / \lambda p\right)x^2\right] \tag{3-13}$$

where w is an integer number, $b_w = \delta_{w,0} + 0.5(\exp[-j\pi]-1)(-1)^w \operatorname{sinc}(0.5w)$, λ is the wavelength in free space and p is the frequency dependent principle focal length of the zone plate lens. Assuming that the incident parallel beam has a unity amplitude, the angular spectrum of the field distribution after the lens is the spatial Fourier transform of equation (3-13) and is described by

$$T_b(f_x) = \int_{-\infty}^{\infty} t_b(x)\exp[-j f_x]dx \tag{3-14}$$

where f_x is the spatial frequency along the x direction and is related to the wave vector component along the x direction, k_x, by $f_x = k_x / 2\pi$. The angular spectrum of the field distribution directly before the material system (at zi1, see Figure 3-18) can be found by multiplying the angular spectrum after the lens by an exponential function. The angular spectrum at zi1 is described by

$$A_{zi1} = T_b(k_x)\exp\lfloor -j k_{z,0}\, zi1 \rfloor \tag{3-15}$$

where $k_{z,0}$ is the wave vector component along the z direction in free space and is described by

$$k_{z,0} = \sqrt{\left(\frac{\omega}{c}\right)^2 - k_x^2} \tag{3-16}$$

for $\left(\frac{\omega}{c}\right)^2 > k_x^2$ where ω is the angular frequency in radians and c is the speed of light in free space. If $\left(\frac{\omega}{c}\right)^2 < k_x^2$, $k_{z,0}$ is picked to be the negative imaginary value resulting from the square root in (3-16). Under this condition the wave becomes evanescent. In relation to the problem definition of this material characterization technique, A_{zi1} is the angular spectrum (or spatial Fourier transform) of the input field distribution. The material system between zi1 and zi2 can be described by a transmission coefficient, $T(\omega, k_x)$, which is a function of the material system's layers properties and thicknesses. $T(\omega, k_x)$ is described as

$$T(\omega, k_x) = \prod_{i=0}^{N} \exp\left[-jk_{z,i} l_i\right] S_{i,i+1} \text{ , [50]} \tag{3-17}$$

where $i = 0$ and $i = N + 1$ are the air before and after the dielectric material system, l_i is the thickness of layer i of the material system, $k_{z,i}$ is the wave vector component along the z direction and is described by

$$k_{z,i} = \sqrt{k_i^2 - k_x^2} \tag{3-18}$$

where k_i is the wave number in the layer i of the material system and is a function of the complex index of refraction of layer i ($\tilde{n}_i = n_i - jk_i$) by, $k_i = \frac{\omega}{c}\tilde{n}_i$.

Additionally,

$$S_{i,i+1} = \frac{T_{i,i+1}}{1 - R_{i+1,i}\tilde{R}_{i+1,i+2} \exp\left[-2jk_{z,i+1} l_{i+1}\right]}, \tag{3-19}$$

where $T_{i,i+1}$ and $R_{i,i+1}$ are interfacial transmission and reflection coefficients respectively and are described in terms of the wave impedances in each layer, Z_i , as

$$T_{i,i+1} = \frac{2Z_{i+1}}{Z_i + Z_{i+1}}, \tag{3-20}$$

$$R_{i,i+1} = \frac{Z_{i+1} - Z_i}{Z_i + Z_{i+1}}, \tag{3-21}$$

and

$$\tilde{R}_{i,i+1} = \frac{R_{i,i+1} + \tilde{R}_{i+1,i+2} \exp\left[-2jk_{z,i+1}l_{i+1}\right]}{1 + R_{i,i+1}\tilde{R}_{i+1,i+2} \exp\left[-2jk_{z,i+1}l_{i+1}\right]}. \tag{3-22}$$

Given the experi1mental measurement setup, the perpendicular polarization case is considered and as a result the wave impedance in layer i is given by

$$Z_i = \frac{k_i \eta_i}{k_{z,i}}, \tag{3-23}$$

where $\eta_i = \frac{120\pi}{\tilde{n}_i}$ is the intrinsic impedance. The angular spectrum of the output field distribution located at zi11 (or after the material system) is described as

$$A_{zi11} = A_{zi1} T(\omega, k_x). \tag{3-24}$$

It is worthy to note that if the material system was moved to an arbitrary location ziu on the z-axis of Figure 3-18, the angular spectrum of the input field distribution will change to

$$A_{ziu} = T_b(k_x) \exp\left[-j k_{z,0}\, ziu\right] \tag{3-25}$$

thus resulting in changes in the angular spectrum of the output field distribution collected at ziuu to become

$$A_{ziuu} = A_{ziu} T(\omega, k_x). \tag{3-26}$$

The input and output field distributions at locations ziu and ziuu respectively are the inverse spatial Fourier transforms of (3-25) and (3-26) and can be respectively described by

$$E_{ziu} = \int_{-\infty}^{\infty} A_{ziu} \exp\left[j 2\pi f_x x\right] df_x \tag{3-27}$$

and

$$\begin{aligned} E_{ziuu} &= \int_{-\infty}^{\infty} A_{ziuu} \exp\left[j 2\pi f_x x\right] df_x \\ &= \int_{-\infty}^{\infty} A_{ziu} T(\omega, k_x) \exp\left[j 2\pi f_x x\right] df_x \end{aligned} . \tag{3-28}$$

3.2.3 Inverse Problem Root Finding Setup

Given a stack of N dielectric layers, input field distributions, $MIE(z)$, at different locations on the z axis can be measured every time the material system is shifted with respect to the PRZP lens. The output field distribution, $MOE(z+\Delta z)$, associated with each measured $MIE(z)$ is also measured where Δz is the total thickness of the material system. Using the angular spectrum of $MIE(z)$ and a certain calculated material system transmission coefficient, $T_C(\omega, k_x)$, calculated versions of the output field distribution, $COE(z+\Delta z)$, can be obtained through equation (3-27).

The root finding process aims to iteratively approximate the unknown material properties of the material systems used to calculate $T_C(\omega, k_x)$ such that the system of equations,

$$
\begin{aligned}
norm\left(\left|COE(z1+\Delta z)\right| - \left|MOE(z1+\Delta z)\right|\right) &= 0 \\
norm\left(\angle COE(z1+\Delta z) - \angle MOE(z1+\Delta z)\right) &= 0 \\
norm\left(\left|COE(z2+\Delta z)\right| - \left|MOE(z2+\Delta z)\right|\right) &= 0 \\
norm\left(\angle COE(z2+\Delta z) - \angle MOE(z2+\Delta z)\right) &= 0 \\
&\vdots \\
norm\left(\left|COE(zN+\Delta z)\right| - \left|MOE(zN+\Delta z)\right|\right) &= 0 \\
norm\left(\angle COE(zN+\Delta z) - \angle MOE(zN+\Delta z)\right) &= 0
\end{aligned}
\tag{3-29}
$$

is solved. The approximated material properties as a result of the root finding process are the extracted material properties of the layers of the material system.

The amount of input and output field distribution pairs required to carry out the material characterization is determined by the total number of unknown dielectric layers' properties to be solved for. For example, a stack of two dielectric layers of which the thicknesses are known has a total of 4 unknowns. Since two equations can be obtained from each input and output field distribution pair, two different input and output field distribution pairs are required. On the other hand, if the thicknesses of the layers are unknown then the total number of unknowns is 6 thus requiring three different input and output field distribution pairs.

In order to solve the system of equations and obtain approximations to the roots (or dielectric layer characteristics to be found), the secant method [51] was used. A description of the secant method is available in Appendix B. Note that the secant method is highly sensitive to initial guesses. The root finding process takes place in two different phases. The first phase consists of running the extraction procedure at each discrete frequency point starting from a set of initial guesses picked at random from uniform distributions. It is worthy to note that if convergence is achieved at a certain frequency point, the parameters extracted at that frequency are used as the initial guesses for the next frequency. Uniform field distributions are possible for a wide range of values for which the unknowns can be found to lie within. Afterwards, the extracted parameters for the frequency points where the extraction algorithm converged or completed the maximum

number of loops are checked as to whether they lie within certain intervals set prior to running the extraction. If a certain extracted set of parameters satisfies the intervals, then the second phase begins. If not, then the first phase is run again. The second phase is a rerun of the extraction procedure taking the extracted set of parameters satisfying the intervals from the first phase as initial guesses. Again, if convergence is achieved at a certain frequency point, the parameters extracted at that frequency are used as the initial guesses for the next frequency.

3.2.4 Forward Problem Solution from Synthesized Data

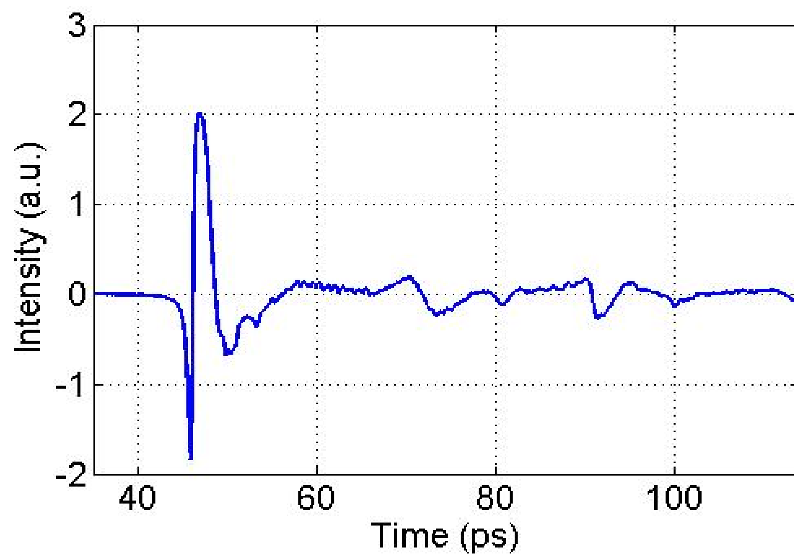

Figure 2-19. Waveform of the incident plane wave upon the PRZP

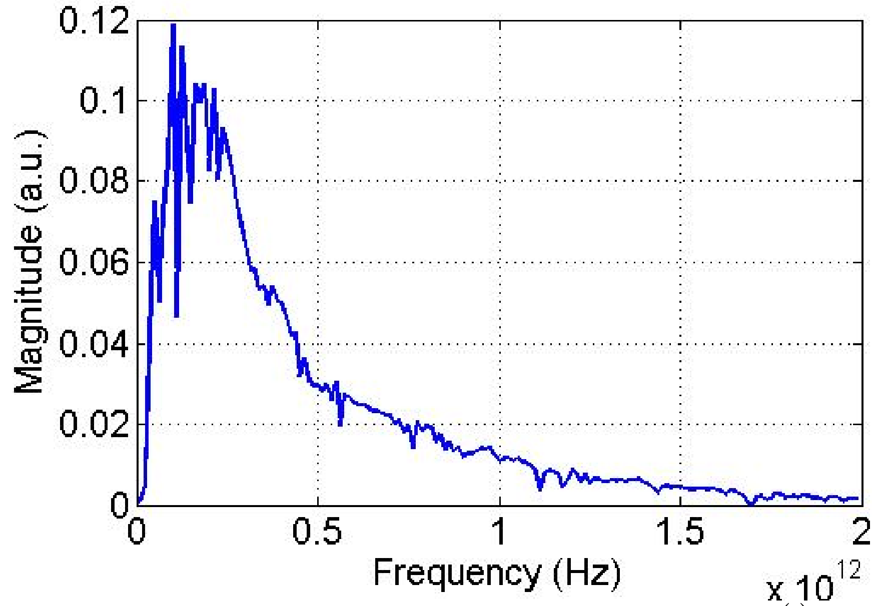

Figure 3-20. Magnitude of the Fourier transform of $E_i(t)$

In this section the evaluation of the forward problem which the method is based upon is carried out. Since the problem is 1-D, only the field distribution in the vertical direction needs to be considered. The field distribution considered at every plane is truncated in a region limited by an assumed PRZP aperture (see dashed green lines in Figure 3-18). The assumed PRZP aperture is located between -19.2mm and 19.2mm on the x-axis. This distance is represented computationally by 1024 discrete points.

Assume that a collimated transient plane wave, $E_i(t)$, is incident upon the PRZP. Furthermore, assume that it has a waveform similar to that of the THz system signal transmitted though air. The waveform of the incident plane wave is shown in Figure 3-19. The discrete Fourier transform of $E_i(t)$ is defined as $E_i(\omega)$. Figure 3-20 shows the magnitude of $E_i(\omega)$.

Now consider the magnitude and phase of $E_i(\omega)$ at each discrete frequency separately. These magnitude and phase values describe the value of the field at each pixel of the field distribution at the plane directly before the PRZP. It is worthy to note that this field distribution is the parallel beam considered in the characterization method theory (see Figure 3-17 and 3-18).

Solving at each frequency, the theory described in the previous section is applicable with the provision that the parallel incident beam is not of magnitude 1 and phase 0 anymore. The resulting field distributions can then be obtained at the planes of interest at each frequency considered.

The PRZP considered in this model is characterized by having a principle focal length equaling approximately 60mm at 600 GHz. The focal length of the PRZP at any other frequency considered can then be found using

$$pf = p\frac{f}{f_d} \tag{3-30}$$

where $p = 60$mm and is the design focal length, $f_d = 600$ GHz and is the design frequency for the design focal length and f is the frequency at which pf is to be found.

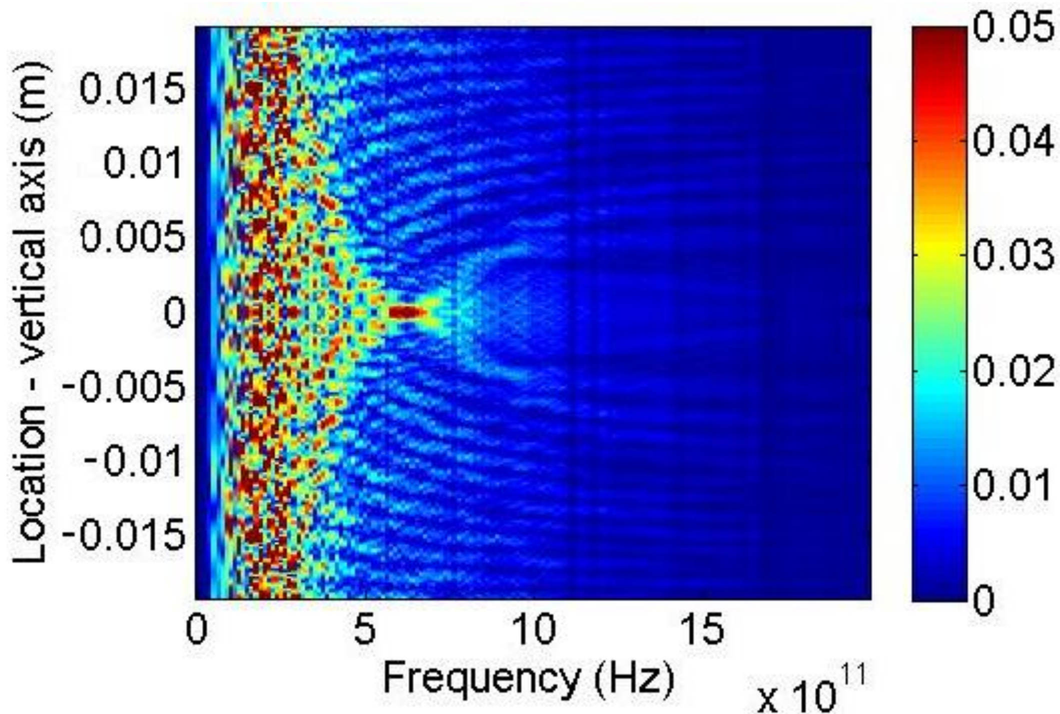

Figure 3-21. Magnitude of the input field distribution at 60mm

The forward problem solution was carried out to find the field distribution at two different locations on the z-axis given that the material system in between these locations is simply air of a

certain thickness. The thickness of the air material system is chosen to be 30mm. The input field distribution was calculated at 60mm (in reference to Figure 3-18, zi1=60mm). Figure 3-21 shows the magnitude of the calculated input field distribution. Given the modeled PRZP and its approximate 60mm focal length at the design frequency of 600 GHz, it can be seen that the calculated results in Figure 3-21 validate the design where the highest intensity focus is located at approximately 600 GHz. Note, the high intensity at the lower frequencies is to a large part due to the emitted THz signal power which decreases as the frequency increases (see Figure 3-20 that shows the signal power as a function of frquency).

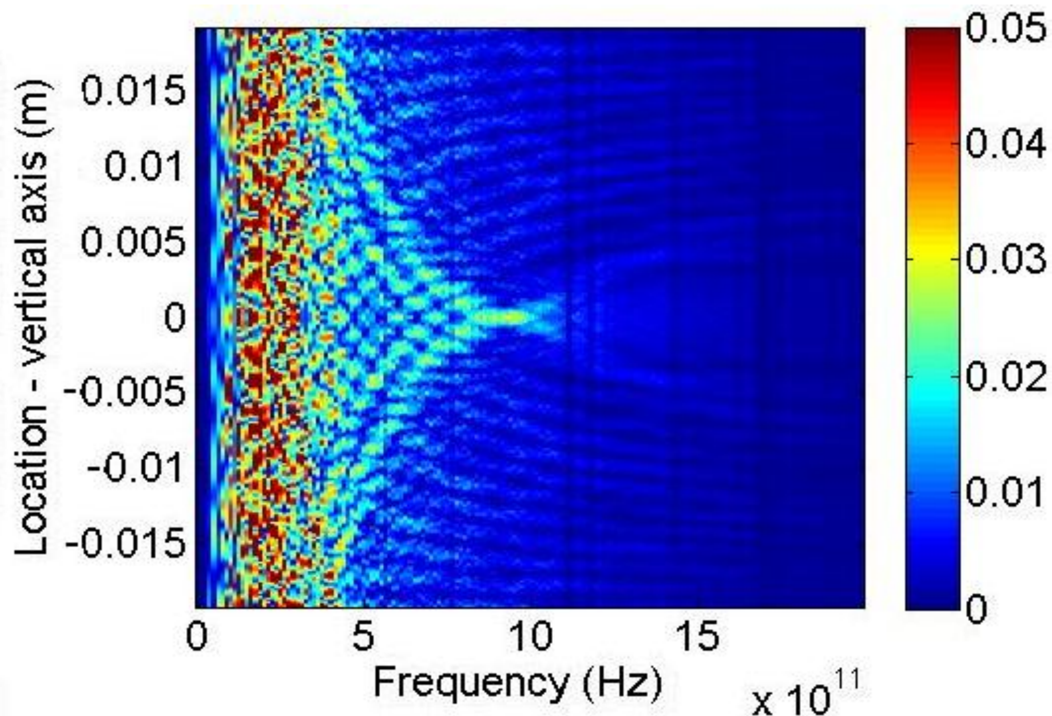

Figure 3-22. Magnitude of the output field distribution for a 30mm material system of air

The material system is composed of 30mm of air hence calculating the output field distribution as a result of the input field distribution and the material system calculated transmission coefficient is equivalent to calculating the field distribution at 90mm away from the PRZP. Using equation (3-30), it can be anticipated that the focal length of around 90mm arises at 900 GHz. Figure 3-22 shows the magnitude of the output field distribution due to the angular

spectrum of the input field distribution propagating through the 30mm material system of air. As was expected, Figure 3-22 shows that the focal frequency has shifted from 600 GHz to 900 GHz as a result of propagating the angular spectrum of the input field distribution through a 30mm material system composed of air.

For the sake of a comparative discussion, the forward problem solution was also carried out to find the output field distribution due to a material system having $n = 3$ and k =0. Figure 3-23 shows the magnitude of the output field distribution if the material system had the same 30mm thickness but $n = 3$ and k =0 as opposed to air's $n = 1$ and k =0.

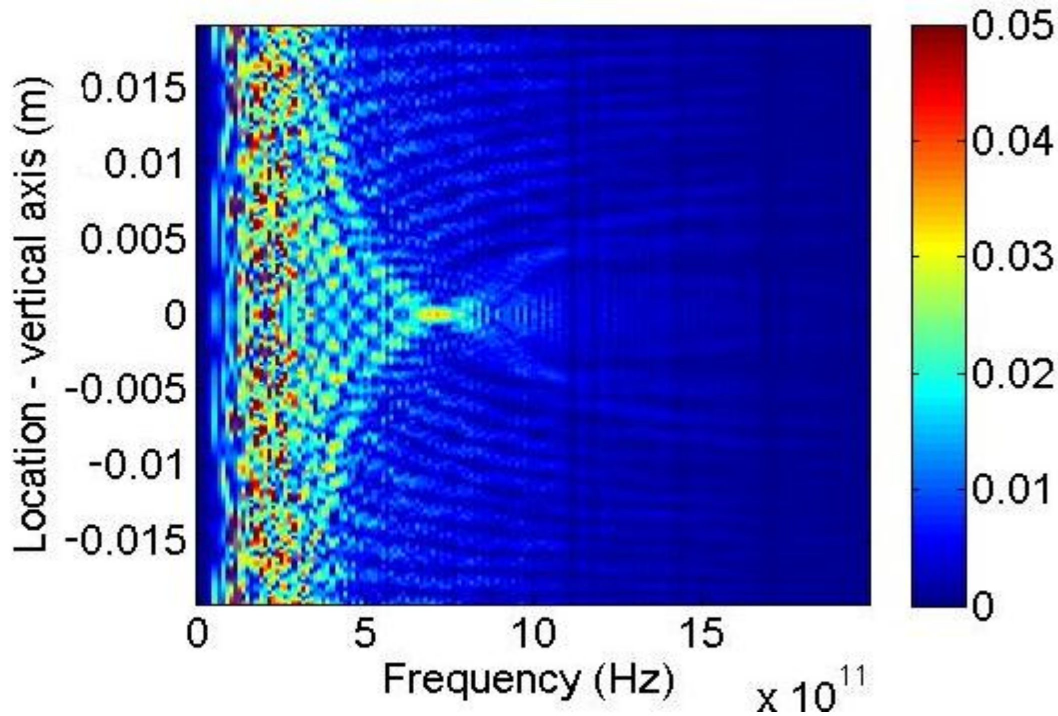

Figure 3-23. Magnitude of the output field distribution for a 30mm thick material having $n = 3$ and k =0

Comparing results obtained for the output field distributions of the 30mm material system of air (Figure 3-22) versus the 30mm material system having $n = 3$ and k =0 (Figure 3-23), it can be seen that the focal frequency in Figure 3-23 is approximately 730 GHz versus the 900 GHz in Figure 3-22. This can be explained by the fact that electromagnetic rays propagating through the

material having $n = 3$ and k =0 propagate a longer optical distance as opposed to the 30mm material system of air thus extending the focal length that would have been relevant to air at a certain frequency.

The forward problem results validate the theoretical model of the input and output field distribution method.

3.2.5 Inverse Problem Solution from Synthesized Data

In this section, inverse problem solutions from synthesized data are carried out. These studies are carried out with the goal of showing the feasibility of using the input and output field distribution method for the characterization of multiple layer dielectric media. Three cases are considered: material characterization of a single dielectric layer along with thickness extraction, material characterization of a two dielectric layer stack along with thickness extraction and material characterization of a three dielectric layer stack with known thicknesses.

The results for the inverse problem solution were obtained between 0.2 THz and 2 THz with 0.0125 THz frequency resolution (found from the sampling period of the measured reference signal =0.0394 ps and the total number of points=2048).

In the first case, it was assumed that the dielectric stack was composed of a single dielectric layer with an unknown thickness. The dielectric layer had a thickness of l =1.982mm. Its refractive index real and imaginary parts across the whole frequency range were n =1.51 and k =0.002, respectively. To sum it up, this problem included three unknowns and as a result three equations were required corresponding to two input field distributions at two distances from the PRZP. The two input field distributions were synthesized at 50mm and 100mm. The layer properties were solved for at each frequency point. The preliminary initial guesses for the first phase of the root finding process were picked at random in the ranges 1.45 to 5, 0 to 0.1 and 0.125mm to 5mm for n, k and l respectively. The first phase ran three times with three

different randomly picked initial guesses before arriving at the extracted parameters used as initial guesses for the second phase of the root finding process. The third and final set of randomly picked initial guesses for the first phase before arriving at the extracted parameters were 2.3050, 0.0453 and 0.0016 for n, k and l respectively. The extracted parameters from the first phase which were used as the initial guesses for the second phase were actually the true parameters for the dielectric layer 1.51, 0.002 and 1.982mm for n, k and l respectively. Figure 3-24 shows the extracted parameters from the second phase of the root finding process.

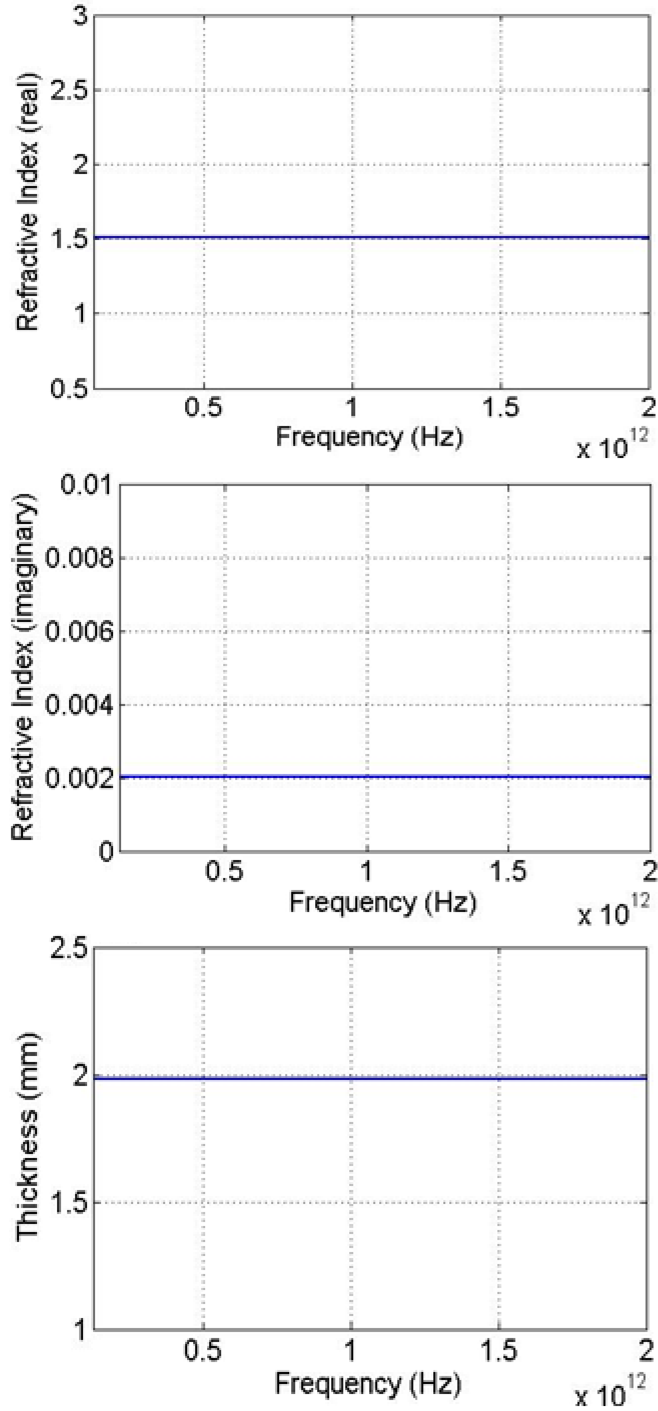

Figure 3-24. Extracted parameters of the single layer stack

In the second inverse problem solution case, it was assumed that the dielectric stack was composed of two layers with unknown thicknesses. The dielectric layers had thicknesses $l1$=0.513mm and $l2$=1.63mm. The refractive indices real and imaginary parts of both dielectric

layers across the whole frequency range were ($n1$=3.4278, $k1$=0.01) and ($n2$=1.96, $k2$=0.008), respectively. To sum it up, this problem included six unknowns and as a result six equations were required corresponding to three input field distributions at three distances from the PRZP. The three input field distributions were synthesized at 20mm, 30mm and 40mm. The layer properties were solved for at each frequency point. The preliminary initial guesses for the first phase of the root finding process were picked at random in the ranges 3.2 to 3.9, 0 to 0.02 and 0.462 mm to 0.5646 mm for $n1$, $k1$ and $l1$ respectively and 1.9 to 2.2, 0 to 0.02 and 1.5 mm to 1.8 mm for $n2$, $k2$ and $l2$ respectively. The first phase ran four times each time with a different set of randomly picked initial guesses before arriving at the extracted parameters used as initial guesses for the second phase of the root finding process. The fourth and final set of randomly picked initial guesses for the first phase before arriving at the extracted parameters were 3.8047, 0.0182 and 0.000472 for $n1$, $k1$ and $l1$ respectively and 1.9324, 0.0029 and 0.0016 for $n2$, $k2$ and $l2$ respectively. The extracted parameters from the first phase which were used as the initial guesses for the second phase were actually the true parameters for the dielectric layers. Figure 3-25 shows the extracted parameters from the second phase of the root finding process.

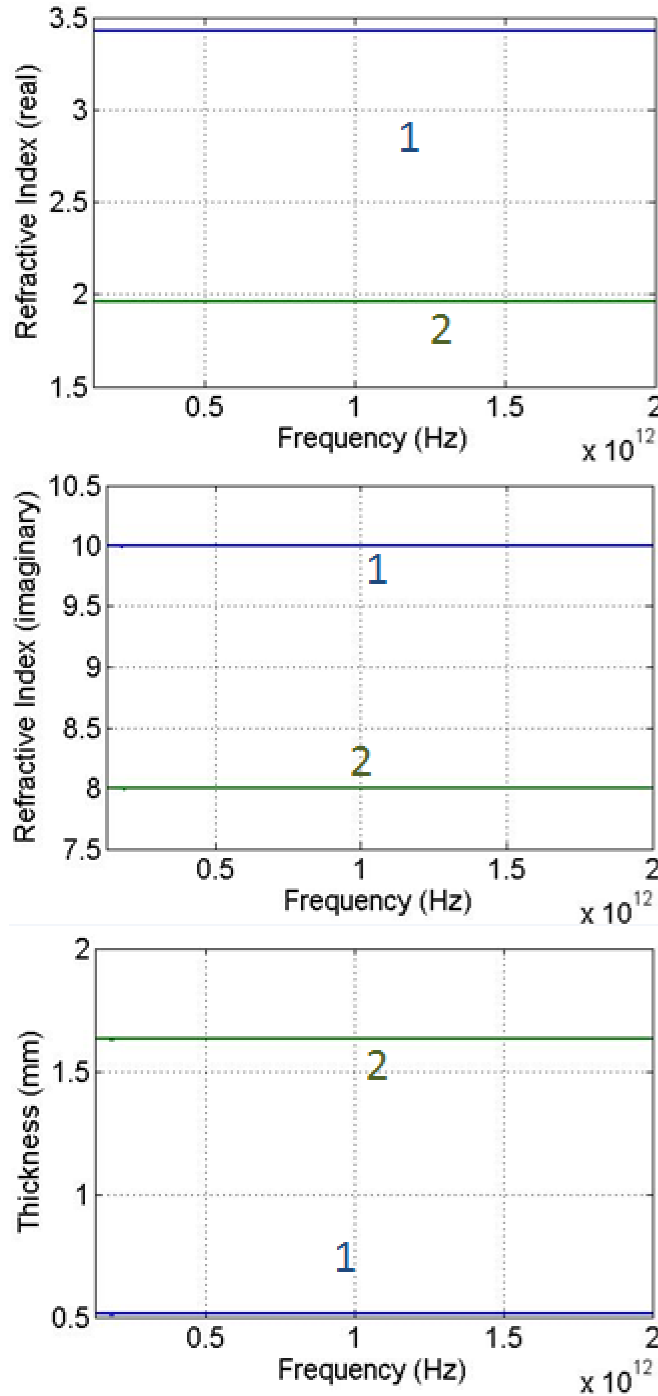

Figure 3-25. Extracted parameters of the two layer stack

In the third inverse problem solution case, it was assumed that the dielectric stack was composed of three dielectric layers with known thicknesses. The dielectric layers had thicknesses $l1$=1mm, $l2$=1.1mm and $l3$=0.85mm. The refractive indices real and imaginary parts of three dielectric layers across the whole frequency range were ($n1$=1.6, $k1$=0.06), ($n2$=1.8,

$k2$=0.001) and ($n3$=1.7, $k3$=0.005) respectively. To sum it up, this problem included six unknowns and as a result six equations were required corresponding to three input field distributions at three distances from the PRZP. The three input field distributions were synthesized at 30mm, 35mm and 45mm. The properties of all layers were solved at each frequency point. The preliminary initial guesses for the first phase of the root finding process were all picked at random in the ranges 1.45 to 1.9 for all the real parts of the indices of refraction and 0 to 0.05 for the imaginary parts of the indices of refraction. The first phase ran four times for each iteration with a different set of randomly picked initial guesses before arriving at the extracted parameters used as initial guesses for the second phase of the root finding process. The fourth and final set of randomly picked initial guesses for the first phase before arriving at the extracted parameters were 1.5526 and 0.0185 for $n1$ and $k1$, 1.8509 and 0.0428 for $n2$ and $k2$ and 1.6311 and 0.0159 for $n3$ and $k3$. The extracted parameters from the first phase which were used as the initial guesses for the second phase were actually the true parameters for the dielectric layers. Figure 3-26 shows the extracted parameters from the second phase of the root finding process.

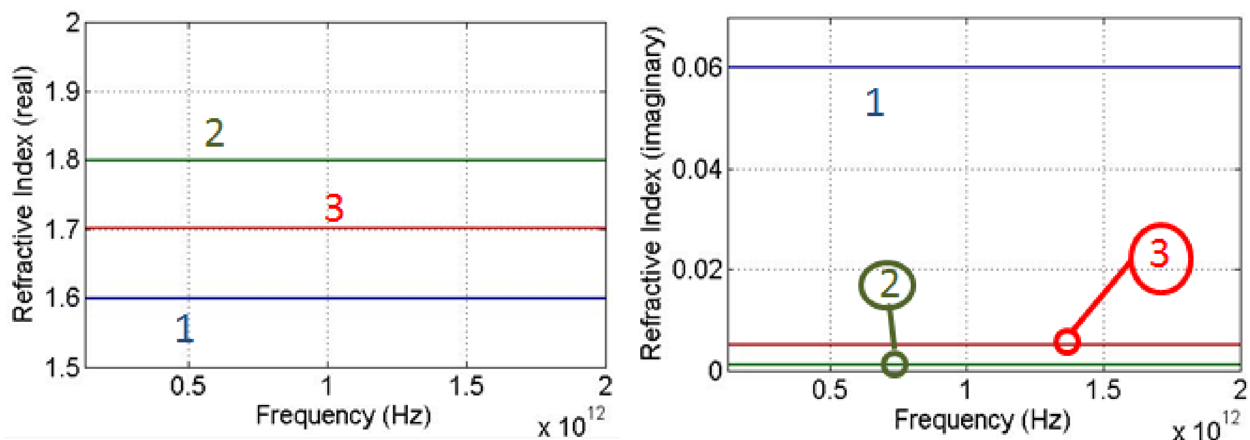

Figure 3-26. Extracted parameters of the three layer stackT

The results from the three cases that were tested show the feasibility of using the material characterization technique for multiple layer characterization in addition to single layer characterization with layer thickness extraction.

3.2.6 Experimental Implementation Discussion

Work on the implementation of the inverse problem solution using measured data is still in the process. Implementation effects pertaining to the THz system noise, instabilities and detection mechanism of the electromagnetic radiation at the receiver are currently being investigated. Due to the need for a slit scan using the single source and single detector setup, a decrease in the effective measured signal to noise ratio (SNR) is prone to happen. This decrease in the SNR has negative results consequences on the root finding method as it is not very robust to noise. The usage of a multi-objective function optimization mechanism instead of a root finding method for the inverse problem solution can be utilized. An optimization can be set up to be more robust to noise which is an issue with a root finding method such as the secant method. The signal power and time drifts occurring over time might prove to be an issue that must be accounted for in the implementation of the inverse problem solution from the measured data. Because field distributions are required to be measured, a pixel imaging scan is needed for each measured field distribution and thus the drifts might cause errors in the measured data especially that imaging scans take a long time. The next subsection presents work done towards the experimental implementation of the input and output field distribution method.

3.2.6.1 Phase Reversal Zone Plate Lens: Design, Fabrication and Testing

Here the design, fabrication and testing of a PRZP lens for the purpose of carrying out the inverse problem solution from measured data is presented. The PRZP designed structure is shown in Figure 3-27. As is seen in Figure 3-27, the 1-D PRZP is composed of a dielectric substrate having periodically spaced grooves in it.

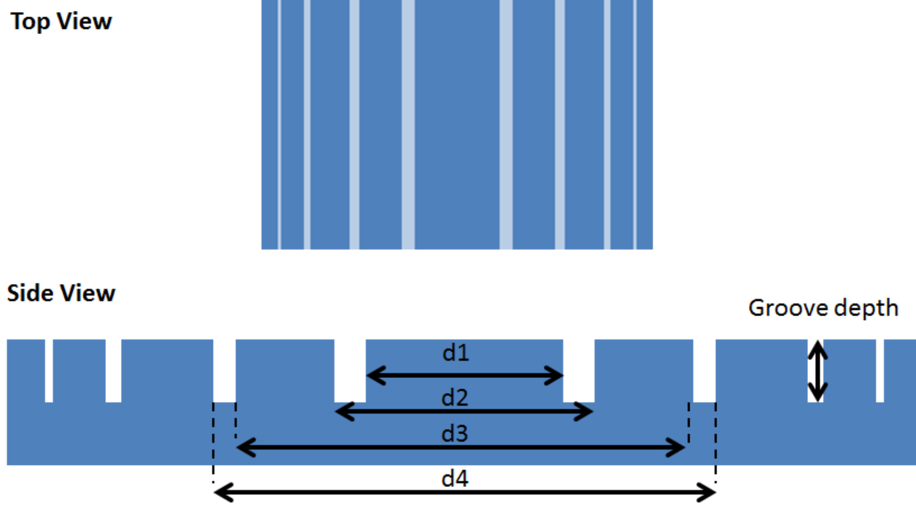

Figure 3-27. PRZP design structure

The zones of the PRZP are the alternating highs and lows in the dielectric substrate representing grooves and protrusions. The size of each zone is defined by a width d_i where i is the index of the zone under consideration. The size of each zone is a function of the design wavelength and design focal length of the PRZP. It is worthy to note that the groove zones are located in such a way where the diffraction caused by them on the wave transmitted through the PRZP adds in phase at the design focal length. On the other hand, the groove depth is designed such that the diffracted wave components from the protrusions add in phase with the diffraction resulting from the grooves. Further explanations and details on the PRZP are given in [60-61]. The expressions to find the width of each zone and the groove depth are respectively,

$$\left(\frac{d_i}{2}\right)^2 = i\frac{\lambda}{p} + \frac{i^2\lambda^2}{4} \tag{3-31}$$

and

$$GrooveDepth = \frac{c}{2f_d\left(\sqrt{\varepsilon_r}-1\right)} \tag{3-32}$$

where ε_r is the dielectric constant of the PRZP substrate. Note that the expression to find the zone widths is an approximation and as a result, the design expected operational performance might be slightly off. Given that the PRZP in this dissertation research is only required to generate different multi-feature input field distributions for different distances away from a material system, minor inconsistencies in the nature of the field distribution versus the design expectations are not crucial as they do not affect the goal or the performance of the material characterization technique.

Using the expressions in (3-31) and (3-32), a PRZP was designed to have 12 zones, and a 30mm design focal length at 600 GHz. The calculated overall cross-section of the design was 27.4 mm*27.4mm while the groove depth was calculated to be around 0.46mm. The chosen material for the PRZP was HDPE ($\varepsilon_r = 2.37$) [37]. The PRZP design was fabricated using a precision computer controlled plastic milling machine. After fabricating the PRZP it was tested using the THz system. The measurement system utilized for measuring the distribution of the PRZP is shown in Figure 3-28. The transmitter, receiver and PRZP apertures are aligned to be parallel to each other. The PRZP is centered within the transmitter collimated beam. A 1.5mm wide slit is attached to the receiver. The receiver along with the slit, scan the field distribution as a result of the PRZP vertically. The number of data points collected at the receiver end is 128 which translates to steps of 0.22mm. The PRZP is mounted on a rail which can be used to modify the distance between the PRZP and the receiver resulting in a different measured field distribution. In order to block any other extraneous signals outside of the PRZP cross-sectional area, a copper screen is utilized with a square hole as big as the PRZP cross-sectional area. It is understood that this might affect the field distribution collected at the receiver. This however does not have any negative effect on the material characterization technique. This is because the

technique requires solely unique input field distributions which result in unique output field distributions regardless of the nature of how they were generated as it is the material system properties that determine the relation between the input and output field distributions

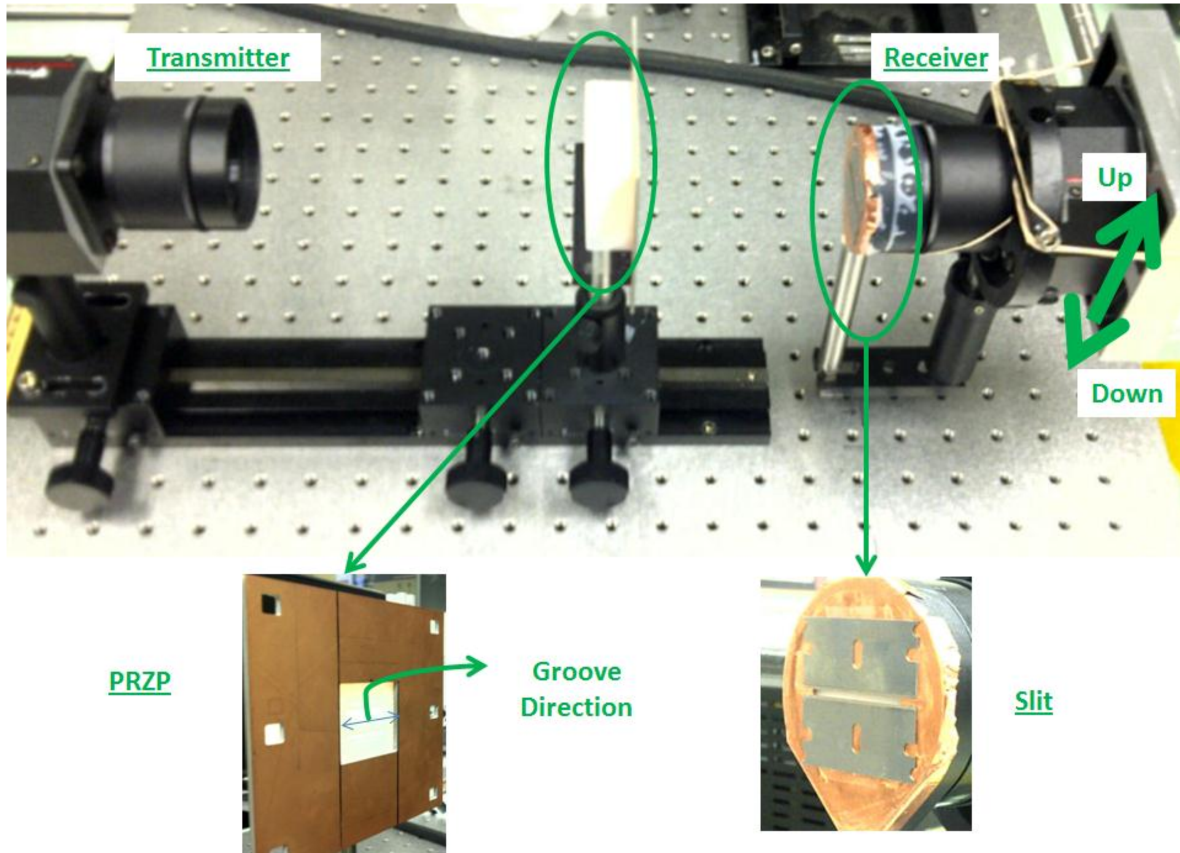

Figure 3-28. PRZP field distribution measurement setup

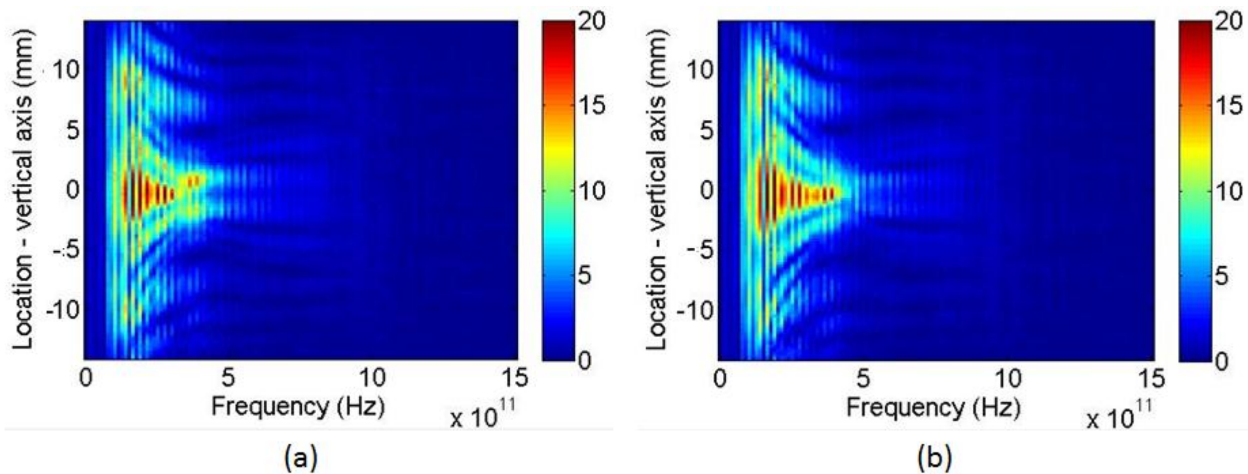

Figure 3-29. Magnitude of field distribution as a result of the PRZP measured at: (a) 15.5mm and (b) 20mm

The field distribution due to the PRZP was measured at two receiver locations (distance). These were at approximately 15.5mm and 20mm. The magnitudes of the measured field distributions are shown in Figure 3-29.

The results shown in Figure 3-29 prove that different field distributions can be obtained as a result of moving the PRZP along the direction normal to its surface. This shows that the PRZP can be used in order to generate different input field distributions to the material system which are used for the material characterization technique. Additionally, the results show that the frequency at which the PRZP obtains focus at 15.5mm is around 325 GHz while the frequency at which the PRZP obtains focus at 20mm is around 437.5 GHz. These results are relatively close to what can be predicted using equation (3-30). The focal lengths calculated from (3-30) at 325 GHz and 437.5 GHz are 16.25mm and 21.8mm respectively. The differences might be partly due to the decreasing trend of the power stored in the THz signal as frequency increases. Additionally, distance setting uncertainty might play a role in these differences aside from that the design equation for the PRZP in (3-30) is an approximation.

CHAPTER 4

SMALL AREA INTERROGATION AND SPECTROSCOPY – CHARACTERIZATION OF 3D COMPOSITE MATERIAL STRUCTURES

4.1 Problem Definition and Motivation

In the preceding chapters of this dissertation, the methods presented for characterizing dielectric properties of material systems have been shown to satisfy material systems that are homogeneous along the direction parallel to the surface of the system. The ability to characterize the properties of material systems which are generally heterogeneous along more directions would have great positive impact in many fields due to the flexibility provided.

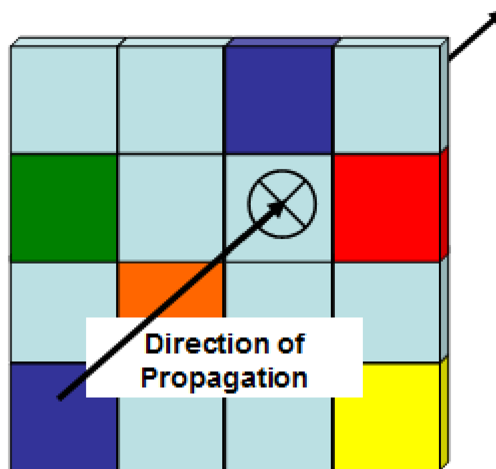

Figure 4-1. Composite structure, homogeneous along the direction normal to its surface

Given certain provisions, the methods presented up to this point can be used to characterize composite material structures. The single layer material characterization methods have the capability to characterize material structures that are homogeneous only along the direction normal to the surface of the material system. Figure 4-1 shows a sketch of such a system. That system can be thought of as composed of small sections of homogeneous materials. If the THz radiation beam can be made (or focused) to have a cross-sectional area that is smaller than the

cross-sectional area of the smallest homogeneous section of the composite structure, then both single layer methods can be used to characterize the structure by scanning the THz beam section by section. Ideally, the way to realize such a beam is by modifying the measurement setup to radiate a collimated beam having a cross-sectional area (or diameter) that is smaller than that of the smallest homogeneous material section. This can be done using a set of plano-convex lenses with decreasing diameters and alternating directions. However, alignment and spacing issues arise with this approach.

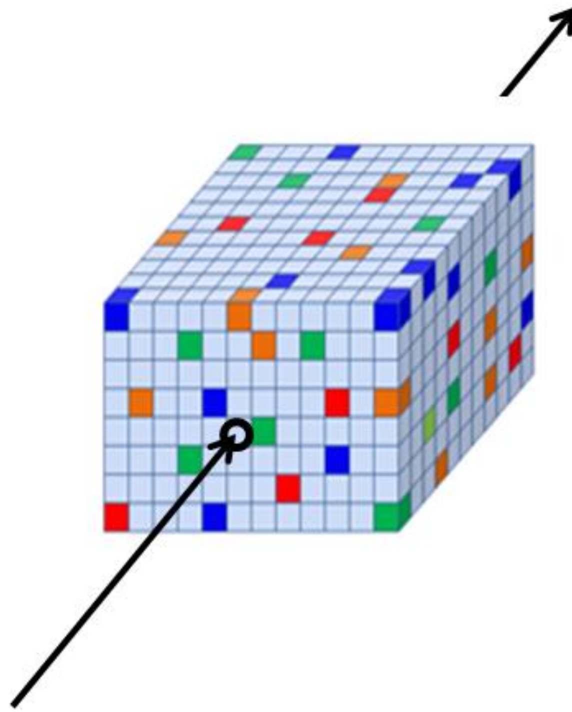

Figure 4-2. Composite structure, heterogeneous along all directions

Additionally, under ideal circumstances the multiple layer methods can be adjusted to characterize the material properties of composite systems that are heterogeneous along all directions. A sketch of a heterogeneous material system is shown in Figure 4-2. For the multiple angle method, not only should the THz radiation beam cross-sectional area be smaller than that of the smallest homogeneous section of the composite structure but also the effects of oblique

wave propagation in the structure due to its thickness must be dealt with (effects ignored under the thin lens approximation). These effects have decreased impact the thinner the composite material structure is optically. The input and output field distribution method can also be used to characterize a heterogeneous material system. This is possible given different input field distributions which can be achieved using a phase reversal zone plate lens or different types of lenses. The provision that would have to be made here is that the field distribution cross sectional area at the input and output would have to be truncated such that it is smaller than that of the smallest homogeneous material section.

In this chapter, a tool for characterizing composite materials at small stand-off distance (especially near field region) in transmission mode using a single source and detector measurement setup is demonstrated. This tool can be used for small area interrogation (or high resolution imaging and/or spectroscopy) or even for extracting material properties of homogeneous sections of a composite material structure when used in conjunction with an accommodating material characterization technique. The tool has sub-wavelength focusing characteristics and maintains a wide operational bandwidth. It overcomes alignment issues encountered when using lenses for small volume interrogation. This is because it focuses at small stand-off distance.

4.2 Terahertz Dielectric Sub-wavelength Focusing Probe

Note: this work is partially documented in [62].

4.2.1 Probe Design

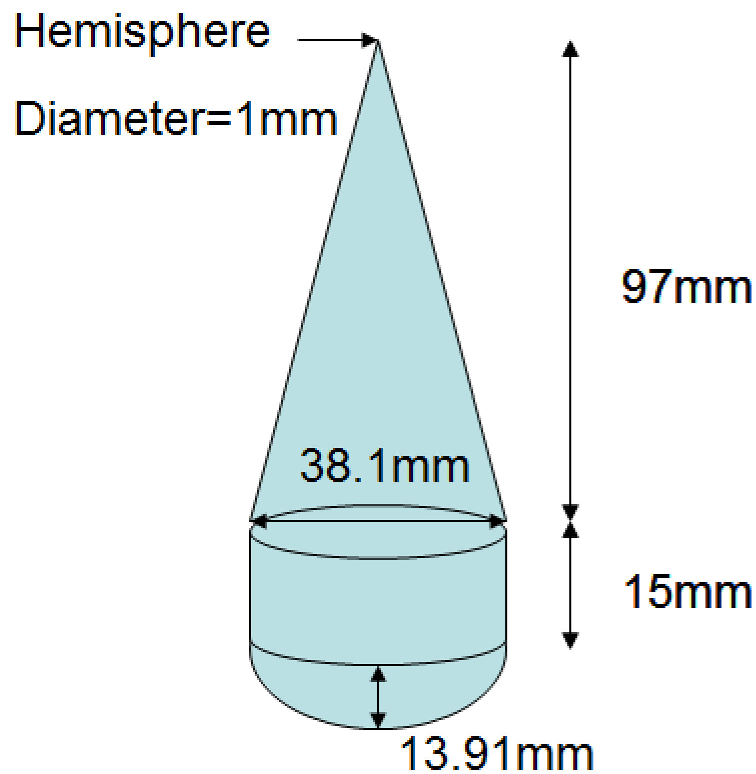

Figure 4-3. Conical probe geometry

Recently, a Teflon dielectric probe was demonstrated [63]. This work showed that a simple pencil-tip shaped dielectric probe can be used in high resolution imaging in the millimeter wave frequency range. Building upon this design, it was found that by using simple geometric shaping of low-loss dielectrics, desired probe characteristics for THz applications can be achieved. The desired characteristics include sub-wavelength focusing, wide-bandwidth, low signal attenuation and ease of fabrication. The signal attenuation caused by the probe is largely dictated by the material properties, geometry and fabrication imperfections. The focusing resolution on the other hand is largely determined by the geometry of the probe. High-density polyethylene was chosen as the probe material because of its low-loss over a wide frequency band, ease of machining and

relative low-cost. High density polyethylene (HDPE) has relatively unchanging dielectric properties from (0.2 THz up to around 1.8 THz) [24-25, 37]. It also has a relatively low dielectric constant (ε_r = 2.37) and thus the need for anti-reflection coatings is less. The shape of the probe borrows principles from quasi optical component design such as lenses, dielectric tapering and polarization maintaining approaches.

The probes are designed for the THz time-domain system, which has separate transmitter and receiver heads. The optics on these heads are designed to transmit and receive linearly polarized collimated electromagnetic pulses. To couple the probes with these heads, the ends of the probes were designed to be plano-convex lenses with a radius (20mm) to cover the whole collimating beam cross section (38.1mm diameter). A cylinder of height equaling 15mm and diameter equaling 38.1mm was added as a delay medium and also to be used in holding and mounting the probe. A shallowly tapered cone (with a 22° vertex angle) with a length of about 97mm is built on top of this cylinder. The small tip of the probe was shaped like a small hemisphere having a diameter of approximately 1mm. The plano-convex lens focuses the collimated beam into the beginning of the cone. The cone then guides the wave to the small tip of the probe. Figure 4-3 shows a sketch diagram of the conical probe.

4.2.2 Probe Simulation

The probe design (see Figure 4-3) was simulated in order to observe its focusing resolution. The simulation was carried out using Ansoft HFSS 13. The source in the simulation setup was set to be a linearly polarized plane wave traveling along the axial direction of the probe. The simulation was carried out at 200 GHz. The results examined were in the form of the magnitude of the field distribution at different locations with respect to the dielectric probe.

The computational cost of simulating such a structure is very high. The structure dimensions are large with respect to a wavelength and as a result a very large number of unknowns is needed in order to complete the simulation (>200000 unknowns). A desktop computer with 16GB of RAM failed to complete the simulation. Had the collimated beam diameter been smaller, most of the design dimensions would have been smaller as well. This is because the probe design dimensions were dependent on the 38.1mm diameter collimated beam. While maintaining the same taper angle and diameter of the hemispherical tip, it is hypothesized that similar focusing can be obtained using a scaled version of the probe design from Figure 4-3 given that the collimated beam is scaled by the same factor. Note that this remains true as long as the scaling of the dimensions keeps the simulated structure large with respect to the wavelength (similar to focusing lens size requirements). The simulated structure dimensions were scaled by 5 from the true design dimensions. Figure 4-4 shows the simulated structure in red while the true design is shown in blue.

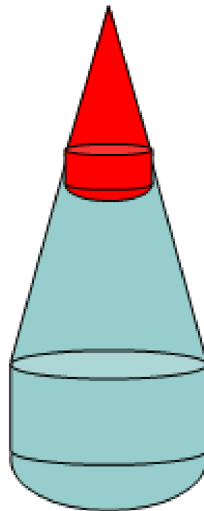

Figure 4-4. True design (blue) versus simulated design (red)

Figure 4-5 shows the cross-sectional field distribution in and around the probe. It is clear that the plano-convex lens succeeds in focusing the wave to a focal spot at the beginning of the

tapered cone. Afterwards the wave is accumulated further and further into a smaller cross-sectional area as the cone cross section becomes smaller. The field distribution shows a high intensity focal spot close to the tip. The distribution shows less field confinement away from the probe tip.

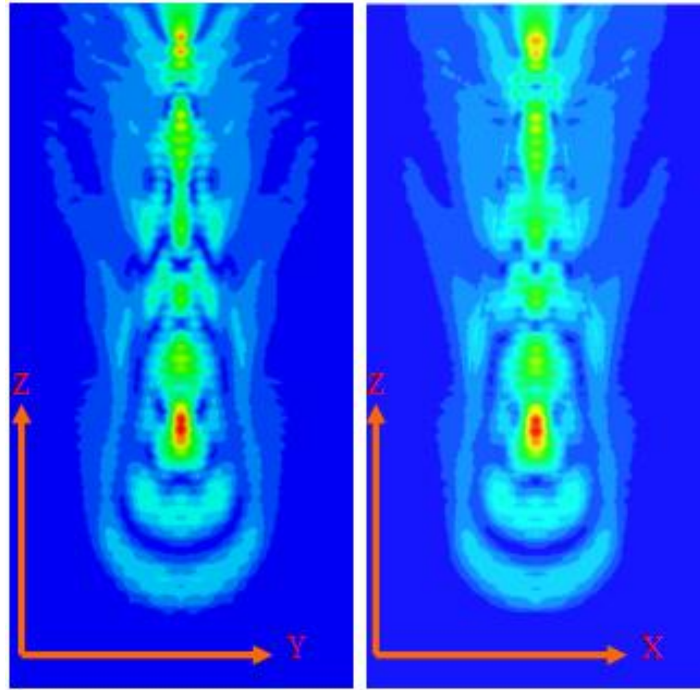

Figure 4-5. Complex field distribution magnitude (red=highest intensity, blue=lowest intensity)

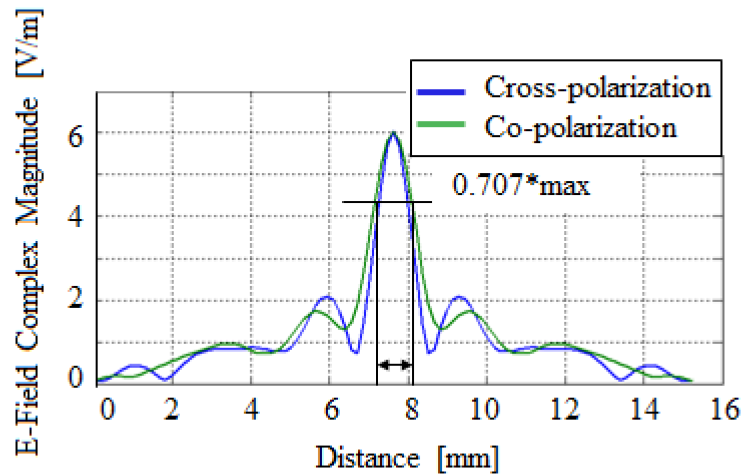

Figure 4-6. Electric field complex magnitude 0.15mm away from the tip

Figure 4-6 shows the field distribution along the cross- and co-polarization lines at 0.15mm away from the tip of the probe. Taking the half power of these distributions results in a resolution

of around 0.7mm which is sub-wavelength (wavelength at 200 GHz = 1.5 mm). In conclusion, the simulation results show that the probe design can achieve the intended sub-wavelength resolution property. As a result, the probe design was adopted for fabrication.

4.2.3 Probe Fabrication and Experimental Testing

Figure 4-7. Probe measurement setup

The conical probe was fabricated using a CNC machine. It was ensured that the surface of the probe was smooth. The probes were characterized using the T-ray 2000 time domain terahertz system from Picometrix. All the measurements were carried out in transmission mode, where the signal from the transmitter passes through two probes facing each other and is received on the opposite end. A photograph of this setup is shown in Figure 4-7. Using this setup, the operational bandwidth and spatial resolution of the probes were measured. Additionally, a leaf imaging experiment utilizing the wide bandwidth and sub-wavelength focusing properties of the probe simultaneously was carried out.

4.2.3.1 Bandwidth Testing

The bandwidth of the probe was found by measuring the transmission through both probes facing each other with their tips barely in contact (see Figure 4-7). The operational frequency

band was defined as the frequency range limited by noise on the lower end below 50 GHz and by the noise floor on the higher end of the magnitude of the Fourier transform of the time domain signal transmitted through both probes. Figure 4-8 shows the magnitude of the Fourier transform of the time domain signal transmitted through the probes. The measured bandwidth of the probe is approximately 900 GHz ranging from 50 GHz to 950 GHz. The decreasing trend in the transmitted signal is to a large part due to the power generated by the transmitter and not only to losses or scattering in the probes.

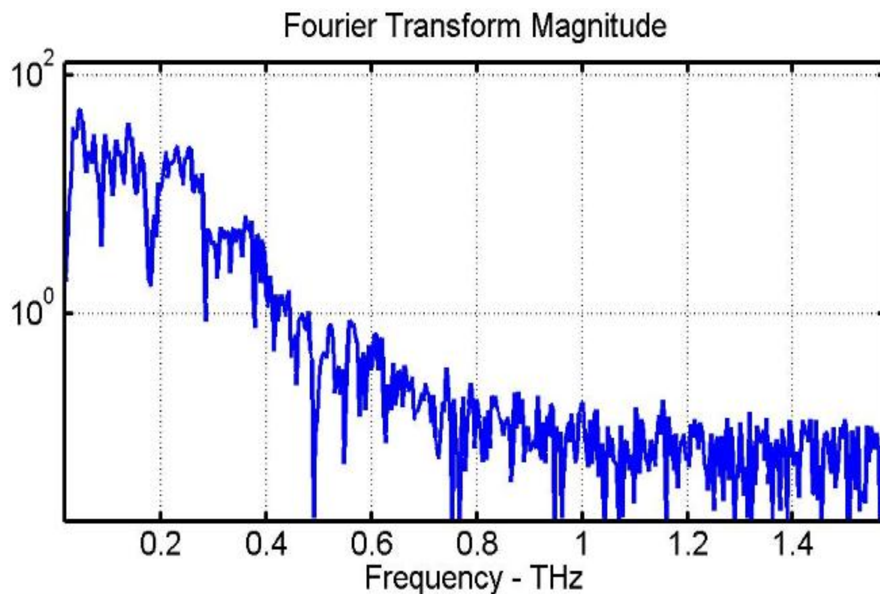

Figure 4-8. Transmitted signal magnitude spectrum

4.2.3.2 Imaging Resolution Testing

Terahertz imaging has the characteristic, unlike infrared, of being transparent to a wide range of dielectric substrates [64]. Unlike X-rays, THz radiation is nonionizing. This is very attractive for imaging of biological tissue. In comparison to microwave and millimeter wave imaging, higher resolution imaging can be generated using THz because of its inherent smaller wavelength.

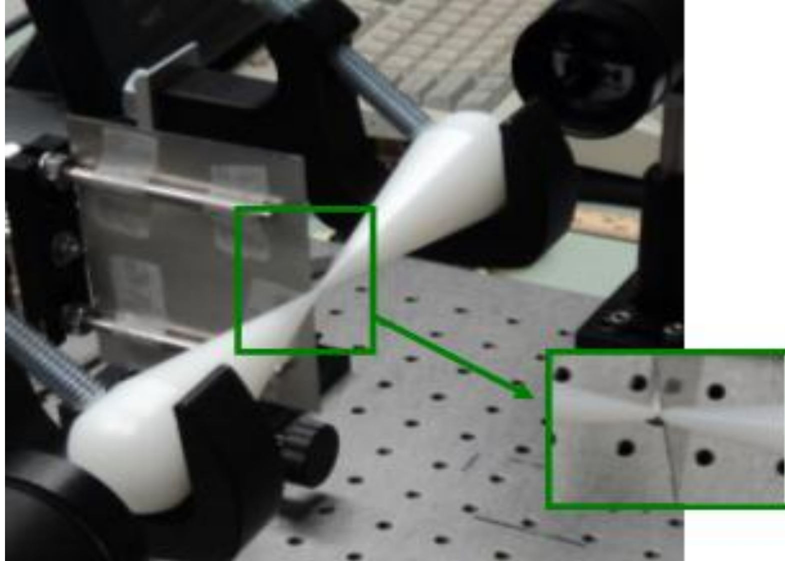

Figure 4-9. Resolution measurement for the conical focusing probes

Knowing that the focusing resolution of the probes is essential information for carrying out imaging scans. The resolution of the probes was obtained through measurement by setting the probes opposite to each other separated at their tips by approximately a 0.75mm air gap. In the gap, a thin metal plate with a sharp edge was moved along a line in 0.1mm increments for a total line length of 10mm (see Figure 4-9). The time domain transmitted signal was measured as a function of metal plate edge raster location. The magnitude of the Fourier transform of every time domain signal was then found, giving a broad band frequency signal. Figure 4-10 shows the measured magnitude of the Fourier transform for a fixed frequency (212.5 GHz) as a function of metal plate edge raster location. A first order smoothing function is fitted to the measured data. The data trend appears to be a step function with a high magnitude value corresponding to the transmitted signal when no metal is present between the probes. The finesse of the focusing of the probe corresponds to a more ideal step function. The gradient of the obtained step functions hence provides a Gaussian like curve. The half power of the Gaussian curve corresponds to the resolution of the probe at the corresponding frequency. This approach to measuring spatial resolution is based upon work presented in [65].

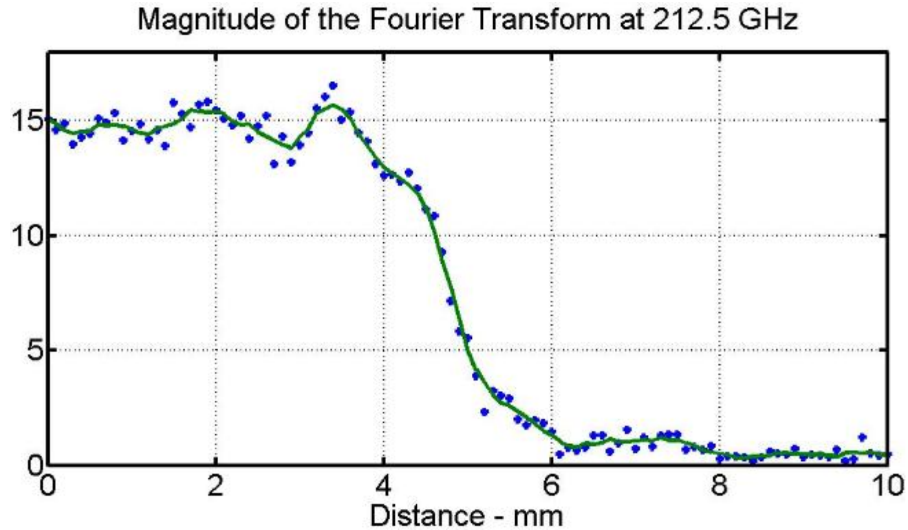

Figure 4-10. Fourier transform magnitude at 212.5 GHz

Figure 4-11 shows the gradient of the smoothened version of the magnitude of the Fourier transform of the transmitted signal in addition to its half power resolution. Finally, Figure 4-12 presents the resolution of the probe at different frequencies using the same approach. It is clear from Figure 4-12 that the probe is characterized by having sub-wavelength focusing resolution varying between 0.2 wavelengths to 0.45 wavelengths in a frequency band ranging from 75 GHz up to 212.5 GHz. At higher frequencies, the sub-wavelength resolution characteristic is lost. However, the actual resolution is expected to be better. The loss of sub-wavelength focusing for this probe can be attributed to the distance between the probes, misalignments and coarse movement of the robotic arm and more importantly the machining of the probe tip ends. Thus there is significant room for the improvement of the probe. These results, however, do show that the probe can be used for fine resolution imaging and probing which holds promise for many applications.

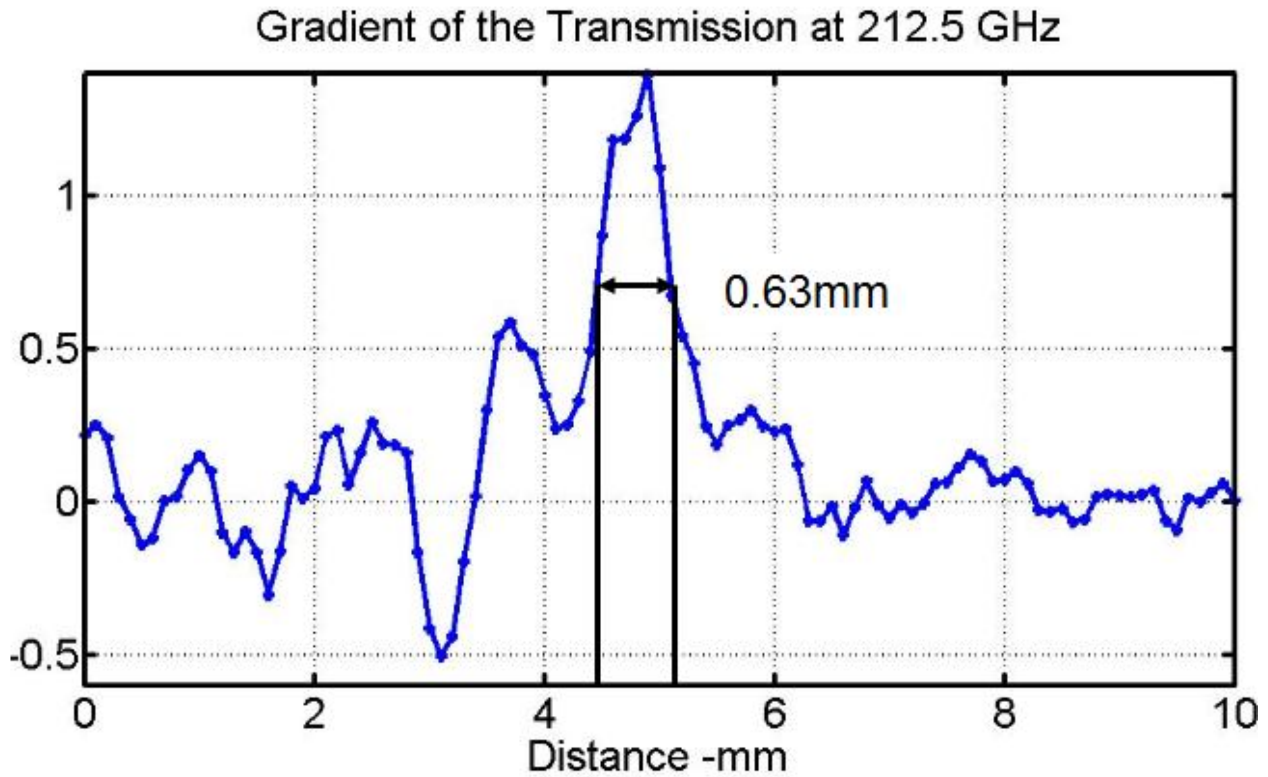

Figure 4-11. Gradient of the magnitude of the Fourier transform with it half power resolution

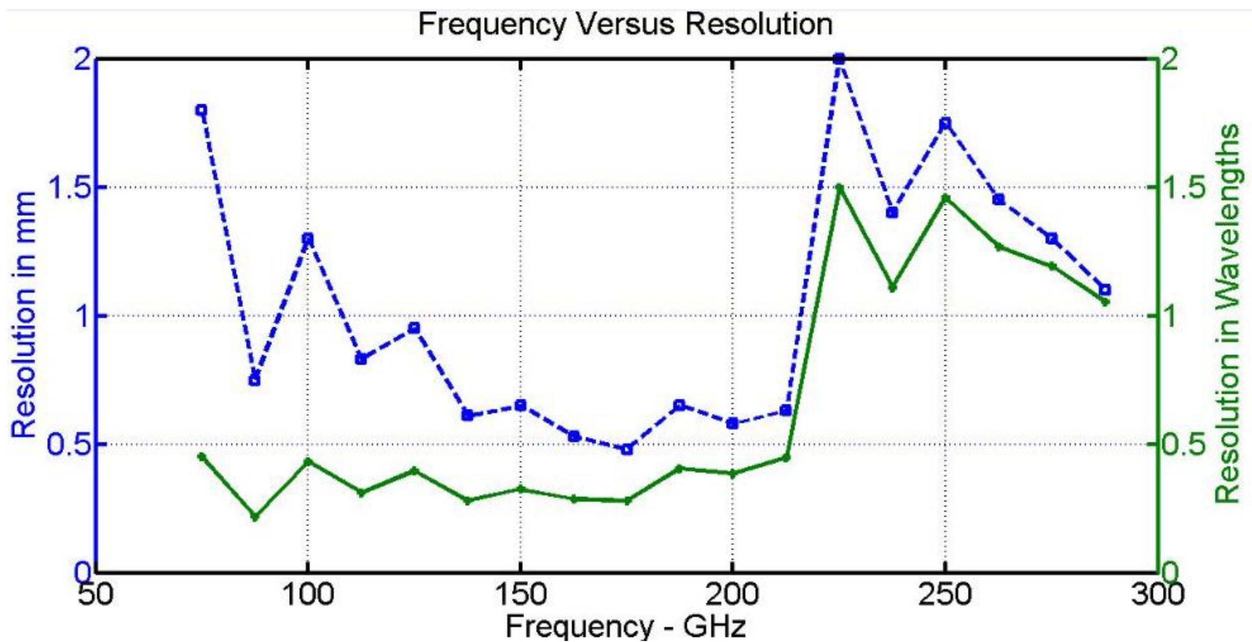

Figure 4-12. Resolution as a function of frequency for the conical probe

4.2.3.3 Simultaneous Imaging and Spectroscopy Experiment

The sub-wavelength focusing ability and wideband characteristic of the probe was used for simultaneous imaging and spectroscopy of a green leaf. The imaging was carried out in

transmission mode. A green leaf from a tree was placed between two thin porous paper based pieces of tape. The tape was used in order to hold the leaf between the two probes and stretch it without damaging it. The total average thickness of the leaf along with its tape holders was approximately 0.65 mm. The total distance between the probes was 0.75 mm. The imaged window section of the leaf was 8mm*10mm. The leaf along with its imaged window is shown in Figure 4-13.

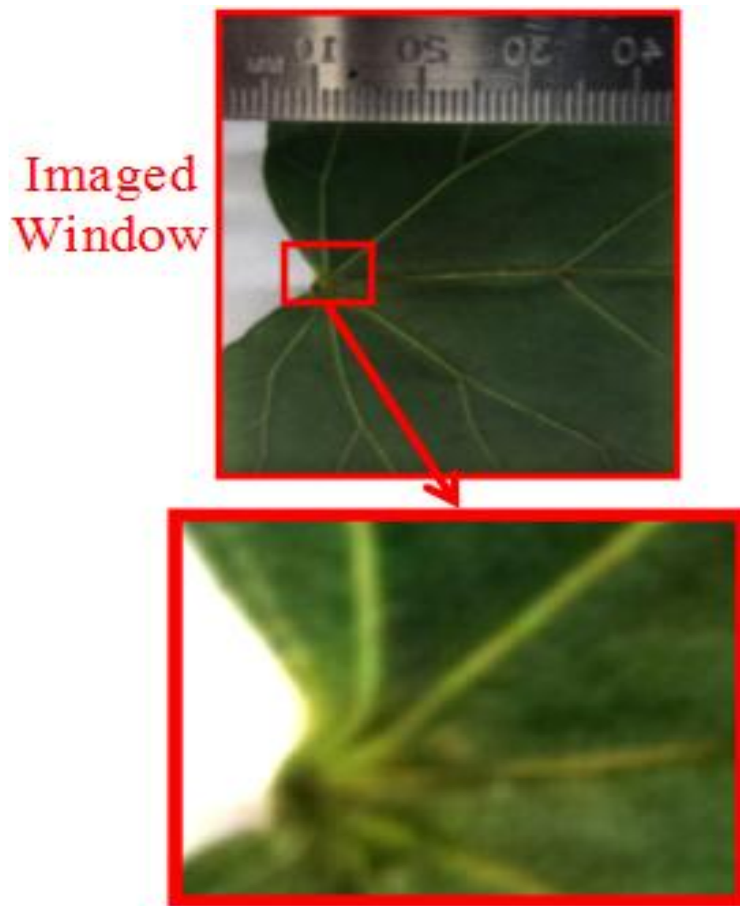

Figure 4-13. Leaf imaged window

The imaging results obtained show high transmission through the regions of the leaf that have low quantities of water while lower transmission is apparent when water is abundant in the leaf (such as the leaf veins). The explanation behind this phenomenon is traced back to the fact the water is highly attenuating in the THz frequency range. Additionally the broadband nature of

the probes makes use of the time domain THz pulse in order to image at a wide frequency range at each pixel in a single measurement. Figure 4-14 shows the images obtained at 137.5, 175 and 200 GHz. Refering back to Figure 4-12, it is clear that the finest imaging resolution for the probe is at 175 GHz. This can be correlated to the resolution of the imaging results obtained in Figure 4-14 where the finest level of detail is seen in the 175 GHz image.

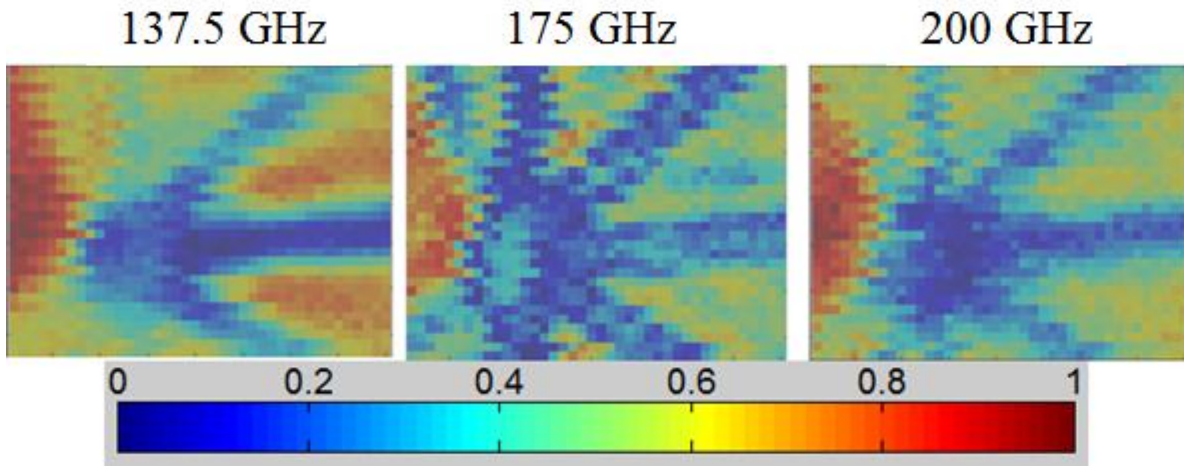

Figure 4-14. Leaf images at different frequencies

Consider the imaged leaf to be a composite structure. Based on the results of the experiment, it can be prospected that another purpose for which the probe was designed is feasible: composite structure material characterization. The frequency dependent information obtained at every pixel of the leaf can be used to extract the pixel's material properties using one of the characterization methods outlined in the previous chapters. Carrying out this operation at every pixel ultimately results in characterizing the material properties of the leaf (or the composite material system).

CHAPTER 5

CONCLUSIONS AND FUTURE WORK

5.1 Conclusions

In this dissertation, tools and techniques for characterizing layered dielectric materials in the THz spectral region have been presented. These have been devised to work for many special cases of material characterization scenarios providing a variety of solutions for previously encountered challenges in the area of THz material characterization. In general, the research work carried out under this dissertation serves as a stepping stone towards characterization of complex 3-D composite material systems.

Two methods for characterizing single layer dielectric material samples have been presented. The first of these is the reference requiring method. This method builds upon the THz material characterization techniques documented in the literature (especially [27]). In particular, improvements to the method presented in [27] include the usage of the Nelder and Mead optimization method which is robust to noise. Also, here the optimization was carried out at discrete frequency points independently instead of the whole frequency range at once thus decreasing the possibility for errors in the extracted parameters. This allows for the preservation of spectral data at all measured frequencies and is important for attaining the spectral content of a sample. Using this method, a library of material characteristics in the THz frequency range was produced. The material properties which were extracted as a result of this method have been made available to the scientific community on an online webpage. Additionally, the reference requiring method was used in order to examine moisture content in polyimide films. It was shown that the extracted dielectric constant and loss tangent of polyimide films increase with higher moisture content. In the reference requiring method, the thickness of the sample under test

has to be known accurately. In order to determine the sensitivity of extracted material parameters to the thickness, an error analysis studying the effect of the dielectric sample thickness measurement accuracy on the reference requiring method was carried out. It was concluded that the reference requiring method becomes increasingly sensitive to the thickness measurement accuracy as the physical thickness of the sample to be characterized becomes smaller and as the dielectric constant of samples having the same physical thickness increases. It was also observed that the reference requiring method is not equally sensitive to dielectric samples having the same optical thickness.

The second of the single layer dielectric material characterization methods presented in this dissertation is the self-calibrating method. Unlike the reference requiring method, the self-calibrating technique only requires a single sample measurement to extract the dielectric material properties and avoids the use of a separate reference measured signal. The self-calibrating technique relates parts of the sample signal measurement to the whole signal in order to carry out the material parameter extraction. The need for only a sample measurement also contributes to saving valuable data collection time which becomes crucial in long imaging and spectroscopy scans. More importantly, the self-calibrating technique overcomes errors faced by reference requiring methods due to differences between reference and sample signals occurring as a result of THz system drifts. Post processing of measured data prior to extracting material parameters is presented. The main aim of the post processing is to remove any system artifacts from the measured sample signal which are not accounted for in the theoretical model. The material characterization results obtained using the self-calibrating method match to within small margins of difference material parameters documented in the literature. The method limitations are also discussed. Similar to the reference requiring method, the self-calibrating technique also requires

prior knowledge of sample thickness for material parameter extraction. As a result, an error analysis study to examine the sensitivity of the self-calibrating technique to the thickness measurement accuracy was carried out. The observations made from the error analysis results are similar to those obtained for the reference requiring method thickness accuracy error analysis. However, it was also concluded that the self-calibrating method is more sensitive to the thickness measurement accuracy then the reference requiring method while maintaining lesser ringing in the extracted parameters as a function of frequency.

Two methods for characterizing multiple layer dielectric material samples were presented. These methods can also be used in carrying out single layer material characterization along with layer thickness extraction. The first of these methods is the multiple angle method. The relationship between a reference signal transmitted through air and signals transmitted through a material system at different angles of incidence are utilized to extract the unknown material properties. The total number of different incidence angle sample measurements required for the material characterization process is dependent on the number of unknown parameters to be extracted. The material characterization method's root finding process which solves a system of equations was the secant method. The root finding process setup is presented. The forward problem solution results show good matching between measured and calculated data. The inverse problem solution results of the multiple angle method from synthesized signals show the feasibility of the application of the material characterization method for single and multiple layer material characterization. It should be noted that the secant method fails to converge to a solution at some discrete frequency points as the complexity of the problem increases. The material characterization results obtained using the multiple angle method for single layer characterization along with thickness extraction match to within small margins of difference

material parameters documented in the literature. For the two layer dielectric stacks, the extracted dielectric constants match to within a small margin of difference the dielectric constants documented in the literature. The extracted loss tangents on the other hand are larger than the true values in the literature. Possible reasons for the mismatch include air gaps between the layers of the stack and/or THz source instabilities effects on the measured sample signals. The multiple angle method requires the sample signal angle settings as inputs. As a result, an error analysis study to examine the sensitivity of the technique to the angle setting accuracy was carried out through characterizing a single layer dielectric sample with known and unknown thicknesses. The observations made from the error analysis results show that the technique is more sensitive to the accuracy of the angle setting as the angle of incidence approaches the Brewster's angle when extracting the dielectric constant. This effect however is not true for the loss tangent. Also, given the choice to pick the equations for the root finding process such as in the case of a single layer characterization with thickness extraction which requires three equations but has four available equations (from two sample measurements); the choice of the equation must not be arbitrary. The error analysis study shows that the sensitivity of the technique differs for the choice of equations.

The second of the multiple layer dielectric material characterization methods presented in this dissertation is the input and output field distribution method. While the other material characterization methods work for single source and detector measurement setups, this method is devised for a single source and multiple detector setup. The method is based upon the idea that if the field distributions at two parallel planes (before and after the sample respectively) are known then the material properties of the medium (or a material system) between the two planes can be found. For a material system composed of multiple dielectric layers, the knowledge of several

input field distributions and output field distributions are required. By using a phase reversal zone plate (PRZP) Fresnel lens and its placement distance from the sample different field distributions can be attained. The total number of input and output field distribution pairs required for the material characterization process is dependent on the number of unknown parameters to be extracted. The material characterization method's root finding process which solves a system of equations was the secant method. The root finding process setup is presented. The forward problem solution from synthesized signals proves the validity of the theoretical model. The inverse problem solution from synthesized signals validates the use of this technique for characterization of multi-layered dielectric structures. The design and experimental testing of a PRZP lens is carried out towards implementing the material characterization method from measured field distributions.

By employing the dielectric sub-wavelength focusing probes presented in chapter 4 in a single source and detector setup, a means to achieving material characterization of 3-D composite material systems is provided. To extract material information about the composite 3-D structure, this setup has to be used in conjunction with one of the material characterization techniques described in chapters 2 and 3. The designed probes have wide operational bandwidth and fine sub-wavelength focusing resolution characteristics which were verified experimentally.

5.2 Future Work

The measured signals needed for the reference requiring method are prone to the THz system amplitude and time drifts. These effects result in errors in the extracted parameters. To determine how much the THz system drifts affect the technique, possible future work in this arena includes error analysis studies examining the sensitivity of the reference requiring method to THz system drifts and instabilities. Additionally, approaches for improving the THz system to decrease its amplitude and time drifts would be highly useful.

The self-calibrating method requires post measurement processing of data in order to remove system artifacts from the measurements prior to extracting the material properties. The system artifacts removal procedure demonstrated in this dissertation does not account for all the dispersion effects in the material, and hence the self-calibrating technique currently works better for materials with low dispersion. Future work can include alternative system artifacts removal solutions that do account better for dispersion in order to widen the scope of material properties that can be extracted accurately using the self-calibrating technique. Solutions can include post measurement processing procedures or improvements to the measurement system.

Future work on the multiple angle method must include the usage of a more robust root finding algorithm or a constrained multi-objective function optimization for the inverse problem solution. Additionally to fully realize the sensitivities of the multiple angle method, further error analysis studies to examine the sensitivity of the technique to possible air gaps between the layers of a stack and THz system drifts and instabilities are needed. Additionally, the incorporation of a self-calibrating technique in the characterization theory of the multiple angle method can be investigated in order to decrease the effect of the THz system drifts and instabilities on the extracted parameters.

Pertaining to the input and output field distribution method, future work includes carrying out the inverse problem solution from measured data. This requires accounting for the THz system issues such as the measured signal to noise ratio, detection mechanism, system instabilities and the usage of an optimization method that is more robust to noise then the root finding secant method if needed.

Finally with respect to the dielectric sub-wavelength THz focusing probes, possible future work routes include the design and fabrication of a better performance probe in terms of bandwidth and resolution. Additionally the implementation of a 3-D composite structure material characterization should be carried out using the probes in a single source and detector measurement setup along with one of the material characterization techniques demonstrated in chapters 2 and 3 in order to realize their full capacity.

APPENDICES

Appendix A

The Nelder and Mead Modified Simplex Optimization Method

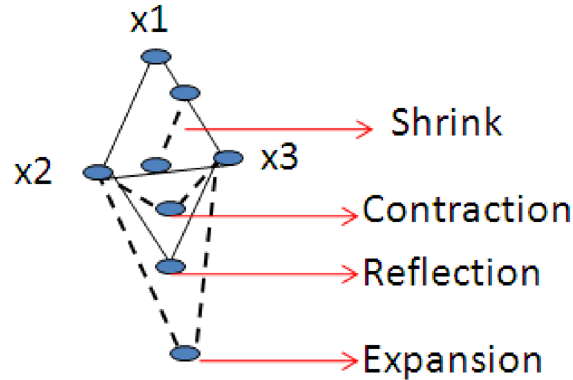

Figure A-1. Nelder and Mead Simplex method possible movements

The Nelder and Mead modified Simplex method doesn't require the knowledge of an analytic expression for the derivative of the objective function and hence is a direct search method. It is an unconstrained optimization method making it computationally robust [39]. The method is also applicable on problems solving for several variables making it useful in the case of single layer material characterization methods as there is a need to extract the real and imaginary parts of the refractive index, n and k respectively. In this method, $N+1$ function values are evaluated in the multivariable space where N is the number of variables for the optimization and the $N+1$ vertices are equidistantly separated composing a polyhedron in space. The polyhedron is called a simplex. The vertex with the highest function value is then substituted with a vertex having a lower function value through a reflection, expansion, contraction or shrinking operation. Figure A-1 shows the possible movement alterations of a simplex as a result of the Nelder and Mead Simplex method. If x1, x2, and x3 are the vertices that compose the initial simplex, and assuming that x1 is the vertex with the worst function value, going through the method will result in one of the four modifications on the initial simplex

to produce a new one. It is worthy to note that the shrink alteration is done by preserving the vertex with the least function value and shrinking the simplex spread accordingly [40].

The choice of alteration is specified by a set of rules. These go as follow for a single iteration of the Nelder Mead Simplex Method: [40]

1. Given a simplex polyhedron, the fitness function is evaluated at every vertex. The fitness function values are then ordered from the least to the highest. In this case, assuming the simplex is two dimensional; three vertices are present in the simplex at any instant. Assume these vertices to be x_{low}, x_{mid}, and x_{high} corresponding to the vertex producing the lowest, middle, and highest function values respectively ($f\ at\ x_{low}$, $f\ at\ x_{mid}$, and $f\ at\ x_{high}$).

2. The centroid x_c is calculated using all the points except x_{high} by,

$$x_c = \frac{1}{2}\left(x_{low} + x_{mid}\right). \tag{A-1}$$

3. The reflected point is then computed using,

$$x_{ref} = (1+\sigma)x_c - \sigma x_{high}. \tag{A-2}$$

   The fitness function $f\ at\ x_{ref}$ is then evaluated. If $f\ at\ x_{low} \le f\ at\ x_{ref} < f\ at\ x_{mid}$, then x_{high} is substituted with x_{ref} and the iteration is ended proceeding back to step 1 for a new iteration.

4. If $f\ at\ x_{ref} < f\ at\ x_{low}$, then the expanded point is calculated using,

$$x_{\exp} = (1-\gamma)x_c + x_{ref}. \tag{A-3}$$

The fitness function $f \; at \; x_{\exp}$ is then evaluated. If $f \; at \; x_{ref} > f \; at \; x_{\exp}$, then x_{high} is substituted with $x_{\exp}$ and the iteration is ended proceeding back to step 1 for a new iteration. If not, then x_{high} is substituted with x_{ref} and the iteration is ended proceeding back to step 1 for a new iteration.

5. If $f \; at \; x_{ref} \geq f \; at \; x_{mid}$, then a contraction operation must be carried out.

   If $f \; at \; x_{ref} \geq f \; at \; x_{high}$, then the contracted point is determined using,

$$x_{cont} = \beta x_{high} + (1 - \beta) x_c . \qquad \text{(A-4)}$$

   The fitness function $f \; at \; x_{cont}$ is then evaluated. If $f \; at \; x_{cont} < f \; at \; x_{high}$, then x_{high} is substituted with x_{cont} and the iteration is ended proceeding back to step 1 for a new iteration. If not, then a shrinking operation is performed after proceeding to step 6.

   If $f \; at \; x_{mid} \leq f \; at \; x_{ref} < f \; at \; x_{high}$, the contracted point is determined using,

$$x_{cont} = \beta x_{ref} + (1 - \beta) x_c . \qquad \text{(A-5)}$$

   The fitness function $f \; at \; x_{cont}$ is then evaluated. If $f \; at \; x_{cont} < f \; at \; x_{ref}$, then x_{high} is substituted with x_{cont} and the iteration is ended proceeding back to step 1 for a new iteration. If not, then a shrinking operation is performed after proceeding to step 6.

6. The shrinking operation is carried out by shrinking the polyhedron towards the vertex with the lowest function value by,

$$x_i = x_{low} + \varepsilon (x_i - x_{low}), \qquad \text{(A-6)}$$

   where, i covers all the vertices except for x_{low}. The iteration is then ended proceeding back to step 1 for a new iteration.

If the value of the fitness function at one of the vertices of the simplex becomes too small or the function values at each vertex become very close to each other, then the search is terminated and the obtained variables at the vertex with the lowest function value are taken to be the solution. The initial simplex before the iterative procedure is initiated is found using the following steps: [39]

- Let $x^{(0)}$ be the N-dimensional initial guess (base point) for the simplex.
- The N initial vertices left to complete the initial simplex are then calculated using the base point and a scale factor, α. α is a quantity that determines the initial size of the simplex. The vertices are found using,

$$x_j^{(i)} = \begin{cases} x_j^{(0)} + \delta_1 \ \mathit{if} \ j = i \\ x_j^{(0)} + \delta_2 \ \mathit{if} \ j \neq i \end{cases}, \tag{A-7}$$

where, both i and j vary from 1 up to N. δ_1 and δ_2 are a function of N and α through the equations,

$$\delta_1 = \left[\frac{(N+1)^{1/2} + N - 1}{N\sqrt{2}} \right] \alpha, \tag{A-8}$$

and

$$\delta_2 = \left[\frac{(N+1)^{1/2} - 1}{N\sqrt{2}} \right] \alpha, \tag{A-9}$$

respectively.

Appendix B

The Secant Method

The secant method in order to solve a system of nonlinear equations is presented here. This is a root finding method that solves equations using the Newton-Raphson algorithm [50] with a provision in which the function derivatives are approximated using finite differences.

The problem to be solved is to find N unknowns $x = [x_1 \quad x_2 \quad ... \quad x_N]^l$ satisfying the N equations, $f(x) = [f_1(x) \quad f_2(x) \quad ... \quad f_N(x)]^l = 0$. The method process goes as follows, [66]

1. N initial guesses $x^0 = \lfloor x_1^0 \quad x_2^0 \quad ... \quad x_N^0 \rfloor$ to the N unknowns are made. Δx which is a small increment to the unknowns is specified.
2. $f(x^0)$ is evaluated. If $f(x^0) < \varepsilon$, then the solution process stops and x^0 is taken as the solution. If not then the method proceeds to step 3.

For n=0,1,2,…., P-1 do:

3. Given $x^n = \lfloor x_1^n \quad x_2^n \quad ... \quad x_N^n \rfloor$ and $f(x^n) = [f_1(x^n) \quad f_2(x^n) \quad ... \quad f_N(x^n)]^l = 0$, the Jacobian matrix,

$$J = \begin{bmatrix} \frac{\partial f_1(x^n)}{\partial x_1^n} & \frac{\partial f_1(x^n)}{\partial x_2^n} & ... & \frac{\partial f_1(x^n)}{\partial x_N^n} \\ \frac{\partial f_2(x^n)}{\partial x_1^n} & \frac{\partial f_2(x^n)}{\partial x_2^n} & ... & \frac{\partial f_2(x^n)}{\partial x_N^n} \\ \downarrow & \downarrow & ... & \downarrow \\ \frac{\partial f_N(x^n)}{\partial x_1^n} & \frac{\partial f_N(x^n)}{\partial x_2^n} & ... & \frac{\partial f_N(x^n)}{\partial x_N^n} \end{bmatrix}, \tag{B-1}$$

is then calculated using a finite difference approximation to calculate $\partial f_i\left(x^n\right) / \partial x_j^n$ described by

$$\frac{\partial f_i\left(x^n\right)}{\partial x_j^n} = \frac{f_i\left(x_1^n, x_2^n, .., x_j^n + \Delta x, .., x_N^n\right) - f_i\left(x_1^n, x_2^n, .., x_j^n, .., x_N^n\right)}{\Delta x}.$$

(B-2)

If $\left|\det(J)\right| < \varepsilon$, then the process is stopped and taken back to step 1 where new initial guesses and Δx are made. If not, then the process moves to step 4.

4. The values for the unknowns, x^n, are then updated using

$$x^{n+1} = x^n - J^{-1} f\left(x^n\right). \quad \text{(B-3)}$$

5. If $f\left(x^{n+1}\right) < \varepsilon$ (convergence criteria), then the root finding process stops and x^{n+1} is taken to be the solution. If not and $n < P-1$, the process goes back to step 3 and repeats. If $n = P-1$ the root finding process stops with no solution. Note, that the choice of ε is dependent on the problem. In certain cases the procedure might be converging to a solution but ε is set to be too low and as such the result might be interpreted as no convergence achieved.

   For the multiple angle method, the following parameters were picked:

   $\varepsilon = 10^{-16}$

   $P = 50$

   $\Delta x = 0.000000000001$

Note: In this research, if $n = P-1$ iterations have been carried out, while $f\left(x^{n+1}\right) < \varepsilon$ is not satisfied; the unknowns from that frequency iteration are taken to be the extracted parameters at

that frequency. For the material characterization methods presented in this dissertation, it was observed that when the root finding method completes the number of iterations while not achieving the convergence criteria ($f\left(x^{n+1}\right) < \varepsilon$); the function values $f\left(x^{n+1}\right)$ although not less than ε have iteratively decreased in a converging like fashion to very small values and staggered around there. This provision was made to account for measurement system effects (such as power) affecting certain frequency samples while not affecting others thus preventing or allowing the convergence criteria to be satisfied or not. The extracted parameters obtained using the secant method with this provision were validated against the literature and found to be sound.

Appendix C

Reference Requiring Method Material Characterization Matlab Code

Description: This code extracts the material parameters (dielectric constant and loss tangent) of a dielectric substrate using the reference requiring method. The code allows for slight substrate thickness optimization. However, if a good estimate of the thickness is available this optimization is not recommended due to its un-robustness to noise. Refer to Mittleman-Dorney 2001 ([27]) for the thickness optimization background (total variation method). The code requires certain inputs. These are:

-Reference measurement and sample measurement files names

-Thickness estimate

-Noise floor for upper frequency limit

-Lower frequency limit

-Next power of two above the number of data points in measured signal (example, if 2000 data points were collected enter 2048)

Note:

**The measured data text files, must have two columns with one being time and the other being signal intensity. The unit for time should be picoseconds. Delete any other text from the text files.

*The optimization method used is the modified NELDER MEAD SIMPLEX METHOD in two dimensions.

→ The code for the reference requiring method is:

```
clc%clearing command window
close all%closing all previously open figures
clear all%clearing MATLAB workspace memory
```

```
format long

%%%%%%%%%%%%%%%%%%%%%%%%%%%%%%%%%%%%%%%%%%%%%%%%%%%%%%%%%%%%%%%%
%%%%%%%%%%%%%
%%%%%%%%%%%%%%%%%%%inputs%%%%%%%%%%%%%%%%%%%%%%%%%%%%%%%%%%%%%%%
%%%%%%%%%%%%%
%%%%%%%%%%%%%%%%%%%%%%%%%%%%%%%%%%%%%%%%%%%%%%%%%%%%%%%%%%%%%%%%
%%%%%%%%%%%%%

flow=120e9; %lower frequency limit
upfl=2.5*(10^12); %noise floor frequency limit
thickest=1.58*(10^-3); %thickness estimate
nex_pw2_nsamples=2048; %next power of two above the number of
data points in                                   %measured
signal

%%loading reference and sample data
Ref_Air=textread('HDPE_Ref_Air_1_p_575_mm.txt', '%s');%reference
measurement
Ref_Air=str2double(Ref_Air);
sample=textread('HDPE_Test_1_p_575_mm.txt', '%s');%sample
measurement
sample=str2double(sample);

%%%%%%%%%%%%%%%%%%%%%%%%%%%%%%%%%%%%%%%%%%%%%%%%%%%%%%%%%%%%%%%%
%%%%%%%%%%%%%
%%%%%%%%%%%%%%%%%%%%%%%%%%%%%%%%%%%%%%%%%%%%%%%%%%%%%%%%%%%%%%%%
%%%%%%%%%%%%%

%%Building Reference and Sample(Test) Matrices for
j=1;
for i=1:size(sample,1)
    if mod(i,2)~=0
        Ref_Air_c(j,1)=Ref_Air(i,1);
        sample_c(j,1)=sample(i,1);
    end
    if mod(i,2)==0
        Ref_Air_c(j,2)=Ref_Air(i,1);
        sample_c(j,2)=sample(i,1);
        j=j+1;
    end
end

Ts=(Ref_Air_c(2,1)-Ref_Air_c(1,1))*10^(-12);%sampling period
Fs=1/Ts;%sampling frequency

%%Reference and Sample Signals Collected from THz system Plot
```

```
figure
plot((Ref_Air_c(:,1)),Ref_Air_c(:,2),':',...
    (sample_c(:,1)),sample_c(:,2))
grid
legend('Air - No Sample', ' Sample')
xlabel('Time (ps)')
ylabel('Recieved Signal Intensity (a.u.)')
title('Time Domain Signals')
x=(0:1:(size(Ref_Air_c,1)-1))*Ts;%updated x axis - time axis
(shortened)
Num_samples=nex_pw2_nsamples;%n points to calculate DFT for
f=0:Fs/Num_samples:(Fs-Fs/Num_samples);%frequency axis for DFT

tots=sample_c(:,2);
totr=Ref_Air_c(:,2);

delt=0;%(find(tots==max(tots))-...
    %(find(totr==max(totr)));%time indices delay between the
peaks of the %reference and sample signals

NFFT=Num_samples;
gh=(fft(totr(1:(end-delt)),NFFT));
jh=(fft(tots,NFFT));

fff=find(f>=upfl);%upper frequency limit for noise floor
noise_level=20*mean(abs(jh(fff(1):end/2)));%obtaining a measure
for noise %level (20*noise_floor)

fr=find(f>=flow);%lower frequency limit to start
characterization at
mista=abs(jh((fr(1):end/2)));
sss=find(mista<=noise_level);
fr1=find(abs(jh(1:end/2))==mista(sss(1)));
fr1(end)=fr1(end)-3;
f_worth=f(fr(1):fr1(end));%frequencies to extract material
parameters at

figure
plot(f,abs(gh(1:size(f,2))),':',...
    f,abs(jh(1:size(f,2))))
grid
legend('Air - No Sample', ' Sample')
xlabel('Frequency - Hz')
ylabel('Magnitude (a.u.)')
title('Frequency Domain - Magnitude Spectrum')

figure
```

```
plot(f,unwrap(angle(gh(1:size(f,2)))),':',...
    f,unwrap(angle(jh(1:size(f,2)))))
grid
legend('Air - No Sample', ' Sample')
xlabel('Frequency - Hz')
ylabel('Phase (degrees)')
title('Frequency Domain - Phase Spectrum')

A=jh./gh;%measured transfer function, frequency domain

figure %measured transfer function magnitude plot
plot(f,abs(A))
grid
xlabel('Frequency - Hz')
title('Frequency Domain Measured Transfer Function - Magnitude
Spectrum')
figure %measured transfer function phase plot
plot(f,phase(A))
grid
xlabel('Frequency - Hz')
title('Frequency Domain Measured Transfer Function - Phase
Spectrum')

lp=thickest;%thickness of substrate
lup=lp*0.03+lp;%upper thickness range limit
ldn=lp-lp*0.03;%lower thickness range limit
num_p=40;%number of points in thickness vector
lvec=ldn:(lup-ldn)/num_p:lup;%thickness vector
lvec=lp;%uncomment this if no thickness optimization is needed
(uncommenting
        %is recommended if possible)

for wj=1:size(lvec,2)%extracting parameters of each thickness

%%initializing refractive index n
xstar=x;
del_t=abs(xstar(1,(find(totr==max(totr))))-...
xstar(1,(find(tots==max(tots)))));
c=3e8;%speed of light in air m/s
nair=1.00027;%refractive index of air
l_eval=lvec(wj);
Thickness=l_eval;
index_initc=del_t*c./Thickness + nair;
index_init=ones(size(gh,1),1)*index_initc;

%%initializing extinction coefficient k
k_init=zeros(size(index_init));
```

```
A=jh./gh;%measured transfer function, frequency domain
A_hat_init=(exp(sqrt(-1)*2*pi*f'*(nair).*Thickness./c).*...
           (2*nair./(nair+index_init-sqrt(-1).*k_init)).*...
    (2*(index_init-sqrt(-1)*k_init)./(nair+index_init-sqrt(-
1)*k_init)).*...
      exp(-sqrt(-1)*2*pi*f'.*(index_init-sqrt(-
1)*k_init)*Thickness/c))./...
      (1+(((index_init-sqrt(-1)*k_init)-nair)./...
     (index_init-sqrt(-1)*k_init+nair)).*...
      ((nair-(index_init-sqrt(-1)*k_init))./...
     (index_init-sqrt(-1)*k_init+nair)).*...
exp(-2*sqrt(-1)*2*pi*f'.*(index_init-sqrt(-
1)*k_init)*Thickness/c));
    jhi=real(NFFT*ifft(A(fr(1):fr1(end))));
    maxjhi=max(abs(jhi));
    lj=1;
    for clap=1:200000
        k_init=k_init+0.00001;
        A_hat_init=(exp(sqrt(-
1)*2*pi*f'*(nair).*Thickness./c).*...
            (2*nair./(nair+index_init-sqrt(-1).*k_init)).*...
    (2*(index_init-sqrt(-1)*k_init)./(nair+index_init-sqrt(-
1)*k_init)).*...
      exp(-sqrt(-1)*2*pi*f'.*(index_init-sqrt(-
1)*k_init)*Thickness/c))./...
(1+(((index_init-sqrt(-1)*k_init)-nair)./...
(index_init-sqrt(-1)*k_init+nair)).*...
            ((nair-(index_init-sqrt(-1)*k_init))./...
(index_init-sqrt(-1)*k_init+nair)).*...
     exp(-2*sqrt(-1)*2*pi*f'.*(index_init-sqrt(-
1)*k_init)*Thickness/c));
        ghi=real(NFFT*ifft(A_hat_init(fr(1):fr1(end))));
        maxghi=max(abs(ghi));
        if abs(maxghi)<=abs(maxjhi)
            break
        end
    end

    %% Nelder Mead simplex search method
    index=index_init(fr(1):fr1(end),:);
    k=k_init(fr(1):fr1(end),:);
    bam=[index, k]';
    N=2;
    alfa=1;
    beta=0.5;
    gamma=2;
    cla=1;
```

```
    swf=0.01;%change swf, only if optimization gets stuck
    del1=swf*((sqrt(N+1)+N-1)/(N*sqrt(2)));
    del2=swf*((sqrt(N+1)-1)/(N*sqrt(2)));
    A1=A;
    clear A
    A=A1(fr(1):fr1(end));

    wght=1;
    ttt=zeros(1,size(f_worth,2));
    for ik=1:size(f_worth,2)
        cla=1;
        xnew0=[bam(1,ik); bam(2,ik)];
        xnew1=[bam(1,ik)+del1; bam(2,ik)+del2];
        xnew2=[bam(1,ik)+del2; bam(2,ik)+del1];
        counting=0;
        alfa=alfa;
        P=phase(A(ik));
        P=P
        while cla==1
            counting=counting+1;
            new0=(exp(sqrt(-
1)*2*pi*f_worth(ik)*(nair).*Thickness./c).*...
                (2*nair./(nair+xnew0(1,1)-sqrt(-
1).*xnew0(2,1))).*...
(2*(xnew0(1,1)-sqrt(-1).*xnew0(2,1))./...
(nair+xnew0(1,1)-sqrt(-1).*xnew0(2,1))).*...
exp(-sqrt(-1)*2*pi*f_worth(ik).*(xnew0(1,1)-sqrt(-1).*...
xnew0(2,1))*Thickness/c))./...
                (1+(((xnew0(1,1)-sqrt(-1).*xnew0(2,1))-
nair)./...
(xnew0(1,1)-sqrt(-1).*xnew0(2,1)+nair)).*...
                ((nair-(xnew0(1,1)-sqrt(-1).*xnew0(2,1)))./...
(xnew0(1,1)-sqrt(-1).*xnew0(2,1)+nair)).*...
                exp(-2*sqrt(-1)*2*pi*f_worth(ik).*...
(xnew0(1,1)-sqrt(-1).*xnew0(2,1))*Thickness/c));
            anglenew0=angle(new0);
            anglebla0=((phase(A(ik)))-(anglenew0));
            if abs(anglebla0)>pi && abs(anglebla0)<2*pi
                if counting==1
                    ttt(ik)=ik;
                end
                anglebla0=abs(anglebla0)-2*pi;
            end
            fxnew0=abs(abs(abs(A(ik))-
abs(new0))+wght*abs(anglebla0));
            (abs(fxnew0))
```

```
            new1=(exp(sqrt(-
1)*2*pi*f_worth(ik)'*(nair).*Thickness./c).*...
                (2*nair./(nair+xnew1(1,1)-sqrt(-
1).*xnew1(2,1))).*...
                (2*(xnew1(1,1)-sqrt(-1).*xnew1(2,1))./...
(nair+xnew1(1,1)-sqrt(-1).*xnew1(2,1))).*...
                exp(-sqrt(-1)*2*pi*f_worth(ik)'.*...
(xnew1(1,1)-sqrt(-1).*xnew1(2,1))*Thickness/c))./...
                (1+(((xnew1(1,1)-sqrt(-1).*xnew1(2,1))-
nair)./...
(xnew1(1,1)-sqrt(-1).*xnew1(2,1)+nair)).*...
                ((nair-(xnew1(1,1)-sqrt(-1).*xnew1(2,1)))./...
(xnew1(1,1)-sqrt(-1).*xnew1(2,1)+nair)).*...
                exp(-2*sqrt(-1)*2*pi*f_worth(ik)'.*...
(xnew1(1,1)-sqrt(-1).*xnew1(2,1))*Thickness/c));
            anglenew1=angle(new1);
            anglebla1=((phase(A(ik)))-(anglenew1));
            if abs(anglebla1)>pi && abs(anglebla1)<2*pi
                if counting==1
                    ttt(ik)=ik;
                end
                anglebla1=abs(anglebla1)-2*pi;
            end
            fxnew1=abs(abs(abs(A(ik))-
abs(new1))+wght*abs(anglebla1));
             (abs(fxnew1))
            new2=(exp(sqrt(-
1)*2*pi*f_worth(ik)'*(nair).*Thickness./c).*...
                (2*nair./(nair+xnew2(1,1)-sqrt(-
1).*xnew2(2,1))).*...
(2*(xnew2(1,1)-sqrt(-1).*xnew2(2,1))./...
(nair+xnew2(1,1)-sqrt(-1).*xnew2(2,1))).*...
                exp(-sqrt(-1)*2*pi*f_worth(ik)'.*...
(xnew2(1,1)-sqrt(-1).*xnew2(2,1))*Thickness/c))./...
                (1+(((xnew2(1,1)-sqrt(-1).*xnew2(2,1))-
nair)./...
(xnew2(1,1)-sqrt(-1).*xnew2(2,1)+nair)).*...
                ((nair-(xnew2(1,1)-sqrt(-1).*xnew2(2,1)))./...
(xnew2(1,1)-sqrt(-1).*xnew2(2,1)+nair)).*...
                exp(-2*sqrt(-1)*2*pi*f_worth(ik)'.*...
(xnew2(1,1)-sqrt(-1).*xnew2(2,1))*Thickness/c));
            anglenew2=angle(new2);
            anglebla2=((phase(A(ik)))-(anglenew2));
            if abs(anglebla2)>pi && abs(anglebla2)<2*pi
                if counting==1
                    ttt(ik)=ik;
                end
```

```
                    anglebla2=abs(anglebla2)-2*pi;
                end
                fxnew2=abs(abs(abs(A(ik))-
abs(new2))+wght*abs(anglebla2));
                (abs(fxnew2))
                if (abs(fxnew0))<0.000000000000001
                    bam(:,ik)=xnew0;
                    bamp(:,ik)=angle(new0);
                    bamm(:,ik)=abs(new0);
                    cla=2;
                    continue
                elseif (abs(fxnew1))<0.000000000000001
                    bam(:,ik)=xnew1;
                    bamp(:,ik)=angle(new1);
                    bamm(:,ik)=abs(new1);
                    cla=2;
                    continue
                elseif (abs(fxnew2))<0.000000000000001
                    bam(:,ik)=xnew2;
                    bamp(:,ik)=angle(new2);
                    bamm(:,ik)=abs(new2);
                    cla=2;
                    continue
                elseif
std([(abs(fxnew0)),(abs(fxnew1)),(abs(fxnew2))])<=0.0000000001
              if abs(abs(fxnew0))<=(abs(fxnew1)) &&
(abs(fxnew0))<=(abs(fxnew2))
                        bam(:,ik)=xnew0;
                        bamp(:,ik)=angle(new0);
                        bamm(:,ik)=abs(new0);
                        cla=2;
                        continue
                    end
                   if(abs(fxnew0))>=(abs(fxnew1)) &&
(abs(fxnew1))<=(abs(fxnew2))
                        bam(:,ik)=xnew1;
                        bamp(:,ik)=angle(new1);
                        bamm(:,ik)=abs(new1);
                        cla=2;
                        continue
                    end
                   if(abs(fxnew2))<=(abs(fxnew1)) &&
(abs(fxnew0))>=(abs(fxnew2))
                        bam(:,ik)=xnew2;
                        bamp(:,ik)=angle(new2);
                        bamm(:,ik)=abs(new2);
                        cla=2;
```

```
                    continue
                end
            end
            %%%%%
            if abs(fxnew0)>abs(fxnew1) &&
abs(fxnew1)>abs(fxnew2)
                fl=abs(fxnew2);
                xl=xnew2;
                fg=abs(fxnew1);
                xg=xnew1;
                fh=abs(fxnew0);
                xh=xnew0;
                centroid=0.5*(xnew1+xnew2);
                xrf=centroid+alfa*(centroid-xh);
        newrf=(exp(sqrt(-
1)*2*pi*f_worth(ik)'*(nair).*Thickness./c).*...
                    (2*nair./(nair+xrf(1,1)-sqrt(-
1).*xrf(2,1))).*...
  (2*(xrf(1,1)-sqrt(-1).*xrf(2,1))./(nair+xrf(1,1)-sqrt(-
1).*xrf(2,1))).*...
 exp(-sqrt(-1)*2*pi*f_worth(ik)'.*...
(xrf(1,1)-sqrt(-1).*xrf(2,1))*Thickness/c))./...
                    (1+(((xrf(1,1)-sqrt(-1).*xrf(2,1))-
nair)./...
(xrf(1,1)-sqrt(-1).*xrf(2,1)+nair)).*...
                    ((nair-(xrf(1,1)-sqrt(-
1).*xrf(2,1)))./(xrf(1,1)-sqrt(-1).*xrf(2,1)+nair)).*...
                    exp(-2*sqrt(-
1)*2*pi*f_worth(ik)'.*(xrf(1,1)-sqrt(-
1).*xrf(2,1))*Thickness/c));
                anglenewrf=angle(newrf);
                angleblarf=((phase(A(ik)))-(anglenewrf));
                if abs(angleblarf)>pi && abs(angleblarf)<2*pi
                    angleblarf=abs(angleblarf)-2*pi;
                end
                fxrf=abs(abs(abs(A(ik))-
abs(newrf))+wght*abs(angleblarf));
                (abs(fxrf))
                if fxrf<fg && fxrf>fl
                    xnew0=xrf;
                    continue
                end
                if fxrf<fl
                    xe=centroid+gamma*(centroid-xh);
             newe=(exp(sqrt(-
1)*2*pi*f_worth(ik)'*(nair).*Thickness./c).*...
```

```
                                (2*nair./(nair+xe(1,1)-sqrt(-
1).*xe(2,1))).*...
       (2*(xe(1,1)-sqrt(-1).*xe(2,1))./(nair+xe(1,1)-sqrt(-
1).*xe(2,1))).*...
      exp(-sqrt(-1)*2*pi*f_worth(ik)'.*...
(xe(1,1)-sqrt(-1).*xe(2,1))*Thickness/c))./...
(1+(((xe(1,1)-sqrt(-1).*xe(2,1))-nair)./...
(xe(1,1)-sqrt(-1).*xe(2,1)+nair)).*...
 ((nair-(xe(1,1)-sqrt(-1).*xe(2,1)))./(xe(1,1)-sqrt(-
1).*xe(2,1)+nair)).*...
exp(-2*sqrt(-1)*2*pi*f_worth(ik)'.*(xe(1,1)-sqrt(-
1).*xe(2,1))*Thickness/c));
                    anglenewe=angle(newe);
                    angleblae=((phase(A(ik)))-(anglenewe));
                    if abs(angleblae)>pi && abs(angleblae)<2*pi
                        angleblae=abs(angleblae)-2*pi;
                    end
                    fxe=abs(abs(abs(A(ik))-
abs(newe))+wght*abs(angleblae));
                    (abs(fxe))
                    if fxe<fxrf
                        xnew0=xe;
                        continue
                    end
                    if fxe>fxrf
                        xnew0=xrf;
                        continue
                    end
                end
                if fxrf>fg
                    if fxrf>=fh
                        xc=xh+beta*(centroid-xh);
       newc=(exp(sqrt(-
1)*2*pi*f_worth(ik)'*(nair).*Thickness./c).*...
                            (2*nair./(nair+xc(1,1)-sqrt(-
1).*xc(2,1))).*...
     (2*(xc(1,1)-sqrt(-1).*xc(2,1))./(nair+xc(1,1)-sqrt(-
1).*xc(2,1))).*...
exp(-sqrt(-1)*2*pi*f_worth(ik)'.*...
(xc(1,1)-sqrt(-1).*xc(2,1))*Thickness/c))./...
(1+(((xc(1,1)-sqrt(-1).*xc(2,1))-nair)./...
(xc(1,1)-sqrt(-1).*xc(2,1)+nair)).*...
((nair-(xc(1,1)-sqrt(-1).*xc(2,1)))./(xc(1,1)-sqrt(-
1).*xc(2,1)+nair)).*...
exp(-2*sqrt(-1)*2*pi*f_worth(ik)'.*(xc(1,1)-sqrt(-
1).*xc(2,1))*Thickness/c));
                        anglenewc=angle(newc);
```

```
                            angleblac=((phase(A(ik)))-(anglenewc));
                            if abs(angleblac)>pi &&
abs(angleblac)<2*pi
                                angleblac=abs(angleblac)-2*pi;
                            end
                       fxc=abs(abs(abs(A(ik))-
abs(newc))+wght*abs(angleblac));
                            (abs(fxc))
                            if fxc<fh
                                xnew0=xc;
                                continue
                            else
                                xnew0=xl+beta*(xnew0-xl);
                                xnew1=xl+beta*(xnew1-xl);
                                continue
                            end
                        else
                            xh=xrf;
                            xc=xh+beta*(centroid-xh);
   newc=(exp(sqrt(-
1)*2*pi*f_worth(ik)'*(nair).*Thickness./c).*...
                                (2*nair./(nair+xc(1,1)-sqrt(-
1).*xc(2,1))).*...
      (2*(xc(1,1)-sqrt(-1).*xc(2,1))./(nair+xc(1,1)-sqrt(-
1).*xc(2,1))).*...
    exp(-sqrt(-1)*2*pi*f_worth(ik)'.*...
(xc(1,1)-sqrt(-1).*xc(2,1))*Thickness/c))./...
(1+(((xc(1,1)-sqrt(-1).*xc(2,1))-nair)./...
(xc(1,1)-sqrt(-1).*xc(2,1)+nair)).*...
 ((nair-(xc(1,1)-sqrt(-1).*xc(2,1)))./(xc(1,1)-sqrt(-
1).*xc(2,1)+nair)).*...
exp(-2*sqrt(-1)*2*pi*f_worth(ik)'.*(xc(1,1)-sqrt(-
1).*xc(2,1))*Thickness/c));
                            anglenewc=angle(newc);
                            angleblac=((phase(A(ik)))-(anglenewc));
                            if abs(angleblac)>pi &&
abs(angleblac)<2*pi
                                angleblac=abs(angleblac)-2*pi;
                            end
               fxc=abs(abs(abs(A(ik))-
abs(newc))+wght*abs(angleblac));
                            (abs(fxc))
                            if fxc<fxrf
                                xnew0=xc;
                                continue
                            else
                                xnew0=xl+beta*(xnew0-xl);
```

```
                        xnew1=xl+beta*(xnew1-xl);
                        continue
                    end
                end
            end
        end
        %%%%%
        if abs(fxnew1)>abs(fxnew0) &&
abs(fxnew0)>abs(fxnew2)
            fl=abs(fxnew2);
            xl=xnew2;
            fg=abs(fxnew0);
            xg=xnew0;
            fh=abs(fxnew1);
            xh=xnew1;
            centroid=0.5*(xnew0+xnew2);
            xrf=centroid+alfa*(centroid-xh);
     newrf=(exp(sqrt(-
1)*2*pi*f_worth(ik)'*(nair).*Thickness./c).*...
                (2*nair./(nair+xrf(1,1)-sqrt(-
1).*xrf(2,1))).*...
(2*(xrf(1,1)-sqrt(-1).*xrf(2,1))./(nair+xrf(1,1)-sqrt(-
1).*xrf(2,1))).*...
exp(-sqrt(-1)*2*pi*f_worth(ik)'.*...
(xrf(1,1)-sqrt(-1).*xrf(2,1))*Thickness/c))./...
(1+(((xrf(1,1)-sqrt(-1).*xrf(2,1))-nair)./...
(xrf(1,1)-sqrt(-1).*xrf(2,1)+nair)).*...
((nair-(xrf(1,1)-sqrt(-1).*xrf(2,1)))./...
(xrf(1,1)-sqrt(-1).*xrf(2,1)+nair)).*...
 exp(-2*sqrt(-1)*2*pi*f_worth(ik)'.*...
(xrf(1,1)-sqrt(-1).*xrf(2,1))*Thickness/c));
            anglenewrf=angle(newrf);
            angleblarf=((phase(A(ik)))-(anglenewrf));
            if abs(angleblarf)>pi && abs(angleblarf)<2*pi
                angleblarf=abs(angleblarf)-2*pi;
            end
            fxrf=abs(abs(abs(A(ik))-
abs(newrf))+wght*abs(angleblarf));
             (abs(fxrf))
            if fxrf<fg && fxrf>fl
                xnew1=xrf;
                continue
            end
            if fxrf<fl
                xe=centroid+gamma*(centroid-xh);
       newe=(exp(sqrt(-
1)*2*pi*f_worth(ik)'*(nair).*Thickness./c).*...
```

```
                              (2*nair./(nair+xe(1,1)-sqrt(-
1).*xe(2,1))).*...
        (2*(xe(1,1)-sqrt(-1).*xe(2,1))./(nair+xe(1,1)-sqrt(-
1).*xe(2,1))).*...
exp(-sqrt(-1)*2*pi*f_worth(ik)'.*...
(xe(1,1)-sqrt(-1).*xe(2,1))*Thickness/c))./...
(1+(((xe(1,1)-sqrt(-1).*xe(2,1))-nair)./...
(xe(1,1)-sqrt(-1).*xe(2,1)+nair)).*...
 ((nair-(xe(1,1)-sqrt(-1).*xe(2,1)))./(xe(1,1)-sqrt(-
1).*xe(2,1)+nair)).*...
exp(-2*sqrt(-1)*2*pi*f_worth(ik)'.*(xe(1,1)-sqrt(-
1).*xe(2,1))*Thickness/c));
                    anglenewe=angle(newe);
                    angleblae=((phase(A(ik)))-(anglenewe));
                    if abs(angleblae)>pi && abs(angleblae)<2*pi
                        angleblae=abs(angleblae)-2*pi;
                    end
                    fxe=abs(abs(abs(A(ik))-
abs(newe))+wght*abs(angleblae));
                    (abs(fxe))
                    if fxe<fxrf
                        xnew1=xe;
                        continue
                    end
                    if fxe>fxrf
                        xnew1=xrf;
                        continue
                    end
                end
                if fxrf>fg
                    if fxrf>=fh
                        xc=xh+beta*(centroid-xh);
        newc=(exp(sqrt(-
1)*2*pi*f_worth(ik)'*(nair).*Thickness./c).*...
                            (2*nair./(nair+xc(1,1)-sqrt(-
1).*xc(2,1))).*...
    (2*(xc(1,1)-sqrt(-1).*xc(2,1))./(nair+xc(1,1)-sqrt(-
1).*xc(2,1))).*...
 exp(-sqrt(-1)*2*pi*f_worth(ik)'.*...
(xc(1,1)-sqrt(-1).*xc(2,1))*Thickness/c))./...
(1+(((xc(1,1)-sqrt(-1).*xc(2,1))-nair)./...
(xc(1,1)-sqrt(-1).*xc(2,1)+nair)).*...
 ((nair-(xc(1,1)-sqrt(-1).*xc(2,1)))./(xc(1,1)-sqrt(-
1).*xc(2,1)+nair)).*...
exp(-2*sqrt(-1)*2*pi*f_worth(ik)'.*(xc(1,1)-sqrt(-
1).*xc(2,1))*Thickness/c));
                        anglenewc=angle(newc);
```

```
                        angleblac=((phase(A(ik)))-(anglenewc));
                        if abs(angleblac)>pi &&
abs(angleblac)<2*pi
                            angleblac=abs(angleblac)-2*pi;
                        end
                fxc=abs(abs(abs(A(ik))-
abs(newc))+wght*abs(angleblac));
                        (abs(fxc))
                        if fxc<fh
                            xnew1=xc;
                            continue
                        else
                            xnew0=xl+beta*(xnew0-xl);
                            xnew1=xl+beta*(xnew1-xl);
                            continue
                        end
                    else
                        xh=xrf;
                        xc=xh+beta*(centroid-xh);
       newc=(exp(sqrt(-
1)*2*pi*f_worth(ik)'*(nair).*Thickness./c).*...
                            (2*nair./(nair+xc(1,1)-sqrt(-
1).*xc(2,1))).*...
  (2*(xc(1,1)-sqrt(-1).*xc(2,1))./(nair+xc(1,1)-sqrt(-
1).*xc(2,1))).*...
exp(-sqrt(-1)*2*pi*f_worth(ik)'.*...
(xc(1,1)-sqrt(-1).*xc(2,1))*Thickness/c))./...
(1+(((xc(1,1)-sqrt(-1).*xc(2,1))-nair)./...
(xc(1,1)-sqrt(-1).*xc(2,1)+nair)).*...
((nair-(xc(1,1)-sqrt(-1).*xc(2,1)))./(xc(1,1)-sqrt(-
1).*xc(2,1)+nair)).*...
exp(-2*sqrt(-1)*2*pi*f_worth(ik)'.*(xc(1,1)-sqrt(-
1).*xc(2,1))*Thickness/c));
                        anglenewc=angle(newc);
                        angleblac=((phase(A(ik)))-(anglenewc));
                        if abs(angleblac)>pi &&
abs(angleblac)<2*pi
                            angleblac=abs(angleblac)-2*pi;
                        end
     fxc=abs(abs(abs(A(ik))-abs(newc))+wght*abs(angleblac));
                        (abs(fxc))
                        if fxc<fxrf
                            xnew1=xc;
                            continue
                        else
                            xnew0=xl+beta*(xnew0-xl);
                            xnew1=xl+beta*(xnew1-xl);
```

```
                            continue
                        end
                    end
                end
            end
            %%%%%
            if abs(fxnew2)>abs(fxnew0) &&
abs(fxnew0)>abs(fxnew1)
                fl=abs(fxnew1);
                xl=xnew1;
                fg=abs(fxnew0);
                xg=xnew0;
                fh=abs(fxnew2);
                xh=xnew2;
                centroid=0.5*(xnew0+xnew1);
                xrf=centroid+alfa*(centroid-xh);
   newrf=(exp(sqrt(-
1)*2*pi*f_worth(ik)'*(nair).*Thickness./c).*...
                    (2*nair./(nair+xrf(1,1)-sqrt(-
1).*xrf(2,1))).*...
(2*(xrf(1,1)-sqrt(-1).*xrf(2,1))./(nair+xrf(1,1)-sqrt(-
1).*xrf(2,1))).*...
 exp(-sqrt(-1)*2*pi*f_worth(ik)'.*...
(xrf(1,1)-sqrt(-1).*xrf(2,1))*Thickness/c))./...
(1+(((xrf(1,1)-sqrt(-1).*xrf(2,1))-nair)./...
(xrf(1,1)-sqrt(-1).*xrf(2,1)+nair)).*...
((nair-(xrf(1,1)-sqrt(-1).*xrf(2,1)))./...
(xrf(1,1)-sqrt(-1).*xrf(2,1)+nair)).*...
exp(-2*sqrt(-1)*2*pi*f_worth(ik)'.*...
(xrf(1,1)-sqrt(-1).*xrf(2,1))*Thickness/c));
                anglenewrf=angle(newrf);
                angleblarf=((phase(A(ik)))-(anglenewrf));
                if abs(angleblarf)>pi && abs(angleblarf)<2*pi
                    angleblarf=abs(angleblarf)-2*pi;
                end
                fxrf=abs(abs(abs(A(ik))-
abs(newrf))+wght*abs(angleblarf));
                (abs(fxrf))
                if fxrf<fg && fxrf>fl
                    xnew2=xrf;
                    continue
                end
                if fxrf<fl
                    xe=centroid+gamma*(centroid-xh);
       newe=(exp(sqrt(-
1)*2*pi*f_worth(ik)'*(nair).*Thickness./c).*...
```

```
                              (2*nair./(nair+xe(1,1)-sqrt(-
1).*xe(2,1))).*...
      (2*(xe(1,1)-sqrt(-1).*xe(2,1))./(nair+xe(1,1)-sqrt(-
1).*xe(2,1))).*...
 exp(-sqrt(-1)*2*pi*f_worth(ik)'.*...
(xe(1,1)-sqrt(-1).*xe(2,1))*Thickness/c))./...
(1+(((xe(1,1)-sqrt(-1).*xe(2,1))-nair)./...
(xe(1,1)-sqrt(-1).*xe(2,1)+nair)).*...
((nair-(xe(1,1)-sqrt(-1).*xe(2,1)))./(xe(1,1)-sqrt(-
1).*xe(2,1)+nair)).*...
exp(-2*sqrt(-1)*2*pi*f_worth(ik)'.*(xe(1,1)-sqrt(-
1).*xe(2,1))*Thickness/c));
                    anglenewe=angle(newe);
                    angleblae=((phase(A(ik)))-(anglenewe));
                    if abs(angleblae)>pi && abs(angleblae)<2*pi
                        angleblae=abs(angleblae)-2*pi;
                    end
                    fxe=abs(abs(abs(A(ik))-
abs(newe))+wght*abs(angleblae));
                    (abs(fxe))
                    if fxe<fxrf
                        xnew2=xe;
                        continue
                    end
                    if fxe>fxrf
                        xnew2=xrf;
                        continue
                    end
                end
                if fxrf>fg
                    if fxrf>fh
                        xc=xh+beta*(centroid-xh);
       newc=(exp(sqrt(-
1)*2*pi*f_worth(ik)'*(nair).*Thickness./c).*...
                                  (2*nair./(nair+xc(1,1)-sqrt(-
1).*xc(2,1))).*...
   (2*(xc(1,1)-sqrt(-1).*xc(2,1))./(nair+xc(1,1)-sqrt(-
1).*xc(2,1))).*...
exp(-sqrt(-1)*2*pi*f_worth(ik)'.*...
(xc(1,1)-sqrt(-1).*xc(2,1))*Thickness/c))./...
(1+(((xc(1,1)-sqrt(-1).*xc(2,1))-nair)./...
(xc(1,1)-sqrt(-1).*xc(2,1)+nair)).*...
 ((nair-(xc(1,1)-sqrt(-1).*xc(2,1)))./(xc(1,1)-sqrt(-
1).*xc(2,1)+nair)).*...
exp(-2*sqrt(-1)*2*pi*f_worth(ik)'.*(xc(1,1)-sqrt(-
1).*xc(2,1))*Thickness/c));
                        anglenewc=angle(newc);
```

```
                        angleblac=((phase(A(ik)))-(anglenewc));
                        if abs(angleblac)>pi &&
abs(angleblac)<2*pi
                            angleblac=abs(angleblac)-2*pi;
                        end
   fxc=abs(abs(abs(A(ik))-abs(newc))+wght*abs(angleblac));
                        (abs(fxc))
                        if fxc<fh
                            xnew2=xc;
                            continue
                        else
                            xnew0=xl+beta*(xnew0-xl);
                            xnew2=xl+beta*(xnew2-xl);
                            continue
                        end
                    else
                        xh=xrf;
                        xc=xh+beta*(centroid-xh);
      newc=(exp(sqrt(-
1)*2*pi*f_worth(ik)'*(nair).*Thickness./c).*...
                            (2*nair./(nair+xc(1,1)-sqrt(-
1).*xc(2,1))).*...
 (2*(xc(1,1)-sqrt(-1).*xc(2,1))./(nair+xc(1,1)-sqrt(-
1).*xc(2,1))).*...
exp(-sqrt(-1)*2*pi*f_worth(ik)'.*...
(xc(1,1)-sqrt(-1).*xc(2,1))*Thickness/c))./...
(1+(((xc(1,1)-sqrt(-1).*xc(2,1))-nair)./...
(xc(1,1)-sqrt(-1).*xc(2,1)+nair)).*...
((nair-(xc(1,1)-sqrt(-1).*xc(2,1)))./(xc(1,1)-sqrt(-
1).*xc(2,1)+nair)).*...
exp(-2*sqrt(-1)*2*pi*f_worth(ik)'.*(xc(1,1)-sqrt(-
1).*xc(2,1))*Thickness/c));
                        anglenewc=angle(newc);
                        angleblac=((phase(A(ik)))-(anglenewc));
                        if abs(angleblac)>pi &&
abs(angleblac)<2*pi
                            angleblac=abs(angleblac)-2*pi;
                        end
            fxc=abs(abs(abs(A(ik))-
abs(newc))+wght*abs(angleblac));
                        (abs(fxc))
                        if fxc<fxrf
                            xnew2=xc;
                            continue
                        else
                            xnew0=xl+beta*(xnew0-xl);
                            xnew2=xl+beta*(xnew2-xl);
```

```
                              continue
                          end
                      end
                  end
              end
              %%%%%
              if abs(fxnew0)>abs(fxnew2) &&
abs(fxnew2)>abs(fxnew1)
                  fl=abs(fxnew1);
                  xl=xnew1;
                  fg=abs(fxnew2);
                  xg=xnew2;
                  fh=abs(fxnew0);
                  xh=xnew0;
                  centroid=0.5*(xnew1+xnew2);
                  xrf=centroid+alfa*(centroid-xh);
     newrf=(exp(sqrt(-
1)*2*pi*f_worth(ik)'*(nair).*Thickness./c).*...
                      (2*nair./(nair+xrf(1,1)-sqrt(-
1).*xrf(2,1))).*...
 (2*(xrf(1,1)-sqrt(-1).*xrf(2,1))./(nair+xrf(1,1)-sqrt(-
1).*xrf(2,1))).*...
exp(-sqrt(-1)*2*pi*f_worth(ik)'.*...
(xrf(1,1)-sqrt(-1).*xrf(2,1))*Thickness/c))./...
(1+(((xrf(1,1)-sqrt(-1).*xrf(2,1))-nair)./...
(xrf(1,1)-sqrt(-1).*xrf(2,1)+nair)).*...
((nair-(xrf(1,1)-sqrt(-1).*xrf(2,1)))./...
(xrf(1,1)-sqrt(-1).*xrf(2,1)+nair)).*...
exp(-2*sqrt(-1)*2*pi*f_worth(ik)'.*...
(xrf(1,1)-sqrt(-1).*xrf(2,1))*Thickness/c));
                  anglenewrf=angle(newrf);
                  angleblarf=((phase(A(ik)))-(anglenewrf));
                  if abs(angleblarf)>pi && abs(angleblarf)<2*pi
                      angleblarf=abs(angleblarf)-2*pi;
                  end
                  fxrf=abs(abs(abs(A(ik))-
abs(newrf))+wght*abs(angleblarf));
                  (abs(fxrf))
                  if fxrf<fg && fxrf>fl
                      xnew0=xrf;
                      continue
                  end
                  if fxrf<fl
                      xe=centroid+gamma*(centroid-xh);
    newe=(exp(sqrt(-
1)*2*pi*f_worth(ik)'*(nair).*Thickness./c).*...
```

```
                              (2*nair./(nair+xe(1,1)-sqrt(-
1).*xe(2,1))).*...
   (2*(xe(1,1)-sqrt(-1).*xe(2,1))./(nair+xe(1,1)-sqrt(-
1).*xe(2,1))).*...
 exp(-sqrt(-1)*2*pi*f_worth(ik)'.*...
(xe(1,1)-sqrt(-1).*xe(2,1))*Thickness/c))./...
(1+(((xe(1,1)-sqrt(-1).*xe(2,1))-nair)./...
(xe(1,1)-sqrt(-1).*xe(2,1)+nair)).*...
((nair-(xe(1,1)-sqrt(-1).*xe(2,1)))./(xe(1,1)-sqrt(-
1).*xe(2,1)+nair)).*...
exp(-2*sqrt(-1)*2*pi*f_worth(ik)'.*(xe(1,1)-sqrt(-
1).*xe(2,1))*Thickness/c));
                    anglenewe=angle(newe);
                    angleblae=((phase(A(ik)))-(anglenewe));
                    if abs(angleblae)>pi && abs(angleblae)<2*pi
                        angleblae=abs(angleblae)-2*pi;
                    end
                    fxe=abs(abs(abs(A(ik))-
abs(newe))+wght*abs(angleblae));
                    (abs(fxe))
                    if fxe<fxrf
                        xnew0=xe;
                        continue
                    end
                    if fxe>fxrf
                        xnew0=xrf;
                        continue
                    end
                end
                if fxrf>fg
                    if fxrf>fh
                        xc=xh+beta*(centroid-xh);
      newc=(exp(sqrt(-
1)*2*pi*f_worth(ik)'*(nair).*Thickness./c).*...
                            (2*nair./(nair+xc(1,1)-sqrt(-
1).*xc(2,1))).*...
  (2*(xc(1,1)-sqrt(-1).*xc(2,1))./(nair+xc(1,1)-sqrt(-
1).*xc(2,1))).*...
exp(-sqrt(-1)*2*pi*f_worth(ik)'.*...
(xc(1,1)-sqrt(-1).*xc(2,1))*Thickness/c))./...
(1+(((xc(1,1)-sqrt(-1).*xc(2,1))-nair)./...
(xc(1,1)-sqrt(-1).*xc(2,1)+nair)).*...
((nair-(xc(1,1)-sqrt(-1).*xc(2,1)))./(xc(1,1)-sqrt(-
1).*xc(2,1)+nair)).*...
exp(-2*sqrt(-1)*2*pi*f_worth(ik)'.*(xc(1,1)-sqrt(-
1).*xc(2,1))*Thickness/c));
                        anglenewc=angle(newc);
```

```
                        angleblac=((phase(A(ik))-(anglenewc));
                        if abs(angleblac)>pi &&
abs(angleblac)<2*pi
                            angleblac=abs(angleblac)-2*pi;
                        end
              fxc=abs(abs(abs(A(ik))-
abs(newc))+wght*abs(angleblac));
                        (abs(fxc))
                        if fxc<fh
                            xnew0=xc;
                            continue
                        else
                            xnew0=xl+beta*(xnew0-xl);
                            xnew2=xl+beta*(xnew2-xl);
                            continue
                        end
                    else
                        xh=xrf
                        xc=xh+beta*(centroid-xh);
      newc=(exp(sqrt(-
1)*2*pi*f_worth(ik)'*(nair).*Thickness./c).*...
                            (2*nair./(nair+xc(1,1)-sqrt(-
1).*xc(2,1))).*...
    (2*(xc(1,1)-sqrt(-1).*xc(2,1))./(nair+xc(1,1)-sqrt(-
1).*xc(2,1))).*...
 exp(-sqrt(-1)*2*pi*f_worth(ik)'.*...
(xc(1,1)-sqrt(-1).*xc(2,1))*Thickness/c))./...
(1+(((xc(1,1)-sqrt(-1).*xc(2,1))-nair)./...
(xc(1,1)-sqrt(-1).*xc(2,1)+nair)).*...
((nair-(xc(1,1)-sqrt(-1).*xc(2,1)))./(xc(1,1)-sqrt(-
1).*xc(2,1)+nair)).*...
exp(-2*sqrt(-1)*2*pi*f_worth(ik)'.*(xc(1,1)-sqrt(-
1).*xc(2,1))*Thickness/c));
                        anglenewc=angle(newc);
                        angleblac=((phase(A(ik))-(anglenewc));
                        if abs(angleblac)>pi &&
abs(angleblac)<2*pi
                            angleblac=abs(angleblac)-2*pi;
                        end
                fxc=abs(abs(abs(A(ik))-
abs(newc))+wght*abs(angleblac));
                        (abs(fxc))
                        if fxc<fxrf
                            xnew0=xc;
                            continue
                        else
                            xnew0=xl+beta*(xnew0-xl);
```

```
                            xnew2=xl+beta*(xnew2-xl);
                            continue
                        end
                    end
                end
            end
            %%%%
            if abs(fxnew2)>abs(fxnew1) &&
abs(fxnew1)>abs(fxnew0)
                fl=abs(fxnew0);
                xl=xnew0;
                fg=abs(fxnew1);
                xg=xnew1;
                fh=abs(fxnew2);
                xh=xnew2;
                centroid=0.5*(xnew1+xnew0);
                xrf=centroid+alfa*(centroid-xh);
     newrf=(exp(sqrt(-
1)*2*pi*f_worth(ik)'*(nair).*Thickness./c).*...
                    (2*nair./(nair+xrf(1,1)-sqrt(-
1).*xrf(2,1))).*...
 (2*(xrf(1,1)-sqrt(-1).*xrf(2,1))./(nair+xrf(1,1)-sqrt(-
1).*xrf(2,1))).*...
exp(-sqrt(-1)*2*pi*f_worth(ik)'.*...
(xrf(1,1)-sqrt(-1).*xrf(2,1))*Thickness/c))./...
(1+(((xrf(1,1)-sqrt(-1).*xrf(2,1))-nair)./...
(xrf(1,1)-sqrt(-1).*xrf(2,1)+nair)).*...
((nair-(xrf(1,1)-sqrt(-1).*xrf(2,1)))./...
(xrf(1,1)-sqrt(-1).*xrf(2,1)+nair)).*...
exp(-2*sqrt(-1)*2*pi*f_worth(ik)'.*...
(xrf(1,1)-sqrt(-1).*xrf(2,1))*Thickness/c));
                anglenewrf=angle(newrf);
                angleblarf=((phase(A(ik))-(anglenewrf));
                if abs(angleblarf)>pi && abs(angleblarf)<2*pi
                    angleblarf=abs(angleblarf)-2*pi;
                end
                fxrf=abs(abs(abs(A(ik))-
abs(newrf))+wght*abs(angleblarf));
                 (abs(fxrf))
                if fxrf<fg && fxrf>fl
                    xnew2=xrf;
                    continue
                end
                if fxrf<fl
                    xe=centroid+gamma*(centroid-xh);
           newe=(exp(sqrt(-
1)*2*pi*f_worth(ik)'*(nair).*Thickness./c).*...
```

```
                          (2*nair./(nair+xe(1,1)-sqrt(-
1).*xe(2,1))).*...
(2*(xe(1,1)-sqrt(-1).*xe(2,1))./(nair+xe(1,1)-sqrt(-
1).*xe(2,1))).*...
exp(-sqrt(-1)*2*pi*f_worth(ik)'.*...
(xe(1,1)-sqrt(-1).*xe(2,1))*Thickness/c))./...
(1+(((xe(1,1)-sqrt(-1).*xe(2,1))-nair)./...
(xe(1,1)-sqrt(-1).*xe(2,1)+nair)).*...
 ((nair-(xe(1,1)-sqrt(-1).*xe(2,1)))./(xe(1,1)-sqrt(-
1).*xe(2,1)+nair)).*...
exp(-2*sqrt(-1)*2*pi*f_worth(ik)'.*(xe(1,1)-sqrt(-
1).*xe(2,1))*Thickness/c));
                    anglenewe=angle(newe);
                    angleblae=((phase(A(ik)))-(anglenewe));
                    if abs(angleblae)>pi && abs(angleblae)<2*pi
                        angleblae=abs(angleblae)-2*pi;
                    end
                    fxe=abs(abs(abs(A(ik))-
abs(newe))+wght*abs(angleblae));
                    (abs(fxe))
                    if fxe<fxrf
                        xnew2=xe;
                        continue
                    end
                    if fxe>fxrf
                        xnew2=xrf;
                        continue
                    end
                end
                if fxrf>fg
                    if fxrf>fh
                        xc=xh+beta*(centroid-xh);
        newc=(exp(sqrt(-
1)*2*pi*f_worth(ik)'*(nair).*Thickness./c).*...
                              (2*nair./(nair+xc(1,1)-sqrt(-
1).*xc(2,1))).*...
 (2*(xc(1,1)-sqrt(-1).*xc(2,1))./(nair+xc(1,1)-sqrt(-
1).*xc(2,1))).*...
exp(-sqrt(-1)*2*pi*f_worth(ik)'.*...
(xc(1,1)-sqrt(-1).*xc(2,1))*Thickness/c))./...
(1+(((xc(1,1)-sqrt(-1).*xc(2,1))-nair)./...
(xc(1,1)-sqrt(-1).*xc(2,1)+nair)).*...
((nair-(xc(1,1)-sqrt(-1).*xc(2,1)))./(xc(1,1)-sqrt(-
1).*xc(2,1)+nair)).*...
exp(-2*sqrt(-1)*2*pi*f_worth(ik)'.*(xc(1,1)-sqrt(-
1).*xc(2,1))*Thickness/c));
                        anglenewc=angle(newc);
```

```
                        angleblac=((phase(A(ik)))-(anglenewc));
                        if abs(angleblac)>pi &&
abs(angleblac)<2*pi
                            angleblac=abs(angleblac)-2*pi;
                        end
              fxc=abs(abs(abs(A(ik))-
abs(newc))+wght*abs(angleblac));
                        (abs(fxc))
                        if fxc<fh
                            xnew2=xc;
                            continue
                        else
                            xnew1=xl+beta*(xnew1-xl);
                            xnew2=xl+beta*(xnew2-xl);
                            continue
                        end
                    else
                        xh=xrf;
                        xc=xh+beta*(centroid-xh);
       newc=(exp(sqrt(-
1)*2*pi*f_worth(ik)'*(nair).*Thickness./c).*...
                            (2*nair./(nair+xc(1,1)-sqrt(-
1).*xc(2,1))).*...
 (2*(xc(1,1)-sqrt(-1).*xc(2,1))./(nair+xc(1,1)-sqrt(-
1).*xc(2,1))).*...
exp(-sqrt(-1)*2*pi*f_worth(ik)'.*...
(xc(1,1)-sqrt(-1).*xc(2,1))*Thickness/c))./...
(1+(((xc(1,1)-sqrt(-1).*xc(2,1))-nair)./...
(xc(1,1)-sqrt(-1).*xc(2,1)+nair)).*...
((nair-(xc(1,1)-sqrt(-1).*xc(2,1)))./(xc(1,1)-sqrt(-
1).*xc(2,1)+nair)).*...
exp(-2*sqrt(-1)*2*pi*f_worth(ik)'.*(xc(1,1)-sqrt(-
1).*xc(2,1))*Thickness/c));
                        anglenewc=angle(newc);
                        angleblac=((phase(A(ik)))-(anglenewc));
                        if abs(angleblac)>pi &&
abs(angleblac)<2*pi
                            angleblac=abs(angleblac)-2*pi;
                        end
                   fxc=abs(abs(abs(A(ik))-
abs(newc))+wght*abs(angleblac));
                        (abs(fxc))
                        if fxc<fxrf
                            xnew2=xc;
                            continue
                        else
                            xnew1=xl+beta*(xnew1-xl);
```

```
                            xnew2=xl+beta*(xnew2-xl);
                            continue
                        end
                    end
                end
            end
            %%%%%
            if abs(fxnew1)>abs(fxnew2) &&
abs(fxnew2)>abs(fxnew0)
                fl=abs(fxnew0);
                xl=xnew0;
                fg=abs(fxnew2);
                xg=xnew2;
                fh=abs(fxnew1);
                xh=xnew1;
                centroid=0.5*(xnew0+xnew2);
                xrf=centroid+alfa*(centroid-xh);
      newrf=(exp(sqrt(-
1)*2*pi*f_worth(ik)'*(nair).*Thickness./c).*...
                    (2*nair./(nair+xrf(1,1)-sqrt(-
1).*xrf(2,1))).*...
 (2*(xrf(1,1)-sqrt(-1).*xrf(2,1))./(nair+xrf(1,1)-sqrt(-
1).*xrf(2,1))).*...
 exp(-sqrt(-1)*2*pi*f_worth(ik)'.*...
(xrf(1,1)-sqrt(-1).*xrf(2,1))*Thickness/c))./...
 (1+(((xrf(1,1)-sqrt(-1).*xrf(2,1))-nair)./...
(xrf(1,1)-sqrt(-1).*xrf(2,1)+nair)).*...
((nair-(xrf(1,1)-sqrt(-1).*xrf(2,1)))./...
(xrf(1,1)-sqrt(-1).*xrf(2,1)+nair)).*...
exp(-2*sqrt(-1)*2*pi*f_worth(ik)'.*...
(xrf(1,1)-sqrt(-1).*xrf(2,1))*Thickness/c));
                anglenewrf=angle(newrf);
                angleblarf=((phase(A(ik)))-(anglenewrf));
                if abs(angleblarf)>pi && abs(angleblarf)<2*pi
                    angleblarf=abs(angleblarf)-2*pi;
                end
                fxrf=abs(abs(abs(A(ik))-
abs(newrf))+wght*abs(angleblarf));
                 (abs(fxrf))
                if fxrf<fg && fxrf>fl
                    xnew1=xrf;
                    continue
                end
                if fxrf<fl
                    xe=centroid+gamma*(centroid-xh);
       newe=(exp(sqrt(-
1)*2*pi*f_worth(ik)'*(nair).*Thickness./c).*...
```

```
                            (2*nair./(nair+xe(1,1)-sqrt(-
1).*xe(2,1))).*...
     (2*(xe(1,1)-sqrt(-1).*xe(2,1))./(nair+xe(1,1)-sqrt(-
1).*xe(2,1))).*...
exp(-sqrt(-1)*2*pi*f_worth(ik)'.*...
(xe(1,1)-sqrt(-1).*xe(2,1))*Thickness/c))./...
(1+(((xe(1,1)-sqrt(-1).*xe(2,1))-nair)./...
(xe(1,1)-sqrt(-1).*xe(2,1)+nair)).*...
((nair-(xe(1,1)-sqrt(-1).*xe(2,1)))./(xe(1,1)-sqrt(-
1).*xe(2,1)+nair)).*...
exp(-2*sqrt(-1)*2*pi*f_worth(ik)'.*(xe(1,1)-sqrt(-
1).*xe(2,1))*Thickness/c));
                    anglenewe=angle(newe);
                    angleblae=((phase(A(ik)))-(anglenewe));
                    if abs(angleblae)>pi && abs(angleblae)<2*pi
                        angleblae=abs(angleblae)-2*pi;
                    end
                    fxe=abs(abs(abs(A(ik))-
abs(newe))+wght*abs(angleblae));
                    (abs(fxe))
                    if fxe<fxrf
                        xnew1=xe;
                        continue
                    end
                    if fxe>fxrf
                        xnew1=xrf;
                        continue
                    end
                end
                if fxrf>fg
                    if fxrf>fh
                        xc=xh+beta*(centroid-xh);
       newc=(exp(sqrt(-
1)*2*pi*f_worth(ik)'*(nair).*Thickness./c).*...
                                (2*nair./(nair+xc(1,1)-sqrt(-
1).*xc(2,1))).*...
(2*(xc(1,1)-sqrt(-1).*xc(2,1))./(nair+xc(1,1)-sqrt(-
1).*xc(2,1))).*...
exp(-sqrt(-1)*2*pi*f_worth(ik)'.*...
(xc(1,1)-sqrt(-1).*xc(2,1))*Thickness/c))./...
(1+(((xc(1,1)-sqrt(-1).*xc(2,1))-nair)./...
(xc(1,1)-sqrt(-1).*xc(2,1)+nair)).*...
((nair-(xc(1,1)-sqrt(-1).*xc(2,1)))./(xc(1,1)-sqrt(-
1).*xc(2,1)+nair)).*...
exp(-2*sqrt(-1)*2*pi*f_worth(ik)'.*(xc(1,1)-sqrt(-
1).*xc(2,1))*Thickness/c));
                        anglenewc=angle(newc);
```

```
                        angleblac=((phase(A(ik)))-(anglenewc));
                        if abs(angleblac)>pi &&
abs(angleblac)<2*pi
                            angleblac=abs(angleblac)-2*pi;
                        end
                 fxc=abs(abs(abs(A(ik))-
abs(newc))+wght*abs(angleblac));
                        (abs(fxc))
                        if fxc<fh
                            xnew1=xc;
                            continue
                        else
                            xnew1=xl+beta*(xnew1-xl);
                            xnew2=xl+beta*(xnew2-xl);
                            continue
                        end
                    else
                        xh=xrf;
                        xc=xh+beta*(centroid-xh);
      newc=(exp(sqrt(-
1)*2*pi*f_worth(ik)'*(nair).*Thickness./c).*...
                            (2*nair./(nair+xc(1,1)-sqrt(-
1).*xc(2,1))).*...
(2*(xc(1,1)-sqrt(-1).*xc(2,1))./(nair+xc(1,1)-sqrt(-
1).*xc(2,1))).*...
exp(-sqrt(-1)*2*pi*f_worth(ik)'.*...
(xc(1,1)-sqrt(-1).*xc(2,1))*Thickness/c))./...
(1+(((xc(1,1)-sqrt(-1).*xc(2,1))-nair)./...
(xc(1,1)-sqrt(-1).*xc(2,1)+nair)).*...
((nair-(xc(1,1)-sqrt(-1).*xc(2,1)))./(xc(1,1)-sqrt(-
1).*xc(2,1)+nair)).*...
exp(-2*sqrt(-1)*2*pi*f_worth(ik)'.*(xc(1,1)-sqrt(-
1).*xc(2,1))*Thickness/c));
                        anglenewc=angle(newc);
                        angleblac=((phase(A(ik)))-(anglenewc));
                        if abs(angleblac)>pi &&
abs(angleblac)<2*pi
                            angleblac=abs(angleblac)-2*pi;
                        end
                 fxc=abs(abs(abs(A(ik))-
abs(newc))+wght*abs(angleblac));
                        (abs(fxc))
                        if fxc<fxrf
                            xnew1=xc;
                            continue
                        else
                            xnew1=xl+beta*(xnew1-xl);
```

```
                                        xnew2=xl+beta*(xnew2-xl);
                                        continue
                                    end
                                end
                            end
                        end
                    end
                end
                par=1;
                indexar(par,:)=bam(1,:);
                kar(par,:)=bam(2,:);
                magar(par,:)=bamm;
                phasar(par,:)=bamp;

                k_f=abs(kar);
                index_f=indexar;

                k_f=abs(k_f);
                real_perm=index_f.^2-k_f.^2;
                imaginary_perm=(2*index_f.*k_f);
                loss_tan=(imaginary_perm./real_perm);
                ind(wj,:)=index_f;
                kd(wj,:)=k_f;

rp(wj,:)=real_perm;ip(wj,:)=imaginary_perm;lt(wj,:)=loss_tan;
    ph(wj,:)=phasar;
    mg(wj,:)=magar;

    clear A
end

D=0;
cima=0;
%total variation - degree 1
for ac=1:size(ind,1)
    for bc=1:fr1(end)-fr(1)+1
        if bc>1
            cima=cima+1;
        D(ac,cima)=abs(ind(ac,bc-1)-ind(ac,bc))+abs(kd(ac,bc-1)-
kd(ac,bc));
        end
    end
    TV(ac)=sum(D(ac,:));
    cima=0;
end
%total variation - degree 2
D1=0;
```

```
for ac=1:size(ind,1)
    for ghj=1:(size(D,2)-1)
        cima=cima+1;
        D1(ac,ghj)=abs(D(ac,cima)-D(ac,cima+1));
    end
    TV1(ac)=sum(D1(ac,:));
    cima=0;
end
figure;plot(lvec,TV,lvec,TV1);grid;
title('total variation degrees one and two')
figure;plot(TV1);grid;title('total variation degree two')

mintv1ind=find(TV1==min(TV1));
bista1=rp(mintv1ind,:);
bista2=lt(mintv1ind,:);
bista3=ind(mintv1ind,:);
bista4=kd(mintv1ind,:);

%extracted parameters (refractive index, extinction coefficient,
%dielectric constant, loss tangent)
figure;plot(f_worth,bista3);grid;title('Refractive Index')
figure;plot(f_worth,bista4);grid;title('Extinction Coefficient')
figure;plot(f_worth,bista1);grid;title('Dielectric Constant')
figure;plot(f_worth,bista2);grid;title('Loss Tangent')
```

Appendix D

The Self-Calibrating Method Matlab Material Characterization Code

Description: This code extracts the material parameters (dielectric constant and loss tangent) of a dielectric substrate using the self-calibrating method. Prior to running, the self-calibrating method code the system artifacts removal procedure should be carried out. The code for the system artifacts removal procedure requires the following inputs:

-Sample measurement file name

-Archived measurement through air file name (for signal artifacts removal procedure)

-number of multiple transmissions to remove the system response pattern from (specified by the number of transmissions due to a certain samples in the time window of the measured sample signal)

Note:

*The measured data text files, must have two columns with one being time and the other being signal intensity. The unit for time should be picoseconds. Delete any other text from the text files.

*The signal artifacts removal procedure is set up to remove the system response from four multiple transmissions at most.

After running the system artifacts removal procedure, the self calibrating technique code is executed. The code for the self-calibrating technique requires the following inputs:

-Thickness estimate

-Upper frequency limit for material characterization

-Lower frequency limit for material characterization

Note:

*The optimization method used is the modified NELDER MEAD SIMPLEX METHOD in two dimensions.

→ The code for the signal artifacts removal procedure is:

```
clc
close all
clear all

format long
%%%%%%%%%%%%%%%%%%%%%%%%%%%%%%%%%%%%%%%%%%%%%%%%%%%%%%%%%%%%%%%%
%%%%%%%%%%%%%%%%%%%%%%%%%%%%%%%%%%%%%%%%%%%%%%%%%Inputs%%%%%%%%%
%%%%%%%%%%%%%%%%%%%%%%%%%%%%%%%%%%%%%%%%%%%%%%%%%%%%%%%%%%%%%%%%
%%%%%%%%%%%%%%%%%%%%%%%%%%%%%%%%%%%%%%%

Ref_Air=textread('Alumina_Ref_Air_0_p_025_in2.txt', '%s'); %
archived
%measurement through air
Ref_Air=str2double(Ref_Air);
sample=textread('Alumina_Test_0_p_025_in1.txt', '%s'); % sample
measurement
sample=str2double(sample);
cla=4;% number of multiple transmissions to remove system
response from

%%%%%%%%%%%%%%%%%%%%%%%%%%%%%%%%%%%%%%%%%%%%%%%%%%%%%%%%%%%%%%%%
%%%%%%%%%%%%%%%%%%%%%%%%%%%%%%%%%%%%%%%%%%%%%%%%%%%%%%%%%%%%%%%%
%%%%%%%%%%%%%%%%%%%%%%%%%%%%%%%%%%%%%%%%%%%%%%%%%%%%%%%%%%%%%%%%
%%%%%%%%%%%%%%%%%%%%%%%%%%%%%%%%%%%%%%%

%%%Building Reference and Sample(Test) Matrices for
j=1;
for i=1:size(sample,1)
    if mod(i,2)~=0
    Ref_Air_c(j,1)=Ref_Air(i,1);
    sample_c(j,1)=sample(i,1);
    end
    if mod(i,2)==0
    Ref_Air_c(j,2)=Ref_Air(i,1);
    sample_c(j,2)=sample(i,1);
    j=j+1;
    end
end
dff=find(abs(Ref_Air_c(:,2))==max(abs(Ref_Air_c(:,2))));
del=find(abs(Ref_Air_c(dff:dff+70,2))==min(abs(Ref_Air_c(dff:dff
+70,2))));
```

```
del=del+dff-2;



Ts=(Ref_Air_c(2,1)-Ref_Air_c(1,1))*10^(-12);
Fs=1/Ts;

%%% Reference and Sample Signals Collected from THz system
figure
plot((Ref_Air_c(:,1)),Ref_Air_c(:,2),':',...
    (sample_c(:,1)),sample_c(:,2))
grid
legend('Air - No Sample', ' Sample')
xlabel('Time (ps)')
ylabel('Recieved Signal Intensity (a.u.)')
title('Time Domain Signals')

himma=0;
sample_c1=sample_c;
clear sample_c
sample_c=sample_c1(1:end-himma,:);

Ref_Air_c1=Ref_Air_c;
clear Ref_Air_c
Ref_Air_c=Ref_Air_c1(1:end-himma,:);

figure;plot(Ref_Air_c(:,1),Ref_Air_c(:,2),sample_c(:,1),sample_c
(:,2));grid

if cla>=1
max_ref=find(Ref_Air_c(:,2)==max(Ref_Air_c(:,2)));%maximum of
reference %signal index
max_sample=find(sample_c(:,2)==max(sample_c(:,2)));%maximum of
sample signal %index
diff=max_sample-max_ref;%difference of indices between
aformentioned maximums


one_ref=Ref_Air_c(1:(end-1*diff),2);%updated reference signal,
tail cut off
two_ref=sample_c(diff+1:(end),2);%update sample signal, aligned
in time with %reference signal
x=(0:1:(size(sample_c(:,1),1)-diff-1))*Ts;%updated x axis - time
axis
```

```
diff_sigs=-
one_ref*max(sample_c(:,2))/max(Ref_Air_c(:,2))+two_ref;%signal=(
updated %sample signal)-(updated reference_signal)
blip=one_ref*max(sample_c(:,2))/max(Ref_Air_c(:,2));
%%% Plot of the updated ref and sample signals with their
difference signal
figure;plot(x,one_ref,x,two_ref,x,diff_sigs);grid

diff_sigs_mod=[zeros(1,diff)'; zeros(1,del)';
diff_sigs(del+1:end,1)]';%zero 5first pulse location in diff
signal

%%%plot of diff signal with zeroed out first pulse location
figure;plot(diff_sigs_mod);grid
end

if cla>=2
max_diff_sigs_mod=find(diff_sigs_mod==max(diff_sigs_mod));%maxim
um of sample %signal index


diff1=max_diff_sigs_mod-max_ref;%difference of indices between
aforementioned %maximums

mult_peak_index_distance=diff1-diff;
mult_tran_method_left_total_indices=size(sample_c(:,2),1)-diff-
max_ref;


one_ref1=Ref_Air_c(1:(end-1*diff1),2);%updated reference signal,
tail cut off
two_ref1=diff_sigs_mod(diff1+1:(end))';%update sample signal,
aligned in time %with reference signal
x1=(0:1:(size(sample_c(:,1),1)-diff1-1))*Ts;%updated x axis -
time axis

diff_sigs1=-one_ref1*max(diff_sigs_mod)/max(Ref_Air_c(:,2))+...
two_ref1;%signal=(updated %sample signal)-(updated
reference_signal)

%%% Plot of the updated ref and sample signals with their
difference signal
figure;plot(x1,one_ref1,x1,two_ref1,x1,diff_sigs1);grid
```

```
diff_sigs1_mod=[zeros(1,diff1)';zeros(1,del)';
diff_sigs1(del+1:end,1)]';%zero first pulse location in diff
signal

%%%plot of diff signal with zeroed out first pulse location
figure;plot(diff_sigs1_mod);grid
end

if cla>=3
max_diff_sigs1_mod=find(diff_sigs1_mod==max(diff_sigs1_mod(round
(del+...
diff1+(diff1-diff)/2):end)));%maximum of sample signal index
diff2=max_diff_sigs1_mod-max_ref;%difference of indices between
aformentioned %maximums

one_ref2=Ref_Air_c(1:(end-1*diff2),2);%updated reference signal,
tail cut off
two_ref2=diff_sigs1_mod(diff2+1:(end))';%update sample signal,
aligned in %time with reference signal
x2=(0:1:(size(sample_c(:,1),1)-1*diff2-1))*Ts;%updated x axis -
time axis

diff_sigs2=-
one_ref2*max(diff_sigs1_mod)/max(Ref_Air_c(:,2))+two_ref2;%signa
l=(updated %sample signal)-(updated reference_signal)

%%% Plot of the updated ref and sample signals with their
difference signal
figure;plot(x2,one_ref2,x2,two_ref2,x2,diff_sigs2);grid


diff_sigs2_mod=[zeros(1,diff2)';zeros(1,del)';
diff_sigs2(del+1:end,1)]';%zero first pulse location in diff
signal

%%%plot of diff signal with zeroed out first pulse location
figure;plot(diff_sigs2_mod);grid
end


if cla>=4
max_diff_sigs2_mod=find(diff_sigs2_mod==max(diff_sigs2_mod(round
(del+...
diff2+(diff1-diff)/2):end)));%maximum of sample signal index
diff3=max_diff_sigs2_mod-max_ref;%difference of indices between
aformentioned %maximums
```

```
one_ref3=Ref_Air_c(1:(end-1*diff3),2);%updated reference signal,
tail cut off
two_ref3=diff_sigs2_mod(diff3+1:(end))';%update sample signal,
aligned in %time with reference signal
x3=(0:1:(size(sample_c(:,1),1)-1*diff3-1))*Ts;%updated x axis -
time axis

diff_sigs3=-
one_ref3*max(diff_sigs2_mod)/max(Ref_Air_c(:,2))+two_ref3;%signa
l=(updated %sample signal)-(updated reference_signal)

%%% Plot of the updated ref and sample signals with their
difference signal
figure;plot(x2,one_ref2,x2,two_ref2,x3,diff_sigs3);grid


diff_sigs3_mod=[zeros(1,diff3)';zeros(1,del)';
diff_sigs3(del+1:end,1)]';%zero first pulse location in diff
signal

%%%plot of diff signal with zeroed out first pulse location
figure;plot(diff_sigs3_mod);grid
end

if cla==4
    uv=diff1-diff;
ux=diff2-diff1;
uy=diff3-diff2;
    if del<=mult_peak_index_distance
clean_diff_sigs_mod=[sample_c(1:diff,2); two_ref(1:del);
diff_sigs_mod(diff+del+1:diff1)';...
    two_ref1(1:del); diff_sigs1_mod(diff1+del+1:diff2)';
two_ref2(1:del);...
    diff_sigs2_mod(diff2+del+1:diff3)'; two_ref3(1:del);
diff_sigs3_mod(diff3+del+1:end)'];

    end
    if del>mult_peak_index_distance
clean_diff_sigs_mod=[sample_c(1:diff,2); two_ref(1:del);
diff_sigs_mod(diff+del:diff1)';...
    two_ref1(1+(del-uv):del); diff_sigs1_mod(diff1+del:diff2)';
two_ref2(1+(del-ux):del);...
    diff_sigs2_mod(diff2+del:diff3)'; two_ref3(1+(del-uy):del);
diff_sigs3_mod(diff3+del+1:end)'];
    end
end
if cla==3
```

```
    uv=diff1-diff;
ux=diff2-diff1;
    if del<=mult_peak_index_distance
clean_diff_sigs_mod=[sample_c(1:diff,2); two_ref(1:del);
diff_sigs_mod(diff+del+1:diff1)';...
    two_ref1(1:del); diff_sigs1_mod(diff1+del+1:diff2)';
two_ref2(1:del);...
    diff_sigs2_mod(diff2+del+1:end)'];
    end
        if del>mult_peak_index_distance
clean_diff_sigs_mod=[sample_c(1:diff,2); two_ref(1:del);
diff_sigs_mod(diff+del:diff1)';...
    two_ref1(1+(del-uv):del); diff_sigs1_mod(diff1+del:diff2)';
two_ref2(1+(del-ux):del);...
    diff_sigs2_mod(diff2+del+1:end)'];
    end
end
if cla==2
    uv=diff1-diff;
    if del<=mult_peak_index_distance
clean_diff_sigs_mod=[sample_c(1:diff,2); two_ref(1:del);
diff_sigs_mod(diff+del+1:diff1)';...
    two_ref1(1:del); diff_sigs1_mod(diff1+del+1:end)'];
    end
        if del>mult_peak_index_distance
clean_diff_sigs_mod=[sample_c(1:diff,2); two_ref(1:del);
diff_sigs_mod(diff+del:diff1)';...
    two_ref1(1+(del-uv):del); diff_sigs1_mod(diff1+del+1:end)'];
    end
end
if cla==1
clean_diff_sigs_mod=[sample_c(1:diff,2); two_ref(1:del);
diff_sigs_mod(diff+del+1:end)'];
end
if cla==0
clean_diff_sigs_mod=[sample_c(:,2)];
end

x=(0:1:(size(sample_c(:,1),1)-1))*Ts;%updated x axis - time axis

%%%plot of diff signal with first pulse from sample signal
figure;plot(x,clean_diff_sigs_mod);grid

%%%plot of diff signal with first pulse from sample signal and
sample signal
figure;plot(x,clean_diff_sigs_mod,x,sample_c(:,2));grid
```

```
x=(0:1:size(sample_c,1)-1)*Ts;
tot=[clean_diff_sigs_mod; zeros(himma,1)];
xstar=x;
save total tot
save xal xstar
save himmal himma
%%%%%%%%%%%%%%%%%%%%%%%%%%%%%%%%%%%%%%%%%%%%%%%%%%%%%%%%%%%%%%%%
%%%%%%%%%%%%%%%%%%%%%%%%%%%%%%%%%%%%%%%%%%%%%%%%%%%%%%%%%%%%%%%%
%%%%%%%%%%%%%%%%%%%%%%%%%%%%%%%%%%%%%%%%%%%%%%%%%%%%%%%%%%%%%%%%
%%%%%%%%%%%%%%%%%%%%%%%%%%%%%%%%%%%%%%%%%%%%%%%%%%%%%%%%%%%%%%%%
%%%%%%%%%%%%%%%%%%%%%%%%%%%%%%%%%%%%%%%%%%%%%%%%%%%%%%%%%%%%%%%%
```

→The code for the self calibrating technique is:

```
clc
close all
clear all
format long
load himmal
load total
load xal
x=xstar;
tot1=tot';
clear tot
tot=tot1;
Num_samples=size(x,2);
%%%%%%%%%%%%%%%%%%%%%%%%%%%%%%%%%%%%%%%%%%%%%%%%%%%%%%%%%%%%%%%%
%%%%%%%%%%%%%%%%%%%%%%%%%%%%%%%%%%%%%%%%%%%%%%Inputs%%%%%%%%%%%%
%%%%%%%%%%%%%%%%%%%%%%%%%%%%%%%%%%%%%%%%%%%%%%%%%%%%%%%%%%%%%%%%
%%%%%%%%%%%%%%%%%%%%%%%%%%%%%%%%%%%%%%%

l=0.637*10^(-3);%thickness of substrate
flow=200*(10^9);%lower frequency limit for material
characterization
fhigh=1600*(10^9);%upper frequency limit for material
characterization

%%%%%%%%%%%%%%%%%%%%%%%%%%%%%%%%%%%%%%%%%%%%%%%%%%%%%%%%%%%%%%%%
%%%%%%%%%%%%%%%%%%%%%%%%%%%%%%%%%%%%%%%%%%%%%%%%%%%%%%%%%%%%%%%%
%%%%%%%%%%%%%%%%%%%%%%%%%%%%%%%%%%%%%%%%%%%%%%%%%%%%%%%%%%%%%%%%
%%%%%%%%%%%%%%%%%%%%%%%%%%%%%%%%%%%%%%%


figure
plot(x,tot)
grid
legend('Sample')
xlabel('Time (s)')
```

```
ylabel('Recieved Signal Intensity (a.u.)')
title('Time Domain Signal')

x1=x;
clear x
bimma=0;
x=x1(:,1:end);

tot1=tot;
clear tot
tot2=tot1(1:end-bimma-himma);

tot=[tot2, zeros(1,bimma+himma)];
tot=tot';


figure
plot(x,tot)
grid
legend('Sample')
xlabel('Time (s)')
ylabel('Recieved Signal Intensity (a.u.)')
title('Time Domain Signal')

lupper=0.1*10^(-3)+l;%upper bound of the substrate thickness
llower=l-0.1*10^(-3);%lower bound of the substrate thickness
many=0;
l_eval=llower:(lupper-llower)/many:lupper;% thickness to try in
the first %iteration of optimization
l_eval=l;

for par=1:(many+1)
    l=l_eval(par)
    nair=1.00027;%index of refraction of air
    c=3e8;%speed of light in free space

    %finding first pulse max
    max_first_pulse=max(tot);
    index_first_max=find(tot==max_first_pulse);

    %finding second pulse max
    min_del_t=2*l*nair^2/c;
    min_index=find((x>=(x(index_first_max)+min_del_t)));
    max_second_pulse = max(tot(min_index(1):end));
    index_second_max=find(tot==max_second_pulse);

    %initializing the index of refraction
```

```
    del_t=(x(index_second_max)-x(index_first_max-1));
    Thickness=l;
    index_initc=del_t*c./(2*Thickness);
    index_init=ones(size(tot(:,1),1),1)*index_initc;

    %initializing the extinction coefficient at k=0
    k_init=0.0*ones(size(index_init));

    %creating zero padded tukey window, for first transmission
multiple
    %extraction
    L=index_second_max+round((index_first_max-
index_second_max)*0.5);
    ri=0.1;
    tukey=tukeywin(L,ri);
    tukeyzp=padarray(tukey,(Num_samples-L),'post');
    figure; plot(x(:),tukeyzp); grid

    %applying window on complete signal to take out the first
multiple
    %transmission
    first_multiple=tukeyzp.*tot;

    %finding measured ratio

first_multiple_ft=fft(first_multiple,size(first_multiple,1));
    Complete_signal_ft=fft(tot,Num_samples);
    ratio_meas=first_multiple_ft./Complete_signal_ft;
    Ts=x(1,2)-x(1,1);
    Fs=1/Ts;
    f=0:Fs/Num_samples:Fs-Fs/Num_samples;%Frequency axis
    %measured ratio spectrum

    fff=find(f>=2.5*(10^12));
    noise_level=20*mean(abs(Complete_signal_ft(fff(1):end/2)));

    fr=find(f>=flow);
    mista=abs(Complete_signal_ft((fr(1):end/2)));
    sss=find(mista<=noise_level);
    fr1=find(abs(Complete_signal_ft(1:end/2))==mista(sss(1)));
    fg=find(f>=fhigh);
    fr1(end)=fg(1);
    f_worth=f(fr(1):fr1(end));

    init_calc_ration=1-(((index_init-sqrt(-1)*k_init-nair)./...
(index_init-sqrt(-1)*k_init+nair)).^2).*...
```

```
    ((exp(-sqrt(-1)*2*(index_init-sqrt(-
1)*k_init)*2*pi.*f'*Thickness/c)));
    jhi=real(Num_samples*ifft(ratio_meas(fr(1):fr1(end))));
    maxjhi=max(abs(jhi(5:end)));

ghi=real(Num_samples*ifft(init_calc_ration(fr(1):fr1(end))));

    lj=1;
    for clap=1:15000
        k_init=k_init+0.00001;
        init_calc_ration=1-(((index_init-sqrt(-1)*k_init-
nair)./...
(index_init-sqrt(-1)*k_init+nair)).^2).*...
    ((exp(-sqrt(-1)*2*(index_init-sqrt(-
1)*k_init)*2*pi.*f'*Thickness/c)));

ghi=real(Num_samples*ifft(init_calc_ration(fr(1):fr1(end))));
        maxghi=max(abs(ghi(5:end)));
        if abs(maxghi)<=abs(maxjhi)
            break
        end
    end

    %simplex search method
    index=index_init(fr(1):fr1(end),:);
    k=k_init(fr(1):fr1(end),:);
    bam=[index, k]';
    N=2;
    alfa=1;
    beta=0.5;
    gamma=2;

    cla=1;

    del1=0.1*((sqrt(N+1)+N-1)/(N*sqrt(2)));
    del2=0.1*((sqrt(N+1)-1)/(N*sqrt(2)));
    ration=ratio_meas(fr(1):fr1(end));
    save rational ration
    ik=5;
    save ikal ik
    save f_worthal f_worth
    save nairal nair

    wght=1;
    for ik=1:size(f_worth,2)
        cla=1;
        xnew0=[bam(1,ik); bam(2,ik)];
```

```
        xnew1=[bam(1,ik)+del1; bam(2,ik)+del2];
        xnew2=[bam(1,ik)+del2; bam(2,ik)+del1];
        counting=0;
        alfa=alfa;
        P=phase(ration(ik));
        P=P;
        while cla==1
            counting=counting+1;
new0=1-(((xnew0(1,1)-sqrt(-1)*xnew0(2,1)-nair)/...
(xnew0(1,1)-sqrt(-1)*xnew0(2,1)+nair))^2)*...
((exp(-sqrt(-1)*2*(xnew0(1,1)-sqrt(-...
1)*xnew0(2,1))*2*pi*f_worth(ik)*Thickness/c)));
            anglenew0=angle(new0);
            anglebla0=((phase(ration(ik)))-(anglenew0));
            if abs(anglebla0)>pi && abs(anglebla0)<2*pi
                if counting==1
                    ttt(ik)=ik;
                end
                anglebla0=abs(anglebla0)-2*pi;
            end
            fxnew0=abs(abs(abs(ration(ik))-
abs(new0))+wght*abs(anglebla0));
            (abs(fxnew0))
new1=1-(((xnew1(1,1)-sqrt(-1)*xnew1(2,1)-nair)/...
(xnew1(1,1)-sqrt(-1)*xnew1(2,1)+nair))^2)*...
((exp(-sqrt(-1)*2*(xnew1(1,1)-sqrt(-...
1)*xnew1(2,1))*2*pi*f_worth(ik)*Thickness/c)));
            anglenew1=angle(new1);
            anglebla1=((phase(ration(ik)))-(anglenew1));
            if abs(anglebla1)>pi && abs(anglebla1)<2*pi
                if counting==1
                    ttt(ik)=ik;
                end
                anglebla1=abs(anglebla1)-2*pi;
            end
            fxnew1=abs(abs(abs(ration(ik))-
abs(new1))+wght*abs(anglebla1));
            (abs(fxnew1))
new2=1-(((xnew2(1,1)-sqrt(-1)*xnew2(2,1)-nair)/...
(xnew2(1,1)-sqrt(-1)*xnew2(2,1)+nair))^2)*...
((exp(-sqrt(-1)*2*(xnew2(1,1)-sqrt(-...
1)*xnew2(2,1))*2*pi*f_worth(ik)*Thickness/c)));
            anglenew2=angle(new2);
            anglebla2=((phase(ration(ik)))-(anglenew2));
            if abs(anglebla2)>pi && abs(anglebla2)<2*pi
                if counting==1
                    ttt(ik)=ik;
```

```
                end
                anglebla2=abs(anglebla2)-2*pi;
            end
            fxnew2=abs(abs(abs(ration(ik))-
abs(new2))+wght*abs(anglebla2));
            (abs(fxnew2))

            if (abs(fxnew0))<0.000000000000001
                bam(:,ik)=xnew0;
                bamp(:,ik)=phase(new0);
                bamm(:,ik)=abs(new0);
                cla=2;
                phg(ik)=1;
                continue
            elseif (abs(fxnew1))<0.000000000000001
                bam(:,ik)=xnew1;
                bamp(:,ik)=phase(new1);
                bamm(:,ik)=abs(new1);
                cla=2;
                phg(ik)=2;
                continue
            elseif (abs(fxnew2))<0.000000000000001
                bam(:,ik)=xnew2;
                bamp(:,ik)=phase(new2);
                bamm(:,ik)=abs(new2);
                cla=2;
                phg(ik)=3;
                continue
            elseif
std([(abs(fxnew0)),(abs(fxnew1)),(abs(fxnew2))])<= ...
0.00000000001
    if abs(abs(fxnew0))<=(abs(fxnew1)) &&
(abs(fxnew0))<=(abs(fxnew2))
                    bam(:,ik)=xnew0;
                    bamp(:,ik)=phase(new0);
                    bamm(:,ik)=abs(new0);
                    cla=2;
                    phg(ik)=4;
                    continue
                end
        if(abs(fxnew0))>=(abs(fxnew1)) &&
(abs(fxnew1))<=(abs(fxnew2))
                    bam(:,ik)=xnew1;
                    bamp(:,ik)=phase(new1);
                    bamm(:,ik)=abs(new1);
                    cla=2;
                    phg(ik)=4;
```

```
                    continue
                end
      if(abs(fxnew2))<=(abs(fxnew1)) &&
(abs(fxnew0))>=(abs(fxnew2))
                    bam(:,ik)=xnew2;
                    bamp(:,ik)=phase(new2);
                    bamm(:,ik)=abs(new2);
                    cla=2;
                    phg(ik)=4;
                    continue
                end
            end

            %%%%%
            if abs(fxnew0)>abs(fxnew1) &&
abs(fxnew1)>abs(fxnew2)
                fl=abs(fxnew2);
                xl=xnew2;
                fg=abs(fxnew1);
                xg=xnew1;
                fh=abs(fxnew0);
                xh=xnew0;
                centroid=0.5*(xnew1+xnew2);
                xrf=centroid+alfa*(centroid-xh);
newrf=1-(((xrf(1,1)-sqrt(-1)*xrf(2,1)-nair)/...
(xrf(1,1)-sqrt(-1)*xrf(2,1)+nair))^2)*...
((exp(-sqrt(-1)*2*(xrf(1,1)-sqrt(-...
1)*xrf(2,1))*2*pi*f_worth(ik)*Thickness/c)));
                anglenewrf=angle(newrf);
                angleblarf=((phase(ration(ik)))-(anglenewrf));
                if abs(angleblarf)>pi && abs(angleblarf)<2*pi
                    angleblarf=abs(angleblarf)-2*pi;
                end
      fxrf=abs(abs(abs(ration(ik))-
abs(newrf))+wght*abs(angleblarf));
                (abs(fxrf))
                if fxrf<fg && fxrf>fl
                    xnew0=xrf;
                    continue
                end
                if fxrf<fl
                    xe=(gamma)*xrf+(1-gamma)*(centroid);
newe=1-(((xe(1,1)-sqrt(-1)*xe(2,1)-nair)/...
(xe(1,1)-sqrt(-1)*xe(2,1)+nair))^2)*...
((exp(-sqrt(-1)*2*(xe(1,1)-sqrt(-
1)*xe(2,1))*2*pi*f_worth(ik)*Thickness/c)));
                    anglenewe=angle(newe);
```

```
                    angleblae=((phase(ration(ik)))-(anglenewe));
                    if abs(angleblae)>pi && abs(angleblae)<2*pi
                        angleblae=abs(angleblae)-2*pi;
                    end
         fxe=abs(abs(abs(ration(ik))-
abs(newe))+wght*abs(angleblae));
                    (abs(fxe))
                    if fxe<fxrf
                        xnew0=xe;
                        continue
                    end
                    if fxe>fxrf
                        xnew0=xrf;
                        continue
                    end
                end
                if fxrf>=fg
                    if fxrf>=fh
                        xc=beta*xh+(1-beta)*(centroid);
newc=1-(((xc(1,1)-sqrt(-1)*xc(2,1)-nair)/(xc(1,1)-sqrt(-...
1)*xc(2,1)+nair))^2)*...
((exp(-sqrt(-1)*2*(xc(1,1)-sqrt(-
1)*xc(2,1))*2*pi*f_worth(ik)*Thickness/c)));
                        anglenewc=angle(newc);
                        angleblac=((phase(ration(ik)))-
(anglenewc));
                        if abs(angleblac)>pi &&
abs(angleblac)<2*pi
                            angleblac=abs(angleblac)-2*pi;
                        end
       fxc=abs(abs(abs(ration(ik))-
abs(newc))+wght*abs(angleblac));
                        (abs(fxc))
                        if fxc<fh
                            xnew0=xc;
                            continue
                        else
                            xnew0=xl+beta*(xnew0-xl);
                            xnew1=xl+beta*(xnew1-xl);
                            continue
                        end
                    else
                        xh=xrf;
                        xc=beta*xh+(1-beta)*(centroid);
 newc=1-(((xc(1,1)-sqrt(-1)*xc(2,1)-nair)/(xc(1,1)-sqrt(-...
1)*xc(2,1)+nair))^2)*...
```

```
((exp(-sqrt(-1)*2*(xc(1,1)-sqrt(-
1)*xc(2,1))*2*pi*f_worth(ik)*Thickness/c)));
                        anglenewc=angle(newc);
                        angleblac=((phase(ration(ik)))-
(anglenewc));
                        if abs(angleblac)>pi &&
abs(angleblac)<2*pi
                            angleblac=abs(angleblac)-2*pi;
                        end
        fxc=abs(abs(abs(ration(ik))-
abs(newc))+wght*abs(angleblac));
                        (abs(fxc))
                        if fxc<=fxrf
                            xnew0=xc;
                            continue
                        else
                            xnew0=xl+beta*(xnew0-xl);
                            xnew1=xl+beta*(xnew1-xl);
                            continue
                        end
                    end
                end
            end

            %%%%%
            if abs(fxnew1)>abs(fxnew0) &&
abs(fxnew0)>abs(fxnew2)
                fl=abs(fxnew2);
                xl=xnew2;
                fg=abs(fxnew0);
                xg=xnew0;
                fh=abs(fxnew1);
                xh=xnew1;
                centroid=0.5*(xnew0+xnew2);
                xrf=centroid+alfa*(centroid-xh);
newrf=1-(((xrf(1,1)-sqrt(-1)*xrf(2,1)-nair)/(xrf(1,1)-sqrt(-...
1)*xrf(2,1)+nair))^2)*...
((exp(-sqrt(-1)*2*(xrf(1,1)-sqrt(-...
1)*xrf(2,1))*2*pi*f_worth(ik)*Thickness/c)));
                anglenewrf=angle(newrf);
                angleblarf=((phase(ration(ik)))-(anglenewrf));
                if abs(angleblarf)>pi && abs(angleblarf)<2*pi
                    angleblarf=abs(angleblarf)-2*pi;
                end
      fxrf=abs(abs(abs(ration(ik))-
abs(newrf))+wght*abs(angleblarf));
                (abs(fxrf))
```

```
                if fxrf<fg && fxrf>fl
                    xnew1=xrf;
                    continue
                end
                if fxrf<fl
                    xe=(gamma)*xrf+(1-gamma)*(centroid);
newe=1-(((xe(1,1)-sqrt(-1)*xe(2,1)-nair)/(xe(1,1)-sqrt(-...
1)*xe(2,1)+nair))^2)*...
((exp(-sqrt(-1)*2*(xe(1,1)-sqrt(-
1)*xe(2,1))*2*pi*f_worth(ik)*Thickness/c)));
                    anglenewe=angle(newe);
                    angleblae=((phase(ration(ik)))-(anglenewe));
                    if abs(angleblae)>pi && abs(angleblae)<2*pi
                        angleblae=abs(angleblae)-2*pi;
                    end
 fxe=abs(abs(abs(ration(ik))-abs(newe))+wght*abs(angleblae));
                    (abs(fxe))
                    if fxe<fxrf
                        xnew1=xe;
                        continue
                    end
                    if fxe>fxrf
                        xnew1=xrf;
                        continue
                    end
                end
                if fxrf>=fg
                    if fxrf>=fh
                        xc=beta*xh+(1-beta)*(centroid);
newc=1-(((xc(1,1)-sqrt(-1)*xc(2,1)-nair)/(xc(1,1)-sqrt(-...
1)*xc(2,1)+nair))^2)*...
((exp(-sqrt(-1)*2*(xc(1,1)-sqrt(-
1)*xc(2,1))*2*pi*f_worth(ik)*Thickness/c)));
                        anglenewc=angle(newc);
                        angleblac=((phase(ration(ik)))-
(anglenewc));
                        if abs(angleblac)>pi &&
abs(angleblac)<2*pi
                            angleblac=abs(angleblac)-2*pi;
                        end
      fxc=abs(abs(abs(ration(ik))-
abs(newc))+wght*abs(angleblac));
                        (abs(fxc))
                        if fxc<fh
                            xnew1=xc;
                            continue
                        else
```

```
                                xnew0=xl+beta*(xnew0-xl);
                                xnew1=xl+beta*(xnew1-xl);
                                continue
                            end
                        else
                            xh=xrf;
                            xc=beta*xh+(1-beta)*(centroid);
newc=1-((((xc(1,1)-sqrt(-1)*xc(2,1)-nair)/(xc(1,1)-sqrt(-...
1)*xc(2,1)+nair))^2)*...
((exp(-sqrt(-1)*2*(xc(1,1)-sqrt(-
1)*xc(2,1))*2*pi*f_worth(ik)*Thickness/c)));
                            anglenewc=angle(newc);
                            angleblac=((phase(ration(ik))-
(anglenewc));
                            if abs(angleblac)>pi &&
abs(angleblac)<2*pi
                                angleblac=abs(angleblac)-2*pi;
                            end
         fxc=abs(abs(abs(ration(ik))-
abs(newc))+wght*abs(angleblac));
                            (abs(fxc))
                            if fxc<=fxrf
                                xnew1=xc;
                                continue
                            else
                                xnew0=xl+beta*(xnew0-xl);
                                xnew1=xl+beta*(xnew1-xl);
                                continue
                            end
                        end
                    end
                end
                %%%%%
                if abs(fxnew2)>abs(fxnew0) &&
abs(fxnew0)>abs(fxnew1)
                    fl=abs(fxnew1);
                    xl=xnew1;
                    fg=abs(fxnew0);
                    xg=xnew0;
                    fh=abs(fxnew2);
                    xh=xnew2;
                    centroid=0.5*(xnew0+xnew1);
                    xrf=centroid+alfa*(centroid-xh);
newrf=1-((((xrf(1,1)-sqrt(-1)*xrf(2,1)-nair)/(xrf(1,1)-sqrt(-...
1)*xrf(2,1)+nair))^2)*...
((exp(-sqrt(-1)*2*(xrf(1,1)-sqrt(-...
1)*xrf(2,1))*2*pi*f_worth(ik)*Thickness/c)));
```

```
                anglenewrf=angle(newrf);
                angleblarf=((phase(ration(ik)))-(anglenewrf));
                if abs(angleblarf)>pi && abs(angleblarf)<2*pi
                    angleblarf=abs(angleblarf)-2*pi;
                end
       fxrf=abs(abs(abs(ration(ik))-
abs(newrf))+wght*abs(angleblarf));
                (abs(fxrf))
                if fxrf<fg && fxrf>fl
                    xnew2=xrf;
                    continue
                end
                if fxrf<fl
                    xe=(gamma)*xrf+(1-gamma)*(centroid);
newe=1-(((xe(1,1)-sqrt(-1)*xe(2,1)-nair)/(xe(1,1)-sqrt(-...
1)*xe(2,1)+nair))^2)*...
((exp(-sqrt(-1)*2*(xe(1,1)-sqrt(-
1)*xe(2,1))*2*pi*f_worth(ik)*Thickness/c)));
                    anglenewe=angle(newe);
                    angleblae=((phase(ration(ik)))-(anglenewe));
                    if abs(angleblae)>pi && abs(angleblae)<2*pi
                        angleblae=abs(angleblae)-2*pi;
                    end
          fxe=abs(abs(abs(ration(ik))-
abs(newe))+wght*abs(angleblae));
                    (abs(fxe))
                    if fxe<fxrf
                        xnew2=xe;
                        continue
                    end
                    if fxe>fxrf
                        xnew2=xrf;
                        continue
                    end
                end
                if fxrf>=fg
                    if fxrf>=fh
                        xc=beta*xh+(1-beta)*(centroid);
newc=1-(((xc(1,1)-sqrt(-1)*xc(2,1)-nair)/(xc(1,1)-sqrt(-...
1)*xc(2,1)+nair))^2)*...
((exp(-sqrt(-1)*2*(xc(1,1)-sqrt(-
1)*xc(2,1))*2*pi*f_worth(ik)*Thickness/c)));
                        anglenewc=angle(newc);
                        angleblac=((phase(ration(ik)))-
(anglenewc));
                        if abs(angleblac)>pi &&
abs(angleblac)<2*pi
```

```
                            angleblac=abs(angleblac)-2*pi;
                        end
         fxc=abs(abs(abs(ration(ik))-
abs(newc))+wght*abs(angleblac));
                        (abs(fxc))
                        if fxc<fh
                            xnew2=xc;
                            continue
                        else
                            xnew0=xl+beta*(xnew0-xl);
                            xnew2=xl+beta*(xnew2-xl);
                            continue
                        end
                    else
                        xh=xrf;
                        xc=beta*xh+(1-beta)*(centroid);
 newc=1-(((xc(1,1)-sqrt(-1)*xc(2,1)-nair)/(xc(1,1)-sqrt(-...
1)*xc(2,1)+nair))^2)*...
((exp(-sqrt(-1)*2*(xc(1,1)-sqrt(-
1)*xc(2,1))*2*pi*f_worth(ik)*Thickness/c)));
                        anglenewc=angle(newc);
                        angleblac=((phase(ration(ik)))-
(anglenewc));
                        if abs(angleblac)>pi &&
abs(angleblac)<2*pi
                            angleblac=abs(angleblac)-2*pi;
                        end
         fxc=abs(abs(abs(ration(ik))-
abs(newc))+wght*abs(angleblac));
                        (abs(fxc))
                        if fxc<=fxrf
                            xnew2=xc;
                            continue
                        else
                            xnew0=xl+beta*(xnew0-xl);
                            xnew2=xl+beta*(xnew2-xl);
                            continue
                        end
                    end
                end
            end

            %%%%%
            if abs(fxnew0)>abs(fxnew2) &&
abs(fxnew2)>abs(fxnew1)
                fl=abs(fxnew1);
                xl=xnew1;
```

```
                fg=abs(fxnew2);
                xg=xnew2;
                fh=abs(fxnew0);
                xh=xnew0;
                centroid=0.5*(xnew1+xnew2);
                xrf=centroid+alfa*(centroid-xh);
newrf=1-(((xrf(1,1)-sqrt(-1)*xrf(2,1)-nair)/(xrf(1,1)-sqrt(-...
1)*xrf(2,1)+nair))^2)*...
((exp(-sqrt(-1)*2*(xrf(1,1)-sqrt(-...
1)*xrf(2,1))*2*pi*f_worth(ik)*Thickness/c)));
                anglenewrf=angle(newrf);
                angleblarf=((phase(ration(ik)))-(anglenewrf));
                if abs(angleblarf)>pi && abs(angleblarf)<2*pi
                    angleblarf=abs(angleblarf)-2*pi;
                end
      fxrf=abs(abs(abs(ration(ik))-
abs(newrf))+wght*abs(angleblarf));
                (abs(fxrf))
                if fxrf<fg && fxrf>fl
                    xnew0=xrf;
                    continue
                end
                if fxrf<fl
                    xe=(gamma)*xrf+(1-gamma)*(centroid);
newe=1-(((xe(1,1)-sqrt(-1)*xe(2,1)-nair)/(xe(1,1)-sqrt(-...
1)*xe(2,1)+nair))^2)*...
((exp(-sqrt(-1)*2*(xe(1,1)-sqrt(-
1)*xe(2,1))*2*pi*f_worth(ik)*Thickness/c)));
                    anglenewe=angle(newe);
                    angleblae=((phase(ration(ik)))-(anglenewe));
                    if abs(angleblae)>pi && abs(angleblae)<2*pi
                        angleblae=abs(angleblae)-2*pi;
                    end
  fxe=abs(abs(abs(ration(ik))-abs(newe))+wght*abs(angleblae));
                    (abs(fxe))
                    if fxe<fxrf
                        xnew0=xe;
                        continue
                    end
                    if fxe>fxrf
                        xnew0=xrf;
                        continue
                    end
                end
                if fxrf>=fg
                    if fxrf>=fh
                        xc=beta*xh+(1-beta)*(centroid);
```

```
newc=1-(((xc(1,1)-sqrt(-1)*xc(2,1)-nair)/(xc(1,1)-sqrt(-...
1)*xc(2,1)+nair))^2)*...
((exp(-sqrt(-1)*2*(xc(1,1)-sqrt(-
1)*xc(2,1))*2*pi*f_worth(ik)*Thickness/c)));
                        anglenewc=angle(newc);
                        angleblac=((phase(ration(ik)))-
(anglenewc));
                        if abs(angleblac)>pi  &&
abs(angleblac)<2*pi
                            angleblac=abs(angleblac)-2*pi;
                        end
         fxc=abs(abs(abs(ration(ik))-
abs(newc))+wght*abs(angleblac));
                        (abs(fxc))
                        if fxc<fh
                            xnew0=xc;
                            continue
                        else
                            xnew0=xl+beta*(xnew0-xl);
                            xnew2=xl+beta*(xnew2-xl);
                            continue
                        end
                    else
                        xc=beta*xh+(1-beta)*(centroid);
newc=1-(((xc(1,1)-sqrt(-1)*xc(2,1)-nair)/(xc(1,1)-sqrt(-...
1)*xc(2,1)+nair))^2)*...
((exp(-sqrt(-1)*2*(xc(1,1)-sqrt(-
1)*xc(2,1))*2*pi*f_worth(ik)*Thickness/c)));
                        anglenewc=angle(newc);
                        angleblac=((phase(ration(ik)))-
(anglenewc));
                        if abs(angleblac)>pi  &&
abs(angleblac)<2*pi
                            angleblac=abs(angleblac)-2*pi;
                        end
fxc=abs(abs(abs(ration(ik))-abs(newc))+wght*abs(angleblac));
                        (abs(fxc))
                        if fxc<=fxrf
                            xnew0=xc;
                            continue
                        else
                            xnew0=xl+beta*(xnew0-xl);
                            xnew2=xl+beta*(xnew2-xl);
                            continue
                        end
                    end
                end
```

```
            end

            %%%%
            if abs(fxnew2)>abs(fxnew1) &&
abs(fxnew1)>abs(fxnew0)
                fl=abs(fxnew0);
                xl=xnew0;
                fg=abs(fxnew1);
                xg=xnew1;
                fh=abs(fxnew2);
                xh=xnew2;
                centroid=0.5*(xnew1+xnew0);
                xrf=centroid+alfa*(centroid-xh);
newrf=1-(((xrf(1,1)-sqrt(-1)*xrf(2,1)-nair)/(xrf(1,1)-sqrt(-...
1)*xrf(2,1)+nair))^2)*...
((exp(-sqrt(-1)*2*(xrf(1,1)-sqrt(-...
1)*xrf(2,1))*2*pi*f_worth(ik)*Thickness/c)));
                anglenewrf=angle(newrf);
                angleblarf=((phase(ration(ik)))-(anglenewrf));
                if abs(angleblarf)>pi && abs(angleblarf)<2*pi
                    angleblarf=abs(angleblarf)-2*pi;
                end
 fxrf=abs(abs(abs(ration(ik))-abs(newrf))+wght*abs(angleblarf));
                (abs(fxrf))
                if fxrf<fg && fxrf>fl
                    xnew2=xrf;
                    continue
                end
                if fxrf<fl
                    xe=(gamma)*xrf+(1-gamma)*(centroid);
newe=1-(((xe(1,1)-sqrt(-1)*xe(2,1)-nair)/(xe(1,1)-sqrt(-...
1)*xe(2,1)+nair))^2)*...
((exp(-sqrt(-1)*2*(xe(1,1)-sqrt(-
1)*xe(2,1))*2*pi*f_worth(ik)*Thickness/c)));
                    anglenewe=angle(newe);
                    angleblae=((phase(ration(ik)))-(anglenewe));
                    if abs(angleblae)>pi && abs(angleblae)<2*pi
                        angleblae=abs(angleblae)-2*pi;
                    end
 fxe=abs(abs(abs(ration(ik))-abs(newe))+wght*abs(angleblae));
                    (abs(fxe))
                    if fxe<fxrf
                        xnew2=xe;
                        continue
                    end
                    if fxe>fxrf
                        xnew2=xrf;
```

```
                        continue
                    end
                end
                if fxrf>=fg
                    if fxrf>=fh
                        xc=beta*xh+(1-beta)*(centroid);
newc=1-(((xc(1,1)-sqrt(-1)*xc(2,1)-nair)/(xc(1,1)-sqrt(-...
1)*xc(2,1)+nair))^2)*...
((exp(-sqrt(-1)*2*(xc(1,1)-sqrt(-
1)*xc(2,1))*2*pi*f_worth(ik)*Thickness/c)));
                        anglenewc=angle(newc);
                        angleblac=((phase(ration(ik))-
(anglenewc));
                        if abs(angleblac)>pi &&
abs(angleblac)<2*pi
                            angleblac=abs(angleblac)-2*pi;
                        end
   fxc=abs(abs(abs(ration(ik))-abs(newc))+wght*abs(angleblac));
                        (abs(fxc))
                        if fxc<fh
                            xnew2=xc;
                            continue
                        else
                            xnew1=xl+beta*(xnew1-xl);
                            xnew2=xl+beta*(xnew2-xl);
                            continue
                        end
                    else
                        xh=xrf;
                        xc=beta*xh+(1-beta)*(centroid);
newc=1-(((xc(1,1)-sqrt(-1)*xc(2,1)-nair)/(xc(1,1)-sqrt(-...
1)*xc(2,1)+nair))^2)*...
((exp(-sqrt(-1)*2*(xc(1,1)-sqrt(-
1)*xc(2,1))*2*pi*f_worth(ik)*Thickness/c)));
                        anglenewc=angle(newc);
                        angleblac=((phase(ration(ik))-
(anglenewc));
                        if abs(angleblac)>pi &&
abs(angleblac)<2*pi
                            angleblac=abs(angleblac)-2*pi;
                        end
      fxc=abs(abs(abs(ration(ik))-
abs(newc))+wght*abs(angleblac));
                        (abs(fxc))
                        if fxc<=fxrf
                            xnew2=xc;
                            continue
```

```
                    else
                        xnew1=xl+beta*(xnew1-xl);
                        xnew2=xl+beta*(xnew2-xl);
                        continue
                    end
                end
            end
        end

        %%%%%
        if abs(fxnew1)>abs(fxnew2)  &&
abs(fxnew2)>abs(fxnew0)
            fl=abs(fxnew0);
            xl=xnew0;
            fg=abs(fxnew2);
            xg=xnew2;
            fh=abs(fxnew1);
            xh=xnew1;
            centroid=0.5*(xnew0+xnew2);
            xrf=centroid+alfa*(centroid-xh);
newrf=1-(((xrf(1,1)-sqrt(-1)*xrf(2,1)-nair)/(xrf(1,1)-sqrt(-...
1)*xrf(2,1)+nair))^2)*...
((exp(-sqrt(-1)*2*(xrf(1,1)-sqrt(-...
1)*xrf(2,1))*2*pi*f_worth(ik)*Thickness/c)));
            anglenewrf=angle(newrf);
            angleblarf=((phase(ration(ik)))-(anglenewrf));
            if abs(angleblarf)>pi && abs(angleblarf)<2*pi
                angleblarf=abs(angleblarf)-2*pi;
            end
   fxrf=abs(abs(abs(ration(ik))-
abs(newrf))+wght*abs(angleblarf));
            (abs(fxrf))
            if fxrf<fg && fxrf>fl
                xnew1=xrf;
                continue
            end
            if fxrf<fl
                xe=(gamma)*xrf+(1-gamma)*(centroid);
newe=1-(((xe(1,1)-sqrt(-1)*xe(2,1)-nair)/(xe(1,1)-sqrt(-...
1)*xe(2,1)+nair))^2)*...
((exp(-sqrt(-1)*2*(xe(1,1)-sqrt(-
1)*xe(2,1))*2*pi*f_worth(ik)*Thickness/c)));
                anglenewe=angle(newe);
                angleblae=((phase(ration(ik)))-(anglenewe));
                if abs(angleblae)>pi && abs(angleblae)<2*pi
                    angleblae=abs(angleblae)-2*pi;
                end
```

```
 fxe=abs(abs(abs(ration(ik))-abs(newe))+wght*abs(angleblae));
                    (abs(fxe))
                    if fxe<fxrf
                        xnew1=xe;
                        continue
                    end
                    if fxe>fxrf
                        xnew1=xrf;
                        continue
                    end
                end
                if fxrf>=fg
                    if fxrf>=fh
                        xc=beta*xh+(1-beta)*(centroid);
newc=1-(((xc(1,1)-sqrt(-1)*xc(2,1)-nair)/(xc(1,1)-sqrt(-...
1)*xc(2,1)+nair))^2)*...
((exp(-sqrt(-1)*2*(xc(1,1)-sqrt(-
1)*xc(2,1))*2*pi*f_worth(ik)*Thickness/c)));
                        anglenewc=angle(newc);
                        angleblac=((phase(ration(ik)))-
(anglenewc));
                        if abs(angleblac)>pi  &&
abs(angleblac)<2*pi
                            angleblac=abs(angleblac)-2*pi;
                        end
      fxc=abs(abs(abs(ration(ik))-
abs(newc))+wght*abs(angleblac));
                        (abs(fxc))
                        if fxc<fh
                            xnew1=xc;
                            continue
                        else
                            xnew1=xl+beta*(xnew1-xl);
                            xnew2=xl+beta*(xnew2-xl);
                            continue
                        end
                    else
                        xh=xrf;
                        xc=beta*xh+(1-beta)*(centroid);
newc=1-(((xc(1,1)-sqrt(-1)*xc(2,1)-nair)/(xc(1,1)-sqrt(-...
1)*xc(2,1)+nair))^2)*...
((exp(-sqrt(-1)*2*(xc(1,1)-sqrt(-
1)*xc(2,1))*2*pi*f_worth(ik)*Thickness/c)));
                        anglenewc=angle(newc);
                        angleblac=((phase(ration(ik)))-
(anglenewc));
```

```
                        if abs(angleblac)>pi &&
abs(angleblac)<2*pi
                            angleblac=abs(angleblac)-2*pi;
                        end
    fxc=abs(abs(abs(ration(ik))-abs(newc))+wght*abs(angleblac));
                        (abs(fxc))
                        if fxc<=fxrf
                            xnew1=xc;
                            continue
                        else
                            xnew1=xl+beta*(xnew1-xl);
                            xnew2=xl+beta*(xnew2-xl);
                            continue
                        end
                    end
                end
            end
        end
    end
    indexar(par,:)=bam(1,:);
    kar(par,:)=bam(2,:);
    magar(par,:)=bamm;
    phasar(par,:)=bamp;
end

k_f=abs(kar);
index_f=indexar;
figure
plot(f_worth,index_f)
grid
title('index')
figure
plot(f_worth,k_f)
grid
title('extinction')

figure
plot(f_worth,2*k_f.*f_worth*2*pi/(c*100))
grid
title('abs coeff.')
% k_f=abs(k_f);
%real perm
real_perm=index_f.^2-k_f.^2;
figure
plot(f_worth,real_perm)
grid
title('real perm')
```

```
%imaginary perm
imaginary_perm=(2*index_f.*k_f);
figure
plot(f_worth,imaginary_perm)
grid
title('imag perm')
%loss tangent
loss_tan=(imaginary_perm./real_perm);
figure
plot(f_worth,(loss_tan))
grid
title('loss tan')
```

Appendix E

The Multiple Angle Method Matlab Material Characterization Code

Description: The material characterization codes provided here can be used to extract the material properties of two different cases of dielectric stacks. The first case code is set up to extract the properties of a single layer dielectric stack (dielectric constant and loss tangent) along with thickness extraction. The second case code is set up to extract the properties of a two layer dielectric stack (dielectric constants and loss tangents) having known physical thicknesses.

The codes for both cases require certain inputs. These are:

-Reference measurement and sample measurement files names

-Upper frequency limit for material characterization

-Lower frequency limit for material characterization

-Upper and lower limits for the initial guesses of the unknowns (thickness, refractive index (real and imaginary parts)

-Angles of incidence of the sample measurements

-Dielectric layer thicknesses for the two layer stack

Note:

*The measured data text files, must have two columns with one being time and the other being signal intensity. The unit for time should be picoseconds. Delete any other text from the text files.

*The root finding method to solve the system of equations and extract the properties is the secant method.

→ The code for the first case (single layer material characterization along with thickness extraction) is:

```
clc
clear all
close all
format long

%%%%%%%%%%%%%%%%%%%%%%%%%%%%%%%%%%%%%%%%%%%%%%%%%%%%%%%%%%%%%%%%
%%%%%%%%%%%%%%%%%%%%%%%%%%%%%%%%%%%%%%%%%%%%%%%%%%%%%%%%%%%%%%%%
%%%%%%%%%%%%%%%%%%%%%%%%%%%%%%%%%%%%%%%%%%%%%%%%%%%%%%%%%%%%%%%%
%%%%%%%%%%%%%%%%%%%%%%%%%%%%%%%%%%%%%%%%%%%%%%%%%%%%%%%%%%%%%%%%
%%%%%%%%%%%%%%%%%%%%%%%%%%%%%%%%%%%%%%%%%%%%%%%%%%%%%%%%%%%%%%%%
%%%%%%%%%%%%%%%%%%%%%%%%%%%%%%%%%%%%%%%%%%%%%%%%%%Inputs%%%%%%%%%%
%%%%%%%%%%%%%%%%%%%%%%%%%%%%%%%%%%%%%%%%%%%%%%%%%%%%%%%%%%%%%%%%
%%%%%%%%%%%%%%%%%%%%%%%%%%%%%%%%%%%%%%%

Ref_Air1=textread('ref_air_si.txt', '%s');%loading reference
measurement
Ref_Air1=str2double(Ref_Air1);
Sample1=textread('si_60.txt', '%s');%loading first sample
measurement
Sample1=str2double(Sample1);
Sample2=textread('si_50.txt', '%s');%loading second sample
measurement
Sample2=str2double(Sample2);

theta1=60;%angle of incidence setting, first sample measurement
theta2=50;%angle of incidence setting, second sample measurement
upper_ind_g=3.8;%upper limit of initial guesses for refractive
index (real)
lower_ind_g=3;%lower limit of initial guesses for refractive
index (real)
upper_thi_g=2*(10^-3);%upper limit of initial guesses for
thickness
lower_thi_g=0.2*(10^-3);%lower limit of initial guesses for
thickness
upper_ext_g=0.15;%upper limit of initial guesses for refractive
index (imag)
lower_ext_g=0;%lower limit of initial guesses for refractive
index (imag)

flow=0.2*(10^12);%lower frequency limit for material
characterization
fhigh=1.2*(10^12);%upper frequency limit for material
characterization

%%%%%%%%%%%%%%%%%%%%%%%%%%%%%%%%%%%%%%%%%%%%%%%%%%%%%%%%%%%%%%%%
%%%%%%%%%%%%%%%%%%%%%%%%%%%%%%%%%%%%%%%%%%%%%%%%%%%%%%%%%%%%%%%%
%%%%%%%%%%%%%%%%%%%%%%%%%%%%%%%%%%%%%%%%%%%%%%%%%%%%%%%%%%%%%%%%
%%%%%%%%%%%%%%%%%%%%%%%%%%%%%%%%%%%%%%%

j=1;
```

```
for i=1:size(Ref_Air1,1)%reorganizing data into two columns,
first column is time
    %second column is signal intensity
    if mod(i,2)~=0
        Ref_Air1_c(j,1)=Ref_Air1(i,1);
        Sample1_c(j,1)=Sample1(i,1);
        Sample2_c(j,1)=Sample2(i,1);
    end
    if mod(i,2)==0
        Ref_Air1_c(j,2)=Ref_Air1(i,1);
        Sample1_c(j,2)=Sample1(i,1);
        Sample2_c(j,2)=Sample2(i,1);
        j=j+1;
    end
end

%measured incident signal plot
figure;plot(Ref_Air1_c(:,1),Ref_Air1_c(:,2),Sample1_c(:,1),Sampl
e1_c(:,2),Sample2_c(:,1),Sample2_c(:,2));grid

del_t_ind1=find(Sample1_c(:,2)==max(Sample1_c(:,2)))-
find(Ref_Air1_c(:,2)==max(Ref_Air1_c(:,2)));

Ts=(10^(-12))*(Ref_Air1_c(2,1)-Ref_Air1_c(1,1));%sampling period
Fs=1/Ts;%sampling frequency
N_samples=size(Ref_Air1_c(:,1),1);%number of discrete data
points in the %incident signal
freq=(0:Fs/N_samples:Fs-Fs/N_samples);%frequency array of the
DFT of the time %domain signal

Ref1_mod_freq=fft(Ref_Air1_c(:,2));
Ref_Air1_c_f=Ref1_mod_freq;
sample1_mod_freq=fft(Sample1_c(:,2));
sample2_mod_freq=fft(Sample2_c(:,2));

fr=find(freq>=flow);
fg=find(freq>=fhigh);
fr1=fg(1);
f_worth=freq(fr(1):fr1);

Tm=sample1_mod_freq./Ref_Air1_c_f;
Tm1=Tm(fr(1):end);
Tm=sample2_mod_freq./Ref_Air1_c_f;
Tm2=Tm(fr(1):end);

%inputs
cc=1;
```

```
lops=0;
while cc==1
n=50; %number of iterations for each frequency
c=2.99*(10^8);
fj=1;
lops=lops+1
ninitial=lower_ind_g+(upper_ind_g-lower_ind_g)*rand%initial n
linitial=lower_thi_g+upper_thi_g*rand%initial thickness
kinitial=0+upper_ext_g*rand
delx=0.000000000001;
lops_init(lops,:)=[ninitial,kinitial,linitial];
    for fj=1:size(f_worth,2)
        no=ninitial;
        ko=kinitial;
        lo=linitial;
        optmat=[no;ko;lo];
        for nj=1:n

            w=2*pi*f_worth(fj);
            k1=2*pi*f_worth(fj)*(no-sqrt(-1)*ko)/c;
            k0=2*pi*f_worth(fj)*(1)/c;
            eta1=120*pi/(no-sqrt(-1)*ko);
            eta0=120*pi/(1);
   kz1=2*pi*f_worth(fj)*sqrt((no-sqrt(-1)*ko)^2-
sin(theta1*pi/180)^2)/c;
            kz0=2*pi*f_worth(fj)*sqrt(1-sin(theta1*pi/180)^2)/c;

            hjgop=find(imag(kz0)>0);
            kz0([hjgop])=-kz0([hjgop]);
            hjjop=find(imag(kz1)>0);
            kz1([hjjop])=-kz1([hjjop]);

            Z2=kz1*eta1./k1;
            Z1=kz0*eta0./k0;
            T12=(2*Z2)./(Z2+Z1);
            T21=(2*Z1)./(Z2+Z1);
            R12=(Z2-Z1)./(Z2+Z1);
            R21=-R12;
 Tc1=(exp(-sqrt(-1)*kz1*(lo)).*T12.*T21)./(1+R12.*R21.*exp(-
sqrt(-...
1)*2*kz1*(lo)));

            func1=[abs(Tm1(fj))-abs(Tc1.*exp(sqrt(-1)*kz0*lo))];
            llps=angle(Tm1(fj));
            hyt=angle(Tc1.*exp(sqrt(-1)*kz0*lo));
            anglebla0=(llps-hyt);
            if abs(anglebla0)>pi && abs(anglebla0)<2*pi
```

```
                anglebla0=abs(anglebla0)-2*pi;
            end
            func2=[abs(anglebla0)];

            k1=2*pi*f_worth(fj)*(no-sqrt(-1)*ko)/c;
            k0=2*pi*f_worth(fj)*(1)/c;
            eta1=120*pi/(no-sqrt(-1)*ko);
            eta0=120*pi/(1);
            kz1=2*pi*f_worth(fj)*sqrt((no-sqrt(-1)*ko)^2-...
sin(theta2*pi/180)^2)/c;
            kz0=2*pi*f_worth(fj)*sqrt(1-sin(theta2*pi/180)^2)/c;

            hjgop=find(imag(kz0)>0);
            kz0([hjgop])=-kz0([hjgop]);
            hjjop=find(imag(kz1)>0);
            kz1([hjjop])=-kz1([hjjop]);

            Z2=kz1*eta1./k1;
            Z1=kz0*eta0./k0;
            T12=(2*Z2)./(Z2+Z1);
            T21=(2*Z1)./(Z2+Z1);
            R12=(Z2-Z1)./(Z2+Z1);
            R21=-R12;
Tc2=(exp(-sqrt(-1)*kz1*(lo)).*T12.*T21)./(1+R12.*R21.*exp(-
sqrt(-...
1)*2*kz1*(lo)));


            llps=angle(Tm2(fj));
            hyt=angle(Tc2.*exp(sqrt(-1)*kz0*lo));
            anglebla0=(llps-hyt);
            if abs(anglebla0)>pi && abs(anglebla0)<2*pi
                anglebla0=abs(anglebla0)-2*pi;
            end
            func3=abs(anglebla0);


            func=[func1;func2;func3]

            if abs(func(1,1))< 0.0000000000000001
                if abs(func(2,1))< 0.0000000000000001
                    if abs(func(3,1))< 0.0000000000000001
                        index(fj)=optmat(1,1);
                        ext(fj)=optmat(2,1);
                        thi(fj)=optmat(3,1);
                        break
                    end
```

```
            end
        end

        k1=2*pi*f_worth(fj)*(no+delx-sqrt(-1)*ko)/c;
        k0=2*pi*f_worth(fj)*(1)/c;
        eta1=120*pi/(no+delx-sqrt(-1)*ko);
        eta0=120*pi/(1);
kz1=2*pi*f_worth(fj)*sqrt((no+delx-sqrt(-1)*ko)^2-
sin(theta1*pi/180)^2)/c;
        kz0=2*pi*f_worth(fj)*sqrt(1-sin(theta1*pi/180)^2)/c;

        hjgop=find(imag(kz0)>0);
        kz0([hjgop])=-kz0([hjgop]);
        hjjop=find(imag(kz1)>0);
        kz1([hjjop])=-kz1([hjjop]);

        Z2=kz1*eta1./k1;
        Z1=kz0*eta0./k0;
        T12=(2*Z2)./(Z2+Z1);
        T21=(2*Z1)./(Z2+Z1);
        R12=(Z2-Z1)./(Z2+Z1);
        R21=-R12;
jTc1=(exp(-sqrt(-1)*kz1*(lo)).*T12.*T21)./(1+R12.*R21.*exp(-
sqrt(-...
1)*2*kz1*(lo)));

   Jack11=[(abs(Tm1(fj))-abs(jTc1.*exp(sqrt(-1)*kz0*lo)))-
func(1,1)];
        llps=angle(Tm1(fj));
        hyt=angle(jTc1.*exp(sqrt(-1)*kz0*lo));
        anglebla0=(llps-hyt);
        if abs(anglebla0)>pi && abs(anglebla0)<2*pi
            anglebla0=abs(anglebla0)-2*pi;
        end
        Jack21=[abs(anglebla0)-func(2,1)];

 kz1=2*pi*f_worth(fj)*sqrt((no+delx-sqrt(-1)*ko)^2-
sin(theta2*pi/180)^2)/c;
        kz0=2*pi*f_worth(fj)*sqrt(1-sin(theta2*pi/180)^2)/c;

        hjgop=find(imag(kz0)>0);
        kz0([hjgop])=-kz0([hjgop]);
        hjjop=find(imag(kz1)>0);
        kz1([hjjop])=-kz1([hjjop]);

        Z2=kz1*eta1./k1;
        Z1=kz0*eta0./k0;
```

```
            T12=(2*Z2)./(Z2+Z1);
            T21=(2*Z1)./(Z2+Z1);
            R12=(Z2-Z1)./(Z2+Z1);
            R21=-R12;
jTc2=(exp(-sqrt(-1)*kz1*(lo)).*T12.*T21)./(1+R12.*R21.*exp(-
sqrt(-...
1)*2*kz1*(lo)));

            llps=angle(Tm2(fj));
            hyt=angle(jTc2.*exp(sqrt(-1)*kz0*lo));
            anglebla0=(llps-hyt);
            if abs(anglebla0)>pi && abs(anglebla0)<2*pi
                anglebla0=abs(anglebla0)-2*pi;
            end
            Jack31=[abs(anglebla0)-func(3,1)];

            k1=2*pi*f_worth(fj)*(no-sqrt(-1)*(ko+delx))/c;
            k0=2*pi*f_worth(fj)*(1)/c;
            eta1=120*pi/(no-sqrt(-1)*(ko+delx));
            eta0=120*pi/(1);
kz1=2*pi*f_worth(fj)*sqrt((no-sqrt(-1)*(ko+delx))^2-
sin(theta1*pi/180)^2)/c;
            kz0=2*pi*f_worth(fj)*sqrt(1-sin(theta1*pi/180)^2)/c;

            hjgop=find(imag(kz0)>0);
            kz0([hjgop])=-kz0([hjgop]);
            hjjop=find(imag(kz1)>0);
            kz1([hjjop])=-kz1([hjjop]);

            Z2=kz1*eta1./k1;
            Z1=kz0*eta0./k0;
            T12=(2*Z2)./(Z2+Z1);
            T21=(2*Z1)./(Z2+Z1);
            R12=(Z2-Z1)./(Z2+Z1);
            R21=-R12;
jTc1=(exp(-sqrt(-1)*kz1*(lo)).*T12.*T21)./(1+R12.*R21.*exp(-
sqrt(-...
1)*2*kz1*(lo)));

Jack12=[(abs(Tm1(fj))-abs(jTc1.*exp(sqrt(-1)*kz0*lo)))-
func(1,1)];

            llps=angle(Tm1(fj));
            hyt=angle(jTc1.*exp(sqrt(-1)*kz0*lo));
            anglebla0=(llps-hyt);
            if abs(anglebla0)>pi && abs(anglebla0)<2*pi
                anglebla0=abs(anglebla0)-2*pi;
```

```
            end
            Jack22=[abs(anglebla0)-func(2,1)];

 kz1=2*pi*f_worth(fj)*sqrt((no-sqrt(-1)*(ko+delx))^2-
sin(theta2*pi/180)^2)/c;
            kz0=2*pi*f_worth(fj)*sqrt(1-sin(theta2*pi/180)^2)/c;

            hjgop=find(imag(kz0)>0);
            kz0([hjgop])=-kz0([hjgop]);
            hjjop=find(imag(kz1)>0);
            kz1([hjjop])=-kz1([hjjop]);

            Z2=kz1*eta1./k1;
            Z1=kz0*eta0./k0;
            T12=(2*Z2)./(Z2+Z1);
            T21=(2*Z1)./(Z2+Z1);
            R12=(Z2-Z1)./(Z2+Z1);
            R21=-R12;
jTc2=(exp(-sqrt(-1)*kz1*(lo)).*T12.*T21)./(1+R12.*R21.*exp(-
sqrt(-...
1)*2*kz1*(lo)));

            llps=angle(Tm2(fj));
            hyt=angle(jTc2.*exp(sqrt(-1)*kz0*lo));

            anglebla0=(llps-hyt);
            if abs(anglebla0)>pi && abs(anglebla0)<2*pi
                anglebla0=abs(anglebla0)-2*pi;
            end
            Jack32=[abs(anglebla0)-func(3,1)];

            k1=2*pi*f_worth(fj)*(no-sqrt(-1)*(ko))/c;
            k0=2*pi*f_worth(fj)*(1)/c;
            eta1=120*pi/(no-sqrt(-1)*(ko));
            eta0=120*pi/(1);
 kz1=2*pi*f_worth(fj)*sqrt((no-sqrt(-1)*(ko))^2-
sin(theta1*pi/180)^2)/c;
            kz0=2*pi*f_worth(fj)*sqrt(1-sin(theta1*pi/180)^2)/c;

            hjgop=find(imag(kz0)>0);
            kz0([hjgop])=-kz0([hjgop]);
            hjjop=find(imag(kz1)>0);
            kz1([hjjop])=-kz1([hjjop]);

            Z2=kz1*eta1./k1;
            Z1=kz0*eta0./k0;
            T12=(2*Z2)./(Z2+Z1);
```

```
            T21=(2*Z1)./(Z2+Z1);
            R12=(Z2-Z1)./(Z2+Z1);
            R21=-R12;
 jTc1=(exp(-sqrt(-
1)*kz1*(lo+delx)).*T12.*T21)./(1+R12.*R21.*exp(-sqrt(-...
1)*2*kz1*(lo+delx)));

 Jack13=[(abs(Tm1(fj))-abs(jTc1.*exp(sqrt(-1)*kz0*(lo+delx))))-
func(1,1)];

            llps=angle(Tm1(fj));
            hyt=angle(jTc1.*exp(sqrt(-1)*kz0*(lo+delx)));

anglebla0=(llps-hyt);
            if abs(anglebla0)>pi && abs(anglebla0)<2*pi
                anglebla0=abs(anglebla0)-2*pi;
            end
            Jack23=[abs(anglebla0)-func(2,1)];

  kz1=2*pi*f_worth(fj)*sqrt((no-sqrt(-1)*(ko))^2-
sin(theta2*pi/180)^2)/c;
            kz0=2*pi*f_worth(fj)*sqrt(1-sin(theta2*pi/180)^2)/c;

            hjgop=find(imag(kz0)>0);
            kz0([hjgop])=-kz0([hjgop]);
            hjjop=find(imag(kz1)>0);
            kz1([hjjop])=-kz1([hjjop]);

            Z2=kz1*eta1./k1;
            Z1=kz0*eta0./k0;
            T12=(2*Z2)./(Z2+Z1);
            T21=(2*Z1)./(Z2+Z1);
            R12=(Z2-Z1)./(Z2+Z1);
            R21=-R12;
jTc2=(exp(-sqrt(-
1)*kz1*(lo+delx)).*T12.*T21)./(1+R12.*R21.*exp(-sqrt(-...
1)*2*kz1*(lo+delx)));


            llps=angle(Tm2(fj));
            hyt=angle(jTc2.*exp(sqrt(-1)*kz0*(lo+delx)));
            anglebla0=(llps-hyt);
            if abs(anglebla0)>pi && abs(anglebla0)<2*pi
                anglebla0=abs(anglebla0)-2*pi;
            end
            Jack33=[abs(anglebla0)-func(3,1)];
            Jack=[Jack11, Jack12, Jack13;
```

```
                Jack21, Jack22, Jack23;
                Jack31, Jack32, Jack33]/delx;

            if abs(det(Jack))<0.0000000000000001
                index(fj)=0;
                ext(fj)=0;
                thi(fj)=0;
                break
            end
            optmat=optmat-Jack\func
            no=optmat(1,1);
            ko=optmat(2,1);
            lo=optmat(3,1);
            TF=isnan(optmat);
            Tff=find(TF==1);
            if sum(Tff)>0
                index(fj)=0;
                ext(fj)=0;
                thi(fj)=0;
                break
            end
            if nj==n
                index(fj)=no;
                ext(fj)=ko;
                thi(fj)=lo;
            end
        end
        cnt(fj)=nj;
    end
    if fj==size(f_worth,2)
        fvd=find(index>lower_ind_g & index<upper_ind_g);
        fgh=find(ext>lower_ext_g & ext<upper_ext_g);
        ffi=find(thi>=lower_thi_g & thi<upper_thi_g);
        d=intersect(fvd,fgh);
        cd=intersect(ffi,fvd);
        if size(d,2)>0 && size(cd,2)>0
            cc=0;
        end
    end
end

n=50; %number of iterations for each frequency
for i=1:size(f_worth,2)
    ninitial=index(i);%initial n
    linitial=thi(i);%initial thickness
    kinitial=ext(i);
    if ninitial>=lower_ind_g && kinitial>lower_ext_g &&...
```

```
linitial>lower_thi_g && ninitial<upper_ind_g &&
kinitial<upper_ext_g &&...
linitial<upper_thi_g
        break
    else
        continue
    end
end
delx=0.000000000001;

    for fj=1:size(f_worth,2)
        no=ninitial;
        ko=kinitial;
        lo=linitial;
        optmat=[no;ko;lo];
            if fj==1
        lops_init(lops+1,:)=optmat';
    end
        for nj=1:n

            w=2*pi*f_worth(fj);
            k1=2*pi*f_worth(fj)*(no-sqrt(-1)*ko)/c;
            k0=2*pi*f_worth(fj)*(1)/c;
            eta1=120*pi/(no-sqrt(-1)*ko);
            eta0=120*pi/(1);
kz1=2*pi*f_worth(fj)*sqrt((no-sqrt(-1)*ko)^2-
sin(theta1*pi/180)^2)/c;
            kz0=2*pi*f_worth(fj)*sqrt(1-sin(theta1*pi/180)^2)/c;

            hjgop=find(imag(kz0)>0);
            kz0([hjgop])=-kz0([hjgop]);
            hjjop=find(imag(kz1)>0);
            kz1([hjjop])=-kz1([hjjop]);

            Z2=kz1*eta1./k1;
            Z1=kz0*eta0./k0;
            T12=(2*Z2)./(Z2+Z1);
            T21=(2*Z1)./(Z2+Z1);
            R12=(Z2-Z1)./(Z2+Z1);
            R21=-R12;
Tc1=(exp(-sqrt(-1)*kz1*(lo)).*T12.*T21)./(1+R12.*R21.*exp(-
sqrt(-...
1)*2*kz1*(lo)));

            func1=[abs(Tm1(fj))-abs(Tc1.*exp(sqrt(-1)*kz0*lo))];
            llps=angle(Tm1(fj));
            hyt=angle(Tc1.*exp(sqrt(-1)*kz0*lo));
```

```
            anglebla0=(llps-hyt);
            if abs(anglebla0)>pi && abs(anglebla0)<2*pi
                anglebla0=abs(anglebla0)-2*pi;
            end
            func2=[abs(anglebla0)];

            k1=2*pi*f_worth(fj)*(no-sqrt(-1)*ko)/c;
            k0=2*pi*f_worth(fj)*(1)/c;
            eta1=120*pi/(no-sqrt(-1)*ko);
            eta0=120*pi/(1);
  kz1=2*pi*f_worth(fj)*sqrt((no-sqrt(-1)*ko)^2-
sin(theta2*pi/180)^2)/c;
            kz0=2*pi*f_worth(fj)*sqrt(1-sin(theta2*pi/180)^2)/c;

            hjgop=find(imag(kz0)>0);
            kz0([hjgop])=-kz0([hjgop]);
            hjjop=find(imag(kz1)>0);
            kz1([hjjop])=-kz1([hjjop]);

            Z2=kz1*eta1./k1;
            Z1=kz0*eta0./k0;
            T12=(2*Z2)./(Z2+Z1);
            T21=(2*Z1)./(Z2+Z1);
            R12=(Z2-Z1)./(Z2+Z1);
            R21=-R12;
Tc2=(exp(-sqrt(-1)*kz1*(lo)).*T12.*T21)./(1+R12.*R21.*exp(-
sqrt(-...
1)*2*kz1*(lo)));


            llps=angle(Tm2(fj));
            hyt=angle(Tc2.*exp(sqrt(-1)*kz0*lo));
            anglebla0=(llps-hyt);
            if abs(anglebla0)>pi && abs(anglebla0)<2*pi
                anglebla0=abs(anglebla0)-2*pi;
            end
            func3=abs(anglebla0);


            func=[func1;func2;func3]

            if abs(func(1,1))< 0.0000000000000001
                if abs(func(2,1))< 0.0000000000000001
                    if abs(func(3,1))< 0.0000000000000001
                        index(fj)=optmat(1,1);
                        ext(fj)=optmat(2,1);
                        thi(fj)=optmat(3,1);
```

```
                        ninitial=index(fj);
                        kinitial=ext(fj);
                        linitial=thi(fj);
                    break
                end
            end
        end

        k1=2*pi*f_worth(fj)*(no+delx-sqrt(-1)*ko)/c;
        k0=2*pi*f_worth(fj)*(1)/c;
        eta1=120*pi/(no+delx-sqrt(-1)*ko);
        eta0=120*pi/(1);
 kz1=2*pi*f_worth(fj)*sqrt((no+delx-sqrt(-1)*ko)^2-
sin(theta1*pi/180)^2)/c;
        kz0=2*pi*f_worth(fj)*sqrt(1-sin(theta1*pi/180)^2)/c;

        hjgop=find(imag(kz0)>0);
        kz0([hjgop])=-kz0([hjgop]);
        hjjop=find(imag(kz1)>0);
        kz1([hjjop])=-kz1([hjjop]);

        Z2=kz1*eta1./k1;
        Z1=kz0*eta0./k0;
        T12=(2*Z2)./(Z2+Z1);
        T21=(2*Z1)./(Z2+Z1);
        R12=(Z2-Z1)./(Z2+Z1);
       R21=-R12;
jTc1=(exp(-sqrt(-1)*kz1*(lo)).*T12.*T21)./(1+R12.*R21.*exp(-
sqrt(-...
1)*2*kz1*(lo)));

     Jack11=[(abs(Tm1(fj))-abs(jTc1.*exp(sqrt(-1)*kz0*lo)))-
func(1,1)];
        llps=angle(Tm1(fj));
        hyt=angle(jTc1.*exp(sqrt(-1)*kz0*lo));
        anglebla0=(llps-hyt);
        if abs(anglebla0)>pi && abs(anglebla0)<2*pi
            anglebla0=abs(anglebla0)-2*pi;
        end
        Jack21=[abs(anglebla0)-func(2,1)];

 kz1=2*pi*f_worth(fj)*sqrt((no+delx-sqrt(-1)*ko)^2-
sin(theta2*pi/180)^2)/c;
        kz0=2*pi*f_worth(fj)*sqrt(1-sin(theta2*pi/180)^2)/c;

        hjgop=find(imag(kz0)>0);
        kz0([hjgop])=-kz0([hjgop]);
```

```
            hjjop=find(imag(kz1)>0);
            kz1([hjjop])=-kz1([hjjop]);

            Z2=kz1*eta1./k1;
            Z1=kz0*eta0./k0;
            T12=(2*Z2)./(Z2+Z1);
            T21=(2*Z1)./(Z2+Z1);
            R12=(Z2-Z1)./(Z2+Z1);
            R21=-R12;
jTc2=(exp(-sqrt(-1)*kz1*(lo)).*T12.*T21)./(1+R12.*R21.*exp(-
sqrt(-...
1)*2*kz1*(lo)));

            llps=angle(Tm2(fj));
            hyt=angle(jTc2.*exp(sqrt(-1)*kz0*lo));
            anglebla0=(llps-hyt);
            if abs(anglebla0)>pi && abs(anglebla0)<2*pi
                anglebla0=abs(anglebla0)-2*pi;
            end
            Jack31=[abs(anglebla0)-func(3,1)];

            k1=2*pi*f_worth(fj)*(no-sqrt(-1)*(ko+delx))/c;
            k0=2*pi*f_worth(fj)*(1)/c;
            eta1=120*pi/(no-sqrt(-1)*(ko+delx));
            eta0=120*pi/(1);
 kz1=2*pi*f_worth(fj)*sqrt((no-sqrt(-1)*(ko+delx))^2-
sin(theta1*pi/180)^2)/c;
            kz0=2*pi*f_worth(fj)*sqrt(1-sin(theta1*pi/180)^2)/c;

            hjgop=find(imag(kz0)>0);
            kz0([hjgop])=-kz0([hjgop]);
            hjjop=find(imag(kz1)>0);
            kz1([hjjop])=-kz1([hjjop]);

            Z2=kz1*eta1./k1;
            Z1=kz0*eta0./k0;
            T12=(2*Z2)./(Z2+Z1);
            T21=(2*Z1)./(Z2+Z1);
            R12=(Z2-Z1)./(Z2+Z1);
            R21=-R12;
jTc1=(exp(-sqrt(-1)*kz1*(lo)).*T12.*T21)./(1+R12.*R21.*exp(-
sqrt(-...
1)*2*kz1*(lo)));

  Jack12=[(abs(Tm1(fj))-abs(jTc1.*exp(sqrt(-1)*kz0*lo)))-
func(1,1)];
```

```
            llps=angle(Tm1(fj));
            hyt=angle(jTc1.*exp(sqrt(-1)*kz0*lo));

            anglebla0=(llps-hyt);
            if abs(anglebla0)>pi && abs(anglebla0)<2*pi
                anglebla0=abs(anglebla0)-2*pi;
            end
            Jack22=[abs(anglebla0)-func(2,1)];

kz1=2*pi*f_worth(fj)*sqrt((no-sqrt(-1)*(ko+delx))^2-
sin(theta2*pi/180)^2)/c;
            kz0=2*pi*f_worth(fj)*sqrt(1-sin(theta2*pi/180)^2)/c;

            hjgop=find(imag(kz0)>0);
            kz0([hjgop])=-kz0([hjgop]);
            hjjop=find(imag(kz1)>0);
            kz1([hjjop])=-kz1([hjjop]);

            Z2=kz1*eta1./k1;
            Z1=kz0*eta0./k0;
            T12=(2*Z2)./(Z2+Z1);
            T21=(2*Z1)./(Z2+Z1);
            R12=(Z2-Z1)./(Z2+Z1);
            R21=-R12;
jTc2=(exp(-sqrt(-1)*kz1*(lo)).*T12.*T21)./(1+R12.*R21.*exp(-
sqrt(-...
1)*2*kz1*(lo)));

            llps=angle(Tm2(fj));
            hyt=angle(jTc2.*exp(sqrt(-1)*kz0*lo));

            anglebla0=(llps-hyt);
            if abs(anglebla0)>pi && abs(anglebla0)<2*pi
                anglebla0=abs(anglebla0)-2*pi;
            end
            Jack32=[abs(anglebla0)-func(3,1)];

            k1=2*pi*f_worth(fj)*(no-sqrt(-1)*(ko))/c;
            k0=2*pi*f_worth(fj)*(1)/c;
            eta1=120*pi/(no-sqrt(-1)*(ko));
            eta0=120*pi/(1);
 kz1=2*pi*f_worth(fj)*sqrt((no-sqrt(-1)*(ko))^2-
sin(theta1*pi/180)^2)/c;
            kz0=2*pi*f_worth(fj)*sqrt(1-sin(theta1*pi/180)^2)/c;

            hjgop=find(imag(kz0)>0);
            kz0([hjgop])=-kz0([hjgop]);
```

```
            hjjop=find(imag(kz1)>0);
            kz1([hjjop])=-kz1([hjjop]);

            Z2=kz1*eta1./k1;
            Z1=kz0*eta0./k0;
            T12=(2*Z2)./(Z2+Z1);
            T21=(2*Z1)./(Z2+Z1);
            R12=(Z2-Z1)./(Z2+Z1);
            R21=-R12;
jTc1=(exp(-sqrt(-
1)*kz1*(lo+delx)).*T12.*T21)./(1+R12.*R21.*exp(-sqrt(-...
1)*2*kz1*(lo+delx)));
Jack13=[(abs(Tm1(fj))-abs(jTc1.*exp(sqrt(-1)*kz0*(lo+delx))))-
func(1,1)];
            llps=angle(Tm1(fj));
            hyt=angle(jTc1.*exp(sqrt(-1)*kz0*(lo+delx)));
anglebla0=(llps-hyt);
            if abs(anglebla0)>pi && abs(anglebla0)<2*pi
                anglebla0=abs(anglebla0)-2*pi;
            end
            Jack23=[abs(anglebla0)-func(2,1)];

kz1=2*pi*f_worth(fj)*sqrt((no-sqrt(-1)*(ko))^2-
sin(theta2*pi/180)^2)/c;
            kz0=2*pi*f_worth(fj)*sqrt(1-sin(theta2*pi/180)^2)/c;

            hjgop=find(imag(kz0)>0);
            kz0([hjgop])=-kz0([hjgop]);
            hjjop=find(imag(kz1)>0);
            kz1([hjjop])=-kz1([hjjop]);

            Z2=kz1*eta1./k1;
            Z1=kz0*eta0./k0;
            T12=(2*Z2)./(Z2+Z1);
            T21=(2*Z1)./(Z2+Z1);
            R12=(Z2-Z1)./(Z2+Z1);
            R21=-R12;
jTc2=(exp(-sqrt(-
1)*kz1*(lo+delx)).*T12.*T21)./(1+R12.*R21.*exp(-sqrt(-...
1)*2*kz1*(lo+delx)));


            llps=angle(Tm2(fj));
            hyt=angle(jTc2.*exp(sqrt(-1)*kz0*(lo+delx)));
            anglebla0=(llps-hyt);
            if abs(anglebla0)>pi && abs(anglebla0)<2*pi
                anglebla0=abs(anglebla0)-2*pi;
```

```
            end
            Jack33=[abs(anglebla0)-func(3,1)];
            Jack=[Jack11, Jack12, Jack13;
                Jack21, Jack22, Jack23;
                Jack31, Jack32, Jack33]/delx;

            if abs(det(Jack))<0.0000000000000001
                index(fj)=0;
                ext(fj)=0;
                thi(fj)=0;
                break
            end
            optmat=optmat-Jack\func
            no=optmat(1,1);
            ko=optmat(2,1);
            lo=optmat(3,1);
            TF=isnan(optmat);
            Tff=find(TF==1);
            if sum(Tff)>0
                index(fj)=0;
                ext(fj)=0;
                thi(fj)=0;
                break
            end
            if nj==n
                index(fj)=no;
                ext(fj)=ko;
                thi(fj)=lo;
                end
        end
        cnt(fj)=nj;
    end

figure;plot(f_worth,index);grid
title('refractive index - real')
figure;plot(f_worth,ext);grid
title('refractive index - imaginary')
figure;plot(f_worth,thi);grid
title('thickness - m')
%figure;plot(f_worth,cnt);grid

er=index.^2-ext.^2;
figure;plot(f_worth,er);grid
title('real perm')
tand=2*index.*abs(ext)./er;
figure;plot(f_worth,tand);grid
title('loss tan')
```

```
%%%%%%%%%%%%%%%%%%%%%%%%%%%%%%%%%%%%%%%%%%%%%%%%%%%%%%%%%%%%%%%%
%%%%%%%%%%%%%%%%%%%%%%%%%%%%%%%%%%%%%%%%%%%%%%%%%%%%%%%%%%%%%%%%
%%%%%%%%%%%%%%%%%%%%%%%%%%%%%%%%%%%%%%%%%%%%%%%%%%%%%%%%%%%%%%%%
%%%%%%%%%%%%%%%%%%%%%%%%%%%%%%%%%%%%%%%%%%%%%%%%%%%%%%%%%%%%%%%%
%%%%%%%%%%%%%%%%%%%%%%%%%%%%%%%%%%%%%%%%%%%%%%%%%%%%%%%%%%%%%%%%
```

→ The code for the second case (two layer material characterization with known physical thicknesses) is:

```
clc
clear all
close all
format long

%%%%%%%%%%%%%%%%%%%%%%%%%%%%%%%%%%%%%%%%%%%%%%%%%%%%%%%%%%%%%%%%
%%%%%%%%%%%%%%%%%%%%%%%%%%%%%%%%%%%%%%%%%%%%%%Inputs%%%%%%%%%%%%
%%%%%%%%%%%%%%%%%%%%%%%%%%%%%%%%%%%%%%%%%%%%%%%%%%%%%%%%%%%%%%%%
%%%%%%%%%%%%%%%%%%%%%%%%%%%%%%%%%%%%%%%

Ref_Air1=textread('ref_air_glass_si.txt','%s');%loading
reference measurement
Ref_Air1=str2double(Ref_Air1);
Sample1=textread('glass_si_30.txt', '%s');%loading first sample
measurement
Sample1=str2double(Sample1);
Sample2=textread('glass_si_60.txt', '%s');%loading second sample
measurement
Sample2=str2double(Sample2);

theta1=30;%angle of incidence setting, first sample measurement
theta2=60;%angle of incidence setting, second sample measurement

upper_ind_g1=3.8;%upper limit of initial guesses for refractive
index (real)
               %for the first dielectric
lower_ind_g1=3;%lower limit of initial guesses for refractive
index (real)
               %for the first dielectric
upper_ext_g1=0.08;%upper limit of initial guesses for refractive
index (imag)
                  %for the first dielectric
lower_ext_g1=0;%lower limit of initial guesses for refractive
index (imag)
               %for the first dielectric
```

```
upper_ind_g2=2.5;%upper limit of initial guesses for refractive
index (real)
               %for the second dielectric
lower_ind_g2=1.9;%lower limit of initial guesses for refractive
index (real)
               %for the second dielectric
upper_ext_g2=0.08;%upper limit of initial guesses for refractive
index (imag)
                  %for the second dielectric
lower_ext_g2=0;%lower limit of initial guesses for refractive
index (imag)
               %for the second dielectric

l1=0.52*(10^-3);%thickness of the first dielectric
l2=0.52*(10^-3);%thickness of the second dielectric

flow=0.2*(10^12);%lower frequency limit for material
characterization
fhigh=1.2*(10^12);%upper frequency limit for material
characterization

%%%%%%%%%%%%%%%%%%%%%%%%%%%%%%%%%%%%%%%%%%%%%%%%%%%%%%%%%%%%%%%%
%%%%%%%%%%%%%%%%%%%%%%%%%%%%%%%%%%%%%%%%%%%%%%%%%%%%%%%%%%%%%%%%
%%%%%%%%%%%%%%%%%%%%%%%%%%%%%%%%%%%%%%%%%%%%%%%%%%%%%%%%%%%%%%%%
%%%%%%%%%%%%%%%%%%%%%%%%%%%%%%%%%%%%%%%

j=1;
for i=1:size(Ref_Air1,1)%reorganizing data into two columns,
first column is time
    %second column is signal intensity
    if mod(i,2)~=0
        Ref_Air1_c(j,1)=Ref_Air1(i,1);
        Sample1_c(j,1)=Sample1(i,1);
        Sample2_c(j,1)=Sample2(i,1);
   end
    if mod(i,2)==0
        Ref_Air1_c(j,2)=Ref_Air1(i,1);
        Sample1_c(j,2)=Sample1(i,1);
        Sample2_c(j,2)=Sample2(i,1);
        j=j+1;
    end
end

%measured incident signal plot
figure;plot(Ref_Air1_c(:,1),Ref_Air1_c(:,2),Sample1_c(:,1),Sampl
e1_c(:,2),...
    Sample2_c(:,1),Sample2_c(:,2));grid
```

```
Ts=(10^(-12))*(Ref_Air1_c(2,1)-Ref_Air1_c(1,1));%sampling period
Fs=1/Ts;%sampling frequency
N_samples=size(Ref_Air1_c(:,1),1);%number of discrete data
points in the incident signal
freq=(0:Fs/N_samples:Fs-Fs/N_samples);%frequency array of the
DFT of the time domain signal

Ref1_mod_freq=fft(Ref_Air1_c(:,2));
Ref_Air1_c_f=Ref1_mod_freq;
sample1_mod_freq=fft(Sample1_c(:,2));
sample2_mod_freq=fft(Sample2_c(:,2));


fr=find(freq>=flow);
fg=find(freq>=fhigh);
fr1=fg(1);
f_worth=freq(fr(1):fr1);

Tm=sample1_mod_freq./Ref_Air1_c_f;
Tm1=Tm(fr(1):end);
Tm=sample2_mod_freq./Ref_Air1_c_f;
Tm2=Tm(fr(1):end);

hyt1=phase(Tm1);

%inputs
n=50; %number of iterations for each frequency
c=2.99*(10^8);
l1initial=l1;
l2initial=l2;

delx=0.0000000000001;
fj=1;
cc=1;
lops=0;
while cc~=0
    lops=lops+1;
n1initial=lower_ind_g1+(upper_ind_g1-lower_ind_g1)*rand;
k1initial=lower_ext_g1+upper_ext_g1*rand;
n2initial=lower_ind_g2+(upper_ind_g2-lower_ind_g2)*rand;
k2initial= lower_ext_g2+ upper_ext_g2*rand;
lops_init(lops,:)=[n1initial,k1initial,n2initial,k2initial];
for fj=1:size(f_worth,2)
    n1o=n1initial;
    k1o=k1initial;
    l1o=l1initial;
```

```
    n2o=n2initial;
    k2o=k2initial;
    l2o=l2initial
    optmat=[n1o;k1o;n2o;k2o];
    for nj=1:n

        w=2*pi*f_worth(fj);
        k1=w*(n1o-sqrt(-1)*k1o)/c;
        k0=w/c;
        k2=w*(n2o-sqrt(-1)*k2o)/c;
        eta2=120*pi/(n2o-sqrt(-1)*k2o);
        eta1=120*pi/(n1o-sqrt(-1)*k1o);
        eta0=120*pi;

        kz0=2*pi*f_worth(fj)*sqrt(1-sin(theta1*pi/180)^2)/c;
kz1=2*pi*f_worth(fj)*sqrt((n1o-sqrt(-1)*k1o)^2-...
sin(theta1*pi/180)^2)/c;
   kz2=2*pi*f_worth(fj)*sqrt((n2o-sqrt(-1)*k2o)^2-
sin(theta1*pi/180)^2)/c;
        hjg=find(imag(kz0)>0);
        kz0([hjg])=-kz0([hjg]);
        hjj=find(imag(kz1)>0);
        kz1([hjj])=-kz1([hjj]);
        hja=find(imag(kz2)>0);
        kz2([hja])=-kz2([hja]);

        Z2=kz2*eta2/k2;
        Z1=kz1*eta1/k1;
        Z0=kz0*eta0/k0;

        T01=(2*Z1)./(Z1+Z0);
        T12=(2*Z2)./(Z2+Z1);
        T20=(2*Z0)./(Z2+Z0);
        R01=(Z1-Z0)./(Z1+Z0);
        R12=(Z2-Z1)./(Z2+Z1);
        R20=(Z0-Z2)./(Z0+Z2);

 Tc1=(exp(-sqrt(-1)*kz1*(l1o)).*exp(-sqrt(-
1)*kz2*(l2o)).*T01.*T12.*T20)./...
                (1+R01.*R12.*exp(-sqrt(-1)*2*kz1*(l1o))+...
+R12.*R20.*exp(-sqrt(-1)*2*kz2*(l2o))+R01.*R20.*exp(-sqrt(-
1)*2*kz2*(l2o))...
                .*exp(-sqrt(-1)*2*kz1*(l1o)));


        func1=[abs(Tm1(fj))-abs(Tc1*exp(sqrt(-
1)*kz0*(l1o+l2o)))];
```

```
        llps=angle(Tm1(fj));
        hyt=angle(Tc1.*exp(sqrt(-1)*kz0*(l1o+l2o)));

        anglebla0=(llps-hyt);
        if abs(anglebla0)>pi && abs(anglebla0)<2*pi
           anglebla0=abs(anglebla0)-2*pi;
        end
        func2=[abs(anglebla0)];

        kz0=2*pi*f_worth(fj)*sqrt(1-sin(theta2*pi/180)^2)/c;
        kz1=2*pi*f_worth(fj)*sqrt((n1o-sqrt(-1)*k1o)^2-
sin(theta2*pi/180)^2)/c;
 kz2=2*pi*f_worth(fj)*sqrt((n2o-sqrt(-1)*k2o)^2-
sin(theta2*pi/180)^2)/c;
        hjg=find(imag(kz0)>0);
        kz0([hjg])=-kz0([hjg]);
        hjj=find(imag(kz1)>0);
        kz1([hjj])=-kz1([hjj]);
        hja=find(imag(kz2)>0);
        kz2([hja])=-kz2([hja]);

        Z2=kz2*eta2/k2;
        Z1=kz1*eta1/k1;
        Z0=kz0*eta0/k0;

        T01=(2*Z1)./(Z1+Z0);
        T12=(2*Z2)./(Z2+Z1);
        T20=(2*Z0)./(Z2+Z0);
        R01=(Z1-Z0)./(Z1+Z0);
        R12=(Z2-Z1)./(Z2+Z1);
        R20=(Z0-Z2)./(Z0+Z2);

Tc2=(exp(-sqrt(-1)*kz1*(l1o)).*exp(-sqrt(-
1)*kz2*(l2o)).*T01.*T12.*T20)./...
            (1+R01.*R12.*exp(-sqrt(-1)*2*kz1*(l1o))+...
+R12.*R20.*exp(-sqrt(-1)*2*kz2*(l2o))+R01.*R20.*exp(-sqrt(-
1)*2*kz2*(l2o))...
            .*exp(-sqrt(-1)*2*kz1*(l1o)));

        func3=[abs(Tm2(fj))-abs(Tc2*exp(sqrt(-
1)*kz0*(l1o+l2o)))];

        llps=angle(Tm2(fj));
        hyt=angle(Tc2.*exp(sqrt(-1)*kz0*(l1o+l2o)));

        anglebla0=(llps-hyt);
```

```
        if abs(anglebla0)>pi && abs(anglebla0)<2*pi
           anglebla0=abs(anglebla0)-2*pi;
        end
        func4=[abs(anglebla0)];


        func=[(func1);(func2);func3;func4]

        if abs(func(1,1))<0.0000000000000001
            if abs(func(2,1))<0.0000000000000001
                if abs(func(3,1))<0.0000000000000001
                    if abs(func(4,1))<0.000000000000001
                index1(fj)=optmat(1,1);
                ext1(fj)=optmat(2,1);
                index2(fj)=optmat(3,1);
                ext2(fj)=optmat(4,1);
                break
                    end
                end
            end
        end

        k1=w*((n1o+delx)-sqrt(-1)*k1o)/c;
        k0=w/c;
        k2=w*(n2o-sqrt(-1)*k2o)/c;
        eta2=120*pi/(n2o-sqrt(-1)*k2o);
        eta1=120*pi/((n1o+delx)-sqrt(-1)*k1o);
        eta0=120*pi;

        kz0=2*pi*f_worth(fj)*sqrt(1-sin(theta1*pi/180)^2)/c;
kz1=2*pi*f_worth(fj)*sqrt(((n1o+delx)-sqrt(-1)*k1o)^2-...
sin(theta1*pi/180)^2)/c;
  kz2=2*pi*f_worth(fj)*sqrt((n2o-sqrt(-1)*k2o)^2-
sin(theta1*pi/180)^2)/c;
        hjg=find(imag(kz0)>0);
        kz0([hjg])=-kz0([hjg]);
        hjj=find(imag(kz1)>0);
        kz1([hjj])=-kz1([hjj]);
        hja=find(imag(kz2)>0);
        kz2([hja])=-kz2([hja]);

        Z2=kz2*eta2/k2;
        Z1=kz1*eta1/k1;
        Z0=kz0*eta0/k0;

        T01=(2*Z1)./(Z1+Z0);
        T12=(2*Z2)./(Z2+Z1);
```

```
        T20=(2*Z0)./(Z2+Z0);
        R01=(Z1-Z0)./(Z1+Z0);
        R12=(Z2-Z1)./(Z2+Z1);
        R20=(Z0-Z2)./(Z0+Z2);

 Tc1=(exp(-sqrt(-1)*kz1*(l1o)).*exp(-sqrt(-
1)*kz2*(l2o)).*T01.*T12.*T20)./...
                (1+R01.*R12.*exp(-sqrt(-1)*2*kz1*(l1o))+...
+R12.*R20.*exp(-sqrt(-1)*2*kz2*(l2o))+R01.*R20.*exp(-sqrt(-
1)*2*kz2*(l2o))...
                .*exp(-sqrt(-1)*2*kz1*(l1o)));

      Jack11=[(abs(Tm1(fj))-abs(Tc1*exp(sqrt(-
1)*kz0*(l1o+l2o))))-func(1,1)];

        llps=angle(Tm1(fj));
        hyt=angle(Tc1.*exp(sqrt(-1)*kz0*(l1o+l2o)));

        anglebla0=(llps-hyt);
        if abs(anglebla0)>pi && abs(anglebla0)<2*pi
           anglebla0=abs(anglebla0)-2*pi;
        end
        Jack21=[abs(anglebla0)-func(2,1)];

        k1=w*((n1o+delx)-sqrt(-1)*k1o)/c;
        k0=w/c;
        k2=w*(n2o-sqrt(-1)*k2o)/c;
        eta2=120*pi/(n2o-sqrt(-1)*k2o);
        eta1=120*pi/((n1o+delx)-sqrt(-1)*k1o);
        eta0=120*pi;

        kz0=2*pi*f_worth(fj)*sqrt(1-sin(theta2*pi/180)^2)/c;
kz1=2*pi*f_worth(fj)*sqrt(((n1o+delx)-sqrt(-1)*k1o)^2-...
sin(theta2*pi/180)^2)/c;
 kz2=2*pi*f_worth(fj)*sqrt((n2o-sqrt(-1)*k2o)^2-
sin(theta2*pi/180)^2)/c;
        hjg=find(imag(kz0)>0);
        kz0([hjg])=-kz0([hjg]);
        hjj=find(imag(kz1)>0);
        kz1([hjj])=-kz1([hjj]);
        hja=find(imag(kz2)>0);
        kz2([hja])=-kz2([hja]);

        Z2=kz2*eta2/k2;
        Z1=kz1*eta1/k1;
        Z0=kz0*eta0/k0;
```

```
        T01=(2*Z1)./(Z1+Z0);
        T12=(2*Z2)./(Z2+Z1);
        T20=(2*Z0)./(Z2+Z0);
        R01=(Z1-Z0)./(Z1+Z0);
        R12=(Z2-Z1)./(Z2+Z1);
        R20=(Z0-Z2)./(Z0+Z2);

 Tc2=(exp(-sqrt(-1)*kz1*(l1o)).*exp(-sqrt(-
1)*kz2*(l2o)).*T01.*T12.*T20)./...
                (1+R01.*R12.*exp(-sqrt(-1)*2*kz1*(l1o))+...
+R12.*R20.*exp(-sqrt(-1)*2*kz2*(l2o))+R01.*R20.*exp(-sqrt(-
1)*2*kz2*(l2o))...
                .*exp(-sqrt(-1)*2*kz1*(l1o)));

Jack31=[(abs(Tm2(fj))-abs(Tc2*exp(sqrt(-1)*kz0*(l1o+l2o))))-
func(3,1)];

        llps=angle(Tm2(fj));
        hyt=angle(Tc2.*exp(sqrt(-1)*kz0*(l1o+l2o)));

        anglebla0=(llps-hyt);
        if abs(anglebla0)>pi && abs(anglebla0)<2*pi
           anglebla0=abs(anglebla0)-2*pi;
        end
        Jack41=[abs(anglebla0)-func(4,1)];


        k1=w*(n1o-sqrt(-1)*(k1o+delx))/c;
        k0=w/c;
        k2=w*(n2o-sqrt(-1)*k2o)/c;
        eta2=120*pi/(n2o-sqrt(-1)*k2o);
        eta1=120*pi/(n1o-sqrt(-1)*(k1o+delx));
        eta0=120*pi;

        kz0=2*pi*f_worth(fj)*sqrt(1-sin(theta1*pi/180)^2)/c;
kz1=2*pi*f_worth(fj)*sqrt((n1o-sqrt(-1)*(k1o+delx))^2-...
sin(theta1*pi/180)^2)/c;
kz2=2*pi*f_worth(fj)*sqrt((n2o-sqrt(-1)*k2o)^2-
sin(theta1*pi/180)^2)/c;
        hjg=find(imag(kz0)>0);
        kz0([hjg])=-kz0([hjg]);
        hjj=find(imag(kz1)>0);
        kz1([hjj])=-kz1([hjj]);
        hja=find(imag(kz2)>0);
        kz2([hja])=-kz2([hja]);

        Z2=kz2*eta2/k2;
```

```
        Z1=kz1*eta1/k1;
        Z0=kz0*eta0/k0;

        T01=(2*Z1)./(Z1+Z0);
        T12=(2*Z2)./(Z2+Z1);
        T20=(2*Z0)./(Z2+Z0);
        R01=(Z1-Z0)./(Z1+Z0);
        R12=(Z2-Z1)./(Z2+Z1);
        R20=(Z0-Z2)./(Z0+Z2);

 Tc1=(exp(-sqrt(-1)*kz1*(l1o)).*exp(-sqrt(-
1)*kz2*(l2o)).*T01.*T12.*T20)./...
                (1+R01.*R12.*exp(-sqrt(-1)*2*kz1*(l1o))+...
+R12.*R20.*exp(-sqrt(-1)*2*kz2*(l2o))+R01.*R20.*exp(-sqrt(-
1)*2*kz2*(l2o))...
                .*exp(-sqrt(-1)*2*kz1*(l1o)));

Jack12=[(abs(Tm1(fj))-abs(Tc1*exp(sqrt(-1)*kz0*(l1o+l2o))))-
func(1,1)];

        llps=angle(Tm1(fj));
        hyt=angle(Tc1.*exp(sqrt(-1)*kz0*(l1o+l2o)));

        anglebla0=(llps-hyt);
        if abs(anglebla0)>pi && abs(anglebla0)<2*pi
           anglebla0=abs(anglebla0)-2*pi;
        end
        Jack22=[abs(anglebla0)-func(2,1)];

        k1=w*(n1o-sqrt(-1)*(k1o+delx))/c;
        k0=w/c;
        k2=w*(n2o-sqrt(-1)*k2o)/c;
        eta2=120*pi/(n2o-sqrt(-1)*k2o);
        eta1=120*pi/(n1o-sqrt(-1)*(k1o+delx));
        eta0=120*pi;

        kz0=2*pi*f_worth(fj)*sqrt(1-sin(theta2*pi/180)^2)/c;
kz1=2*pi*f_worth(fj)*sqrt((n1o-sqrt(-1)*(k1o+delx))^2-...
sin(theta2*pi/180)^2)/c;
kz2=2*pi*f_worth(fj)*sqrt((n2o-sqrt(-1)*k2o)^2-
sin(theta2*pi/180)^2)/c;
        hjg=find(imag(kz0)>0);
        kz0([hjg])=-kz0([hjg]);
        hjj=find(imag(kz1)>0);
        kz1([hjj])=-kz1([hjj]);
        hja=find(imag(kz2)>0);
        kz2([hja])=-kz2([hja]);
```

```
        Z2=kz2*eta2/k2;
        Z1=kz1*eta1/k1;
        Z0=kz0*eta0/k0;

        T01=(2*Z1)./(Z1+Z0);
        T12=(2*Z2)./(Z2+Z1);
        T20=(2*Z0)./(Z2+Z0);
        R01=(Z1-Z0)./(Z1+Z0);
        R12=(Z2-Z1)./(Z2+Z1);
        R20=(Z0-Z2)./(Z0+Z2);

 Tc2=(exp(-sqrt(-1)*kz1*(l1o)).*exp(-sqrt(-
1)*kz2*(l2o)).*T01.*T12.*T20)./...
                (1+R01.*R12.*exp(-sqrt(-1)*2*kz1*(l1o))+...
+R12.*R20.*exp(-sqrt(-1)*2*kz2*(l2o))+R01.*R20.*exp(-sqrt(-
1)*2*kz2*(l2o))...
                .*exp(-sqrt(-1)*2*kz1*(l1o)));

 Jack32=[(abs(Tm2(fj))-abs(Tc2*exp(sqrt(-1)*kz0*(l1o+l2o))))-
func(3,1)];

        llps=angle(Tm2(fj));
        hyt=angle(Tc2.*exp(sqrt(-1)*kz0*(l1o+l2o)));

        anglebla0=(llps-hyt);
        if abs(anglebla0)>pi && abs(anglebla0)<2*pi
           anglebla0=abs(anglebla0)-2*pi;
        end
        Jack42=[abs(anglebla0)-func(4,1)];
        k1=w*(n1o-sqrt(-1)*k1o)/c;
        k0=w/c;
        k2=w*((n2o+delx)-sqrt(-1)*k2o)/c;
        eta2=120*pi/((n2o+delx)-sqrt(-1)*k2o);
        eta1=120*pi/(n1o-sqrt(-1)*k1o);
        eta0=120*pi;

        kz0=2*pi*f_worth(fj)*sqrt(1-sin(theta1*pi/180)^2)/c;
 kz1=2*pi*f_worth(fj)*sqrt((n1o-sqrt(-1)*k1o)^2-
sin(theta1*pi/180)^2)/c;
kz2=2*pi*f_worth(fj)*sqrt(((n2o+delx)-sqrt(-1)*k2o)^2-...
sin(theta1*pi/180)^2)/c;
        hjg=find(imag(kz0)>0);
        kz0([hjg])=-kz0([hjg]);
        hjj=find(imag(kz1)>0);
        kz1([hjj])=-kz1([hjj]);
        hja=find(imag(kz2)>0);
```

```
        kz2([hja])=-kz2([hja]);

        Z2=kz2*eta2/k2;
        Z1=kz1*eta1/k1;
        Z0=kz0*eta0/k0;

        T01=(2*Z1)./(Z1+Z0);
        T12=(2*Z2)./(Z2+Z1);
        T20=(2*Z0)./(Z2+Z0);
        R01=(Z1-Z0)./(Z1+Z0);
        R12=(Z2-Z1)./(Z2+Z1);
        R20=(Z0-Z2)./(Z0+Z2);

Tc1=(exp(-sqrt(-1)*kz1*(l1o)).*exp(-sqrt(-
1)*kz2*(l2o)).*T01.*T12.*T20)./...
                (1+R01.*R12.*exp(-sqrt(-1)*2*kz1*(l1o))+...
+R12.*R20.*exp(-sqrt(-1)*2*kz2*(l2o))+R01.*R20.*exp(-sqrt(-
1)*2*kz2*(l2o))...
                .*exp(-sqrt(-1)*2*kz1*(l1o)));

 Jack13=[(abs(Tm1(fj))-abs(Tc1*exp(sqrt(-1)*kz0*(l1o+l2o))))-
func(1,1)];

        llps=angle(Tm1(fj));
        hyt=angle(Tc1.*exp(sqrt(-1)*kz0*(l1o+l2o)));

        anglebla0=(llps-hyt);
        if abs(anglebla0)>pi && abs(anglebla0)<2*pi
           anglebla0=abs(anglebla0)-2*pi;
        end
        Jack23=[abs(anglebla0)-func(2,1)];

        k1=w*(n1o-sqrt(-1)*k1o)/c;
        k0=w/c;
        k2=w*((n2o+delx)-sqrt(-1)*k2o)/c;
        eta2=120*pi/((n2o+delx)-sqrt(-1)*k2o);
        eta1=120*pi/(n1o-sqrt(-1)*k1o);
        eta0=120*pi;

        kz0=2*pi*f_worth(fj)*sqrt(1-sin(theta2*pi/180)^2)/c;
kz1=2*pi*f_worth(fj)*sqrt((n1o-sqrt(-1)*k1o)^2-
sin(theta2*pi/180)^2)/c;
kz2=2*pi*f_worth(fj)*sqrt(((n2o+delx)-sqrt(-1)*k2o)^2-...
sin(theta2*pi/180)^2)/c;
        hjg=find(imag(kz0)>0);
        kz0([hjg])=-kz0([hjg]);
        hjj=find(imag(kz1)>0);
```

```
        kz1([hjj])=-kz1([hjj]);
        hja=find(imag(kz2)>0);
        kz2([hja])=-kz2([hja]);

        Z2=kz2*eta2/k2;
        Z1=kz1*eta1/k1;
        Z0=kz0*eta0/k0;

        T01=(2*Z1)./(Z1+Z0);
        T12=(2*Z2)./(Z2+Z1);
        T20=(2*Z0)./(Z2+Z0);
        R01=(Z1-Z0)./(Z1+Z0);
        R12=(Z2-Z1)./(Z2+Z1);
        R20=(Z0-Z2)./(Z0+Z2);

 Tc2=(exp(-sqrt(-1)*kz1*(l1o)).*exp(-sqrt(-
1)*kz2*(l2o)).*T01.*T12.*T20)./...
                (1+R01.*R12.*exp(-sqrt(-1)*2*kz1*(l1o))+...
+R12.*R20.*exp(-sqrt(-1)*2*kz2*(l2o))+R01.*R20.*exp(-sqrt(-
1)*2*kz2*(l2o))...
                .*exp(-sqrt(-1)*2*kz1*(l1o)));

  Jack33=[(abs(Tm2(fj))-abs(Tc2*exp(sqrt(-1)*kz0*(l1o+l2o))))-
func(3,1)];

        llps=angle(Tm2(fj));
        hyt=angle(Tc2.*exp(sqrt(-1)*kz0*(l1o+l2o)));

        anglebla0=(llps-hyt);
        if abs(anglebla0)>pi && abs(anglebla0)<2*pi
           anglebla0=abs(anglebla0)-2*pi;
        end
        Jack43=[abs(anglebla0)-func(4,1)];

        k1=w*(n1o-sqrt(-1)*k1o)/c;
        k0=w/c;
        k2=w*(n2o-sqrt(-1)*(k2o+delx))/c;
        eta2=120*pi/(n2o-sqrt(-1)*(k2o+delx));
        eta1=120*pi/(n1o-sqrt(-1)*k1o);
        eta0=120*pi;

        kz0=2*pi*f_worth(fj)*sqrt(1-sin(theta1*pi/180)^2)/c;
 kz1=2*pi*f_worth(fj)*sqrt((n1o-sqrt(-1)*k1o)^2-
sin(theta1*pi/180)^2)/c;
kz2=2*pi*f_worth(fj)*sqrt((n2o-sqrt(-1)*(k2o+delx))^2-...
sin(theta1*pi/180)^2)/c;
        hjg=find(imag(kz0)>0);
```

```
        kz0([hjg])=-kz0([hjg]);
        hjj=find(imag(kz1)>0);
        kz1([hjj])=-kz1([hjj]);
        hja=find(imag(kz2)>0);
        kz2([hja])=-kz2([hja]);

        Z2=kz2*eta2/k2;
        Z1=kz1*eta1/k1;
        Z0=kz0*eta0/k0;

        T01=(2*Z1)./(Z1+Z0);
        T12=(2*Z2)./(Z2+Z1);
        T20=(2*Z0)./(Z2+Z0);
        R01=(Z1-Z0)./(Z1+Z0);
        R12=(Z2-Z1)./(Z2+Z1);
        R20=(Z0-Z2)./(Z0+Z2);

 Tc1=(exp(-sqrt(-1)*kz1*(l1o)).*exp(-sqrt(-
1)*kz2*(l2o)).*T01.*T12.*T20)./...
                (1+R01.*R12.*exp(-sqrt(-1)*2*kz1*(l1o))+...
+R12.*R20.*exp(-sqrt(-1)*2*kz2*(l2o))+R01.*R20.*exp(-sqrt(-
1)*2*kz2*(l2o))...
                .*exp(-sqrt(-1)*2*kz1*(l1o)));

Jack14=[(abs(Tm1(fj))-abs(Tc1*exp(sqrt(-1)*kz0*(l1o+l2o))))-
func(1,1)];

        llps=angle(Tm1(fj));
        hyt=angle(Tc1.*exp(sqrt(-1)*kz0*(l1o+l2o)));

        anglebla0=(llps-hyt);
        if abs(anglebla0)>pi && abs(anglebla0)<2*pi
           anglebla0=abs(anglebla0)-2*pi;
        end
        Jack24=[abs(anglebla0)-func(2,1)];

        k1=w*(n1o-sqrt(-1)*k1o)/c;
        k0=w/c;
        k2=w*(n2o-sqrt(-1)*(k2o+delx))/c;
        eta2=120*pi/(n2o-sqrt(-1)*(k2o+delx));
        eta1=120*pi/(n1o-sqrt(-1)*k1o);
        eta0=120*pi;

        kz0=2*pi*f_worth(fj)*sqrt(1-sin(theta2*pi/180)^2)/c;
 kz1=2*pi*f_worth(fj)*sqrt((n1o-sqrt(-1)*k1o)^2-
sin(theta2*pi/180)^2)/c;
kz2=2*pi*f_worth(fj)*sqrt((n2o-sqrt(-1)*(k2o+delx))^2-...
```

```
sin(theta2*pi/180)^2)/c;
        hjg=find(imag(kz0)>0);
        kz0([hjg])=-kz0([hjg]);
        hjj=find(imag(kz1)>0);
        kz1([hjj])=-kz1([hjj]);
        hja=find(imag(kz2)>0);
        kz2([hja])=-kz2([hja]);

        Z2=kz2*eta2/k2;
        Z1=kz1*eta1/k1;
        Z0=kz0*eta0/k0;

        T01=(2*Z1)./(Z1+Z0);
        T12=(2*Z2)./(Z2+Z1);
        T20=(2*Z0)./(Z2+Z0);
        R01=(Z1-Z0)./(Z1+Z0);
        R12=(Z2-Z1)./(Z2+Z1);
        R20=(Z0-Z2)./(Z0+Z2);

 Tc2=(exp(-sqrt(-1)*kz1*(l1o)).*exp(-sqrt(-
1)*kz2*(l2o)).*T01.*T12.*T20)./...
                (1+R01.*R12.*exp(-sqrt(-1)*2*kz1*(l1o))+...
+R12.*R20.*exp(-sqrt(-1)*2*kz2*(l2o))+R01.*R20.*exp(-sqrt(-
1)*2*kz2*(l2o))...
                .*exp(-sqrt(-1)*2*kz1*(l1o)));

 Jack34=[(abs(Tm2(fj))-abs(Tc2*exp(sqrt(-1)*kz0*(l1o+l2o))))-
func(3,1)];

        llps=angle(Tm2(fj));
        hyt=angle(Tc2.*exp(sqrt(-1)*kz0*(l1o+l2o)));

        anglebla0=(llps-hyt);
        if abs(anglebla0)>pi && abs(anglebla0)<2*pi
           anglebla0=abs(anglebla0)-2*pi;
        end
        Jack44=[abs(anglebla0)-func(4,1)];

        Jack=[Jack11, Jack12, Jack13, Jack14;
            Jack21, Jack22, Jack23, Jack24;
            Jack31, Jack32, Jack33, Jack34;
            Jack41, Jack42, Jack43, Jack44]/delx;

        if abs(det(Jack(1:4,:)))<0.0000000000000001
                index1(fj)=0;
                ext1(fj)=0;
                index2(fj)=0;
```

```
                ext2(fj)=0;
         break
        end
        optmat=optmat-Jack\func
        n1o=optmat(1,1);
        k1o=optmat(2,1);
        n2o=optmat(3,1);
        k2o=optmat(4,1);

                    if nj==n
                index1(fj)=n1o;
                ext1(fj)=k1o;
                index2(fj)=n2o;
                ext2(fj)=k2o;
                    end
    end
    cnt(fj)=nj;

end
    if fj==size(f_worth,2)
        fvd=find(index1>lower_ind_g1 & index1<upper_ind_g1);
        fgh=find(ext1>lower_ext_g1 & ext1<upper_ext_g1);
        fvd1=find(index2>lower_ind_g2 & index2<upper_ind_g2);
        fgh1=find(ext2>lower_ext_g2 & ext2<upper_ext_g2);
        d=intersect(fvd,fgh);
        cd=intersect(fvd1,fgh1);
        flav=intersect(d,cd);
        if size(flav,2)>0
            cc=0;
        end
    end

end
%figure;plot(f_worth,index1,f_worth,index2);grid
%figure;plot(f_worth,abs(ext1),f_worth,abs(ext2));grid
%figure;plot(f_worth,cnt);grid

er1=index1.^2-ext1.^2;
er2=index2.^2-ext2.^2;
%figure;plot(f_worth,er1,f_worth,er2);grid

tand1=2*index1.*abs(ext1)./er1;
tand2=2*index2.*abs(ext2)./er2;
%figure;plot(f_worth,tand1,f_worth,tand2);grid

n=50; %number of iterations for each frequency
for i=1:size(f_worth,2)
```

```
    n1initial=index1(i);%initial n
    n2initial=index2(i);
    k1initial=ext1(i);
    k2initial=ext2(i);
    if n1initial>=lower_ind_g1 && k1initial>lower_ext_g1 &&
k2initial>lower_ext_g2 && n2initial>=lower_ind_g2 &&
n2initial<upper_ind_g2 && n1initial<upper_ind_g1 ...
            && k1initial<upper_ext_g1 && k2initial<upper_ext_g2
        break
    else
        continue
    end
end
delx=0.00000000000001;

for fj=1:size(f_worth,2)
    n1o=n1initial;
    k1o=k1initial;
    l1o=l1initial;
    n2o=n2initial;
    k2o=k2initial;
    l2o=l2initial
    optmat=[n1o;k1o;n2o;k2o];
    if fj==1
        lops_init(lops+1,:)=optmat';
    end
    for nj=1:n

        w=2*pi*f_worth(fj);
        k1=w*(n1o-sqrt(-1)*k1o)/c;
        k0=w/c;
        k2=w*(n2o-sqrt(-1)*k2o)/c;
        eta2=120*pi/(n2o-sqrt(-1)*k2o);
        eta1=120*pi/(n1o-sqrt(-1)*k1o);
        eta0=120*pi;

        kz0=2*pi*f_worth(fj)*sqrt(1-sin(theta1*pi/180)^2)/c;
 kz1=2*pi*f_worth(fj)*sqrt((n1o-sqrt(-1)*k1o)^2-
sin(theta1*pi/180)^2)/c;
 kz2=2*pi*f_worth(fj)*sqrt((n2o-sqrt(-1)*k2o)^2-
sin(theta1*pi/180)^2)/c;
        hjg=find(imag(kz0)>0);
        kz0([hjg])=-kz0([hjg]);
        hjj=find(imag(kz1)>0);
        kz1([hjj])=-kz1([hjj]);
        hja=find(imag(kz2)>0);
        kz2([hja])=-kz2([hja]);
```

```
        Z2=kz2*eta2/k2;
        Z1=kz1*eta1/k1;
        Z0=kz0*eta0/k0;

        T01=(2*Z1)./(Z1+Z0);
        T12=(2*Z2)./(Z2+Z1);
        T20=(2*Z0)./(Z2+Z0);
        R01=(Z1-Z0)./(Z1+Z0);
        R12=(Z2-Z1)./(Z2+Z1);
        R20=(Z0-Z2)./(Z0+Z2);

 Tc1=(exp(-sqrt(-1)*kz1*(l1o)).*exp(-sqrt(-
1)*kz2*(l2o)).*T01.*T12.*T20)./...
               (1+R01.*R12.*exp(-sqrt(-1)*2*kz1*(l1o))+...
+R12.*R20.*exp(-sqrt(-1)*2*kz2*(l2o))+R01.*R20.*exp(-sqrt(-
1)*2*kz2*(l2o))...
                .*exp(-sqrt(-1)*2*kz1*(l1o)));


        func1=[abs(Tm1(fj))-abs(Tc1*exp(sqrt(-
1)*kz0*(l1o+l2o)))];

        llps=angle(Tm1(fj));
        hyt=angle(Tc1.*exp(sqrt(-1)*kz0*(l1o+l2o)));

        anglebla0=(llps-hyt);
        if abs(anglebla0)>pi && abs(anglebla0)<2*pi
           anglebla0=abs(anglebla0)-2*pi;
        end
        func2=[abs(anglebla0)];

        kz0=2*pi*f_worth(fj)*sqrt(1-sin(theta2*pi/180)^2)/c;
kz1=2*pi*f_worth(fj)*sqrt((n1o-sqrt(-1)*k1o)^2-
sin(theta2*pi/180)^2)/c;
kz2=2*pi*f_worth(fj)*sqrt((n2o-sqrt(-1)*k2o)^2-
sin(theta2*pi/180)^2)/c;
        hjg=find(imag(kz0)>0);
        kz0([hjg])=-kz0([hjg]);
        hjj=find(imag(kz1)>0);
        kz1([hjj])=-kz1([hjj]);
        hja=find(imag(kz2)>0);
        kz2([hja])=-kz2([hja]);

        Z2=kz2*eta2/k2;
        Z1=kz1*eta1/k1;
        Z0=kz0*eta0/k0;
```

```
        T01=(2*Z1)./(Z1+Z0);
        T12=(2*Z2)./(Z2+Z1);
        T20=(2*Z0)./(Z2+Z0);
        R01=(Z1-Z0)./(Z1+Z0);
        R12=(Z2-Z1)./(Z2+Z1);
        R20=(Z0-Z2)./(Z0+Z2);

Tc2=(exp(-sqrt(-1)*kz1*(l1o)).*exp(-sqrt(-
1)*kz2*(l2o)).*T01.*T12.*T20)./...
            (1+R01.*R12.*exp(-sqrt(-1)*2*kz1*(l1o))+...
+R12.*R20.*exp(-sqrt(-1)*2*kz2*(l2o))+R01.*R20.*exp(-sqrt(-
1)*2*kz2*(l2o))...
            .*exp(-sqrt(-1)*2*kz1*(l1o)));

        func3=[abs(Tm2(fj))-abs(Tc2*exp(sqrt(-
1)*kz0*(l1o+l2o)))];

        llps=angle(Tm2(fj));
        hyt=angle(Tc2.*exp(sqrt(-1)*kz0*(l1o+l2o)));

        anglebla0=(llps-hyt);
        if abs(anglebla0)>pi && abs(anglebla0)<2*pi
           anglebla0=abs(anglebla0)-2*pi;
        end
        func4=[abs(anglebla0)];



        func=[(func1);(func2);func3;func4]

        if abs(func(1,1))<0.0000000000000001
            if abs(func(2,1))<0.0000000000000001
                if abs(func(3,1))<0.0000000000000001
                    if abs(func(4,1))<0.0000000000000001
                index1(fj)=optmat(1,1);
                ext1(fj)=optmat(2,1);
                index2(fj)=optmat(3,1);
                ext2(fj)=optmat(4,1);
                 n1initial=index1(fj);
                 k1initial=ext1(fj);
                 n2initial=index2(fj);
                 k2initial=ext2(fj);
                 fhh(fj,:)=[func'];
                 break
                    end
                end
```

```
            end
        end

        k1=w*((n1o+delx)-sqrt(-1)*k1o)/c;
        k0=w/c;
        k2=w*(n2o-sqrt(-1)*k2o)/c;
        eta2=120*pi/(n2o-sqrt(-1)*k2o);
        eta1=120*pi/((n1o+delx)-sqrt(-1)*k1o);
        eta0=120*pi;

        kz0=2*pi*f_worth(fj)*sqrt(1-sin(theta1*pi/180)^2)/c;
kz1=2*pi*f_worth(fj)*sqrt(((n1o+delx)-sqrt(-1)*k1o)^2-...
sin(theta1*pi/180)^2)/c;
kz2=2*pi*f_worth(fj)*sqrt((n2o-sqrt(-1)*k2o)^2-
sin(theta1*pi/180)^2)/c;
        hjg=find(imag(kz0)>0);
        kz0([hjg])=-kz0([hjg]);
        hjj=find(imag(kz1)>0);
        kz1([hjj])=-kz1([hjj]);
        hja=find(imag(kz2)>0);
        kz2([hja])=-kz2([hja]);

        Z2=kz2*eta2/k2;
        Z1=kz1*eta1/k1;
        Z0=kz0*eta0/k0;

        T01=(2*Z1)./(Z1+Z0);
        T12=(2*Z2)./(Z2+Z1);
        T20=(2*Z0)./(Z2+Z0);
        R01=(Z1-Z0)./(Z1+Z0);
        R12=(Z2-Z1)./(Z2+Z1);
        R20=(Z0-Z2)./(Z0+Z2);

        Tc1=(exp(-sqrt(-1)*kz1*(l1o)).*exp(-sqrt(-
1)*kz2*(l2o)).*T01.*T12.*T20)./...
                (1+R01.*R12.*exp(-sqrt(-1)*2*kz1*(l1o))+...
+R12.*R20.*exp(-sqrt(-1)*2*kz2*(l2o))+R01.*R20.*exp(-sqrt(-
1)*2*kz2*(l2o))...
                .*exp(-sqrt(-1)*2*kz1*(l1o)));

   Jack11=[(abs(Tm1(fj))-abs(Tc1*exp(sqrt(-1)*kz0*(l1o+l2o))))-
func(1,1)];

        llps=angle(Tm1(fj));
        hyt=angle(Tc1.*exp(sqrt(-1)*kz0*(l1o+l2o)));

        anglebla0=(llps-hyt);
```

```
        if abs(anglebla0)>pi && abs(anglebla0)<2*pi
           anglebla0=abs(anglebla0)-2*pi;
        end
        Jack21=[abs(anglebla0)-func(2,1)];

        k1=w*((n1o+delx)-sqrt(-1)*k1o)/c;
        k0=w/c;
        k2=w*(n2o-sqrt(-1)*k2o)/c;
        eta2=120*pi/(n2o-sqrt(-1)*k2o);
        eta1=120*pi/((n1o+delx)-sqrt(-1)*k1o);
        eta0=120*pi;

        kz0=2*pi*f_worth(fj)*sqrt(1-sin(theta2*pi/180)^2)/c;
kz1=2*pi*f_worth(fj)*sqrt(((n1o+delx)-sqrt(-1)*k1o)^2-...
sin(theta2*pi/180)^2)/c;
  kz2=2*pi*f_worth(fj)*sqrt((n2o-sqrt(-1)*k2o)^2-
sin(theta2*pi/180)^2)/c;
        hjg=find(imag(kz0)>0);
        kz0([hjg])=-kz0([hjg]);
        hjj=find(imag(kz1)>0);
        kz1([hjj])=-kz1([hjj]);
        hja=find(imag(kz2)>0);
        kz2([hja])=-kz2([hja]);

        Z2=kz2*eta2/k2;
        Z1=kz1*eta1/k1;
        Z0=kz0*eta0/k0;

        T01=(2*Z1)./(Z1+Z0);
        T12=(2*Z2)./(Z2+Z1);
        T20=(2*Z0)./(Z2+Z0);
        R01=(Z1-Z0)./(Z1+Z0);
        R12=(Z2-Z1)./(Z2+Z1);
        R20=(Z0-Z2)./(Z0+Z2);

 Tc2=(exp(-sqrt(-1)*kz1*(l1o)).*exp(-sqrt(-
1)*kz2*(l2o)).*T01.*T12.*T20)./...
                (1+R01.*R12.*exp(-sqrt(-1)*2*kz1*(l1o))+...
+R12.*R20.*exp(-sqrt(-1)*2*kz2*(l2o))+R01.*R20.*exp(-sqrt(-
1)*2*kz2*(l2o))...
                .*exp(-sqrt(-1)*2*kz1*(l1o)));

   Jack31=[(abs(Tm2(fj))-abs(Tc2*exp(sqrt(-1)*kz0*(l1o+l2o))))-
func(3,1)];

        llps=angle(Tm2(fj));
        hyt=angle(Tc2.*exp(sqrt(-1)*kz0*(l1o+l2o)));
```

```
        anglebla0=(llps-hyt);
        if abs(anglebla0)>pi && abs(anglebla0)<2*pi
           anglebla0=abs(anglebla0)-2*pi;
        end
        Jack41=[abs(anglebla0)-func(4,1)];


        k1=w*(n1o-sqrt(-1)*(k1o+delx))/c;
        k0=w/c;
        k2=w*(n2o-sqrt(-1)*k2o)/c;
        eta2=120*pi/(n2o-sqrt(-1)*k2o);
        eta1=120*pi/(n1o-sqrt(-1)*(k1o+delx));
        eta0=120*pi;

        kz0=2*pi*f_worth(fj)*sqrt(1-sin(theta1*pi/180)^2)/c;
kz1=2*pi*f_worth(fj)*sqrt((n1o-sqrt(-1)*(k1o+delx))^2-...
sin(theta1*pi/180)^2)/c;
kz2=2*pi*f_worth(fj)*sqrt((n2o-sqrt(-1)*k2o)^2-
sin(theta1*pi/180)^2)/c;
        hjg=find(imag(kz0)>0);
        kz0([hjg])=-kz0([hjg]);
        hjj=find(imag(kz1)>0);
        kz1([hjj])=-kz1([hjj]);
        hja=find(imag(kz2)>0);
        kz2([hja])=-kz2([hja]);

        Z2=kz2*eta2/k2;
        Z1=kz1*eta1/k1;
        Z0=kz0*eta0/k0;

        T01=(2*Z1)./(Z1+Z0);
        T12=(2*Z2)./(Z2+Z1);
        T20=(2*Z0)./(Z2+Z0);
        R01=(Z1-Z0)./(Z1+Z0);
        R12=(Z2-Z1)./(Z2+Z1);
        R20=(Z0-Z2)./(Z0+Z2);

Tc1=(exp(-sqrt(-1)*kz1*(l1o)).*exp(-sqrt(-
1)*kz2*(l2o)).*T01.*T12.*T20)./...
                (1+R01.*R12.*exp(-sqrt(-1)*2*kz1*(l1o))+...
+R12.*R20.*exp(-sqrt(-1)*2*kz2*(l2o))+R01.*R20.*exp(-sqrt(-
1)*2*kz2*(l2o))...
                .*exp(-sqrt(-1)*2*kz1*(l1o)));

Jack12=[(abs(Tm1(fj))-abs(Tc1*exp(sqrt(-1)*kz0*(l1o+l2o))))-
func(1,1)];
```

```
        llps=angle(Tm1(fj));
        hyt=angle(Tc1.*exp(sqrt(-1)*kz0*(l1o+l2o)));

        anglebla0=(llps-hyt);
        if abs(anglebla0)>pi && abs(anglebla0)<2*pi
           anglebla0=abs(anglebla0)-2*pi;
        end
        Jack22=[abs(anglebla0)-func(2,1)];

        k1=w*(n1o-sqrt(-1)*(k1o+delx))/c;
        k0=w/c;
        k2=w*(n2o-sqrt(-1)*k2o)/c;
        eta2=120*pi/(n2o-sqrt(-1)*k2o);
        eta1=120*pi/(n1o-sqrt(-1)*(k1o+delx));
        eta0=120*pi;

        kz0=2*pi*f_worth(fj)*sqrt(1-sin(theta2*pi/180)^2)/c;
kz1=2*pi*f_worth(fj)*sqrt((n1o-sqrt(-1)*(k1o+delx))^2-...
sin(theta2*pi/180)^2)/c;
kz2=2*pi*f_worth(fj)*sqrt((n2o-sqrt(-1)*k2o)^2-
sin(theta2*pi/180)^2)/c;
        hjg=find(imag(kz0)>0);
        kz0([hjg])=-kz0([hjg]);
        hjj=find(imag(kz1)>0);
        kz1([hjj])=-kz1([hjj]);
        hja=find(imag(kz2)>0);
        kz2([hja])=-kz2([hja]);

        Z2=kz2*eta2/k2;
        Z1=kz1*eta1/k1;
        Z0=kz0*eta0/k0;

        T01=(2*Z1)./(Z1+Z0);
        T12=(2*Z2)./(Z2+Z1);
        T20=(2*Z0)./(Z2+Z0);
        R01=(Z1-Z0)./(Z1+Z0);
        R12=(Z2-Z1)./(Z2+Z1);
        R20=(Z0-Z2)./(Z0+Z2);

Tc2=(exp(-sqrt(-1)*kz1*(l1o)).*exp(-sqrt(-
1)*kz2*(l2o)).*T01.*T12.*T20)./...
                (1+R01.*R12.*exp(-sqrt(-1)*2*kz1*(l1o))+...
+R12.*R20.*exp(-sqrt(-1)*2*kz2*(l2o))+R01.*R20.*exp(-sqrt(-
1)*2*kz2*(l2o))...
                .*exp(-sqrt(-1)*2*kz1*(l1o)));
```

```
  Jack32=[(abs(Tm2(fj))-abs(Tc2*exp(sqrt(-1)*kz0*(l1o+l2o))))-
func(3,1)];

        llps=angle(Tm2(fj));
        hyt=angle(Tc2.*exp(sqrt(-1)*kz0*(l1o+l2o)));

        anglebla0=(llps-hyt);
        if abs(anglebla0)>pi && abs(anglebla0)<2*pi
           anglebla0=abs(anglebla0)-2*pi;
        end
        Jack42=[abs(anglebla0)-func(4,1)];


        k1=w*(n1o-sqrt(-1)*k1o)/c;
        k0=w/c;
        k2=w*((n2o+delx)-sqrt(-1)*k2o)/c;
        eta2=120*pi/((n2o+delx)-sqrt(-1)*k2o);
        eta1=120*pi/(n1o-sqrt(-1)*k1o);
        eta0=120*pi;

        kz0=2*pi*f_worth(fj)*sqrt(1-sin(theta1*pi/180)^2)/c;
kz1=2*pi*f_worth(fj)*sqrt((n1o-sqrt(-1)*k1o)^2-
sin(theta1*pi/180)^2)/c;
kz2=2*pi*f_worth(fj)*sqrt(((n2o+delx)-sqrt(-1)*k2o)^2-...
sin(theta1*pi/180)^2)/c;
        hjg=find(imag(kz0)>0);
        kz0([hjg])=-kz0([hjg]);
        hjj=find(imag(kz1)>0);
        kz1([hjj])=-kz1([hjj]);
        hja=find(imag(kz2)>0);
        kz2([hja])=-kz2([hja]);

        Z2=kz2*eta2/k2;
        Z1=kz1*eta1/k1;
        Z0=kz0*eta0/k0;

        T01=(2*Z1)./(Z1+Z0);
        T12=(2*Z2)./(Z2+Z1);
        T20=(2*Z0)./(Z2+Z0);
        R01=(Z1-Z0)./(Z1+Z0);
        R12=(Z2-Z1)./(Z2+Z1);
        R20=(Z0-Z2)./(Z0+Z2);

Tc1=(exp(-sqrt(-1)*kz1*(l1o)).*exp(-sqrt(-
1)*kz2*(l2o)).*T01.*T12.*T20)./...
                (1+R01.*R12.*exp(-sqrt(-1)*2*kz1*(l1o))+...
```

```
+R12.*R20.*exp(-sqrt(-1)*2*kz2*(l2o))+R01.*R20.*exp(-sqrt(-
1)*2*kz2*(l2o))...
                .*exp(-sqrt(-1)*2*kz1*(l1o)));

Jack13=[(abs(Tm1(fj))-abs(Tc1*exp(sqrt(-1)*kz0*(l1o+l2o))))-
func(1,1)];

        llps=angle(Tm1(fj));
        hyt=angle(Tc1.*exp(sqrt(-1)*kz0*(l1o+l2o)));

        anglebla0=(llps-hyt);
        if abs(anglebla0)>pi && abs(anglebla0)<2*pi
           anglebla0=abs(anglebla0)-2*pi;
        end
        Jack23=[abs(anglebla0)-func(2,1)];

        k1=w*(n1o-sqrt(-1)*k1o)/c;
        k0=w/c;
        k2=w*((n2o+delx)-sqrt(-1)*k2o)/c;
        eta2=120*pi/((n2o+delx)-sqrt(-1)*k2o);
        eta1=120*pi/(n1o-sqrt(-1)*k1o);
        eta0=120*pi;

        kz0=2*pi*f_worth(fj)*sqrt(1-sin(theta2*pi/180)^2)/c;
kz1=2*pi*f_worth(fj)*sqrt((n1o-sqrt(-1)*k1o)^2-
sin(theta2*pi/180)^2)/c;
kz2=2*pi*f_worth(fj)*sqrt(((n2o+delx)-sqrt(-1)*k2o)^2-...
sin(theta2*pi/180)^2)/c;
        hjg=find(imag(kz0)>0);
        kz0([hjg])=-kz0([hjg]);
        hjj=find(imag(kz1)>0);
        kz1([hjj])=-kz1([hjj]);
        hja=find(imag(kz2)>0);
        kz2([hja])=-kz2([hja]);

        Z2=kz2*eta2/k2;
        Z1=kz1*eta1/k1;
        Z0=kz0*eta0/k0;

        T01=(2*Z1)./(Z1+Z0);
        T12=(2*Z2)./(Z2+Z1);
        T20=(2*Z0)./(Z2+Z0);
        R01=(Z1-Z0)./(Z1+Z0);
        R12=(Z2-Z1)./(Z2+Z1);
        R20=(Z0-Z2)./(Z0+Z2);
```

```
 Tc2=(exp(-sqrt(-1)*kz1*(l1o)).*exp(-sqrt(-
1)*kz2*(l2o)).*T01.*T12.*T20)./...
                (1+R01.*R12.*exp(-sqrt(-1)*2*kz1*(l1o))+...
+R12.*R20.*exp(-sqrt(-1)*2*kz2*(l2o))+R01.*R20.*exp(-sqrt(-
1)*2*kz2*(l2o))...
                .*exp(-sqrt(-1)*2*kz1*(l1o)));

Jack33=[(abs(Tm2(fj))-abs(Tc2*exp(sqrt(-1)*kz0*(l1o+l2o))))-
func(3,1)];

        llps=angle(Tm2(fj));
        hyt=angle(Tc2.*exp(sqrt(-1)*kz0*(l1o+l2o)));

        anglebla0=(llps-hyt);
        if abs(anglebla0)>pi && abs(anglebla0)<2*pi
           anglebla0=abs(anglebla0)-2*pi;
        end
        Jack43=[abs(anglebla0)-func(4,1)];


        k1=w*(n1o-sqrt(-1)*k1o)/c;
        k0=w/c;
        k2=w*(n2o-sqrt(-1)*(k2o+delx))/c;
        eta2=120*pi/(n2o-sqrt(-1)*(k2o+delx));
        eta1=120*pi/(n1o-sqrt(-1)*k1o);
        eta0=120*pi;

        kz0=2*pi*f_worth(fj)*sqrt(1-sin(theta1*pi/180)^2)/c;
kz1=2*pi*f_worth(fj)*sqrt((n1o-sqrt(-1)*k1o)^2-
sin(theta1*pi/180)^2)/c;
kz2=2*pi*f_worth(fj)*sqrt((n2o-sqrt(-1)*(k2o+delx))^2-...
sin(theta1*pi/180)^2)/c;
        hjg=find(imag(kz0)>0);
        kz0([hjg])=-kz0([hjg]);
        hjj=find(imag(kz1)>0);
        kz1([hjj])=-kz1([hjj]);
        hja=find(imag(kz2)>0);
        kz2([hja])=-kz2([hja]);

        Z2=kz2*eta2/k2;
        Z1=kz1*eta1/k1;
        Z0=kz0*eta0/k0;

        T01=(2*Z1)./(Z1+Z0);
        T12=(2*Z2)./(Z2+Z1);
        T20=(2*Z0)./(Z2+Z0);
        R01=(Z1-Z0)./(Z1+Z0);
```

```
        R12=(Z2-Z1)./(Z2+Z1);
        R20=(Z0-Z2)./(Z0+Z2);

 Tc1=(exp(-sqrt(-1)*kz1*(l1o)).*exp(-sqrt(-
1)*kz2*(l2o)).*T01.*T12.*T20)./...
                (1+R01.*R12.*exp(-sqrt(-1)*2*kz1*(l1o))+...
+R12.*R20.*exp(-sqrt(-1)*2*kz2*(l2o))+R01.*R20.*exp(-sqrt(-
1)*2*kz2*(l2o))...
                .*exp(-sqrt(-1)*2*kz1*(l1o)));

Jack14=[(abs(Tm1(fj))-abs(Tc1*exp(sqrt(-1)*kz0*(l1o+l2o))))-
func(1,1)];

        llps=angle(Tm1(fj));
        hyt=angle(Tc1.*exp(sqrt(-1)*kz0*(l1o+l2o)));

        anglebla0=(llps-hyt);
        if abs(anglebla0)>pi && abs(anglebla0)<2*pi
           anglebla0=abs(anglebla0)-2*pi;
        end
        Jack24=[abs(anglebla0)-func(2,1)];

        k1=w*(n1o-sqrt(-1)*k1o)/c;
        k0=w/c;
        k2=w*(n2o-sqrt(-1)*(k2o+delx))/c;
        eta2=120*pi/(n2o-sqrt(-1)*(k2o+delx));
        eta1=120*pi/(n1o-sqrt(-1)*k1o);
        eta0=120*pi;

        kz0=2*pi*f_worth(fj)*sqrt(1-sin(theta2*pi/180)^2)/c;
 kz1=2*pi*f_worth(fj)*sqrt((n1o-sqrt(-1)*k1o)^2-
sin(theta2*pi/180)^2)/c;
kz2=2*pi*f_worth(fj)*sqrt((n2o-sqrt(-1)*(k2o+delx))^2-...
sin(theta2*pi/180)^2)/c;
        hjg=find(imag(kz0)>0);
        kz0([hjg])=-kz0([hjg]);
        hjj=find(imag(kz1)>0);
        kz1([hjj])=-kz1([hjj]);
        hja=find(imag(kz2)>0);
        kz2([hja])=-kz2([hja]);

        Z2=kz2*eta2/k2;
        Z1=kz1*eta1/k1;
        Z0=kz0*eta0/k0;

        T01=(2*Z1)./(Z1+Z0);
        T12=(2*Z2)./(Z2+Z1);
```

```
        T20=(2*Z0)./(Z2+Z0);
        R01=(Z1-Z0)./(Z1+Z0);
        R12=(Z2-Z1)./(Z2+Z1);
        R20=(Z0-Z2)./(Z0+Z2);

 Tc2=(exp(-sqrt(-1)*kz1*(l1o)).*exp(-sqrt(-
1)*kz2*(l2o)).*T01.*T12.*T20)./...
                (1+R01.*R12.*exp(-sqrt(-1)*2*kz1*(l1o))+...
+R12.*R20.*exp(-sqrt(-1)*2*kz2*(l2o))+R01.*R20.*exp(-sqrt(-
1)*2*kz2*(l2o))...
                .*exp(-sqrt(-1)*2*kz1*(l1o)));

 Jack34=[(abs(Tm2(fj))-abs(Tc2*exp(sqrt(-1)*kz0*(l1o+l2o))))-
func(3,1)];

        llps=angle(Tm2(fj));
        hyt=angle(Tc2.*exp(sqrt(-1)*kz0*(l1o+l2o)));

        anglebla0=(llps-hyt);
        if abs(anglebla0)>pi && abs(anglebla0)<2*pi
           anglebla0=abs(anglebla0)-2*pi;
        end
        Jack44=[abs(anglebla0)-func(4,1)];
        Jack=[Jack11, Jack12, Jack13, Jack14;
            Jack21, Jack22, Jack23, Jack24;
            Jack31, Jack32, Jack33, Jack34;
            Jack41, Jack42, Jack43, Jack44]/delx;

        if abs(det(Jack(1:4,:)))<0.00000000000000001
                index1(fj)=0;
                ext1(fj)=0;
                index2(fj)=0;
                ext2(fj)=0;
                fhh(fj,:)=[func'];
         break
        end
        optmat=optmat-Jack\func;
        n1o=optmat(1,1);
        k1o=optmat(2,1);
        n2o=optmat(3,1);
        k2o=optmat(4,1);

                    if nj==n
                index1(fj)=n1o;
                ext1(fj)=k1o;
                index2(fj)=n2o;
                ext2(fj)=k2o;
```

```
                fhh(fj,:)=[func'];
                    end
    end
    cnt(fj)=nj;

end

figure;plot(f_worth,index1,f_worth,index2);grid
title('refractive index - real')
figure;plot(f_worth,abs(ext1),f_worth,abs(ext2));grid
title('refractive index - imag')
%figure;plot(f_worth,cnt);grid

er1=index1.^2-ext1.^2;
er2=index2.^2-ext2.^2;
figure;plot(f_worth,er1,f_worth,er2);grid
title('real perm')

tand1=2*index1.*abs(ext1)./er1;
tand2=2*index2.*abs(ext2)./er2;
figure;plot(f_worth,tand1,f_worth,tand2);grid
title('loss tangent')
```

BIBLIOGRAPHY

BIBLIOGRAPHY

[1] B. Freguson, and X. C. Zhang , "Materials for Terahertz Science and Technology," *Nature Materials*, Vol. 1, (2002), pp. 26-33.

[2] X. C. Zhang, "Terahertz Wave Imaging: Horizons and Hurdles," *Phys. Med. Biol.,* Vol. 47, (2002), pp. 3667–3677.

[3] P. H. Seigel, "Terahertz Technology," *IEEE Trans. Microwave Theory Tech.,* Vol. 50, No. 3, (2002), pp. 910–928.

[4] D. Zimdars, J. S. White, G. Stuck, A. Chernovsky, G. Fichter, and S. Williamson, "Large Area Terahertz Imaging and Non-Destructive Evaluation Applications," *Proc The 4th International Workshop on Ultrasonic and Advanced Methods for Nondestructive Testing and Material Characterization*, Dartmouth, MA, (2006), pp. 63-66.

[5] Y. Ju, M. Saka, and H. Abe, "NDI of Delamination in IC Packages Using Millimeter-Waves," *IEEE Trans. Instr. and Meas.,* Vol. 50, No. 4, (2001), pp. 1019-1023.

[6] C. Jordens, F. Rutz, and M. Koch, "Quality assurance of Chocolate Products with Terahertz Imaging," *Proc of ECNDT*, Berlin, Germany, (2006), Post. 67.

[7] R. Anastasia, and E. I. Madaras, "Terahertz NDE for Metallic Surface Roughness Evaluation," *Proc of The 4th International Workshop on Ultrasonic and Advanced Methods for Nondestructive Testing and Material Characterization*, Dartmouth, MA, (2006), pp. 57-62.

[8] J. Fredrici, R. L. Wample, D. Rodriquez, and S. Mukherjee, "Application of Terahertz Gouy Phase Shift from Curved Surfaces for Estimation of Crop Yield," *Appl. Opt.,* Vol. 48, No. 7, (2009), pp. 1382-1388.

[9] H. B. Liu, G. Plopper, S. Earley, Y. Chen, B. Ferguson, and X. C. Zhang, "Sensing Minute Changes in Biological Cell Monolayers with THz Differential Time-Domain Spectroscopy," *Biosens. Bioelectron.,* Vol. 22, (2007), pp. 1075–1080.

[10] C. D. Stoik, M. J. Bohn, J. L. Blackshire, "Nondestructive Evaluation of Aircraft Composites Using Terahertz Time Domain Spectroscopy," *Infrared, Millimeter and Terahertz Waves, 2008. IRMMW-THz 2008. 33rd International Conference on* , vol., no., pp.1-2, 15-19 Sept. 2008

[11] M. C. Kemp, C. Baker, and I. Gregory, "Stand-off explosives detection using terahertz technology," in *Stand-off Detection of Suicide Bombers and Mobile Subjects*, H. Schubert, and A. Rimski-Korsakov, eds.(Springer, 2006), pp.151-165.

[12] S. Wang, *et. Al,* "Pulsed terahertz tomography," *J. Appl. Phy.,* Vol. 37, (2004), pp. R1-R36.

[13] D. Mittleman, *et. Al,* "T-ray tomography," *Opt. Lett.,* Vol. 22, No. 12, (1997), pp. 904-906.

[14] M. V. Exter, *et. Al,* “Terahertz time-domain spectroscopy of water vapor,” *Opt. Lett.,* Vol. 14, No. 29, (1989), pp. 1128-1131.

[15] D. Banerjee, *et. Al,* “Diagnosing water content in paper by terahertz radiation,” *Opt. Exp.,* Vol. 16, No. 12, (2008), pp. 9060-9066.

[16] H. T. Chen, R. kersting, and G. C. Cho, “Terahertz imaging with nanometer resolution,” *Appl. Phy. Lett.,* Vol. 83, No. 15, (2003), pp. 3009-3011.

[17] J. T. Case, F. L. Hepburn, and R. Zoughi, “Inspection of Spray on Foam Insulation (SOFI) Using Microwave and Millimeter Wave Synthetic Aperture Focusing and Holography,” *Proc. of The Instrumentation and Measurement Technology Conference*, Sorrento, Italy, (2006).

[18] S. theerawisitpong, T. Suzuki, T. Negishi, K. Shibahara, and Y. Watanabe, “Void and Pore Detections by the Scanning Near-Field Millimeter-Wave Microscopic Aperture Probe,” *Proc. of The Asia-Pacific Microwave Conference*, Bangkok, Thailand, (2007).

[19] N. S. Greeney, and J. A. Scales, “Dielectric microscopy with submillimeter resolution,” *Appl. Phy. Lett.,* Vol. 91, 222909, (2007).

[20] E. Kume, and S. Sakai, “Properties of a dielectric probe for scanning near-field millimeter-wave microscopy,” *J. Appl. Phy.,* Vol. 99, 056105, (2006).

[21] P. H. Bolivar, J. G. Rivas, R. Gonzalo, I. Ederra, A. L. Reynolds, M. Holker, and P. de Maagt, “Measurement of the dielectric constant and loss tangent of high dielectric-constant materials at terahertz frequencies,” *IEEE Trans. Microwave Theory Tech.,* Vol. 51, No. 4, (2003), pp. 1062–1066.

[22] T. Fujii, A. Ando, and Y. Sakabe, “Charaterization of Dielectric Properties of Oxide Materials in Frequency Range From GHz to THz,” *J. Eur. Ceram. Soc.,* Vol. 26,(2006), pp. 1857–60.

[23] A. K. Azad, J. G. Han, and W. L. Zhang, “Terahertz Dielectric Properties of High-Resistivity Single-Crystal ZnO”, *Appl. Phys. Lett.,* Vol. *88*, (2006), 021103.

[24] A. Podzorov, and G. Gallot, “Low-loss polymers for terahertz applications,” *Appl. Op*t., Vol. 47, (2008), pp. 3254–3257.

[25] M. Naftaly, and R. E. Miles, “Terahertz time-domain spectroscopy for material characterization,” *Proc. IEEE*, Vol. 95, No. 8, (2007), pp. 1658–1665.

[26] M. Hangyo, M. Tani, and T. Nagashima, “Terahertz Time-Domain Spectroscopy of Solids: A Review,” *Intl. Jour. Of Infrared and Millimeter Waves*, Vol. 26, No. 12, (2005), pp.1661-1690.

[27] T. Dorney, R. G. Baraniuk, and D. M. Mittleman, “Material Parameter Estimation with Terahertz Time-Domain Spectroscopy,” *J. Opt. Soc. Amer. A*, Vol. 18, No. 7, (2001), pp. 1562-1571.

[28] L. Duvillaret, F. Garet, and J. Coutaz, “A Reliable Method for Extraction of Material Parameter in Terahertz Time-Domain Spectroscopy,” *IEEE J. Sel. Top. Quantum Electron.*, Vol. 2, No. 3, (1996), pp. 739-746.

[29] L. Duvillaret, F. Garet, and J. Coutaz, “Highly Precise Determination of Both Optical Constants and Sample Thickness in Terahertz Time-Domain Spectroscopy,” *Appl. Opt*., Vol. 38, No. 2, (1999), pp. 409-415.

[30] I. Pupeza, R. Wilk, and M. Koch, “Highly Accurate Optical Material Parameter Determination with THz Time-Domain Spectroscopy,” *Opt. Exp.*, Vol. 15, No. 7, (2007), pp. 4335-4350.

[31] T. Jeon, “Characterization of Doped Silicon from 0.1 to 2.5 THz Using Multiple Reflection,” *J. Opt. Soc. Kor.*, Vol. 3, No. 1, (1999), pp. 10-14.

[32] T. Nagashima, and M. Hangyo, “Measurement of Complex Optical Contstants of a Highly Doped Si Wafer Using Terahertz Ellipsometry,” *Appl. Phy. Lett*, Vol. 29, No. 24, (2001), pp. 3917-3919.

[33] N. Matsumoto, T. Hosokura, T. Nagashima, and M. Hangyo, “Measurement of Dielectric Constant of Thin Films Using Terahertz Time-Domain Spectroscopic Ellipsometry,” *Opt. Lett.*, Vol. 36, No. 2, (2011), pp. 265-267.

[34] Z. Jiang, M. Li, and X.C. Zhang, “Dielectric Constant Measurement of Thin Films by Differential Time-Domain Spectroscopy,” *Appl. Phy. Lett.*, Vol. 76, No. 22, (2000), pp. 3221-3223.

[35] S. Mickan, K. Lee, T. Lu, J. Munch, D. Abbot, and X.C. Zhang, “Double Modulate Differential THz-TDS for Thin Film Characterization,” *Microelec. Jour.*, Vol. 33, (2002), pp. 1033-1042.

[36] M. Feng-Ying, S. Jian-Po, G. Qiao-Xia, Y. Jing, D. Yan-Li, G. Mao-Tian, and Y. Bin, “Measurement of the Optical Constants of Thin Metal Films Using THz Differential Time Domain Spectroscopy,” *Chin. Phys. Lett.*, Vol. 28, No. 9, (2011), 097803.

[37] J. A. Hejase, P. R. Paladhi, and P. Chahal, “THz Characterization of Dielectric Substrates for Component Design and Non-destructive Evaluation of Packages,” *IEEE Trans. Components, Packaging and Manufacturing Tech.*, Vol.1, No.11, (2011), pp.1685-1694.

[38] E. J. Rothwell, and M. J. Cloud, *Electromagnetics*. Boca Raton, FL: CRC Press, (2001), pp. 292–294.

[39] A. Ravindran, K.M. Ragsdell, and G. V. Reklaitis, *Engineering Optimization: Methods and Applications*. New York: Wiley, (2006), pp. 86–91.

[40] J. Lagarias, J. A. Reeds, M. H. Wright, and P. E. Wright, "Convergence Properties of the Nelder–Mead Simplex Method in Low Dimensions," *SIAM J. Optim.*, Vol. 9, No. 1, (1998), pp. 112–147.

[41] J. A. Nelder, and R. Mead, "A Simplex Method for Function Minimization," *Comput. J.*, Vol. 7, No. 4, (1965), pp. 308–313.

[42] P. Chahal, R. R. Tummala, M. G. Allen, and M. Swaminathan, "A Novel Integrated Decoupling Capacitor for MCM-L Technology," *IEEE Trans. Comp., Packag., Manuf. Technol. Part B: Adv. Packag.*, Vol. 21, No. 2, (1998), pp. 184–193.

[43] Y. Jin, G. Kim, and S. Jeon, "Terahertz dielectric properties of polymers," *J. Korean Phys. Soc.*, Vol. 49, No. 2, (2006), pp. 513–517.

[44] K. Naito, Y. Kagawa, S. Utsuno, T. Naganuma, and K. Kurihara "Dielectric Properties of Eigh-Harness-Stain Fabric Glass Fiber Reinforced Polyimide Matrix Composite in the THz Frequency Range," *NDT & E Int.*, Vol. 42, No. 5, (2009), pp. 441–445.

[45] *Kapton Polyimide Film-Summary of Properties*, Industrial Films Division, Polymer Products Dept., DuPont Co., Wilmington, DE, (1989).

[46] J.A. Hejase, E.J. Rothwell, and P. Chahal, "A Self Calibrating Technique for Terahertz Time Domain Material Parameter Extraction", *J. Opt. Soc. Amer. A*, Vol. 28, No. 12, (2011), pp. 2561-2567.

[47] M.V. Exter, and D. Grischowsky, "Optical and Electronic Properties of Doped Silicon between 0.1 to 2 THz," *Appl. Phys. Lett.,* Vol. 56, (1990), pp. 1694-1696.

[48] J. Li, and J. Li, "Dielectric Properties of Silicon in Terahertz Wave Region," *Mic. and Opt. Tech. Lett.*, Vol. 50, (2008), pp. 1143-1146.

[49] J. A. Hejase, E. J. Rothwell, and P. Chahal, "A Multiple Angle Material Parameter Extraction method for Stacked Layers of Dielectrics Using THz Time-domain Spectroscopy," *38th Annual Review of Progress in Quantitative Nondestructive Evaluation*, American Institute of Physics (Sept. 2011).

[50] W. C. Chew, *Waves and Fields in Inhomogeneous Media, 1*st ed. New York: VNR, (1990), pp.48–49.

[51] E. Kreyszig, *Advanced Engineering Mathematics,* New York: Wiley, (1999), pp. 845–846.

[52] J. W. Goodman, *Introduction to Fourier Optics,* Englewood, CO: ROBERTS & COMPANY, (2005), pp. 55–61.

[53] K. Lizuka, *Engineering Optics,* Berlin, Heidelberg (Germany): Springer-Verlag, (1985), pp. 95-102.

[54] J. E. Garrett, and J. C. Wiltse, "Fresnel Zone Plate Antennas at Millimeter Wavelengths," *Intl. Jour. Of Infrared and Millimeter Waves*, Vol. 12, No. 3, (1991), pp.195-222.

[55] J. Jahns, and S. J. Walker, "Two-Dimensional Array of Diffractive Microlenses Fabricated by Thin Film Deposition," *App. Opt.,* Vol. 29, No. 7, (1990), pp.931-936.

[56] S. Wang, and X. C. Zhang, "Tomographic Imaging With a Terahertz Binary Lens," *App. Phy. Lett.,* Vol. 82, No. 12, (2003), pp.1821-1823.

[57] E. D. Walsby, S. Wang, J. Xu, T. Yuan, R. J. Blaikie, S. M. Durbin, X. C. Zhang, and D. R. S. Cumming, "Mutilevel Silicon Diffractive Optics for Terahertz Waves," *J. Vac. Sci. Technol. B.,* Vol. 20, No. 6, (2002), pp.2780-2783.

[58] S. Wang, T. Yuan, E. D. Walsby, R. J. Blaikie, S. M. Durbin, D. R. S. Cumming, J. Xu, and X. C. Zhang, "Characterization of T-ray Binary Lenses," *Opt. Lett.,* Vol. 27, No. 13, (2002), pp.1183-1185.

[59] S. Y. Lei, Z. Q. Li, and Z. C. Lin, "Diffraction of Terahertz Waves After Passing Through a Fresnel Lens," *Chin. Phy. B,* Vol. 18, No. 12, (2009), pp.5511-5517.

[60] M. Howells, C. Jacobsen, T. Warwick, A. Bos, P. W. Hawkes, and J. C. H. Spence, "Principles and Applications of the Zone Plate X-ray Microscopres," in *Science of Microscopy*, (Springer, 2007), pp.835-926.

[61] J. Kirz, "Phase Zone Plates for X-rays and the Extreme UV," *J. Opt. Soc. Amer.,* Vol. 64, No. 3, (1974), pp.301-309.

[62] J. A. Hejase, B. Schulte, and P. Chahal, "Design and test of wide band terahertz dielectric sub-wavelength focusing probes," in *Proc. 61st Electron. Comp. Packag. Conf.*, Lake Buena Vista, FL, May–Jun. 2011, pp. 1035–1040.

[63] E. Kume, and S. Sakai, "Millimeter-wave radiation from a Teflon dielectric probe and its imaging application," *Meas. Sci. and Tech.,* Vol. 19, (2006), 115501-6pp.

[64] W. Chan, J. Deibel, and D. Mittleman, "Imaging with Terahertz Radiation," *Rep. on Prog. in Phys.*, No.70 (2007), pp.1325-1379.

[65] Schade et al., "THz near-field imaging of biological tissues employing synchrotron radiation," Lawrence Berkeley National Laboratory, (2004).

[66] G. E. Urroz (2001). *Solving Nonlinear Equations With SCILAB* [Online]. Available: http://www.infoclearinghouse.com/files/scilab/scilab6a.pdf